VOLUME 78 MARCH 28, 1974 NUMBER 7

JPCHAx

THE JOURNAL OF PHYSICAL CHEMISTRY

PUBLISHED BIWEEKLY BY THE AMERICAN CHEMICAL SOCIETY

THE JOURNAL OF

PHYSICAL CHEMISTRY

AMERICAN CHEMICAL SOCIETY, *1155 Sixteenth St., N.W., Washington, D. C. 20036*

Books and Journals Division

JOHN K CRUM *Director*
RUTH REYNARD *Assistant to the Director*

CHARLES R. BERTSCH *Head, Editorial Processing Department*
D. H. MICHAEL BOWEN *Head, Journals Department*
BACIL GUILEY *Head, Graphics and Production Department*
SELDON W. TERRANT *Head, Research and Development Department*

 Published biweekly by the American Chemical Society at 20th and Northampton Sts., Easton, Pa. 18042. Second-class postage paid at Washington, D. C., and at additional mailing offices.

All manuscripts should be sent to *The Journal of Physical Chemistry*, Department of Chemistry, University of Minnesota, Minneapolis, Minn. 55455.

Additions and Corrections are published once yearly in the final issue. See Volume 77, Number 26 for the proper form.

Extensive or unusual alterations in an article after it has been set in type are made at the author's expense, and it is understood that by requesting such alterations the author agrees to defray the cost thereof.

The American Chemical Society and the Editor of *The Journal of Physical Chemistry* assume no responsibility for the statements and opinions advanced by contributors.

Correspondence regarding accepted copy, proofs, and reprints should be directed to Editorial Processing Department, American Chemical Society, 20th and Northampton Sts., Easton, Pa. 18042. Head: CHARLES R. BERTSCH. Assistant Editor: EDWARD A. BORGER. Editorial Assistant: JOSEPH E. YURVATI.

Advertising Office: Centcom, Ltd., 142 East Avenue, Norwalk, Conn. 06851.

Business and Subscription Information

Send all new and renewal subscriptions *with payment* to: Office of the Controller, 1155 16th Street, N.W., Washington, D. C. 20036. Subscriptions should be renewed promptly to avoid a break in your series. All correspondence and telephone calls regarding changes of address, claims for missing issues, subscription service, the status of records, and accounts should be directed to Manager, Membership and Subscription Services, American Chemical Society, P.O. Box 3337, Columbus, Ohio 43210. Telephone (614) 421-7230.

On changes of address, include both old and new addresses with ZIP code numbers, accompanied by mailing label from a recent issue. Allow four weeks for change to become effective.

Claims for missing numbers will not be allowed (1) if loss was due to failure of notice of change in address to be received before the date specified, (2) if received more than sixty days from date of issue plus time normally required for postal delivery of journal and claim, or (3) if the reason for the claim is "issue missing from files."

Subscription rates (1974): members of the American Chemical Society, $20.00 for 1 year; to nonmembers, $60.00 for 1 year. Those interested in becoming members should write to the Admissions Department, American Chemical Society, 1155 Sixteenth St., N.W., Washington, D. C. 20036. Postage to Canada and countries in the Pan-American Union, $5.00; all other countries, $6.00. Air freight rates available on request. Single copies for current year: $3.00. Rates for back issues from Volume 56 to date are available from the Special Issues Sales Department, 1155 Sixteenth St., N.W., Washington, D. C. 20036.

Subscriptions to this and the other ACS periodical publications are available on microfilm. Supplementary material not printed in this journal is now available in microfiche form on a current subscription basis. For information on microfilm or microfiche subscriptions, write Special Issues Sales Department at the address above.

Notice to Authors last printed in the issue of December 6, 1973

THE JOURNAL OF

PHYSICAL CHEMISTRY

Volume 78, Number 7 March 28, 1974

JPCHAx 78 (7) 653–762 (1974)
ISSN 0022-3654

COMMUNICATIONS TO THE EDITOR

■ Supplementary material for this paper is available separately, in photocopy or microfiche form. Ordering information is given in the paper.

* In papers with more than one author, the asterisk indicates the name of the author to whom inquiries about the paper should be addressed.

AUTHOR INDEX

THE JOURNAL OF
PHYSICAL CHEMISTRY

VOLUME 78, NUMBER 7 MARCH 28, 1974

Reaction of HO_2 with NO and NO_2

R. Simonaitis* and Julian Heicklen

Department of Chemistry and Ionosphere Research Laboratory, Pennsylvania State University, University Park, Pennsylvania 16802

(Received October 9, 1973)

Publication costs assisted by the National Science Foundation

The reaction of HO_2 with NO and NO_2 was studied at 25°. The HO_2 radicals were prepared by the photolysis of N_2O at 2139 Å in the presence of O_2 and excess H_2. In the presence of NO_2, the NO_2 pressure drops with a quantum yield of disappearance just under 2.0 until a final steady-state value, $[NO_2]_{ss}$, is reached. If the irradiation is terminated, the NO_2 pressure rises due to the heterogeneous decay of HONO + O_2 (2). This reaction is so fast that there is no evidence for the competing reaction $2HO_2 \rightarrow H_2O_2$ min^{-1} in our reaction vessel. The initial decay of the NO_2 is caused by the reaction $HO_2 + NO_2 \rightarrow$ HONO O_2 (2). This reaction is so fast that there is no evidence for the competing reaction $2HO_2 \rightarrow H_2O_2$ + O_2 (6). Thus from the data $k_2/k_6^{1/2} > 11.4 \times 10^{-8}$ (cc/sec)$^{1/2}$. If k_6 is taken as 6.0×10^{-12} cc/sec, then $k_2 > 3 \times 10^{-13}$ cc/sec. If small amounts of NO and NO_2 are both present in mixtures of N_2O, O_2, CO, and excess H_2, the NO_2 pressure rises when irradiation is initiated because of the reaction HO_2 + NO $\rightarrow$ HO + NO_2 (1). When the NO is essentially exhausted, the NO_2 pressure passes through a maximum and then decays with a quantum yield of about 2.0. During the initial rise, if [NO] and $[NO_2]$ are sufficiently small, and $[H_2]$ and [CO] sufficiently large, then $\Phi_i[NO_2] = 2(k_1[NO]/k_2[NO_2] - 1)$. From the data, $k_1/k_2 = 7 \pm 1$.

Introduction

The reactions of HO_2 with NO and NO_2 are of interest in both the upper and lower atmosphere. The reaction of HO_2 with NO

$$HO_2 + NO \longrightarrow NO_2 + HO \qquad (1)$$

is believed to be a key reaction in the conversion of NO to NO_2 in polluted atmospheres. We have examined this reaction previously, but only a lower limit has been obtained for its rate coefficient: $k_1 > 1.5 \times 10^{-13}$ cc/sec at 300°K.

As far as we know, the reaction of HO_2 with NO_2

$$HO_2 + NO_2 \longrightarrow HONO + O_2 \qquad (2)$$

has not been studied, nor has it been considered in atmospheric models. The reaction is greatly exothermic, and there is no *a priori* reason why it could not be fast. If so, it would also play an important role in atmospheric chemistry.

In this paper we report the first kinetic study of reaction 2 and provide relative rate coefficients for reactions 1 and 2. The HO_2 radicals are generated by the photolysis of N_2O at 2139 Å in the presence of O_2 and excess H_2.[1]

The sequence of reactions is

$$N_2O + h\nu \longrightarrow N_2 + O(^1D) \quad \text{rate} = I_a$$

$$O(^1D) + H_2 \longrightarrow HO + H \qquad (3)$$

$$HO + H_2 \longrightarrow H_2O + H \qquad (4)$$

$$H + O_2 + M \longrightarrow HO_2 + M \qquad (5)$$

If NO or NO_2 or both are introduced then the HO_2 radicals may react with these compounds or they may disproportionate

$$2HO_2 \longrightarrow H_2O_2 + O_2 \qquad (6)$$

By following NO_2 pressure as a function of reaction conditions, the relative importance of reactions 1, 2, and 6 could be studied.

Experimental Section

The experimental apparatus, procedure, and actinometry were the same as in our previous study,[1] except that the NO_2 pressures were measured continuously as a function time with a sensitive dual-beam spectrophotometer. Light from a 300-W tungsten light bulb was modulated with a PAR Model 125 chopper equipped with a modified

chopping wheel. The wheel consisted alternately of 16 slots and 16 mirrors, providing a modulating frequency of 667 Hz. When the beam impinged upon a slot the light was focused by means of lenses and mirrors onto a RCA 935 phototube. When the beam impinged upon a mirror, the reflected light passed through the reaction cell and was focused onto the phototube. The signal from the phototube was amplified with PAR Model 112 preamplifier and further amplified and detected with a PAR Model 121 lock-in amplifier equipped with a millivolt recorder readout. The minimum NO_2 pressure detectable was ~1 mTorr.

The NO_2 was prepared in the vacuum line from pure NO and O_2. It was purified periodically (when blue N_2O_3 could be seen in the solid) by the addition of excess O_2 and degassing at −196°.

Results

NO Initially Absent. Irradiation of mixtures of N_2O–O_2–H_2 in the presence of small amounts of NO_2 at 2139 Å and 25° leads to the consumption of NO_2. Figure 1 shows a plot of the NO_2 pressure *vs.* irradiation time for an experiment in which the initial NO_2 pressure, $[NO_2]_0$, was 13 mTorr. The consumption is linear with irradiation time, even at 2-mTorr NO_2 pressure, until the NO_2 is exhausted.

Figure 2 shows a similar plot for an experiment with $[NO_2]_0$ = 81 mTorr. As before NO_2 comsumption occurs, but only to a lower limiting steady-state value, $[NO_2]_{ss}$, which in this case is 5 mTorr. When the irradiation is terminated, the NO_2 pressure rises to a final value, $[NO_2]_\infty$, equal to about one-third its starting value.

The results clearly indicate that NO_2 is consumed during irradiation to form a product which thermally decomposes to regenerate NO_2 thermally. Undoubtedly this product is HONO, and the regeneration step is[2]

$$\text{HONO} \xrightarrow{\text{wall}} (1/2)H_2O + (1/2)NO + (1/2)NO_2 \qquad (7)$$

The results of several experiments are listed in Table I. The initial quantum yields of NO_2 disappearance, $-\Phi_i\{NO_2\}$, are almost all just slightly less than 2.0. Three runs have $\Phi_i\{NO_2\}$ slightly above 2.0, and one run at the lowest $[H_2]/[N_2O]$ ratio (*i.e.*, 4.2), has $\Phi_i\{NO_2\}$ = 1.34. However, for the others, $\Phi_i\{NO_2\}$ varies between 1.61 and 1.95 which reflects the experimental uncertainty. Thus as long as $[H_2]/[N_2O] > 8$, $\Phi_i\{NO_2\}$ is essentially independent of the reactant pressures which varied from 13 to 53 Torr for N_2O, 25 to 150 Torr for O_2, 410 to 800 Torr for H_2 (excluding the run with $[H_2]$ = 210 Torr), and 7.5 to 350 mTorr of NO_2. Further the reactant pressure ratios ranged from $[H_2]/[N_2O]$ = 4.2 to 50, $[H_2]/[O_2]$ = 4 to 30, and $[H_2]/[NO_2] = 1.9 \times 10^3$ to 1.0×10^5.

The values for $[NO_2]_{ss}$ were measured in a number of runs and they are listed in Table I. Due to experimental problems, it was difficult to obtain accurate values. In spite of the large experimental uncertainty, it is apparent that $[NO_2]_{ss}$ increases with $[NO_2]_0$. Values of the initial rate of reformation of NO_2 after the irradiation is terminated, $R_d\{NO_2\}$, are given in the table, and they also tend to increase with $[NO_2]_0$.

For four runs, values of $[NO_2]_\infty$ were obtained. Since HONO decays to produce one-half as much NO_2, the sum of [HONO] + $[NO_2]$ at the steady state is obtained from the function $2[NO_2]_\infty - [NO_2]_{ss}$. For the four runs in Table I where this function can be computed, the ratio $(2[NO_2]_\infty - [NO_2]_{ss})/[NO_2]_0$ is 0.82, 0.75, 0.71, and 0.36, respectively, for the runs with $[NO_2]_0$ = 68, 81, 150, and 345 mTorr. Consequently as $[NO_2]_0$ rises a larger percentage of the NO_2 converts to NO, N_2O_5, or $HONO_2$.

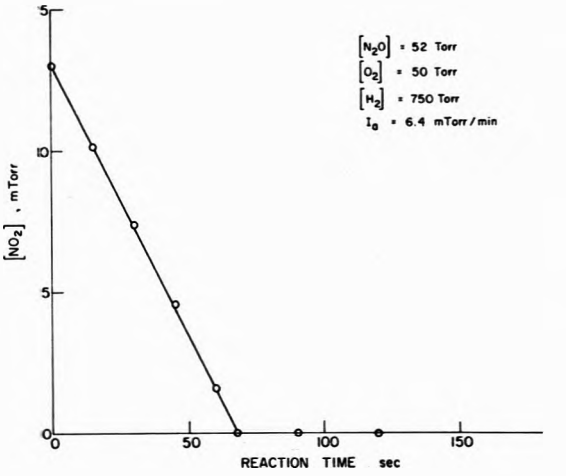

Figure 1 Plot of NO_2 pressure *vs.* reaction time in the photolysis of N_2O–O_2–H_2–NO_2 mixtures at 2139 Å and 25° for $[NO_2]_0$ = 13 mTorr.

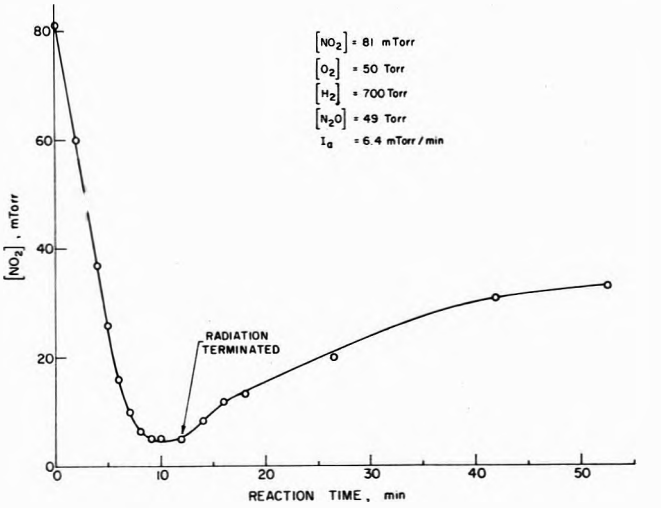

Figure 2. Plot of NO_2 pressure *vs.* reaction time in the photolysis of N_2O–O_2–H_2–NO_2 mixtures at 2139 Å and 25° for $[NO_2]_0$ = 79 mTorr.

A possible route for the loss of NO_2 could be by reaction with H_2O_2.[2]

$$(1 + \epsilon)H_2O_2 + 2NO_2 \longrightarrow 2HONO_2 + \epsilon H_2O + (\epsilon/2)O_2 \qquad (8)$$

To test this possibility, NO_2 and H_2O_2 were mixed, and the initial rate of NO_2 disappearance, $R_i\{NO_2\}$, was measured. The results are in Table II. These rates are smaller than those found by Gray, *et al.*,[2] thus confirming the heterogeneous character of the reaction. The rates are too small to be significant in the early stages of the reaction, but they might account for part of the NO_2 deficiency at the steady state, if in fact H_2O_2 is produced in the reaction.

Another possible route for NO_2 loss is through direct photodecomposition. To test this possibility experiments were done with the N_2O omitted. The results are shown in Table III. The initial rates of NO_2 removal, $R_i\{NO_2\}$, by direct photolysis are too small to make a significant effect at the beginning of the reaction. Even with 320 mTorr of NO_2, the direct photolysis would only have about a 15% effect.

TABLE I: Reaction of HO_2 with NO_2

$[NO_2]_0$, mTorr	$[N_2O]$, Torr	$[O_2]$, Torr	$[H_2]$, Torr	I_a, mTorr/min	$-\Phi_i\{NO_2\}$	$[NO_2]_{ss}$, mTorr	$R_d\{NO_2\}$, mTorr/min	$[NO_2]_\infty$, mTorr
7.5	53	50	750	6.4	1.95	0		
13	52	50	750	6.4	1.59	0		
13	50	25	750	6.4	1.78	0		
15	50	49	750	6.4	1.85	0		
19	50	50	750	6.4	1.95			
24	50	50	800	6.4	1.88			
37	50	50	750	6.4	2.03			
45	20.5	33	410	2.6	1.73	5.3	0.67	
67	50	50	700	6.4	1.72	6.5		
68	53	38	700	6.4	1.90		1.8	30
79	50	50	750	6.4	1.79	8.0		
80	55	53	800	6.4	1.80		2.0	
80	50	50	700	6.4	1.72			
80	50	100	650	6.4	1.80			
81	49	50	700	6.4	1.78		1.55	33
82	50	50	750	6.4	1.85	11.8		
83	50	50	210	6.4	1.34	8.6		
83	20	50	750	2.6	2.54	6.6		
86	50	50	600	6.4	1.61			
98	50	50	700	6.4	1.92	7.5		
99	16	37	800	2.0	2.26	5.0		
100	13	39	430	1.66	1.69	13		
102	50	50	370	6.4	1.63	7.4	1.8	
136	45	50	700	5.8	1.64		2.0	
145	50	50	700	6.4		11		
148	50	50	700	6.4			2.5	
148	50	50	700	6.4	1.89	15		
148	50	50	700	6.4			2.2	
150	50	50	700	6.4	1.89	11	3.3	
150	50	50	700	6.4	1.72		3.0	56
310	50	50	700	6.4	1.80		5.2	
310	50	150	600	6.4	1.87	17		
345	50	120	630	6.4	1.73		7.0	70

TABLE II: Reaction of H_2O_2 with NO_2

$[H_2O_2]$, Torr	$[NO_2]_0$, mTorr	$-R_i\{NO_2\}$, mTorr/min
0.17	95	1.75
1.0	75	3.0
1.2	30	0.75
1.2	90	3.7

NO Initially Present. Irradiation of O_2–N_2O–H_2 and O_2–N_2O–H_2–CO mixtures in the presence of small amounts of NO and NO_2 causes the NO_2 pressure to increase initially at a rate $R_i\{NO_2\}$ (because of reaction 1), reach a maximum, and then decline with a constant rate, $-R_m\{NO_2\}$, of $\sim 2I_a$. A typical run is shown in Figure 3.

Values of $R_i\{NO_2\}$ and $-R_m\{NO_2\}$ for several runs are given in Table IV. Also listed is the initial quantum yield of NO_2 formation computed as $2R_i\{NO_2\}/R_m\{NO_2\}$. The results can be summarized as follows: $\Phi_i\{NO_2\}$ increases with $[NO]_0/[NO_2]_0$ at constant $[NO_2]_0$, but for the same values of $[NO]_0/[NO_2]_0$, $\Phi_i\{NO_2\}$ drops as $[NO_2]_0$ increases from 10 to 20 to 50 mTorr. For $[NO_2]_0 \sim 50$ mTorr, $\Phi_i\{NO_2\}$ rises with [CO], but for $[NO_2]_0 \sim 20$ mTorr the effect of CO is small, an increase of [CO] from 50 to 150 Torr has almost no effect.

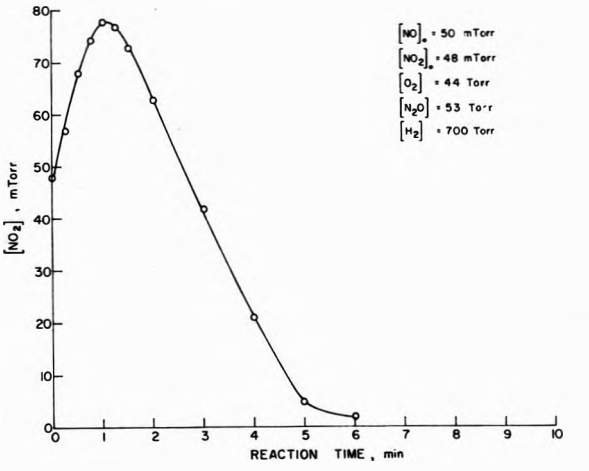

Figure 3. Plot of NO_2 pressure *vs.* reaction time in the photolysis of N_2O–O_2–H_2–NO_2–NO mixtures at 2139 Å and 25° for $[NO]_0/[NO_2]_0 = 1.04$.

Discussion

Mechanism. In order to discuss the results it is convenient to develop the complete mechanism for the early stages of the reaction, *i.e.*, when the reactions of H_2O_2, HONO, $HONO_2$, and N_2O_5 can be ignored. The initial photolytic act is the formation of $O(^1D)$ *via*

$$N_2O + h\nu \longrightarrow N_2 + O(^1D) \quad \text{rate} = I_a$$

The photolysis of NO_2 also occurs to some extent, especially at high NO_2 pressures, but the results in Table III show that this process is not important.

The $O(^1D)$ is removed essentially exclusively by reaction with H_2

$$O(^1D) + H_2 \longrightarrow HO + H \qquad (3)$$

since the rate coefficients for $O(^1D)$ removal by H_2, N_2O, and O_2 have the relative values 1.6, 1.0, and 0.42, respectively,[3] and except for the one run with $[H_2]/[N_2O] = 4.2$, our experimental ratios for $[H_2]/[N_2O] \geq 7.4$ and $[H_2]/[O_2] \geq 4$. Experimental verification that $O(^1D)$ removal

TABLE III: Photolysis of NO_2–O_2–H_2 Mixtures for Conditions where I_a for 50 Torr of N_2O Is 6.4 mTorr/min

$[NO_2]_0$, mTorr	$[O_2]$, Torr	$[H_2]$, Torr	$-R_i\{NO_2\}$, mTorr/min
40	50	700	0.20
80	50	750	0.5
87	40	700	0.42
220	50	700	2.0
290	50	700	4.0

by N_2O or O_2 was unimportant comes from the invariance of $\Phi_i\{NO_2\}$ to the $[H_2]/[N_2O]$ and $[H_2]/[O_2]$ ratios.

The HO radical produced in reaction 3 can react *via*

$$HO + H_2 \longrightarrow H_2O + H \quad (4)$$

$$HO + NO_2 + M \longrightarrow HONO_2 + M \quad (9)$$

$$HO + NO + M \longrightarrow HONO + M \quad (10)$$

$$HO + CO \longrightarrow H + CO_2 \quad (11)$$

Reaction 4 (and 11 if CO is present) is the dominant reaction, but reactions 9 and 10 cannot be neglected, in general, since they are chain-terminating steps. In fact, reaction 9 is probably responsible for the NO_2 deficiency observed at high NO_2 pressures at the steady state (in NO_2) conditions.

The H atom produced in reaction 4 undergoes only one reaction of importance under our conditions

$$H + O_2 + M \longrightarrow HO_2 + M \quad (5)$$

Its rate coefficient is 1.8×10^{-32} cc^6/sec for Ar or He as a chaperone.[3] With the assumption that H_2 is more efficient, the effective second-order rate coefficient under our conditions becomes $>5 \times 10^{-13}$ cc/sec. The possible competing reaction of H with NO_2 has a rate coefficient of 4.8×10^{-11} cc/sec.[4] Thus under our conditions of $[O_2]/[NO_2]_0 > 160$, the reaction of H with NO_2 can account for no more than 38% of the removal of H atoms and probably <15%, even under the most unfavorable conditions. Furthermore the experimental results show no dependence on the $[O_2]/[NO_2]_0$ ratio. We therefore disregard this reaction. The removal of H by NO is third order and proceeds with a rate coefficient no greater than that for reaction 6,[3] so that it can be ignored under our conditions ($[O_2]/[NO] > 1000$).

The HO_2 radical can be removed *via* any of the processes

$$HO_2 + NO \longrightarrow HO + NO_2 \quad (1)$$

$$HO_2 + NO_2 \longrightarrow HONO + O_2 \quad (2)$$

$$2HO_2 \longrightarrow H_2O_2 + O_2 \quad (6)$$

In the later stages of the reaction NO_2 must be reformed because a limiting steady-state value of NO_2 is obtained. Reaction 7 produces NO_2, however analysis shows that if $k_7 = 0.06$ sec^{-1} (see below) reaction 7 is not sufficiently fast to account for the observed values of $[NO_2]_{ss}$.

Other reactions which may produce NO_2 are

$$OH + HONO \longrightarrow H_2O + NO_2 \quad (12)$$

$$HONO + h\nu \longrightarrow OH + NO \text{ or } H + NO_2 \quad (13)$$

$$HO_2 + HONO \longrightarrow H_2O_2 + NO_2 \quad (14)$$

Reaction 12 could account for the observed $[NO_2]_{ss}$ providing $k_{12} \sim 7 \times 10^{-11}$ cm^3/sec. This large value of k_{12} is not impossible, but is very unlikely. Furthermore the mechanism predicts that if reaction 12 is important, $[NO_2]_{ss}$ should depend on $[H_2]$. This is not observed. Reaction 13 would contribute to $[NO_2]_{ss}$ only if reaction 12 is important. The remaining possibility is reaction 14. Analysis shows that this reaction would account for the observed $[NO_2]_{ss}$ provided $k_{14} > 2 \times 10^{-14}$ cm^3/sec. However in view of the uncertainty of the mechanism and the large uncertainty in the measured values of $[NO_2]_{ss}$ this lower limit for k_{14} cannot be accepted with confidence.

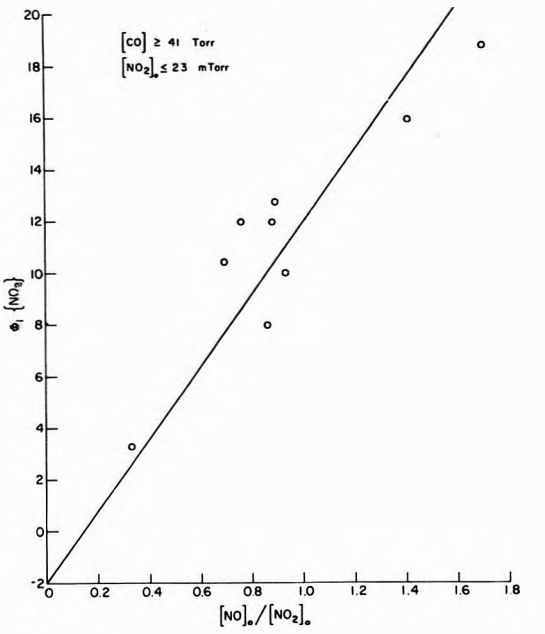

Figure 4. Plot of $\Phi_i\{NO_2\}$ *vs.* $[NO]_0/[NO_2]_0$ in the photolysis of N_2O–O_2–H_2–CO–NO_2–NO mixtures at 2139 Å and 25° for [CO] ≥ 41 Torr and $[NO_2]_0 \leq 23$ mTorr.

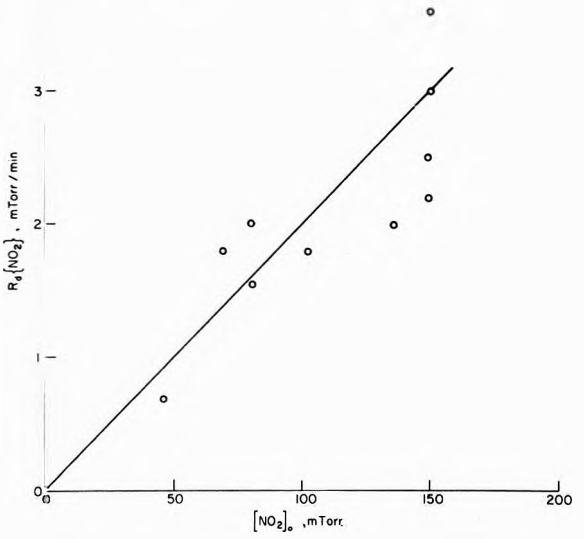

Figure 5. Plot of $R_d\{NO_2\}$ *vs.* $[NO_2]_0$ after radiation is terminated in the photolysis of N_2O–O_2–H_2–NO_2 mixtures at 25°.

Reaction of HO_2 with NO_2. In the absence of NO and CO, the mechansim for the early stages of the reaction predicts that $-\Phi_i\{NO_2\} = 2.0$ if reaction 6 is negligible. Our results give $-\Phi_i\{NO_2\}$ slightly less than 2.0, but this deficiency can be attributed to the small amount of $O(^1D)$ removal by N_2O and O_2. Of more significance is the fact that $-\Phi_i\{NO_2\} \sim 2.0$ even when $[NO_2] \sim 1$ mTorr and $I_a = 6.4$ mTorr/min. Thus under these conditions, reaction 2 is more important than reaction 6, which leads to the inequality

TABLE IV: Reaction of HO_2 with NO and NO_2

$[NO]_0/[NO_2]_0$	$[NO]_0$, mTorr	$[O_2]$, Torr	[CO], Torr	$R_i\{NO_2\}$, mTorr/min	$-R_m\{NO_2\}$, mTorr/min	$\Phi_i\{NO_2\}$
			$[NO_2] \sim 10$ mTorr[a]			
1.41	13.8	42	55	26.0	3.26	16.0
			$[NO_2] \sim 20$ mTorr[a]			
0.33	6.7	51	41	5.1	3.13	3.25
0.69	15.8	44	59	17.6	3.40	10.4
0.76	16.8	40	150	21.5	3.60	12.0
0.86	16.8	40	0	12.0	3.30	7.3
0.86	16.5	33	0	15.8	3.30	4.5
0.86	16.5	47	156	18.0	4.50	8.0
0.88	16.5	33	115	23.4	3.90	12.0
0.89	17.7	22	90	18.5	2.90	12.8
0.93	17.7	88	65	18.0	3.60	10.0
1.69	36.5	44	51	29.0	3.10	18.8
			$[NO_2] \sim 50$ mTorr[b]			
0.40	16.5	41	50	11.0	3.90	5.6
0.74	44	50	0	17.5	11.2	3.1
0.78	43.5	47	120	56	22.0	5.2
0.79	43.3	43	0	26.5	18.4	2.9
0.91	43	40	0	35.0	16.5	4.3
0.97	49	46	110	80	20.7	7.8
1.04	50	44	0	26.0	20.6	3.4

[a] $[N_2O] = 6.5 \pm 0.5$ Torr, $[H_2] = 700 \pm 50$ Torr. [b] $[N_2O] = 53 \pm 3$ Torr, $[H_2] = 700 \pm 50$ Torr.

$$k_2/k_6^{1/2} > 2I_a^{1/2}/[NO_2] = 11.4 \times 10^{-8} \text{ (cc/sec)}^{1/2} \quad \text{(a)}$$

With the average value of $k_6 = 6 \times 10^{-12}$ cc/sec found by Paukert and Johnston[5] and Hochanadel, *et al.*,[6] $k_2 > 3 \times 10^{-13}$ cc/sec.

Determination of k_2/k_1. In the presence of NO, the rate law for $\Phi_i\{NO_2\}$ becomes complex

$$\Phi_i\{NO_2\} = \left(\frac{\alpha - 1}{\alpha + 1} - \beta\right) \times \left(\frac{2\alpha + 1}{1 + (1 + \alpha)(\beta + \gamma)}\right) + \frac{\alpha - 1}{\alpha + 1} \quad \text{(b)}$$

where $\alpha \equiv k_1[NO]/k_2[NO_2]$, $\beta \equiv k_9[NO_2]/(k_4[H_2] + k_{11}[CO])$, and $\gamma \equiv k_{10}[NO]/(k_4[H_2] + k_{11}[CO])$. For sufficiently small values of β and γ the equation simplifies to

$$\Phi_i\{NO_2\} = 2(k_1[NO]/k_2[NO_2] - 1) \quad \text{(c)}$$

Equation c is convenient to use since it can give k_1/k_2 directly. The parameters β and γ can be reduced by reducing $[NO_2]$ and [NO], respectively, or by increasing $[H_2]$ or [CO]. The reason for using CO is because $k_{11} \gg k_4$. These parameters are sufficiently small when further increases in [CO] no longer raise $\Phi_i\{NO_2\}$. Our experiments in Table IV with $[NO_2]_0 \leq 23$ mTorr and $[CO] \geq 40$ Torr meet this requirement. For these experiments $\Phi_i\{NO_2\}$ is plotted *vs.* $[NO]/[NO_2]$ in Figure 4. The plot is linear and the slope gives $k_1/k_2 = 7 \pm 1$.

Now that k_1/k_2 has been obtained, the validity of eq c as an approximation can be computed from known rate constants. The ratio $k_{11}/k_4 = 20$.[7-9] For reaction 9 the rate coefficients cannot exceed the high-pressure limiting rate coefficients which give $k_{11}/k_9^{\infty} = 0.019$.[10] With 1 atm of H_2, the pseudo-second-order rate coefficient for reaction 10 is 6.0×10^{-12} cc/sec.[1] With $k_{11} = 1.35 \times 10^{-13}$ cc/sec,[7-9] $k_{10}/k_{11} = 45$. Thus for the conditions of $[H_2] = 700$ Torr, $[CO] \geq 40$ Torr, $[NO_2]_0 \leq 20$ mTorr, and $0.33 \leq [NO]_0/[NO_2]_0 \leq 1.69$, it is found that $\beta(1 + \alpha)/(1 - \alpha) \leq 0.031$ and $(1 + \alpha)(\beta + \alpha) < 0.39$. Consequently eq c approximates eq b to within 40% error even under the most unfavorable conditions. The largest two data points in Figure 4 should lie somewhat low, and indeed they do.

Thermal Decomposition of HONO. After the irradiation is terminated the HONO decomposes *via* reaction 7. Assuming that the HONO pressure, calculated as $2([NO_2]_\infty - [NO_2]_{ss})$, when the irradiation is interrupted is $0.70[NO_2]_0$ for $[NO_2]_0 \leq 150$ mTorr, as seems to be the case from Table I, we can estimate k_7 from the slope of a plot of $R_d\{NO_2\}$ *vs.* [HONO]. Figure 5 is a plot of $R_d\{NO_2\}$ *vs.* $[NO_2]_0$. The data are badly scattered, but can be fitted by a straight line of slope 0.02 min^{-1}. Thus $k_7 \sim 0.06$ min^{-1}, about a factor of 6 smaller than found by Gray, *et al.*[2] Both the first-order rate law and the different rate coefficients in the two studies confirm the heterogeneous nature of the reaction.

Acknowledgment. The authors wish to thank Professor Marcel Nicolet for his continuing interest and help. This work was supported by the Atmospheric Science Section of the National Science Foundation through Grant No. GA-12385, the National Aeronautics and Space Administration through Grant No. NGL-009-003, and the Climatic Impact Assessment Program, Office of the Secretary, Department of Transportation, for which we are grateful.

References and Notes

(1) R. Simonaitis and J. Heicklen, *J. Phys. Chem.*, **77**, 1096 (1973).
(2) D. Gray, E. Lissi, and J. Heicklen, *J. Phys. Chem.*, **76**, 1919 (1972).
(3) D. Garvin, National Bureau of Standards Report No. NBSIR-203 (1973).
(4) R. F. Hampson, National Bureau of Standards Report No. 10692 (1972).
(5) T. T. Paukert and H. S. Johnston, *J. Chem. Phys.*, **56**, 2824 (1972).
(6) C. J. Hochanadel, J. A. Ghormley, and P. J. Ogren, *J. Chem. Phys.*, **56**, 4426 (1972).
(7) N. R. Greiner, *J. Chem. Phys.*, **51**, 5049 (1969).
(8) F. Stuhl and H. Niki, *J. Chem. Phys.*, **57**, 3671 (1972).
(9) A. A. Westenberg and N. de Haas, *J. Chem. Phys.*, **58**, 4061 (1973).
(10) R. Simonaitis and J. Heicklen, *Int. J. Chem. Kinet.*, **4**, 529 (1972).

Pressure and Phase Dependence of the Stereochemical Course in Hot Tritium for Hydrogen and Chlorine-38 for Chlorine Substitution in *meso*- and *rac*-1,2-Dichloro-1,2-difluoroethane

H. -J. Machulla and G. Stöcklin*

Institut fur Nuklearchemie der Kernforschungsanlage, Jüliche Gmb.H, Jülich, West Germany *(Received March 20, 1973; Revised Manuscript Received January 14, 1974)*

Publication costs assisted by Kernforschungsanlage Jülich GmbH, FRG

The pressure dependence of the stereochemical course in hot homolytic T-for-H and ^{38}Cl-for-Cl substitution in *meso*- and *rac*-1,2-dichloro-1,2-difluoroethane has been studied from 10 to 10^4 Torr. Distinct differences are observed between the yield *vs.* density dependence of the retained and the inverted product. For both recoil tritium and chlorine, substitution with inversion of configuration is almost negligible in the gas phase and its yields remain constant over the entire pressure range studied. Typical pressure effects are observed, however, for substitution with retention of configuration, particularly for recoil chlorine. While the change from the high-pressure gas phase to the liquid leaves T-for-H substitution almost unaffected, ^{38}Cl-for-Cl substitution exhibits a strong phase effect. The absolute yields of the retained product increase by a factor of 2.5, that of the inverted product by about 20, almost identical in both diastereomeric substrates. The density dependence of the HCl and HF elimination products is also different for recoil tritium and chlorine; in the latter case the yields follow the increasing trend observed for substitution. While for recoil tritium the predominant substitution channel seems to be a direct replacement with retention of configuration, even in the liquid phase, ^{38}Cl-for-Cl substitution at higher densities cannot be satisfactorily explained on the basis of the impact model nor by caged radical combination. Alternatively, substitution *via* a caged complex is discussed.

Introduction

Hot homolytic substitution reactions by nucleogenic tritium and halogen atoms at asymmetric carbon atoms proceed predominantly with retention of configuration (for review *cf.* ref 1-3). Recent results of Rowland and coworkers on T-for-H[4,5] and halogen for halogen[7-10] substitution in diastereomeric haloalkanes showed that this is true for the gaseous and, to a lesser extent, also for the liquid phase. The somewhat smaller stereospecificity observed in the condensed phase has been generally ascribed to a contribution from radical-radical cage combination reactions, allowing racemization of the intermediate radical.

In a preceding paper[11] we have, however, demonstrated that ^{38}Cl-for-Cl substitution in liquid 2,3-dichlorobutane can be drastically influenced (from 35 to 85% retention) by various solvents, a result which could clearly be attributed to a conformational effect. This conformational effect provides evidence for a one-step substitution, which in the liquid phase can lead to both retention and inversion. It was therefore postulated that the hot substitution can proceed *via* two channels: (i) a direct replacement without a change in configuration, according to the Wolfgang impact model[3] and (ii) the formation of a longer lived complex, with lifetimes long enough to allow also inversion of configuration. While the direct reaction should be predominant at low pressures, complex formation, if it occurs at all, is most likely to be observed at high pressures and particularly in the liquid phase, because of collisional stabilization and prolonged collision times. It was also expected that the latter process should play a greater role for chlorine than for tritium due to orbital overlap. In order to obtain further evidence for this hypothesis, it was necessary to carry out extensive gas-phase studies on the pressure dependence of the stereochemical course of hot substitution reactions by both recoil tritium and chlorine.

Experimental Section

Sample Preparation and Irradiation. A diastereomeric mixture of 1,2-dichloro-1,2-difluoroethane, $(CHClF)_2$, was obtained from Peninsular Chemical Research (PCR) Inc. The mixture was first prepurified by gas chromatography without separation of the diastereomers, using a 4-m column (8 mm i.d.) with 20% Igepal CO-880 on Chromosorb A 60/80 mesh at 60° and 120 cc/min. The prepurified samples were then separated by glc into the meso and racemic forms, using a 14-m column (8 mm i.d.) with 30% Igepal CO-880 on Chromosorb P-NAW 60/80 mesh at 85° and 200 cc/min. The boiling points of the purified diastereomers are 59.4° for the meso and 59.9° for the racemic form.

For the *in situ* production of recoil ^{38}Cl ($T_{1/2}$ = 37.3 min) the ^{37}Cl(n,γ)^{38}Cl process was used. Neutron irradiations were carried out in a thermal column facility of the FRJ-1 at a thermal neutron flux density of 1.6×10^{10} cm^{-2} sec^{-1} for a period of 120 min. The irradiation temperature was adjusted with a heating cartridge as required up to 260°, and measured by a thermocouple. The accompanying γ-exposure rate was about 10^4 R/hr.

For the irradiations in the gaseous phase, weighed amounts (corresponding to the required vapor pressure during irradiation) of *meso*- or *rac*-$(CHClF)_2$, containing 1 mol % I_2 as scavenger were placed in quartz ampoules of about 1 to 170 ml (1 to 5 cm i.d.), depending on the pressure. They were outgassed on a vacuum line by freezing and melting cycles and then sealed. Liquid samples were prepared and irradiated as described before.[11]

In the case of tritium, the $^3He(n,p)T$ process was used for the gas-phase studies, and about 10 mol % of ^3He was added to the substrate vapor. In the liquid phase the $^6Li(n,\alpha)T$ process was applied for the *in situ* production of recoil tritium, and the samples contained about 10 mg of LiF in 100-μl substrate. About 1 mol % of I_2 scavenger was added to all samples, which were prepared by vacuum techniques and irradiated under conditions described above.

Radioanalytical Procedure. In the case of ^{38}Cl, the irradiated gaseous samples were condensed into the tip of the ampoule, and 5 ml of a 1:1 mixture of an aqueous Na_2SO_3-Na_2CO_3 solution (10%) was added. The organic products were extracted with 1 ml of carrier containing CH_2Cl_2. The small liquid samples were crushed directly under the surface of the extraction mixture. After washing, aliquots of the phases were submitted to radioactivity determination and, in the case of the organic phase, to a radio gas chromatographic analysis. The relatively low ^{38}Cl activity made it necessary to use a discontinuous technique,[12] adsorbing the individual eluated products on charcoal tubes, which were then submitted to radioactivity measurement.[11]

In the case of tritium, samples were stored for several days at −30° to allow decay of short-lived radioactivities. The ampoules were then attached to a vacuum line, immersed into liquid nitrogen, and opened *via* break seal. The gaseous activity (HT) was then removed with H_2 carrier and counted separately in an internal proportional gas counter. After adding carriers to the condensable products, aliquots were submitted to activity determination by liquid scintillation counting and to radio gas chromatography. Again, a discontinuous procedure was used, collecting the individual products in traps containing toluene scintillator solutions, which were then submitted to liquid scintillation counting. Product yields are given in per cent of total induced ^{38}Cl or T activity, respectively (radiochemical yield).

Gas chromatographic separation of the diastereomeric labeled products was achieved by using a 12-m column (5 mm i.d.) with 30% Igepal CO-880 on Chromosorb P-AW 60/80 mesh at temperatures between 20 and 115° and a flow of 100 cc/min. The basic experimental details have been published elsewhere.[13,14] The sequence of net retention times for the compounds of interest was *cis*-ClFC=CFH (18.8 min), *trans*-ClFC=CFH (19.7 min), *cis*-ClFC=CClH (36.2 min), *trans*-ClFC=CClH (38.2 min), *meso*-$(CHClF)_2$ (76 min), and *rac*-$(CHClF)_2$ (104 min). The temperature program used was as follows: from 20° with 2°/min up to 50°, 10 min at 50°, with 10°/min to 105°, after passage of *rac*-$(CHClF)_2$ with 30°/min to 190°.

Results

Pressure and Phase Dependence of Characteristic Product Yields in the ^{38}Cl-rac-$(CHClF)_2$ System. The product yields of interest, arising from ^{38}Cl-for-halogen substitution and from concomitant HF or HCl elimination, have been determined as a function of total substrate pressure ranging from about 50 to 10^4 Torr. The total inorganic yield ($H^{38}Cl$, $^{38}ClCl$, and ^{38}ClF) was also measured. The sum of other undetected and unidentified organic product yields, including those from ^{38}Cl-for-H substitution, was calculated from the activity balance. The wide pressure range could only be achieved by also changing the temperature during irradiation from about 25 to 260°. It was shown by constant pressure experiments at 150 Torr that

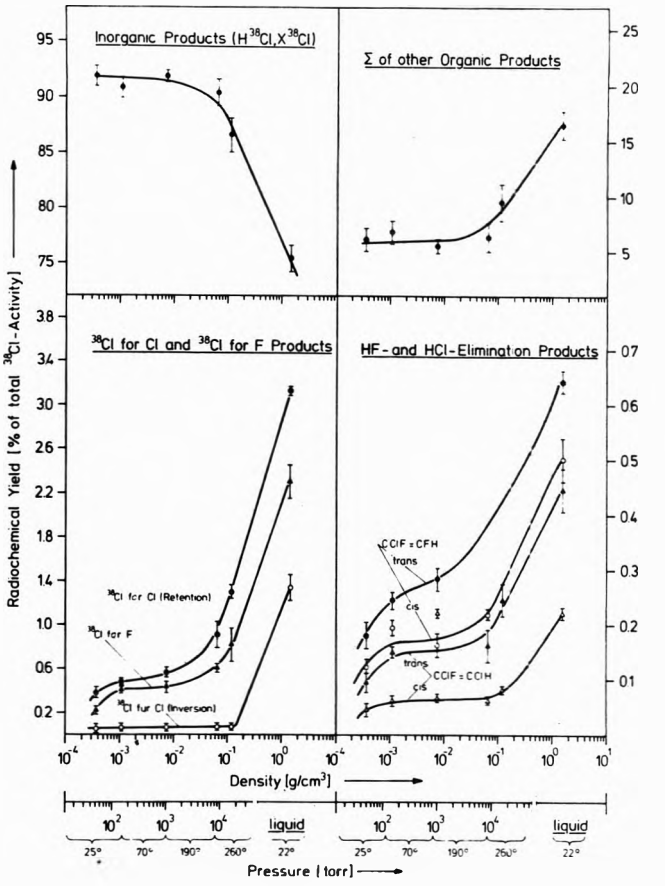

Figure 1. Pressure and phase dependence of characteristic product yields from the reaction of hot ^{38}Cl with *rac*-$(CHClF)_2$. Sum of other organic products (upper right) has been calculated from the activity balance. The HCl elimination product yields have been multiplied by a factor of 2, assuming an equal chance for radioactive and inactive HCl elimination.

in the I_2-scavenged system the product yields and the stereochemical course is not affected by these temperature changes within the experimental error; *e.g.*, for *rac*-$(CHClF)_2$ we obtained at 70° the following radiochemical yields: 0.06 ± 0.01 for *meso*-$(CHClF)_2$ and 0.48 ± 0.03 for *rac*-$(CHClF)_2$, *i.e.*, a ratio retention/inversion of 8.5 ± 1.9.

At 260° we obtained 0.06 ± 0.01 for *meso*-$(CHClF)_2$ and 0.39 ± 0.04 for *rac*-$(CHClF)_2$, *i.e.*, a ratio retention/inversion of 6.7 ± 1.9.

The results of the pressure dependence of the radiochemical product yields including those from the liquid phase are shown in Figure 1. The corresponding densities and the temperatures applied are also given. It can be seen that both the ^{38}Cl-for-halogen substitution and the elimination product yields (lower part of Figure 1) show a qualitatively similar pressure dependence with a point of inflection at about 10^3 Torr, resembling to some extent the density curves obtained by Richardson and Wolfgang[16] for the substitution reactions of ^{18}F in CH_3F. Except for the ^{38}Cl-for-Cl substitution with inversion, the yields of these products increase up to about 10^2 Torr, then level off until about 10^3 Torr. Above 10^3 Torr they slowly start increasing again, finally (at about 10^4 Torr) showing a drastic almost linear increase up to the liquid phase. In contrast to the product with retention of configuration, which shows the typical pressure dependence, the small yield of the inverted product remains constant over

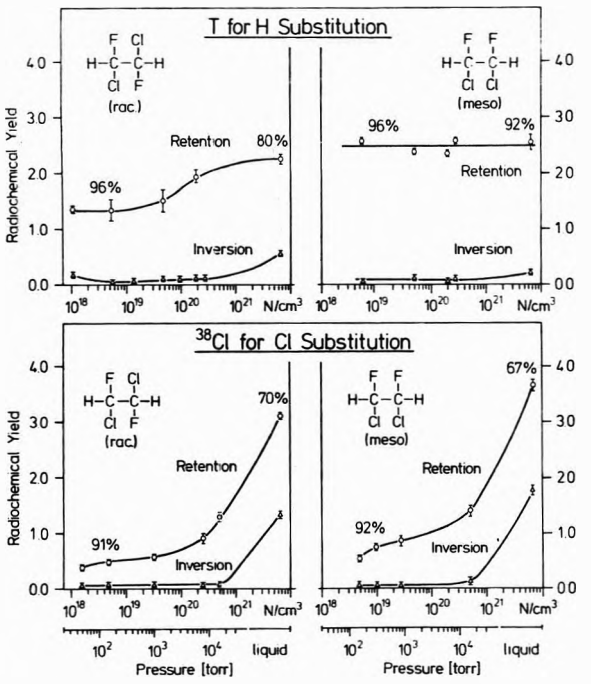

Figure 2. Comparison of pressure and phase dependence of hot T-for-H and ^{38}Cl-for-Cl substitution yields in *rac-* and *meso-*$(CHClF)_2$. For temperatures *cf.* Figure 1.

the entire pressure range, and the jump to higher yields only occurs when going to the liquid phase.

It is also noteworthy to point out that the elimination products do not show the pressure dependence expected for products arising from unimolecular excitation decomposition processes, namely, a decreasing yield with increasing pressure, but instead exhibit a generally increasing trend, typically observed for hot substitution products. Finally, the inorganic yield (upper part of Figure 1) is shown to decrease below about 10^3 Torr, and a concomitant increase is observed for the other, mostly unidentified organic products.

Comparison of Pressure and Phase Dependence of T-for-H and ^{38}Cl-for-Cl Substitution Yields in rac- and meso-$(CHClF)_2$. In Figure 2 we have compared the pressure and phase dependence of the T-for-H and ^{38}Cl-for-Cl substitution yields in both *rac-* and *meso-*$(CHClF)_2$. In addition to the pressure scale the corresponding densities in molecules per cm^3 are also given. From the lower part of Figure 2 it can be seen that ^{38}Cl-for-Cl substitution shows an almost identical pressure and phase dependence in both diastereomeric substrates, exhibiting the trends described above, *i.e.*, pressure *and* phase effect for the retained, and a phase effect only for the inverted product yields. The stereochemical course changes from 91 and 92% at about 150 Torr to 70 and 67% retention in the liquid phase for *meso-* and *rac-*$(CHClF)_2$, respectively.

It is also significant that the density effects, particularly the gas to liquid phase effects on the ^{38}Cl-for-Cl substitution yields, are almost identical in both diastereomeric substrates.

A completely different picture is obtained in T-for-H substitution. Neither a pressure nor a significant phase effect is observed in the *meso-*$(CHClF)_2$ system, and only small changes can be found in *rac-*$(CHClF)_2$, *i.e.*, an increase in the retained substitution product yield above about 10^3 Torr, leveling off before the liquid phase is reached, while the inverted product remains practically

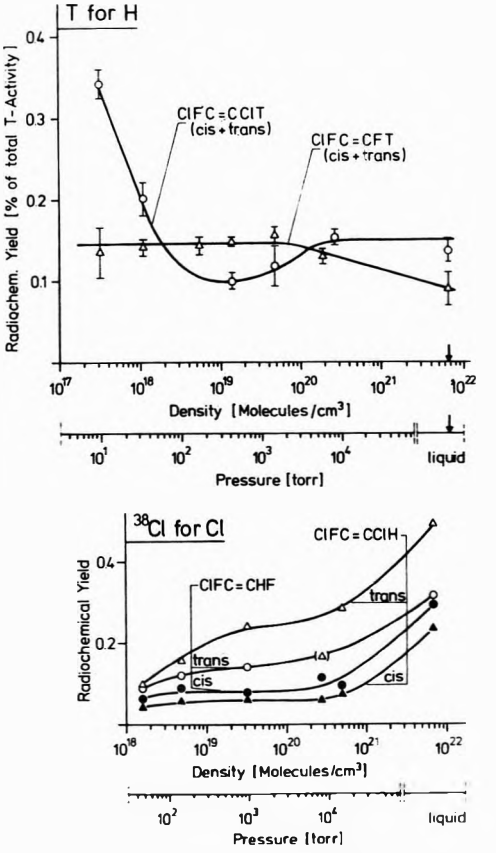

Figure 3. Pressure and phase dependence of HCl and HF elimination product yields accompanying hot T-for-H and ^{38}Cl-for-Cl replacement, respectively, in *rac-*$(CHClF)_2$. For temperatures *cf.* Figure 1.

unaffected over the entire pressure range and only slightly increases when going to the liquid phase. The stereochemical course also shows only small changes from 96% retention at about 150 Torr to 92 and 80% in the liquid phase for *meso-* and *rac-*$(CHClF)_2$, respectively. In contrast to ^{38}Cl-for-Cl substitution an almost complete lack of pressure and phase effects seems to be characteristic for T-for-H substitution. It should be pointed out that the stereochemical course observed in the gaseous and liquid systems agree within the experimental error with those reported by Palino and Rowland[5] for a corresponding density.[6]

Pressure Dependence of HCl and HF Elimination Product Yields. The pressure dependence of the HF and HCl product yields in the T-*rac-*$(CHClF)_2$ system is shown in Figure 3. For comparison the corresponding elimination product yields are also shown for the ^{38}Cl-*rac-*$(CHClF)_2$ system (lower part of Figure 3), as taken from Figure 1. In the case of recoil tritium, HCl and HF elimination, following T-for-H substitution, exhibit a different pressure dependence. The HF elimination product yields first decrease with increasing pressure, then go through a minimum at about 5×10^3 Torr, and finally level off above about 10^4 Torr. The HCl elimination product yields, on the other hand, remain practically constant over the entire pressure range and only show a slight decrease when going to the liquid phase.

Even though the experimental errors for these small yields are quite large (*cf.* Figure 3), it is evident that the elimination products in the recoil tritium case exhibit a completely different pressure dependence than the corresponding products in the recoil chlorine system. HCl and

HF elimination following ^{38}Cl-for-Cl substitution shows a generally increasing trend (lower part of Figure 3), similar to that of the substitution products.

Discussion

Lack of Pressure Effect on Inversion Product Yields. Even though there are obvious marked differences between recoil chlorine and tritium with respect to the pressure and phase dependence for both the substitution and elimination products, there is one important common aspect which should be discussed first. For both recoil tritium and chlorine, substitution with inversion of configuration is almost negligible in the gas phase. While this fact has been demonstrated before by Rowland and coworkers[7-10] at low pressure, it is now interesting to see that this is true for a wide pressure range from about 10 to 10^4 Torr. This finding demonstrates that the almost complete lack of inversion in the gas phase cannot be due to enhanced excitation decomposition. It had been previously pointed out[8] that substitution with inversion might deposit much vibrational energy in the substituted product that the molecules formed will undergo secondary decomposition within about 10^{-10} sec. It can be seen from Figure 2 that an increase of the inverted substitution product yield is only observed when going to the liquid phase, particularly in the case of recoil chlorine. The fact that inversion remains negligibly small and constant over the entire pressure range for both recoil tritium and chlorine indicates that the formation of a complex with lifetimes long enough to allow configurational changes does not take place in the *gas phase* for either tritium or chlorine.

On the other hand, substitution yields in the gaseous phase are generally small and more than 90% of the recoil atoms end up in inorganic form as shown in Figure 1 for recoil chlorine. In the case of recoil chlorine the system is self-scavenging due to fast hydrogen abstraction,[11,14] and those chlorine atoms which have not succeeded in organic bond formation eventually form $H^{38}Cl$, since hydrogen abstraction is the only fast reaction for thermalized chlorine atoms with the substrate. The question remains, why does the organic product yield increase so drastically when going to the liquid phase?

The Gas to Liquid Phase Effect. One is tempted to attribute the sudden increase in substitution yields and the concomitant decrease in stereospecificity accompanying the gas to liquid phase change to cage effects, which would affect chlorine but not so much the smaller tritium atoms,[15] as seems to be indicated by Figure 2. A similar density effect has been observed by Richardson and Wolfgang[16] for the ^{18}F substitution yields in CH_3F. They also found a second stronger rise in yield above the critical density of about 4×10^{21} molecules/cm^3, which they explained on the basis of Franck-Rabinowitsch caging,[17] a central concept in condensed-phase hot atom chemistry.[18-20] Fluorine atoms, however, rapidly abstract hydrogen from the substrate molecules and caging is not expected to play a major role. Another explanation of the enhanced substitution yields at higher densities would be the concept of a caged complex, *i.e.*, an electronically unstable intermediate, which is held together by the surrounding solvent molecules for a time sufficient for configurational changes to occur.

In preceding papers[11,14] we have already pointed out that cage recombination in recoil chlorine–alkyl halide systems is not likely to contribute significantly to the substitution yield, since hydrogen abstraction by thermal chlorine atoms is a fast process with an activation energy of only about 1 kcal/mol, which competes strongly with radical combination. Experimental evidence against a substantial contribution from cage combination was obtained by the lack of mass, temperature, and viscosity effects and, most important, by the observation of a conformational effect, which is indicative for a hot one-step reaction.[11,14]

Further information is now obtained from the phase effect in *rac*- and *meso*-$(CHClF)_2$. If the increase in the ^{38}Cl-for-Cl substitution yield accompanying the gas to liquid phase change (*cf.* Figure 2) would be due to cage recombination between $^{38}Cl\cdot$ atoms and $\cdot CHF\text{-}CHClF$ radicals, both diastereomeric product yields would increase, depending on the thermodynamical or kinetic control of racemization and recombination, respectively. If recombination occurs faster or on a time scale comparable to the time required for racemization, the product will predominantly retain the original configuration. If, on the other hand, racemization reaches its equilibrium, both diastereomers are formed, depending on thermodynamic and/or on steric factors. These latter effects should be negligible in view of the fact that the stereochemical course of the substitution and its density and phase dependence is almost identical in both diastereomeric substrates, *rac*- and *meso*-$(CHClF)_2$. The other case, in which recombination would occur with predominant retention, cannot completely be ruled out. Even though the absolute yield of the retained substitution product increases only by a factor of about 2.5 as compared to roughly 20 for the inverted product, when going from the high-pressure gas (about 10^4 Torr) to the liquid phase in both systems, the incremental increase for the extra material found in the liquid phase is slightly higher for the retained than for the inverted substitution product (namely, 2.3 as compared to 1.5 in the meso and 1.8 as compared to 1.3 in the *rac*-$(CHClF)_2$ system). It should be noted, however, that the yield increase of the retained form already starts in the high-pressure range of the gas phase, and then simply continues to increase almost linearly with increasing density, while a significant inversion is only observed in the liquid phase (*cf.* lower part of Figure 2). The almost linear increase in the yield of the retained product at higher densities can also be interpreted by predominant collisional stabilization of excited product molecules, while the appearance of a significant inversion is only connected with the gas to liquid phase change. Even though the results do not provide conclusive evidence for the absence of caged radical combinations, they suggest that caging does not play a major role in the case of recoil chlorine, particularly in view of our previous results on the conformational effect mentioned above.

Mechanism of Substitution. Hot substitution in the gas phase is generally described as a direct replacement caused by a translationally hot atom $[\cdot Y]^{\ddagger}$

$$[\cdot Y]^{\ddagger} + RX \longrightarrow [RY]^{*} + X\cdot \qquad (1)$$

On the basis of the impact model this reaction should proceed with retention of configuration. The excited product molecule [RY]* can either decompose or become collisionally deexcited

$$[RY]^{*} \xrightarrow{M} RY + X \qquad (2)$$
$$[RY]^{*} \longrightarrow \text{decomposition products, } e.g., \text{ elimination}$$

The excited molecules are known to have a wide spectrum of lifetimes, ranging from 10^{-13} to 10^{-8} sec (for review *cf.* ref 1-3), and can thus already become stabilized in the gas phase over a wide pressure range. This is reflected in Figure 2 by the increase observed for the retained substitution products in the pressure range from about 10^2 to 10^4 Torr. It remains open to question as to why this is not observed for recoil tritium in the *meso*-$(CHClF)_2$ system. The absolute yields in the meso system are generally somewhat higher than those in *rac*-$(CHClF)_2$, and this may be due to the greater stability of the meso form. However, it is not apparent why this is much less pronounced for recoil chlorine than for recoil tritium.

The different density dependence of the retained and the inverted ^{38}Cl-for-Cl substitution yields suggests that in addition to the direct reaction another substitution mechanism must be operative. This channel seems to predominate in the liquid phase. On the basis of the results presented in the preceding sections, we feel that caged radical combination cannot substantially contribute to the product formation in this system. Even though there is no unambiguous evidence for this statement, the present results necessitate the consideration of another substitution mechanism.

At higher densities particularly in the liquid phase the collision times are longer. The tightly packed molecules are kept together and the time of interaction is prolonged. For thermal collision partners typical collision times are about a factor of 100 greater than at normal pressures in the gas phase.[21] In addition, solvation and efficient energy transfer may promote hot radical-molecule interactions, which cannot occur in isolated gas-phase collisions. The formation of a pentacoordinate carbon complex with lifetimes considerably longer than 10^{-14} sec seems unlikely, however, since there is no definitive evidence for local potential energy minima of neutral five-bonded carbon intermediates. On the other hand, the "caged complex," which would explain the experimental results, is to be distinguished from caged radical recombination, by the number of radicals in the solvent cage. In caged recombination, which may lead to racemization, there are at least two, which have to recombine, while in the "caged complex" mechanism there is only one, namely, the (perhaps electronically unstable) adduct formed from the hot atom and substrate molecule. In the latter mechanism, substitution processes leading both to retention and inversion of configuration would occur concomitantly, but racemization *via* a planar radical would not be possible.

The Elimination Products. From the great variety of possible decomposition products, only those arising from HF and HCl elimination have been determined, since their pressure dependence can provide additional information on whether they arise from unimolecular excitation decomposition (eq 2) or *via* complex formation. It can be seen from Figure 3 that in the case of recoil tritium the origin of the elimination products seems to be excitation decomposition, even though the observed pressure dependence is not typical. For recoil chlorine, on the other hand, the pressure dependence of the elimination products clearly reflects that of the substitution products (*cf.* Figures 1 and 3). Hence, these elimination products should not be formed *via* the direct reaction with subsequent excitation decomposition (*cf.* eq 1 and 2), but rather by a process which is expected to be favored with increasing pressure as an alternative channel to substitution.

Conclusion

In gaseous *rac*- and *meso*-$(CHClF)_2$ both T-for-H and Cl-for-Cl substitution proceeds predominantly *via* a direct replacement even at high pressures with almost complete retention of configuration, possibly according to the impact model. In the case of recoil tritium this seems to be the dominating process even in the liquid phase. For recoil chlorine, however, hot ^{38}Cl-for-Cl substitution in the liquid phase cannot be satisfactorily explained by the impact model nor by radical combination but rather by a nondirect process, possibly a caged intermediate the lifetime of which is effectively prolonged by the surrounding molecules.

Acknowledgment. The authors are indebted to Drs. J. T. Muckerman, M. D. Newton, and A. P. Wolf for stimulating discussions and valuable suggestions. They also wish to thank Mr. M. Schüller for experimental assistance.

Supplementary Material Available. The tables corresponding to Figures 1-3 will appear following these pages in the microfilm edition of this volume of the journal. Photocopies of the supplementary material from this paper only or microfiche (105 × 148 mm, 24× reduction, negatives) containing all of the supplementary material for the papers in this issue may be obtained from the Journals Department, American Chemical Society, 1155 16th St., N.W., Washington, D. C. 20036. Remit check or money order for $3.00 for photocopy or $2.00 for microfiche, referring to code number JPC-74-658.

References and Notes

(1) A. P. Wolf, *Advan. Phys. Org. Chem.*, **2**, 201 (1964).
(2) R. Wolfgang, *Progr. React. Kinet.*, **3**, 97 (1965).
(3) G. Stöcklin, "Chemie heisser Atome," Verlag Chemie, Weinheim, Germany, 1969.
(4) Yi-N. Tang, C. T. Ting, and F. S. Rowland, *J. Phys. Chem.*, **74**, 675 (1970).
(5) G. F. Palino and F. S. Rowland, *J. Phys. Chem.*, **75**, 1299 (1971).
(6) See paragraph at end of paper regarding supplementary material.
(7) C. M. Wai, C. T. Ting, and F. S. Rowland, *J. Amer. Chem. Soc.*, **86**, 2525 (1964).
(8) C. M. Wai and F. S. Rowland, *J. Phys. Chem.*, **71**, 2752 (1967).
(9) C. M. Wai and F. S. Rowland, *J. Phys. Chem.*, **74**, 434 (1970).
(10) G. F. Palino and F. S. Rowland, *Radiochim. Acta*, **15**, 57 (1971).
(11) L. Vasáros, H. -J. Machulla, and G. Stöcklin, *J. Phys. Chem.*, **76**, 501 (1972).
(12) G. Stöcklin and W. Tornau, *Radiochim. Acta*, **6**, 86 (1966); **9**, 95 (1968).
(13) L. Vasáros, H. -J. Machulla, and W. Tornau, *J. Chromatogr.*, **62**, 458 (1971).
(14) H. -J. Machulla, Report JÜL-873-NC (1972).
(15) The effect of solute size on the magnitude of caging has recently been discussed by D. L. Bunker and B. S. Jacobson, *J. Amer. Chem. Soc.*, **94**, 1843 (1972).
(16) A. E. Richardson and R. Wolfgang, *J. Amer. Chem. Soc.*, **92**, 3480 (1970).
(17) J. Franck and E. Rabinowitsch, *Trans. Faraday Soc.*, **30**, 120 (1934).
(18) C. Lu and S. Sugden, *J. Chem. Soc.*, 1273 (1939).
(19) W. F. Libby, *J. Amer. Chem. Soc.*, **62**, 1930 (1940).
(20) J. E. Willard, *Annu. Rev. Phys. Chem.*, **6**, 141 (1955).
(21) S. W. Benson, "The Foundation of Chemical Kinetics," McGraw-Hill, New York, N. Y., 1960, p 494.

Determination of Branching Ratios for the Reaction of Oxygen Atoms with Ethylene

Frank J. Pruss, Jr., Irene R. Slagle, and David Gutman*

Department of Chemistry, Illinois Institute of Technology, Chicago, Illinois 60616 *(Received August 20, 1973)*

Publication costs assisted by the National Science Foundation and the Petroleum Research Fund

The absolute specific rate of ketene production in the reaction O + C_2H_4 has been measured using a fast-flow reactor coupled to a photoionization mass spectrometer. The rate constant at 300°K for the reaction O + C_2H_4 → H_2C_2O + H_2 was determined to be 3.81 ± 0.95 × 10^{-14} cc molecule^{-1} sec^{-1}. Branching ratios for the reaction O + C_2H_4 at 300°K were calculated from the results of this study and other studies, and they are O + C_2H_4 → CH_3 + HCO (0.95) and O + C_2H_4 → H_2C_2O + H_2 (0.05).

Introduction

Direct observations of the products produced by the reactions of O atoms with olefins have revealed that each of these highly exothermic reactions proceeds *via* more than one reactive channel.[1,2] Since these elementary reactions are important steps in many thermal and photochemical oxidation systems, knowledge of their branching ratios is essential to achieve successful kinetic modeling of the complex reactive systems in which they are involved. We have undertaken to measure these ratios, and we report here the results obtained for the O + C_2H_4 reaction at 300°K.

Investigations to identify the reactive channels of the O + C_2H_4 reaction began with Cvetanović's study of the identity and amounts of stable products produced by the O + C_2H_4 reaction.[3] Cvetanović concluded that this reaction proceeds by at least two routes

$$\mathrm{O} + \mathrm{C_2H_4} \xrightarrow{k} \begin{cases} \xrightarrow{k_1} \mathrm{CH_3} + \mathrm{HCO} & (1) \\ \xrightarrow{k_2} \mathrm{H_2C_2O} + \mathrm{H_2} & (2) \end{cases}$$

with route 1 accounting for the majority of the overall reaction and route 2 about 4% of the total reaction rate. Four other minor routes were suggested as likely. Indirect evidence from later flow reactor studies of the O + C_2H_4 reaction has supported route 1 as a major one.[4,5] Recently Kanofsky and Gutman studied the O + C_2H_4 reaction in high-intensity room-temperature crossed molecular beams and directly observed the products CH_3, HCO, and H_2C_2O with a photoionization mass spectrometer. They concluded that the reaction proceeds by routes 1 and 2 (H_2 was not observable by their detection method).[1] Their failure to observe other detectable products, particularly CH_2, H_3C_2O, and H_4C_2O, led them to further conclude that the two observed routes are the only significant ones for the O + C_2H_4 reaction at room temperature.[1,2]

The determination of the branching ratios for the O + C_2H_4 reaction reported here essentially consisted of measuring k_2 and k. Since the overall rate constant $k = k_1 + k_2$, k_1 may be calculated (the presumption is made that routes 1 and 2 are the only significant ones). The branching ratios, $R_2 = k_2/k$ and $R_1 = (1 - R_2)$, were then calculated.

Experimental Section

The rate constant k_2 was determined by mixing O and C_2H_4 in a conventional fast-flow reactor and monitoring the absolute rate of H_2C_2O formation. Initial concentrations of O and C_2H_4 were chosen to be so low that their concentrations were negligibly depleted during their flow time through the reactor. Under these conditions stable products such as H_2C_2O (ketene) are produced at a constant rate and their concentrations grow linearly with time.

The fast-flow reactor used is one with a movable central inlet tube and is essentially identical with one described in detail by Niki, Daby, and Weinstock.[4] A small leak in the end of the reactor allows gas from the reactor to flow directly into the ion source of a quadrupole mass spectrometer. Extensive details of the experimental arrangement are to be published elsewhere.[6] Ions are produced in the ion source by photoionization using rare-gas resonance lamps.[1] Ketene and C_2H_4 were monitored with a hydrogen lamp producing primarily the 10.2-eV Lyman-α line. Oxygen atoms were ionized with a windowless lamp containing neon, which emits mainly the 16.67- and 16.85-eV resonance lines of neon.

The absolute sensitivity of the mass filter to ketene was established by metering known flows of this gas into the main carrier gas, which was helium in all the experiments. Ketene was produced by the pyrolysis of diketene[7] and collected in a Dry-Ice cooled trap. Very volatile impurities such as CO_2 were removed by pumping on the cooled trap for several hours. One remaining impurity, allene, was not removable. Its mole fraction in the ketene vapor was accurately determined and the total metered flow was corrected to remove the contribution due to allene. When not in use the ketene was stored at liquid N_2 temperature. Each day the volatile impurities were pumped away and the allene mole fraction redetermined.

Oxygen atoms were produced by adding small amounts of a 1.0%-O_2-in-helium gas mixture to the helium carrier gas flowing through a microwave discharge. Just before flowing through the discharge, the gas passed through a trap cooled to liquid N_2 temperature to remove water and hydrocarbons capable of producing H atoms in the discharge. The O atom concentration was determined by overtitrating with NO_2 and measuring the absolute amount of NO produced. Flow rates of NO, NO_2, and C_2H_4 were determined by routing these gases to a known volume and measuring the rate of pressure rise. Other flows were measured with calibrated rotameters.

In a typical experiment the H_2C_2O ion signal was measured at various positions of the movable inlet, which introduced C_2H_4 into the flow containing O atoms. The ab-

solute sensitivity of the mass spectrometer to H_2C_2O was determined before each run. Four experiments were performed which covered a threefold change in O-atom concentration and a twofold change in C_2H_4 concentration. The data obtained from these four experiments are displayed in Figure 1.

Results

Since both O and C_2H_4 were in essentially constant concentration during their transit time through the flow reactor, the net rate of ketene production is given by

$$\Delta[H_2C_2O]/\Delta t = k_2[O][C_2H_4] \quad (I)$$

since ketene is not significantly consumed in the flow reactor. At the low O-atom concentrations used in this study a negligible fraction (less than 5%) of the ketene is consumed by the relatively slow O + H_2C_2O reaction.[8] Also the very low steady-state concentrations of CH_3 and HCO in the flow reactor (1×10^{10} to 3×10^{10} radicals/cm^3)[5,9] are too low to deplete the ketene concentration even if the rate constants for their reactions with ketene are near the collision rate. The constant rate of ketene production, $\Delta[H_2C_2O]/\Delta t$, for each experiment was obtained from the slope of the least-squares-fitted line drawn through the data points from that experiment shown in Figure 1. The concentrations of O and C_2H_4 were determined from known flow rates, the titrations, and measurements of the pressure in the flow tube. In each experiment the pressure was 1.40 Torr, the flow velocity 12.8 m/sec, and the temperature 300°K. The gas composition was always 99.85% He and nearly 0.15% O_2.

The results for all four runs are given in Table I. Three of the experiments are in close agreement. The fourth is the one with the lowest rate of ketene production. In this last experiment the ketene signals were poorest, yielding a significant uncertainty in the slope, $\Delta(H_2C_2O)/\Delta t$. The experiment, however, was included because it appreciably extends the range of conditions over which this slope was measured. The average value for k_2 determined from the four runs together with the standard deviation is $k_2 = 3.81 \pm 0.76 \times 10^{-14}$ cm^3 $molecule^{-1}$ sec^{-1}. The accuracy of k_2 is estimated to be ±25% (*i.e.*, $\pm 0.95 \times 10^{-14}$) based on the accuracy of flow and pressure measurements and on the scatter of the experimental data points.

An additional experiment was performed in which O atoms were generated by passing N_2 through the discharge and titrating the N atoms with NO to yield O atoms by the reaction N + NO → N_2 + O. The specific rate of ketene production was the same in this experiment as in those in which O atoms were produced by discharging O_2. This result precludes the possibility that ketene production is affected by the presence of O_2 or $C_2(^1\Delta_g)$ (which are present when O_2 is passed through a microwave discharge but absent when N_2 is passed through and NO subsequently added).

Discussion

To calculate the branching ratios for the O + C_2H_4 reaction, a value for k, the overall rate constant for the O + C_2H_4 reaction, is needed. Using the same flow reactor, gas handling equipment, and monitoring techniques k was measured using three different sets of flow conditions. The details of these experiments are published elsewhere.[6] The result obtained was $k = 7.7 \times 10^{-13}$ cm^3 $molecule^{-1}$ sec^{-1} at 300°K. This result is very close to a recently recommended consensus value for k at 298°K, 8.44×10^{-13} cm^3 $molecule^{-1}$ sec^{-1}.[10] Using our value for k to calculate R_2 and R_1, the values are $R_2 = 0.05$ and $R_1 = 0.95$.

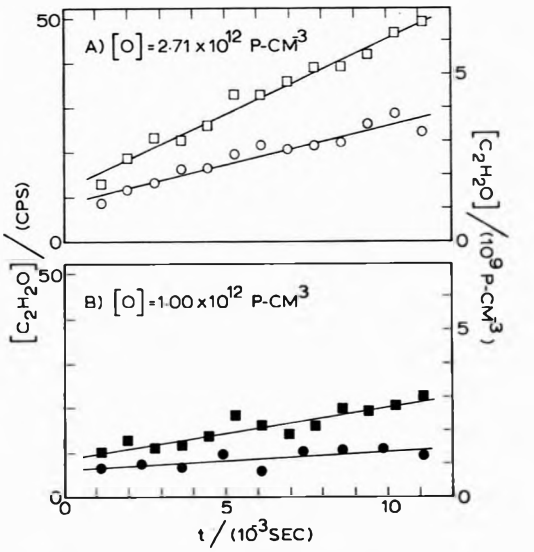

Figure 1. Plot of ketene ion signal and concentration *vs.* time for the four experiments listed in Table I: (a) two experiments in which [O] = 2.71×10^{12} atoms cc^{-1}; (b) two experiments in which [O] = 1.00×10^{12} atoms cc^{-1}.

TABLE I: Reaction Conditions and Results of Flow Reactor Experiments

[O] × 10^{-12}, atoms cc^{-1}	[C_2H_4] × 10^{-12}, molecules cc^{-1}	$k_2 \times 10^{14}$, cc $molecule^{-1}$ sec^{-1}
2.71	4.11	4.30
2.71	2.03	4.50
1.00	4.16	3.81
1.00	2.06	2.80

The branching ratio R_2 is in good agreement with the value 0.04 suggested by Cvetanović, whose result is based on a rather extended set of inferences (ketene was not actually detected), none of which, however, involves knowledge of the identity or importance of the other reaction channels.[11] The branching ratio $R_1 = 0.95$ is higher than the value 0.75 reported by Cvetanović solely because he presumed the presence of other reactive channels. There is nevertheless agreement that route 1 accounts for most of the overall reaction.

In the crossed-beam study of the O + C_2H_4 reaction by Kanofsky and Gutman,[1] the ketene mass peak is nearly as high as that for the major products CH_3 and HCO, which gives the "appearance" that route 2 is a major one. We have measured the relative sensitivity for the detection of CH_3 and H_2C_2O at 10.2 eV to determine whether the inordinately high ketene peak was caused by a large difference in detection efficiency for these two products. At 10.2 eV the ketene sensitivity is twice that for CH_3 under the conditions of the crossed-beam study. Thus, the relatively high ketene peak seen in Figure 1 of ref 1 is due to another cause, possibly to the different kinematics of the two reactive channels. The scattering of ketene from route 2 could possibly be more favorable along the direction of the O atom beam, where products were detected. In such crossed-beam studies with fixed-angle detectors, caution must therefore be used in associating peak heights of products with the relative importance of the respective reactive channels.

Acknowledgments. The authors gratefully acknowledge the support for this research from the Donors of the Petro-

leum Research Fund, administered by the American Chemical Society, and from the National Science Foundation. One of us (F. J. P.) thanks the National Science Foundation for support in the summer 1972 under the NSF Undergraduate Research Participation Program.

References and Notes

(1) J. R. Kanofsky and D. Gutman, *Chem. Phys. Lett.*, **15**, 236 (1972).
(2) J. R. Kanofsky, D. Lucas, and D. Gutman, *Symp. (Int.) Combust., [Proc.], 14th, 1972*, 285 (1973).
(3) R. J. Cvetanović, *J. Chem. Phys.*, **23**, 1375 (1955).
(4) H. Niki, E. E. Daby, and B. Weinstock, *Symp. (Int.) Combust., [Proc.], 12th, 1968*, 277 (1969).
(5) J. M. Brown and B. A. Thrush, *Trans. Faraday Soc.*, **63**, 630 (1967).
(6) I. R. Slagle, F. Pruss, and D. Gutman, *Int. J. Chem. Kinet.*, in press.
(7) "Organic Synthesis," Collect. Vol. V, 679 (1973).
(8) R. W. Carr, Jr., I. D. Gay, G. P. Glass, and H. Niki, *J. Chem. Phys.*, **49**, 846 (1968).
(9) N. Washida, R. I. Martinez, and K. D. Bayes, manuscript in preparation.
(10) D. D. Davis, R. E. Huie, J. T. Herron, M. S. Kurylo, and W. Braun, *J. Chem. Phys.*, **56**, 4868 (1972).
(11) R. J. Cvetanović, *Can. J. Chem.*, **33**, 1684 (1955).

Photochemistry of Halogenated Acetones. I. Spectroscopic Studies

Peter A. Hackett and David Phillips*

Department of Chemistry, The University, Southampton S09 5NH, England *(Received June 19, 1973; Revised Manuscript Received January 14, 1974)*

Absorption, fluorescence, phosphorescence, fluorescence excitation, and phosphorescence excitation spectra for 1-chloropentafluoroacetone (CPFA), 1,3-dichlorotetrafluoroacetone (DCTFA), and 1,1,3-trichlorotrifluoroacetone (TCTFA) have been measured. Similar spectral data for 1-fluoroacetone (FA) and 1,1,1-trifluoroacetone (TFA) are also reported. Measurements of fluorescence quantum yields and decay times for the vibrationally relaxed singlet states of these molecules were used to calculate values of rate constants for radiative (k_R) and nonradiative (k_{NR}) decay. Trends of these results with increasing halogen substitution are discussed and compared with other literature values.

Introduction

The photochemistry and photophysics of halogen-substituted acetones have attracted considerable interest during the past few years. The literature was reviewed in 1964.[1] The luminescence of hexafluoroacetone (HFA) has been the subject of several recent reports. The phosphorescence of the compound was first reported by Bowers and Porter,[2] and much work on the luminescence of the compound was reported by Kutschke and coworkers.[3-6] Fluorescence decay time measurements on HFA,[7,8] acetone,[8] and acetone-d_6[8] allowed comparison of rate constants for radiative and nonradiative decay, and these were discussed in the light of simple theories. Photodecomposition in 1-chloropentafluoroacetone (CPFA), 1,3-dichlorotetrafluoroacetone (DCTFA), 1,1,3-trichlorotrifluoroacetone (TCTFA), and other similar ketones has been described.[9] Recently some aspects of the photophysics of CPFA[10] and DCTFA[11] have been discussed. The present series of papers is concerned with aspects of the photochemistry of halogentated acetones not widely studied to date. In this first paper various spectroscopic measurements are reported. Subsequent papers will discuss luminescence quantum yield measurements, vibrational relaxation, and quenching of these molecules in the gas phase. These papers have been abstracted in part from the Ph.D. thesis of P. A. Hackett, University of Southampton, 1973.

Experimental Section

Absorption spectra were obtained on a Pye-Unicam S.P. 700 recording spectrophotometer using a 6-cm long quartz gas cell. Samples of vapor were introduced to the cell using vacuum systems described in earlier papers.[11] Uncorrected fluorescence and total emission spectra were obtained using a Farrand Mk. 1 spectrofluorimeter (SPF) in the conventional mode.

Phosphorescence spectra were determined using the system shown in Figure 1. Samples were introduced into a capillary phosphorescence cell on a mercury-free vacuum line by freezing down from a constant volume. Pressures of ether and isopentane were also frozen from this known volume to give a solution of known molarity. The solution was then degassed and transferred to the quartz Aminco-Bowman dewar which was filled with nitrogen and placed in the SPF. Cylindrical quartz lenses were used to focus the exciting light onto the sample tube and the emitted light onto the entrance slit of the monochromator. Square wave modulation (75 Hz) of the exciting light was provided by a three-bladed mechanical chopper placed between lamp and excitation monochromator. A light emitting diode and phototransistor were placed either side of the chopper to derive a reference waveform. The reference waveform and the output from the photomultiplier were fed into the Brookdeal phase sensitive detector

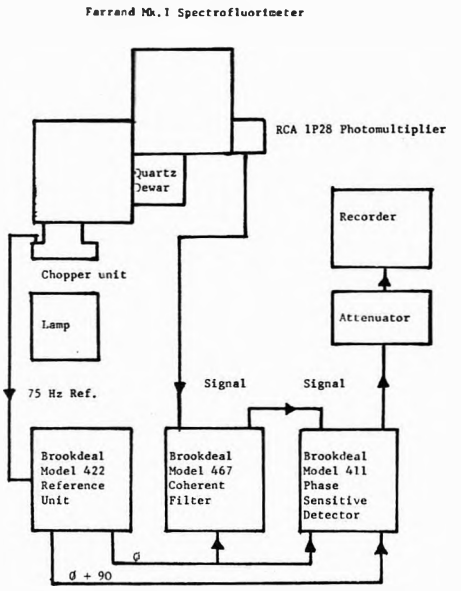

Figure 1. Apparatus for measurement of phosphorescence spectra.

(PSD) system in the configuration shown in Figure 1. The reference unit phase shift was adjusted with both monochromators set at 600 nm, until zero output was recorded by the PSD. The PSD was then used to record the 90° out of phase emission intensity. It is easily shown that this intensity corresponds only to delayed emission. A phosphorescence spectrum was then recorded.

In principle this apparatus could be used to measure phosphorescence decay times by measuring the intensity of the emission in the in-phase and 90° out-of-phase positions but the in-phase signal contains contributions from scattered light and ketone fluorescence and hence the measured phase shift would be distorted. Phosphorescence lifetimes were thus measured by photographing an oscilloscope trace of the photomultiplier output recorded on a Tektronix oscilloscope with 1A1 plug in. The trace was photographed in the single shot mode using the reference square wave as a trigger, by a Land Thompson oscilloscope camera. The response time, 0.3 msec, was inherent in the system due to the input impedance of the oscilloscope (1 MΩ and 100 pF) and the cable capacitance of the signal lead (100 pF). However this response time was not prohibitive in measuring the phosphorescence decay times required ($\approx$1 msec).

Moderately high resolution fluorescence excitation spectra were measured as follows. Excitation wavelengths were selected by a Hilger and Watts Monospex 1000 grating monochromator from an Osram XBO 450, 450-W xenon lamp. This monochromator has an f number of 10 and uses a grating blazed at 3000 Å with a reciprocal dispersion of 8 Å/mm. Excitation wavelengths passed through the cell (Figure 2) which was designed to reduce scattered light and hence allow the use of low pressures of sample without difficulty. Emission wavelengths were selected by a Corning CS-0-52 filter and viewed by a 20th Century Electronics Q4249BA photomultiplier. This photomultiplier was maintained at 1 kV by a Farnell EHT2 power supply. Photocurrents were measured using the Victoreen VTE-1 electrometer with a 3 sec time constant. The output signal was displayed on a Heathkit x-t recorder. A voltage subtractor was necessary since the output of the

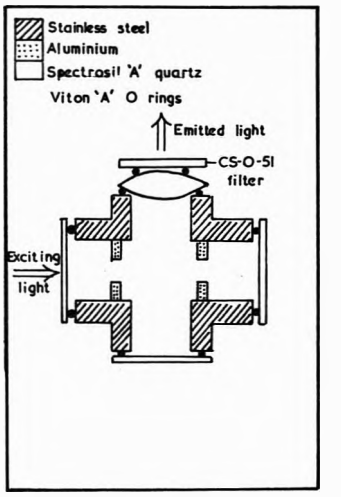

Figure 2. Fluorescence excitation cell.

electrometer was 0–10 mV floated on −3.8 V and the recorder could only accept an input referenced to ground.

Fluorescence quantum yields and decay times were measured by procedures to be described in a later paper.

Materials. The purity of all compounds used in this study was tested by gas liquid chromatography (glc) using a Perkin-Elmer Model 452 glc with flame ionization and thermal conductivity detectors. The carrier gas used was helium.

The columns used were (1) 20% silicone grease on celite inside 0.25-in. o.d. copper tubing; (2) 1 m of dinonylphthalate on Chromosorb W packed in 0.25-in. o.d. copper tubing.

Purity of Ketone Compounds. Biacetyl was obtained from British Drug Houses. It was distilled in the vacuum line. Glc analyses showed it to be substantially pure and free from acetone and dienes.

Fluoroacetone (FA) was obtained from Fluorochem Ltd. and was used without analysis.

1,1,1-Trifluoroacetone (TFA) was obtained from Bristol Organic Chemicals Ltd. Analysis on column 2 failed to reveal any impurity.

Hexafluoroacetone (HFA). The author wishes to thank Dr. M. C. Flowers of this department for the gift of purified hexafluoroacetone.

Chloropentafluoroacetone (CPFA) was obtained from Bristol Organic Chemicals Ltd. Analysis of column 2 failed to reveal any impurity.

1,3-Dichlorotetrafluoroacetone (DCTFA) was obtained from Koch Light Laboratories and was distilled on the vacuum line. Glc analysis failed to reveal any impurity but the mass spectrum showed a peak due to $CFCl_2$. This could be due to the presence of 1,1-dichlorotetrafluoroacetone.

1,1,3-Trichlorotrifluoroacetone (TCTFA) was obtained from Bristol Organic Chemicals Ltd. and was distilled on the vacuum line. No impurities were detected using columns 1 and 2.

Results

The ultraviolet absorption and fluorescence emission spectra of CPFA, DCTFA, and TCTFA are shown in Figures 3a, 3b, and 3c, respectively. The emission from these compounds was identified as fluorescence, since addition of up to 200 Torr of molecular oxygen had no effect upon the intensity of the fluorescence excited by 340-nm radiation. This assignment was verified by quenching studies

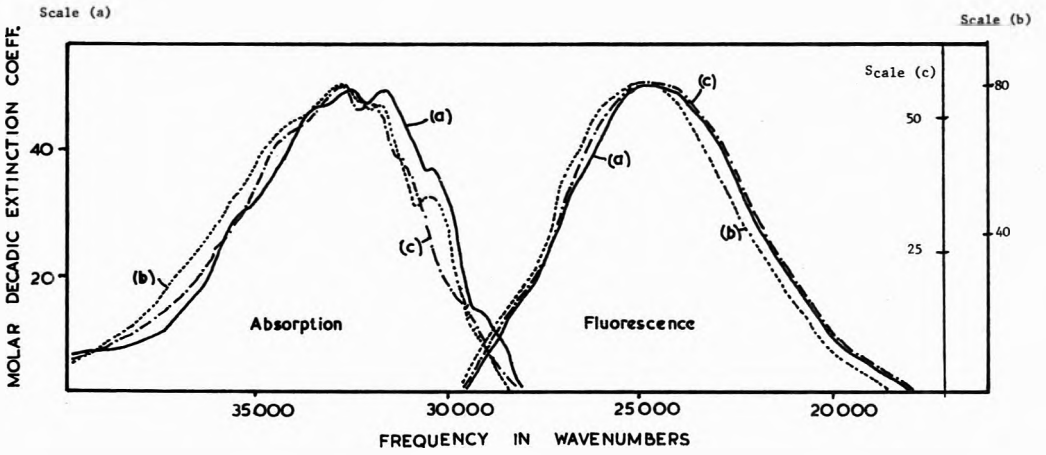

Figure 3. Absorption and fluorescence spectra of CPFA (a), DCTFA (b), and TCTFA (c): vapor phase, 20°. Fluorescence normalized to absorption scale.

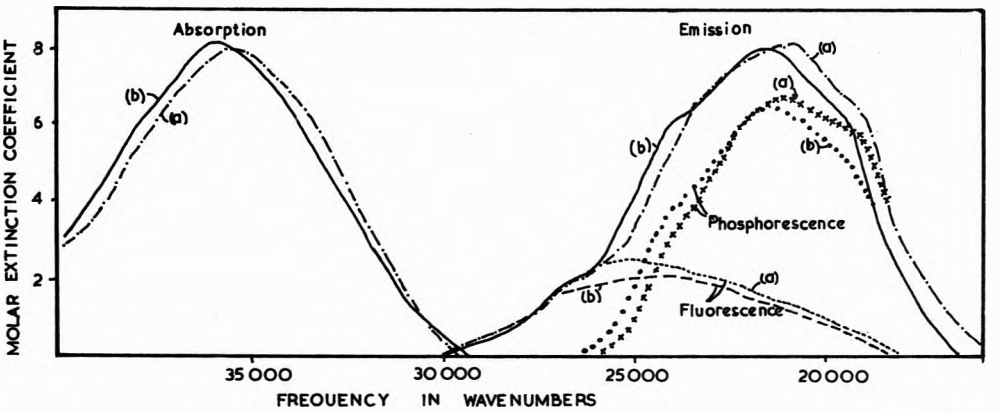

Figure 4. Absorption and emission spectra of FA (a) and TFA (b): (- - - -) emissiom not quenched by oxygen (fluorescence). Difference spectra are phosphorescence spectra.

which showed that 4 Torr of *cis*-2-butene would quench out all of the phosphorescence from biacetyl sensitized by DCTFA, but had little or no effect upon the emission of DCTFA itself.

The emission from TFA and FA, however, was partially quenched by addition of 2–22 Torr of molecular oxygen. The emission remaining in the presence of oxygen was designated fluorescence, and that quenched by oxygen was designated phosphorescence. The absorption spectrum, total emission, fluorescence, and phosphorescence emission spectrum of TFA and FA are shown in Figures 4a and 4b, respectively.

High (0.3 Å) resolution fluorescence excitation spectra of 3 Torr of TCPFA, DCTFA, and TCTFA are shown in Figure 5. This figure also shows the effect on these spectra of addition of 500 Torr of perfluoro-2-butene.

CPFA, DCTFA, and TCTFA phosphoresce in isopentane–ether glasses at liquid nitrogen temperatures. The phosphorescence emission and excitation spectra of these compounds are shown in Figure 6. The phosphorescence decay times are shown in Table I.

Selected fluorescence quantum yields and decay times for the various ketones are given in Table II.

Discussion

The frequency at which crossing of the fluorescence and absorption spectra occurs for the five compounds studied here was used to establish the 0–0 frequency of the transition from the ground state to first $n\pi^*$ singlet state. These

TABLE I: Phosphorescence Decay Times of Halogenated Ketones

Compd	τ_p, msec	Conditions
HFA	6.6[a]	0.06 *M* 3-methylpentane glass
CPFA	4.7[a]	0.02 *M* EPA
CPFA	3.1[a]	0.02 *M* 3-methylpentane glass
DCTFA	5.8[b]	0.02 *M* ether–isopentane glass
TCTFA	4.3[b]	0.02 *M* ether–isopentane glass

[a] Reference 10. [b] This work.

frequencies together with those of acetone and HFA are shown in Table II. The difference between the onset of the fluorescence and phosphorescence emission spectra, or the difference between the phosphorescence maximum and the fluorescence maximum, may be used to define the energy difference between the $^3n\pi^*$ and $^1n\pi^*$ excited states. These values were subtracted from the 0–0 frequencies defined above the lead to the triplet energies also listed in Table II.

The effect of chlorine substitution upon extinction coefficient for the nominal ground state to $^1n\pi^*$ state transition is shown by comparison of Figures 3 and 4, from which it can be seen that the oscillator strength is greatly enhanced. It is also evident that whereas the envelope of the absorption curves for the fluorine-substituted acetones is featureless, as is that for acetone itself, vibrational structure appears in the chlorine-substituted compounds. This is also seen in the fluorescence excitation spectra, and more dramati-

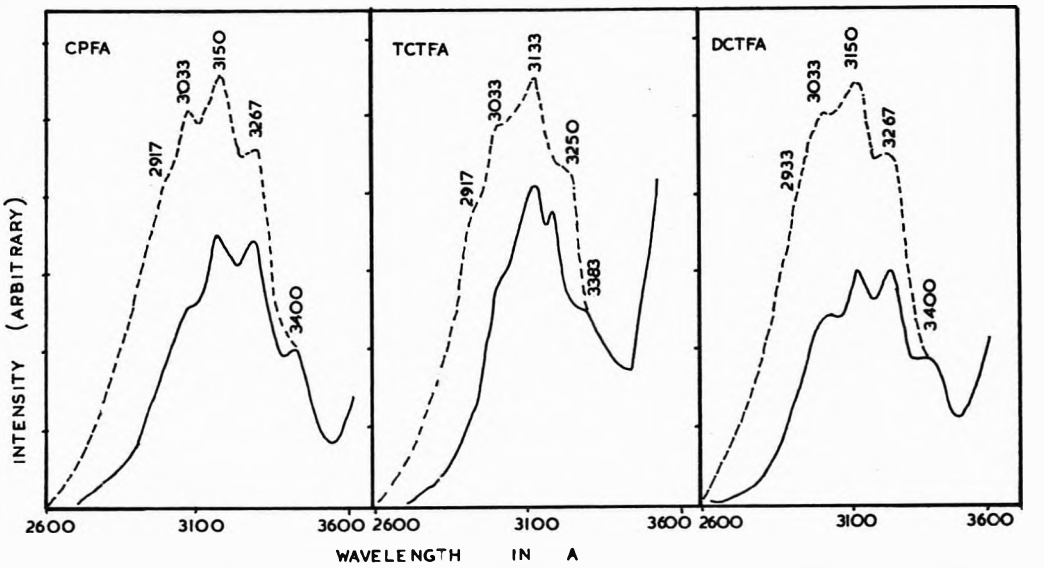

Figure 5. Fluorescence excitation spectra for CPFA, TCTFA, and DCTFA: (——) 3 Torr of ketone, (- - - -) 3 Torr of ketone + 500 Torr of perfluoro-2-butene; resolution 0.3 Å.

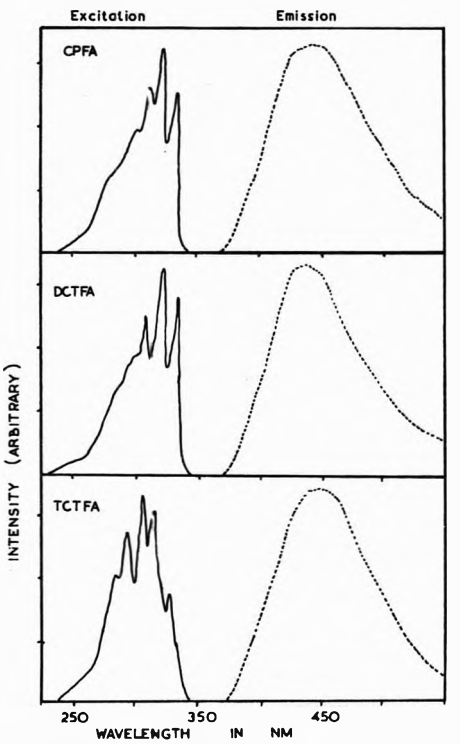

Figure 6. Phosphorescence spectra of CPFA, DCTFA, and TCTFA at 77°K, in ether–isopentane glass.

cally so in the phosphorescence excitation spectra where the features are much better resolved. The coincidence of the spacing of the vibrational bands in absorption, fluorescence excitation, and phosphorescence excitation spectra has been established.

The fluorescence excitation spectra are interesting. Lee, *et al.*,[12] have shown that in the fluorescence excitation spectrum of cyclobutanone a predissociation in the excited singlet state is clearly evident. Thus for photon energies which give rise to a state with a few kilocalories of energy above the zero-point energy, little or no fluorescence is observed. The fluorescence excitation spectrum thus differs appreciably from the absorption spectrum. In the present case, however, the fluorescence excitation spectrum (uncorrected) is quite similar to that for absorption, showing that a fast predissociation is absent from the $^1n\pi^*$ manifolds of CPFA, DCTFA, and TCTFA. At sufficiently high photon energies, singlet decomposition does however occur, but this process has been shown to be competitive with vibrational relaxation, at least for DCTFA.[11] Figure 5 shows that addition of a large pressure of an inert gas gives rise to FES spectra in all cases which extend to shorter wavelengths, supporting the idea that vibrational relaxation to the fluorescent lower levels can be effected in the three systems studied, which thus excludes the possibility that singlet decomposition occurs *via* a rapid predissociation within the time scale of a few vibrations in the molecule.

The behavior of the ketones studied following excitation by radiation near to the 0–0 transition (FA, TFA 330 nm; DCTFA, CPFA, TCTFA, 340 nm) can be described by the following simple mechanism

$$h\nu + A \longrightarrow {}^1A_0 \quad \text{absorption} \tag{1}$$

$${}^1A_0 \longrightarrow A + h\nu_F \quad k_R \text{ fluorescence} \tag{2}$$

$${}^1A_0 \longrightarrow \quad k_{NR} \text{ nonradiative transition} \tag{3}$$

The mechanism is validated by the observation that the fluorescence quantum yield observed under such excitation conditions is very much less than unity and is pressure independent. Now k_R and k_{NR} are given by

$$k_R = \Phi_F/\tau_F \tag{4}$$

$$k_{NR} = (1 - \Phi_F)/\tau_F \tag{5}$$

and values for the equilibrated levels of halogenated acetones are given in Table II (data taken from the following paper). For an orbitally allowed transition k_R may be calculated from the Strickler–Berg equations[13] and such values are also given in Table II.

Effect of Substitution on k_R

In the case of the $n \rightarrow \pi^*$ transition in formaldehyde the transition is orbitally forbidden but made allowed by out-of-plane vibrational frequency which distorts the planar ground state into the pyramidal geometry of the $n\pi^*$ state.[14] If the nature of the transition in the acetones were similar, then the Strickler–Berg (SB) equation should not give realistic estimates of k_R. Halpern and Ware demon-

TABLE II: Results of Lifetime, Quantum Yield, and Spectral Measurements on Gas-Phase Samples of Halogenated Ketones[a]

Compd	$S_0 \rightarrow S_1$ 0–0 frequency, cm^{-1}	Triplet energy, cm^{-1}	$(\bar{\nu}_F^{-3})_{AV}^{-1}$ $k_R(SB) \times 10^{13}$ cm^3	$(\bar{\nu}_F^{-2})_{AV}^{-1}$ $k_R(SB) \times 10^6$ sec^{-1}	Φ_F	τ_F, nsec	$k_R \times 10^{-6}$, sec^{-1}	$k_{NR} \times 10^{-7}$, sec^{-1}
A[b]			1.3	1.0	0.0012	2.4	5.0	42
HFA[b]			1.21	0.56	0.0185	8.4	2.2	1.2
CPFA	28,800	26,000	1.2	3.8	0.021	36.1	5.6	2.7
DCTFA	29,000	26,000	1.2	6.0	0.015	30.0	5.0	3.3
TCTFA	29,100	26,600	1.2	3.8	0.004_2	12.5	3.4	8.0
TFA	29,500	26,200	1.3	0.6	0.001_0	4.0	2.5	25.0
FA	29,800	25,800	1.3	0.7	0.001_1	2 ± 1[c]	1.1–3.7[c]	11–37[c]
Acetone-d_6			1.3	0.86	0.0016	3.4	4.7	29

[a] Rate constant data that for equilibrated levels taken from following paper. [b] Data from ref 8. [c] Fluorescence decay time very difficult to measure. Upper limit of 3 nsec gives best fit with data, and is used throughout.

TABLE III: Relative Radiative Rate Constant Data for Fluoroacetones

Compd	k_R(acetone)/k_R[a]	ω(acetone)/ω[b]	[ω(acetone)/ω][2]	ω^{HT},[c] cm^{-1}	ω^{BO},[d] cm^{-1}
Acetone	(1.00)	(1.00)	(1.00)		
Acetone-d_6	1.06	1.29	1.99		
FA	1.35[e]			358	435
TFA	2.00			242	378
HFA	2.27	1.32	2.26		
	k_R(acetone)/k_R[a]	k_R/k_R(HFA)[a]			
CPFA	0.89	2.55			
DCTFA	1.00	2.27			
TCTFA	1.47	1.54			

[a] Data from Table II. [b] Data from ref 8b. [c] Promoting mode frequency estimated from rate constant ratio using HT scheme (eq 6). [d] Promoting mode frequency estimated from rate constant ratio using BO scheme (eq 7). [e] Value obtained using the upper limit of lifetime.

strated this point for acetone, acetone-d_6, and HFA,[8] and as can be seen from Table II, k_R and k_R(SB) are noticeably different for FA and TFA also. For the chlorine-containing acetones however k_R(SB) and k_R are of similar magnitude. Halpern and Ware analyzed their data in terms of the theory of Albrecht which describes vibronic transitions[15] using the conventional Herzberg–Teller approach. The treatment indicates that the intensity of absorption will be linearly dependent upon the excited state promoting mode frequency, and the value of k_R will depend linearly upon the ground-state promoting mode frequency. Since isotopic substitution would in general reduce the value of the promoting mode frequency, results for acetone, acetone-d_6, and HFA can be rationalized on this basis. It is evident that the present results for TFA and for FA if the upper limit of lifetime is taken also fit the same broad trend.[16]

The Herzberg–Teller (HT) approach has recently been criticized as being too simple however.[17,18] It involves both the adiabatic Born–Oppenheimer approximation and the Condon approximation, and deviations from the former can give rise to terms which are significant, but which are neglected in the HT scheme. Orlandi and Siebrand[18] have shown that in absorption the intensity ratio for isotopically substituted species in the HT scheme will be given by the ratio of (excited state) promoting mode frequencies, whereas in the case of their recent approach, termed the Born–Oppenheimer (BO) approach,[18] the intensity ratio dependence will be cubic with respect to promoting mode frequencies, *i.e.*

$$I_H^{HT}/I_D^{HT} \approx \omega_H/\omega_D \quad (6)$$

$$I_H^{BO}/I_D^{BO} \approx (\omega_H/\omega_D)^3 \quad (7)$$

Similar relationships will hold for the relative values of k_R except that promoting mode frequencies will be ground-state parameters. It should therefore be possible to determine the relative importance of the two coupling schemes given data for k_R and promoting mode frequencies. Table III shows values of k_R for a variety of fluorinated acetones relative to that for acetone, together with values of the relative promoting mode frequencies to the first and third power where these data are available. Where promoting mode frequencies are not known they have been calculated from rate constant ratios using both the HT and BO schemes, and these values are also shown in Table III. The data for acetone-d_6 clearly do not support either the HT or BO schemes, but those for HFA clearly favor the BO coupling scheme proposed. Further support for this is obtained from the calculation of frequencies using the HT and BO mechanisms in the cases of FA and TFA.

An infrared absorption spectrum was taken of a gas-phase sample of TFA in a cell using cesium iodide windows. Absorptions were observed at 428, 372, and 362 cm^{-1}. Similar spectra were taken of a sample of FA vapor and the presence of weak absorptions at 425, 400, 378, and 357 cm^{-1} was revealed. While no attempt has been made to assign normal coordinates to these frequencies, the results do show that for both compounds a frequency exists which has the right magnitude to fit the radiative rate constant data according to the BO scheme, but at least in the case of TFA, no such frequency exists for the HT scheme.

However, it is clear from Table III that the values of k_R for the chlorinated ketones are all greater than those for HFA, which is difficult to rationalize in terms of the treatment above. The reason for this discrepancy may be seen from a consideration of the extinction coefficients of these and other α-chlorinated ketones shown in Table IV. Similar marked increases in extinction coefficient and red shifts have been noted when an amine group is substituted α to a carbonyl group.[19] These effects have been as-

TABLE IV: Spectral Characteristics of α-Chloro Ketones

Compd	$\lambda_{(\epsilon_{max})}$, nm	ϵ_{max}	Ref
Acetone	275	17	1
Chloroacetone	300	32	No. B1/8[a]
1,1-Dichloroacetone	295	65	1
HFA	305	8	1
CPFA	305	49	9
DCTFA	300	80	1
TCTFA	302	43	1
Cyclohexanone	280	18	20
1-Chlorocyclohexanone[b]	300	35	No. B1/4[a]

[a] H. H. Perkampas, I. Sandeman, and C. J. Timmons in "UV Atlas of Organic Compounds," Butterworths, London, 1966. [b] 37% equitorial isomer.

cribed to a mixing of the substituent nonbonding electrons in the n–π* transition, for which there is much further evidence in the literature.[20,21]

It is not unreasonable to propose that α-chlorinated acetones should show all of these effects and hence the "n–π*" transition in CPFA, DCTFA, and TCTFA would involve more orbital allowedness than the corresponding n–π* transitions in nonchlorinated acetones. The manifestations of this mixing are the enhancement of the oscillator strength of the nominal n–π* transition in the chloro ketones, and better agreement between k_R and k_R(SB) for these compounds. Table II shows that this is what is observed in the present case.

Nonradiative Decay

The mixing of chlorine nonbonding electrons, or carbon–chlorine σ* molecular orbitals into the n–π* transition has important consequences on the rate of nonradiative processes. In the case of CPFA and DCTFA this nonradiative process can be unambiguously defined as intersystem crossing since the triplet state yield under these conditions was shown to be close to unity.[10,11] Triplet TCTFA has a lifetime which is too short to enable the biacetyl technique to adequately determine the triplet state yield but under conditions of excitation at 340 nm with ketone pressures greater than 20 Torr it is not unreasonable to suppose the nonradiative process to be solely intersystem crossing by analogy with CPFA and DCTFA. The values of the intersystem crossing rate constant determined in this way are 2.7×10^7 sec^{-1} for CPFA, $3.3 \times 10^7 \times$ sec^{-1} for DCTFA, and 8×10^7 sec^{-1} for TCTFA (Table III). Halpern and Ware[8] found k_{NR} to vary from 41.7×10^7 sec^{-1} in acetone to 29.4×10^7 sec^{-1} in acetone-d_6 and 1.2×10^7 sec^{-1} in hexafluoroacetone.

A calculation (using ground-state vibrational frequencies) using the method of Haarhoff[22] revealed that the maximum density of states (ρ) isoenergetic with the vibrationless excited singlet is 1.2 cm for acetone, 4.2 cm for acetone-d_6, and 5×10^4 cm for HFA; substitution of these values into the golden rule expression for the intersystem crossing rate constant

$$k_{NR} = (2\pi/h)\rho V^2$$

where V is the matrix element associated with the perturbation responsible for the nonradiative decay allows an estimation of ρV. Values obtained were 2×10^{-2} for acetone, 4×10^{-2} for acetone-d_6, and 6.9×10^{-2} for HFA. As the authors point out these values are considerably less than unity although these molecules show all the other characteristics of molecules in the statistical limit.[23] It must be stated that the calculation of ρV is probably invalid because of the lack of knowledge of triplet state vibrational frequencies. However it can be seen that substitution affects the electronic part of the nonradiative transition probability. Presumably the vibronic coupling, spin–orbit coupling, and Frank–Condon factors may all change as well as the density of states.

It is interesting that the nonradiative rate constant for 1,1,1-trifluoroacetone fits into the series investigated by Halpern and Ware as does that for FA if the upper limit of the lifetime is taken. However, as with the radiative rates the intersystem crossing rates in the series HFA, CPFA, DCTFA, and TCTFA change in the opposite direction to that predicted. Since the singlet–triplet energy gap is relatively constant (3000 cm^{-1}) throughout the chlorinated acetone series it is reasonable to suppose that the density of states will increase with successive chlorination due to the introduction of low-frequency modes, and this may explain the trend in the intersystem crossing rate constants. However, the Frank–Condon factors and factors affecting the electronic part (β) of the nonradiative transition probability will change also and it has been pointed out that decreases in the former factor frequently tend to cancel out changes in the density of states. Thus the enhancement of intersystem crossing may be due to changes in β. These changes could be due to an enhanced spin–orbit coupling due to "heavy atom" effects of the chlorine atoms. Such internal heavy atom effects on k_{ISC} have been frequently observed in aromatic molecules although El-Sayed has shown[24] that heavy atoms should have a negligible effect on n–π* transitions of carbonyl compounds. This calculation was based upon the assumption that the orbitals involved in the nπ* transition have zero coefficients on the halogen atoms. Clearly if the configurational interaction proposed to explain the variation of the radiative rate constant with chlorine substitution does occur this assumption will be invalid and the spin–orbit coupling matrix elements will contain one center terms on the halogens.

Kanda has measured the oscillator strength for ($T_1 \leftarrow S_0$) transitions for oxalyl bromide, oxalyl chloride, and biacetyl.[25] The results (3.3×10^{-6}, 1.34×10^{-7}, and 1.12×10^{-7}, respectively) support the view that internal spin–orbit coupling can effect nπ* transitions.

Were such effects of importance in the present case, it might have been anticipated that progressive chlorination would have led to a decrease in the observed phosphorescence decay time. However, Table I shows little discernible affect. It is noticeable from Table I that the solvent plays a large part in determining phosphorescence decay times (results for CPFA), and it is not perhaps useful to compare these data.

Acknowledgments. We wish to thank the Science Research Council, The Royal Society, and Monsanto Chemicals Ltd. for financial assistance. We are grateful to Dr. A. W. Sloman for his helpful advice in setting up equipment.

References and Notes

(1) J. R. Majer and J. P. Simons, *Advan. Photochem.*, **2**, 137 (1964).
(2) P. G. Bowers and G. B. Porter, *J. Phys. Chem.*, **68**, 2982 (1964).
(3) A. Gandini and K. O. Kutschke, *Can. J. Chem.*, **44**, 1720 (1966).
(4) R. K. Boyd, G. B. Carter, and K. O. Kutschke, *Can. J. Chem.*, **46**, 175 (1968).
(5) A. Gandini, D. A. Whytock, and K. O. Kutschke, *Ber. Bunsenges. Phys. Chem.*, **72**, 296 (1968).
(6) D. A. Whytock and K. O. Kutschke, *Proc. Roy. Soc., Ser. A*, **306**, 503 (1968); A. Gandini and K. O. Kutschke, *ibid.*, 511 (1968); A. Gandini, D. A. Whytock, and K. O. Kutschke, *ibid.*, 529, 537, 541 (1968).

(7) W. R. Ware and M. L. Dutton, *J. Chem. Phys.*, **47**, 4670 (1967).
(8) (a) A. M. Halpern and W. R. Ware, *J. Chem. Phys.*, **53**, 1969 (1970); (b) *ibid.*, **54**, 1271 (1971).
(9) J. R. Majer, C. Olavesen, and J. C. Robb, *J. Chem. Soc. A*, 893 (1969); *J. Chem. Soc. B*, 48 (1971).
(10) H. S. Samant and A. J. Yarwood, *Can. J. Chem.*, **48**, 2611, 2937 (1970); *Can. J. Chem.*, **49**, 2053 (1971); A. J. Yarwood, *ibid.*, **50**, 1429 (1972).
(11) P. A. Hackett and D. Phillips, *J. Chem. Soc., Faraday Trans. 1*, **68**, 323, 329, 335 (1972).
(12) R. C. Shortridge, Jr., C. F. Rusbult, and E. K. C. Lee, *J. Amer. Chem. Soc.*, **93**, 863 (1971).
(13) S. Strickler and R. A. Berg, *J. Chem. Phys.*, **37**, 814 (1962).
(14) H. L. McMurray, *J. Chem. Phys.*, **9**, 241 (1941).
(15) A. Albrecht, *J. Chem. Phys.*, **33**, 1120 (1960).
(16) P. A. Hackett and D. Phillips, *J. Photochem.*, **2**, 325 (1973).
(17) P. A. Geldof, R. P. H. Rettschnick, and G. J. Hoytink, *Chem. Phys. Lett.*, **10**, 549 (1971).
(18) G. Orlandi and W. Siebrand, *Chem. Phys. Lett.*, **15**, 465 (1972).
(19) J. Hudec, *Chem. Commun.*, 829 (1970).
(20) N. L. Allinger, J. C. Tai, and M. A. Miller, *J. Amer. Chem. Soc.*, **88**, 4495 (1966).
(21) R. Hoffmann, *Accounts Chem. Res.*, **4**, 1 (1971).
(22) P. C. Haarhoff, *Mol. Phys.*, **7**, 101 (1963).
(23) J. Jortner, S. A. Rice, and R. M. Hochstrasser, *Advan. Photochem.*, **7**, 149 (1970).
(24) M. F. A. El-Sayed, *J. Chem. Phys.*, **41**, 2462 (1964).
(25) Y. Kanda, R. Shimada, H. Shimada, H. Kaseda, and T. Matumura, "Reprints of Tokyo Symposium (IUPAC) on Molecular Structure and Spectra," Tokyo, 1962, p B304.

Photochemistry of Halogenated Acetones. II. Rate Constant Measurements

Peter A. Hackett and David Phillips*

Department of Chemistry, The University, Southampton SO9 5NH, England *(Received June 19, 1973; Revised Manuscript Received January 14, 1974)*

Fluorescence decay times of FA, TFA, CPFA, DCTFA, and TCTFA have been measured for a variety of vapor-phase conditions. Fluorescence quantum yields for the last three compounds are also reported. Variations in rate constants for radiative (k_R) and nonradiative (k_{NR}) decay as a function of photon energy are discussed. It is shown that increase in photon energy causes an exponential increase in k_{NR} for the compounds studied which is attributable either to decomposition from the singlet manifold or an enhancement of nonradiative decay to a short-lived, presumably dissociative, triplet state.

Introduction

The previous paper was concerned with spectroscopic measurements on several halogenated acetones. In the present paper we present luminescence quantum yield and decay time measurements under a variety of conditions from which absolute rate constants for radiative and nonradiative decay may be determined.

Experimental Section

Luminescence Quantum Yields. The quantum yields of emission of the carbonyl molecules in the gas phase were measured using the system described below.

Monochromatic light emergent from a lamp and monochromator combination was collimated by a lens and traversed the long axis of a T-shaped fluorescence cell which contained the compound of interest at a known pressure. This exciting light then fell upon an RCA 935 photodiode, allowing absorption measurements to be made. Light emitted by the compound in the cell was observed normal to the exciting light by an RCA 1P28 photomultiplier powered by a Farnell E2 constant voltage power supply. A glass filter was interposed between the detector and the cell to reduce scattered light. Photocurrents from these two detectors were monitored using a Victoreen VTE-1 electrometer. The lamp used throughout this work was an Osram XBO/150 W1 high-pressure xenon lamp. The monochromator used was either a Bausch and Lomb 33-86-07 uv visible monochromator or a Bausch and Lomb 33-86-07 uv monochromator fitted with a collimating lens. The former monochromator has a grating with a reciprocal dispersion of 64 Å/mm blazed at 2200 Å. The latter was blazed at 2500 Å with a reciprocal dispersion of 32 Å/mm. The emergent beam from the monochromator was made parallel by a quartz lens. The monochromators were wavelength calibrated by observing the peaks in the emission of a Hanovia SH/100 medium-pressure mercury arc lamp and comparing these with the standard spectrum. The fluorescence cell was 6 cm long, 3 cm diameter, with a 2-cm diameter centrally placed T window and was made from Spectrosil A nonfluorescent quartz using 1-mm thick optical flats. All exterior surfaces of the cell with the exception of the three optical flats were painted with matt black paint, substantially reducing the scattered light signal. The cell and photodetectors were housed in a brass casing, isolating them from ambient light. A discussion of the geometrical effects operative in a cell of this design has been given[1] and the relevant correction factors were applied wherever the absorption by the compound in the cell was high.

A Corning CS0.52 filter was placed between cell and photomultiplier tube to isolate ketone fluorescence and a Corning CS3.71 filter to isolate the sensitized phosphorescence of biacetyl. A mask was placed between the filter and the 1P28 photomultiplier to constrict the field of view

of the photomultiplier to the area of the cell excited by the incident radiation. The spectral response of both photodetectors was nominally S5 but it was considered important to calibrate that of the RCA 935 used to observe the intensity of the excitation beam. This was achieved using a sodium salicylate quantum counter. Absolute quantum yields of fluorescence were obtained by calibration with 500 Torr of HFA excited at 313 nm in the presence of 5 Torr of oxygen, for which the fluorescence quantum yield has been given as 0.018_5.[2]

The procedure for measurement of fluorescence quantum yields has been stressed here since previous measurements on DCTFA have been shown to be greatly overestimated.[3] This is unfortunate and was due to the use of benzene vapor as a standard, which has very different absorption and fluorescence spectral characteristics from those of the ketone investigated. In making corrections for the spectral sensitivities of the photodetectors in the original studies, maker's curves only were used. Present results indicate that for the particular photomultiplier tube used in the original investigation the sensitivity curve assumed was invalid. In the present case use of a new 935 phototube, the sodium salicylate quantum counter, and HFA as a standard removes these difficulties and leads to the correct values of fluorescence quantum yields given in the Results section.

Values of the quantum yield of emission from biacetyl sensitized by the ketones were obtained absolutely by comparison with relative yields from biacetyl excited directly at 404.7 nm extrapolated to zero pressure, for which the quantum yield is 0.15 ± 0.3.[4,5]

At certain wavelengths of excitation the measurement of the quantum yield of sensitized phosphorescence of biacetyl ϕ_S, was complicated by absorption of the incident exciting radiation by biacetyl. This effect was corrected for by the standard method of Ishikawa and Noyes.[6]

The sensitivity of the biacetyl triplet state to oxygen is well known and so several checks were made to test the validity of the measurements. ϕ_S was shown to be independent of the number of times the mixture was degassed in the cell. It was also shown to be independent of the storage time in the cell for a period of 12 hr; hence it could be concluded that there were no significant pressures of oxygen in the cell and that little leakage of oxygen into the cell or desorption of oxygen from the cell walls occurred.

The bandpass of exciting radiation used in these studies was 3 nm, and the precision of measurements on ϕ_F at low pressure was reproducibly 10%. Low-resolution spectral measurements showed no significant change in the fluorescence spectra of the ketones under different excitation wavelength and pressure conditions.

Fluorescence Decay Time Measurements. A block diagram of the apparatus used is shown in Figure 1. The lamp was obtained from Applied Photophysics Ltd but was considerably modified. The resistor chain was replaced with a single 150 MΩ resistor obtained from the Victoreen Co. (MOX-4) rated at 40 kV and which was connected to the Brandenberg 800 EHT power supply by 30-kV coaxial cable. The screening of this cable was connected to the lamp body (metal) and to the ground of the power supply. The resistor was surrounded by ⅛-in. thick Teflon sheeting formed into a tube. The lamp discharge was usually run at 28 kV to give optimum intensity and repetition rate. The high voltage electrode of the discharge was a tungsten point made from 1/16-in. diameter rod. It was found that the mass of the electrode had a marked effect on the characteristics of the discharge. A large electrode gave high light intensity pulses at a low repetition rate (2 kHz) while a smaller electrode gave a high repetition rate of smaller amplitude light pulses. An electrode of ⅜ in. of 18 gauge platinum wire soldered directly to the end of the 150-MΩ resistor gave a stable 45-kHz output of low-intensity light pulses.

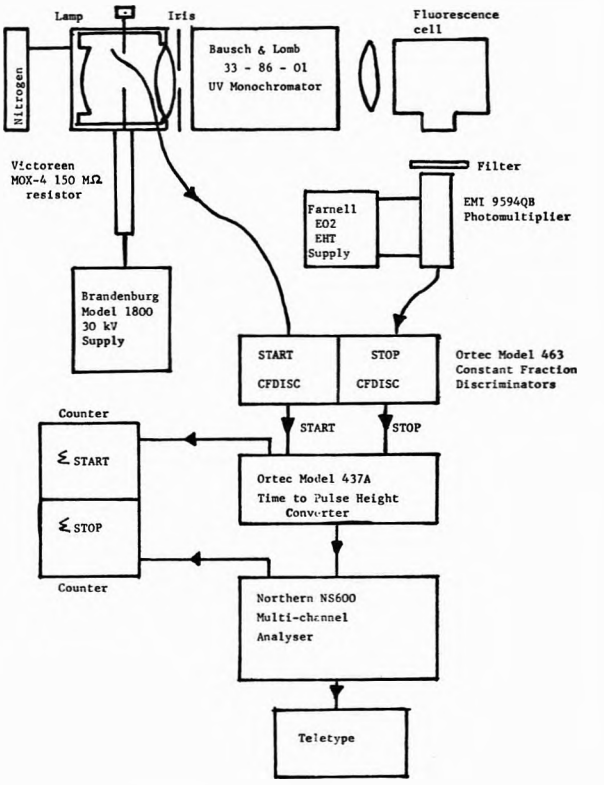

Figure 1. Block diagram of time-correlated single-photon counting apparatus.

The ground electrode was threaded in order that the spark gap could be adjusted. The electrode was either a rounded tungsten rod or a ball made by fusing platinum wire. The optimum spark gap was found by experiment; small gaps giving high reptition rates of smaller amplitude pulses, the repetition rate decreasing and intensity increasing as the gap was increased until the discharge became unstable. The position of the electrodes was then adjusted until the required gap was centered in the collecting lens.

All experiments reported here were carried out with the lamp filled with nitrogen. The nitrogen pressure was kept at 30 lbs/in.^{2} since this gave the shortest lamp decay. The lamp gave light pulses, 4 nsec wide at half-height at a stable frequency of 2–40 kHz.

The photomultiplier used was an uncooled EMI 9594QB biased at 2350 V by a Farnell E2 regulated supply. The photomultiplier dynode chain was wired according to the maker's specifications and was terminated in a 50-Ω pulse counting mode. The "focus" and "deflection" potentiometers were adjusted such that the observed signal of the lamp excitation pulse was of minimum width at half-height and of maximum amplitude. These adjustments were made using a Tektronix 1S1 sampling oscilloscope.

Start pulses were generated from a single Teflon-insulated wire which passed through the lamp body. Ortec 463

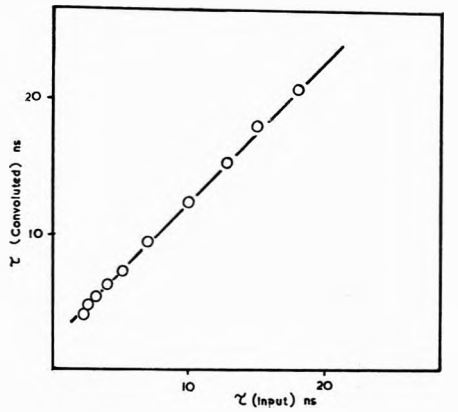

Figure 2. Results of convolution of trial decay times with lamp excitation function as function of input decay time.

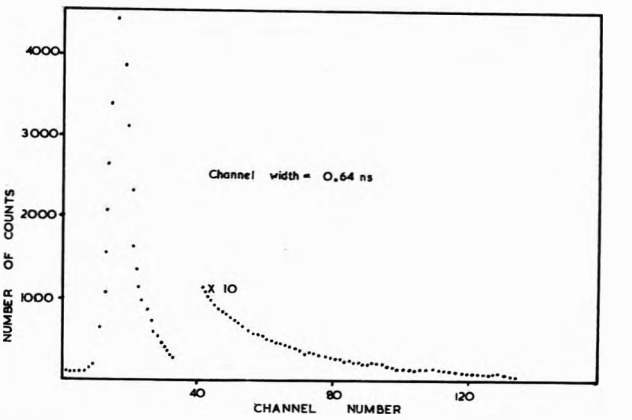

Figure 3. Typical lamp decay curve used as excitation function in Figure 2.

constant fraction discriminators were used to give proper pulse shaping and time derivation of the outputs from the photomultiplier and the lamp trigger. The time-to-pulse height converter (TPHC) used was an Ortec 437A and the multichannel pulse height analyzer (MCPHA) was a Northern NS-600. Data readout from the MCPHA was achieved with a teletype printer. Problems arising from "pile-up" were avoided by ensuring that the ratio of number of photons counted, N_t, to start pulses N, was less than 0.05.

Start pulses generated from the output of TPHC and stop pulses generated from the output of the MCPHA were counted in an eight-digit dual scaler designed and built by Dr. A. W. Sloman of this department. Pulses were counted independently in two separate counters. The counters were zeroed and held by the same control, ensuring that both counted over identical periods of time. The accumulated counts from either counter were displayed by a buffered eight-digit display continuously or on command. The counters could remain operative while the display was stationary and hence N_t/N could be computed at intervals throughout any run.

Data were analyzed using three different techniques. In the first, the lamp excitation function was used to convolute expected decay curves for actual fluorescence lifetimes using a computer. A log plot was made of the exponential tail of these decay curves and the predicted generated decay time was obtained. A graph of inputed fluorescence decay time against predicted generated decay time was obtained (Figure 2). The lamp excitation function used to generate these curves is shown in Figure 3. A log plot of the experimental observed decay curve with the experimental scattered light subtracted was then made and the observed decay time was then used to interpolate the true decay time from Figure 2.

The second method employed a computer curve-fitting routine. The lamp excitation function and the experimental decay curve were read in to the computer which used an estimated value of the fluorescence decay curve to convolute a predicted experimental decay curve. The two "experimental curves" were then normalized such that their areas were equal and the sum of the squares of the deviations between the curves was found. This latter function was then minimized by the Newton–Raphson curve-fitting procedure; changing the value of the fluorescence decay time until the best fit was obtained. This curve-fitting procedure proved to be extremely fast.

The third method was used to analyze data obtained at low pressures of ketone and short excitation wavelength. Under these conditions the fluorescence intensity varies with time according to the kinetic scheme under test and such effects were taken into account in the convolution procedure. The calculated curve was fitted to the experimental curve by an iterative procedure.

Results and Discussion

Fluorescence decay times for the ketones studied are shown in Table I together with excitation conditions. The variation in fluorescence quantum yield with pressure of ketone for CPFA, DCTFA, and TCTFA are shown in Figures 4–6.

The dependence of the radiative and nonradiative rate constants on the vibrational energy content of the excited singlet state was investigated by taking the fluorescence decay time and fluorescence quantum yield measurements for CPFA, DCTFA, and TCTFA at five wavelengths (340, 325, 310, 300, and 280 nm), at pressure low enough such that the vibrational levels formed by optical excitation could be observed in the absence of collisions. This pressure was calculated by assuming that the vibrational relaxation constant was equal to $7 \times 10^{10}\ M^{-1}\ \text{sec}^{-1}$ and that vibrational relaxation removes the state from the system. The values calculated were CPFA (fluorescence decay time 36 nsec) 0.2 Torr, DCTFA (fluorescence decay time 30 nsec) 0.3 Torr, and TCTFA (fluorescence decay time 12.5 nsecs) 0.7 Torr. However vibrational relaxation leads to a state which may still emit and thus higher pressures may be used without distortion of the decay times and fluorescence yields. This was the observed result of Halpern and Ware[7] who calculated a pressure of 0.1 Torr for HFA (fluorescence decay time 84 nsecs) but observed that decay times measured at 0.5 Torr were equal to those measured at 0.1 Torr. This is what was observed with CPFA, DCTFA, and TCTFA.

At pressures in excess of 25 Torr the fluorescence decay times of CPFA, DCTFA, and TCTFA were precisely exponential and independent of both pressure and wavelength, and thus correspond to emission from the Boltzmann distribution of excited state levels. At pressures below approximately 1 Torr, exponential fluorescence decay was also observed, but the lifetimes were dependent upon excitation energy, decreasing with increase in photon energy. At intermediate pressures, nonexponential decay curves were obtained.

The behavior here parallels that observed earlier by Halpern and Ware[7] for HFA, and the pressure dependence

TABLE I: Fluorescence Decay Times of Halogenated Ketones

Compd	Excitation wavelength, nm	Sample conditions, Torr	τ_F, nsec
CPFA	340	40	36.1
	310	40	36.0
	340	80	36.1
	340	7	36.1
	340	7	36.0
	300	5	*a*
	300	2	*a*
	300	4	*a*
	300	11	*a*
	300	7	*a*
	340	0.5	36.0
	325	0.5	34.3
	310	0.5	29.8
	300	0.5	21.8
	290	0.5	15.7
	280	0.5	8.9
DCTFA	340	80	30.0
	340	40	28.0
	300	40	30.0
	340	30	28.0
	300	12	*a*
	300	7.8	*a*
	300	5.5	*a*
	300	4	*a*
	340	0.6	25.6
	325	0.6	19.9
	310	0.6	16.4
	300	0.6	14.1
	280	0.6	6.2
	310	PFMCH (soln)	26.1
TCTFA	340	40	12.5
	340	30	12.6
	340	1.2	12.0
	325	1.2	13.1
	310	1.2	11.0
	300	1.2	8.6
TFA	310	200	4.0
FA	310	50	≈2

[a] Nonexponential decay observed; PFMCH perfluoromethylcyclohexane.

of the lifetimes is a manifestation of vibrational relaxation from initially "isolated" molecules to the Boltzmann distribution. This relaxation process is discussed further in the following paper. Values of k_R and k_{NR} obtained in the low-pressure limit are shown in Table II. It should be noted that because of the relatively broad bandpass of excitation used in this study, and sequence congestion in the absorption spectra of the compounds studied, and further, the possibility of intramolecular vibrational redistribution the low-pressure results are characteristic of a distribution of emitting states rather than single vibronic levels.

Wavelength Dependence of k_R

It can be seen from Table III that k_R tends to decrease with decreasing wavelength. This effect is most pronounced below 300 nm. This effect may be real or an experimental artifact. Thus optical excitation may result in partitioning between excited singlet states which dissociate and excited states which may fluoresce. The quantum yield of fluorescence of emitting states would then be underestimated yielding a value of k_R which is too low. Halpern and Ware[7] found no similar discernable trend in his experiments on HFA, however, no measurements of quantum yields were made in that study. The quantum yields used were interpolated from the zero pressure fluorescence quantum yields measured by Kutschke, *et al.*,[8] at excitation wavelengths of 313, 265, and 254 nm. These values were 0.0095, 0.0045, and 0.0015, respectively. Kutschke's value of 0.0138 for excitation at 366 nm was not used since this result is probably influenced by the effects of direct singlet–triplet absorption. Hence a value of the high-pressure quantum yield at 313 nm (0.0185) was used for the zero pressure yield at 358 nm. Linear interpolations based upon these values may not yield valid estimates of the zero pressure fluorescence quantum yield, and hence Ware's values of k_R may be subject to errors.

Herzberg–Teller theory for forbidden transitions can be

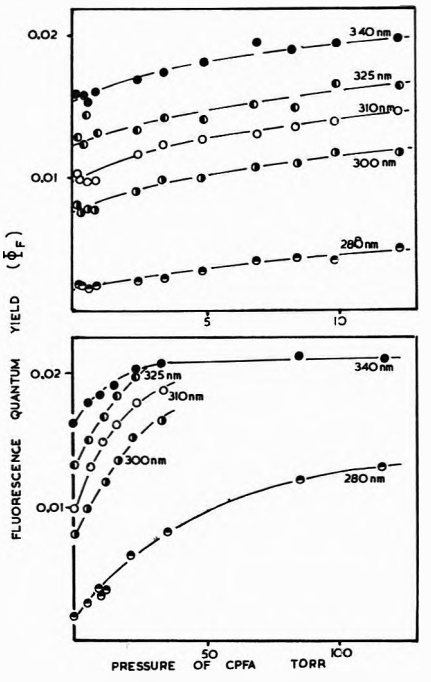

Figure 4. Fluorescence quantum yields of CPFA at 20° as a function of pressure at different excitation wavelengths.

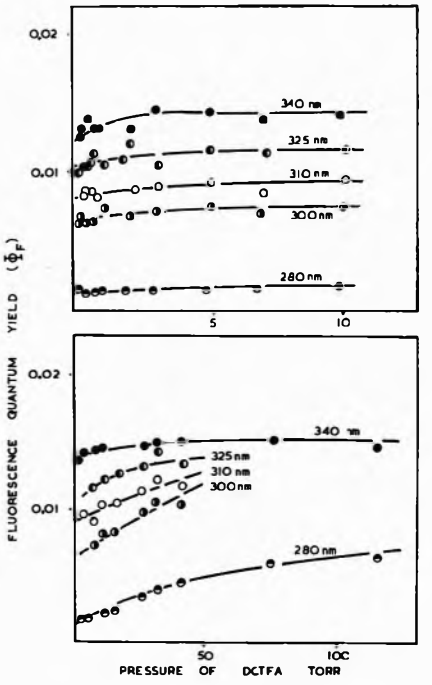

Figure 5. Fluorescence quantum yields of DCTFA at 20° as a function of pressure at different excitation wavelengths.

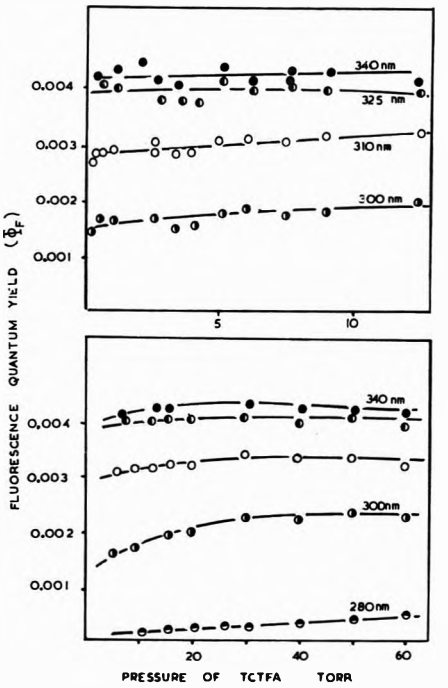

Figure 6. Fluorescence quantum yields of TCTFA at 20° as a function of pressure at different excitation wavelengths.

TABLE II: Zero Pressure Lifetimes and Quantum Yield Data for CPFA, DCTFA, and TCTFA

Compd	Excitation wavelength, nm	τ_F, nsec	ϕ_F	$k_R \times 10^{-5}$, sec^{-1}	$k_{NR} \times 10^{-7}$, sec^{-1}
CPFA	340	36.0	0.0154	4.3	2.8
	325	34.3	0.0126	3.7	2.9
	310	29.8	0.0095	3.2	3.3
	300	21.8	0.0075	3.5	4.6
	290	15.7			6.4
	280	8.9	0.0018	2.0	11.0
DCTFA	340	25.6	0.0131	5.1	3.9
	325	19.9	0.010	5.0	5.0
	310	16.4	0.0081	4.9	6.0
	300	14.1	0.0062	4.4	7.0
	280	6.2	0.0012	1.9	16.1
TCTFA	340	12.0	0.0043	3.6	8.3
	325	13.1	0.0041	3.1	7.6
	310	11.0	0.0027	2.4	9.1
	300	8.6	0.0015	1.7	11.6

used[9] to show that the integrated absorption coefficient should increase with temperature according to the equation

$$\int \frac{\epsilon(\bar{\nu})\, d\bar{\nu}}{\bar{\nu}} \alpha \coth (h\bar{\nu}_{1m}/2kT) \qquad (1)$$

where $\bar{\nu}_{1m}$ is the frequency of the promoting mode. Ware[10] has shown that this quantity obeys the above equation over 300–600°K in HFA, which implies that k_R should increase with increase in photon energy.

The results found for CPFA, DCTFA, and TCTFA are thus in contradiction with vibronic coupling theory. It is possible that the value of k_R is determined by the magnitude of the configurational interaction discussed in the previous paper. The temperature dependence of such interactions is not well understood but it is not unreasonable to propose that interactions which are highly conformationly dependent would be "smeared out" at high internal energies, leading to a reduction in k_R. Alternatively the reduction in magnitude of k_R with increasing photon energy may simply reflect decreases in the Franck–Condon factors for the radiative transition. A recent paper by Lin, *et al.*,[11] is relevant to the discussion above. These authors have shown that within the harmonic oscillator approximation for both symmetry allowed and symmetry forbidden transitions, k_R should vary linearly with excess vibrational energy in the excited state, both in the case of single vibronic level excitation, and in cases in which unimolecular vibrational redistribution occurs. k_R may increase or decrease with excess energy depending upon vibrational frequency changes and the nature of the modes excited. For the case of excitation in a progression in which the frequency of the mode excited is less in the upper state than in the ground state, k_R will decrease linearly with excess energy. The same is true for an ensemble of levels if an averaged frequency term is less in the upper state than the ground state. For excitation of the promoting mode with successive quanta, however, k_R should increase with excess energy. For the molecules studied here excited state frequencies will undoubtedly be smaller than ground state, and thus the decrease in k_R with excess energy can be understood. The apparently anomalous results for HFA could on this basis be due to a fortuitous excitation of successive quanta of the promoting mode at the wavelengths studied.

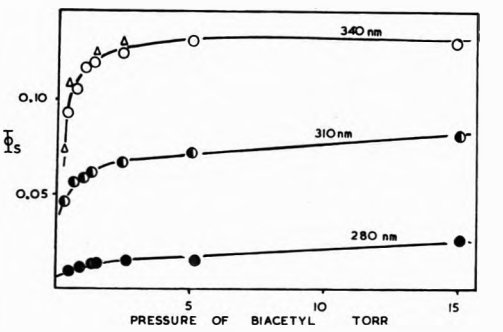

Figure 7. Quantum yields of sensitized phosphorescence of biacetyl from 30 Torr of DCTFA as a function of biacetyl pressure at 20°: O mercury-free system, Δ results from mercury-saturated system.

TABLE III: Quantum Yields of Intersystem Crossing (ϕ_{ISC}) for Halogenated Ketones Determined by the Sensitized Phosphorescence of Biacetyl Technique

Compd	Pressure of compound, Torr	Excitation wavelength, nm	ϕ_{ISC}
CPFA	29	340	0.92
	29	310	0.65
	29	280	0.23
DCTFA	30	340	0.91
	30	310	0.45
	30	280	0.09
	80	340	0.92
	80	310	0.76
	80	280	0.42
	40	280	0.20
	25	280	0.11
	15	280	0.07
	10	280	0.05
	5	280	0.01
TCTFA	30	340	0.37
	30	310	0.12
	30	280	0.01

Wavelength Dependence of k_{NR}

Table II indicates that for the three chlorinated ketones considered here, the value of k_{NR} increases markedly with increase in photon energy, as is seen in HFA. It is necessary to understand the nature of the nonradiative process to explain such results. The results for each compound will be discussed in turn.

DCTFA. The results discussed so far may be explained by the following mechanism

$$A + h\nu \longrightarrow {}^1A_n \quad (2)$$

$${}^1A_n \longrightarrow A + h\nu_f \quad (3)$$

$${}^1A_n \longrightarrow \text{nonradiative decay} \quad (4)$$

$${}^1A_n + A \longrightarrow {}^1A_0 + A \quad (5)$$

$${}^1A_0 \longrightarrow A + h\nu_f \quad (6)$$

$${}^1A_0 \longrightarrow \text{nonradiative decay} \quad (7)$$

where A is the ketone, superscripts refer to multiplicity of excited states, and subscripts to vibrational content. Ambiguous points are (i) the number of steps in the vibrational relaxation mechanism which is represented here as a one step process for simplicity (discussed in a subsequent paper); and (ii) the nature and the products of the radiationless processes 4 and 7.

The second point was investigated using the technique of the sensitization of the phosphorescence of biacetyl to probe S_1–T_1 intersystem crossing in the ketone. Before investigation of the emission from biacetyl sensitized by DCTFA, it was necessary to establish the effect of biacetyl upon the fluorescence of DCTFA. The results which will be discussed in a subsequent paper show that the fluorescence is quenched at all wavelengths with rate constant $2.8 \times 10^{10}\ M^{-1}\ \text{sec}^{-1}$.

The emission of biacetyl sensitized by 40 Torr of DCTFA excited at 340, 310, and 280 nm is shown in Figure 7. Equivalent plots for 5, 10, 15, and 25 Torr of DCTFA excited at 280 nm are shown in Figure 8.

The results were obtained on the mercury-free system, however, it was found that the presence of mercury did not affect the shape of the sensitization curve and hence it was concluded that mercury did not quench the triplet state of DCTFA. One such plots obtained on a mercury-saturated system is shown in Figure 7.

The following additional steps are consistent with these observations

$${}^1A_n + B \longrightarrow A + {}^1B \quad (8)$$

$${}^1A_0 + B \longrightarrow A + {}^1B \quad (9)$$

$${}^3A_m + B \longrightarrow {}^3B + A \quad (10)$$

$${}^1B \longrightarrow {}^3B \quad (11)$$

$${}^3B \longrightarrow B + h\nu_p \quad (12)$$

$${}^3B \longrightarrow B \quad (13)$$

$${}^3A_m \longrightarrow D \quad (14)$$

where B = biacetyl.

^3A_m arises wholly from reactions 4 and/or 7. The observed quenching of the fluorescence of DCTFA is undoubtedly a consequence of electronic energy transfer to give singlet biacetyl. The vibrational energy of the excited singlet biacetyl molecule will be governed by the overlap of the biacetyl absorption spectrum and the emission spectrum of ^1A_n. Thus the excited singlet state biacetyl molecule is formed with a range of vibrational energy equivalent to optical excitation with wavelengths less than 350 nm. It has been shown that at pressures greater than 50 Torr such excitation results in a phosphorescence quantum yield of 0.145,[4] however, at pressures below 40 Torr this yield is pressure dependent. Thus at experimental pressures of above 50 Torr singlet energy transfer cannot decrease the yield of sensitized phosphorescence of biacetyl as has been noted for aromatic molecules. Indeed, if reaction 4 and/or 7 is partitioned between decomposition and intersystem crossing singlet–singlet energy transfer will result in an increase in ϕ_s. Following excitation at 340 nm steps 3, 4, and 5 can be neglected since absorption produces the equilibrated level of the excited singlet state, and the quantum yield of sensitized phosphorescence of biacetyl ϕ_s is given by

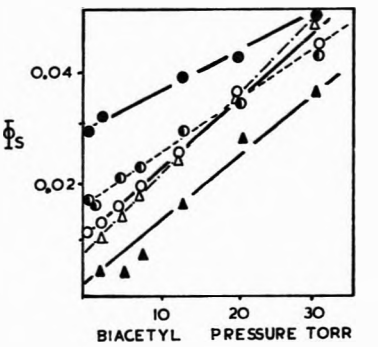

Figure 8. Quantum yields of sensitized phosphorescence of biacetyl against biacetyl pressure for DCTFA-sensitized, 280-nm excitation: filled circles, 40 Torr of DCTFA; half-filled circles, 25 Torr; open circles, 15 Torr; open triangles, 10 Torr, filled triangles, 5 Torr DCTFA.

$$\phi_S = \frac{k_{12}}{k_{12} + k_{13}}\left[\frac{k_9[B]}{k_6 + k_7 + k_9[B]} + \frac{k_7}{(k_6 + k_7 + k_9[B])}\,\frac{k_{10}[B]}{(k_{14} + k_{10}[B])}\right] \quad (15)$$

Inspection of Figure 7 shows that for pressures of biacetyl above about 5 Torr $k_{10}[B] \gg k_{14}$, and thus

$$\phi_S = \frac{k_{12}}{k_{12} + k_{13}}\left[\frac{k_7 + k_9[B]}{k_6 + k_7 + k_9[B]}\right] \quad (16)$$

We require the value of ϕ_S would have in the absence of singlet energy transfer, and an estimate may be obtained by extrapolation of the values obtained at pressures of biacetyl of 5 Torr and above to zero pressure of biacetyl. Such treatment introduces inaccuracies, but the values may nevertheless be used to give an estimate of the intersystem crossing quantum yield ϕ_{ISC} under these conditions where ϕ_{ISC} is given by $k_6/(k_6 + k_7)$ and where $k_{12}/(k_{12} + k_{13}) = 0.145$.[4]

Table III shows that at 340-nm excitation, the sum of fluorescence and intersystem crossing yields is within experimental error of unity, and thus the assumption that $k_7 = k_{ISC}$ is justified. Under these conditions the decomposition observed by Bowles, Majer, and Robb[12] must originate in the triplet state of the ketone since the decomposition yield is greater than 0.85, as shown earlier.[3,13,14] Table III shows that under conditions such that the excited singlet state of the ketone is not fully equilibrated, the sum of intersystem crossing determined as above and fluorescence quantum yields is considerably less than unity. There are at least two indistinguishable mechanisms which can explain this trend. In the first it may be postulated that the excited singlet DCTFA molecule suffers

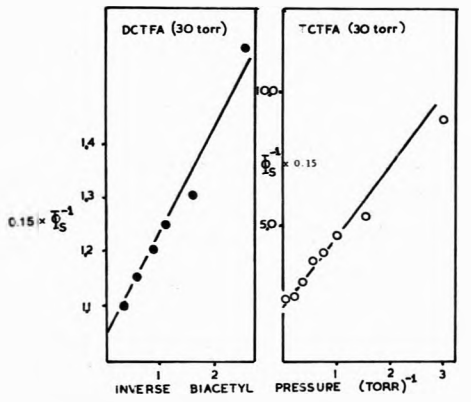

Figure 9. Inverse quantum yield of sensitized phosphorescence of biacetyl against inverse biacetyl pressure for DCTFA and TCTFA sensitizers, 340-nm excitation. Ordinate plotted is $0.15/\phi_B$.

some fate other than intersystem crossing. This is probably decomposition. This mechanism would explain the increasing k_{NR} with decreasing wavelength in terms of the increasing importance of decomposition. The increase in ϕ_S at pressures of biacetyl greater than 5 Torr would then be ascribed to singlet–singlet energy transfer.

In the second mechanism, the increase in k_{NR} is ascribed solely to intersystem crossing with the provision that ISC from high vibrational levels of the singlet state will produce triplet state molecules which are themselves highly vibrationally excited and more prone to decomposition and hence of shorter lifetime. In this model the increase in ϕ_S at pressures of biacetyl greater than 5 Torr is ascribed to the shorter lifetime of the triplet state formed by ISC from vibrationally excited singlets. It can be seen that the two mechanisms become completely indistinguishable when the lifetime of the triplet state produced by ISC becomes equal to the lifetime of the singlet state which produces the triplet state. Processes which shorten the lifetime of the triplet state at high internal vibrational energies can be envisaged as decomposition or crossing of the triplet state by another (possibly dissociative) electronic energy level of the same multiplicity.

Given the above observations it would seem improbable that quenching technique would be able to distinguish between processes occurring from the singlet and triplet manifolds, especially in view of the noted similarity in the quenching rate constants of singlet and triplet carbonyl molecules. However, our mechanism and treatment of the data is able to distinguish, albeit crudely, between "long-lived" excited triplet states and "short-lived" excited states. Since the decomposition quantum yield is greater than 0.85 under all the conditions studied, the long-lived triplet states must, in the absence of quencher, all eventually decompose.[12]

The biacetyl-sensitized emission plots can be used to obtain an estimate of the lifetime of the long-lived triplet states of DCTFA. Following excitation at 340 nm of 30 Torr of DCTFA and ignoring singlet–singlet electronic transfer at low pressures of biacetyl eq 15 reduces to

$$\phi_S = \frac{k_{12}}{k_{12} + k_{13}} \left[\frac{k_7}{k_6 + k_7} \frac{k_{10}[B]}{k_{14} + k_{10}[B]} \right] \quad (17)$$

Thus a plot of ϕ_S^{-1} against $[B]^{-1}$ will have a slope to intercept ratio of k_{14}/k_{10}. Such a plot is shown in Figure 9. The ratio k_{14}/k_{10} derived from this plot is $k_{14}/k_{10} = 0.93 \times 10^{-5}$ M. If we assume that $k_{10} = 3 \times 10^{10}$ M^{-1} sec^{-1} then $k_{14} = 2.8 \times 10^5$ sec^{-1}, or the DCTFA triplet has a lifetime of 3.6 μsec.

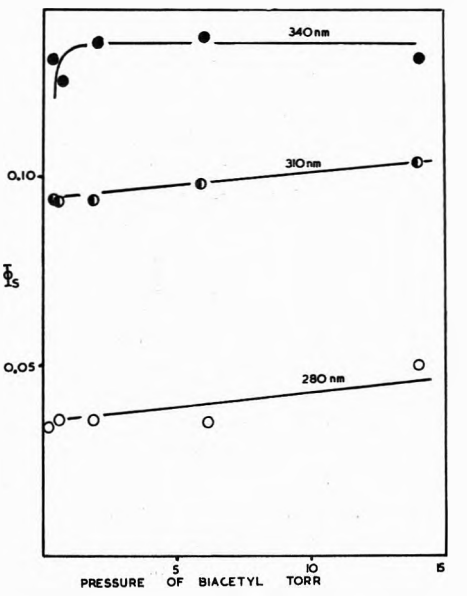

Figure 10. Quantum yield of sensitized phosphorescence of biacetyl from 30 Torr of CPFA as a function of biacetyl pressure for various excitation wavelengths, 20°.

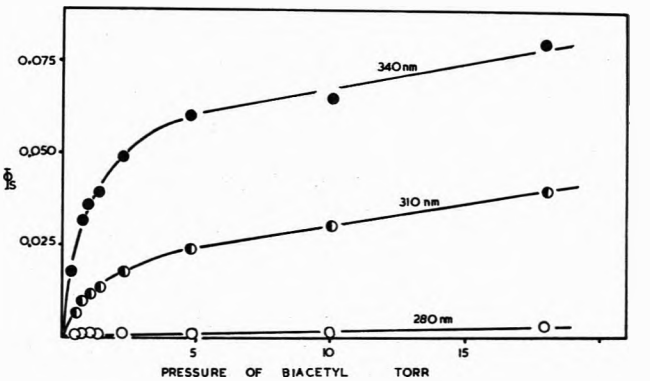

Figure 11. Quantum yields of sensitized phosphorescence of biacetyl from 30 Torr of TCTFA at 20° as a function of biacetyl pressure at different wavelengths of excitation.

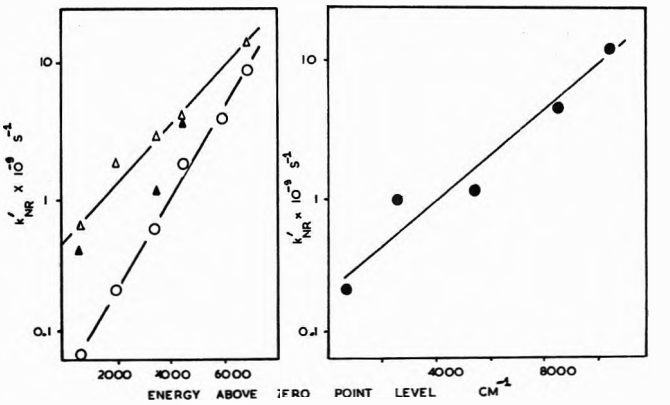

Figure 12. Plots of k_{NR}' as a function of excess vibrational energy in the singlet manifolds for HFA (filled circles), CPFA (open circles), DCTFA (open triangles), and TCTFA (filled triangles). k_{NR}' is difference between k_{NR} at any wavelength and that for excitation to zero-point level of excited singlet state.

CPFA. The photochemistry of this compound parallels

that of DCTFA discussed above. Values of ϕ_{ISC} deduced by extrapolation of eq 16, Figure 10 as for DCTFA, are shown in Table III. Unfortunately no quantum yields of decomposition have been measured. The lifetime of CPFA triplet must be greater than that of DCTFA since the smallest pressure of biacetyl used (0.3 Torr) was sufficient to quench all the CPFA triplet, following excitation at 340 nm.

TCTFA. The quantum yields of intersystem crossing deduced by extrapolation of eq 16, Figure 11, are shown in Table III. The lifetime of TCTFA deduced from a plot of ϕ_S^{-1} against $[B]^{-1}$ (Figure 9) assuming that $k_{10} = 3 \times 10^{10}\ M^{-1}\ sec^{-1}$ is 0.5 μsecs. The quantum yield of CO production at 20° of 45 Torr of TCTFA following excitation at 313 nm has been measured as 0.92,[15] and it is evident therefore that as for DCTFA, either there is considerable singlet decomposition at 310-nm excitation, or there are short-lived dissociative triplet states formed which are not quenched by biacetyl. It can be seen that even at the longest wavelengths used in this study the quantum yield of intersystem crossing to detectable triplet levels for TCTFA is smaller than that for CPFA and DCTFA. In the case of TCTFA, therefore, some other process of energy dissipation is of importance at long wavelengths of excitation.

It is evident from Table III that increase in photon energy causes a rapid increase in k_{NR} for all three ketones studied here, and this increase is not associated with an increase in detectable triplet state formation. Figure 12 shows a plot of $(k_{NR} - (k_{NR})_0)$ against excess vibrational energy in the singlet manifold. $(k_{NR})_0$ is the value of k_{NR} for excitation to the zero-point level of the singlet state. These data were obtained from the zero pressure results at the appropriate wavelengths. It can be seen that k_{NR}' $[k_{NR}' = (k_{NR} - (k_{NR})_0)]$ increases exponentially with excess energy for CPFA, DCTFA, and HFA. Data for TCTFA are less satisfactory, but this is expected in view of the fact that intersystem crossing does not account for the entire magnitude of $(k_{NR})_0$ for this compound.

Halpern and Ware[7] have compared their observed increase in k_{NR} for HFA with that predicted by Bowers[16] from an RRKM calculation of the dissociation of singlet hexafluoroacetone and have rejected the singlet decomposition on the basis of the disagreement of the two trends.

It should be noted that Bowers' calculation is only of an approximate nature, is based upon data measured upon mercury-saturated vacuum lines, and makes no distinction between singlet and triplet decomposition. The RRKM calculation should also include factors which account for the fact that intersystem crossing might be favored in some modes.

In view of the fact that singlet decomposition would lead to an exponential dependence of rate constant upon excess energy as observed, and that earlier studies showed that for DCTFA the concept of singlet decomposition could account for observed quenching behavior, it is tempting to associate the increase in k_{NR} with photon energy for the compounds studied here with a new dissociative decay channel in the singlet manifold. However, the reservation quoted earlier still applies in that an enhancement of nonradiative decay to a dissociative triplet level would show similar behavior.

Acknowledgments. We wish to thank Dr. A. W. Sloman for his able assistance in setting up the photon-counting equipment. We gratefully acknowledge the financial support of the Science Research Council, The Royal Society, and Monsanto Chemicals Ltd.

References and Notes

(1) D. Phillips, D. Gray, and K. Al-Ani, *J. Chem. Soc.*, 905 (1971).
(2) A. Gandini and K. O. Kutschke, *Proc. Roy. Soc.*, **306**, 511 (1968).
(3) P. A. Hackett and D. Phillips, *J. Chem. Soc., Faraday Trans. 1*, **68**, 323 (1972).
(4) G. M. Almy and P. R. Gillett, *J. Chem. Phys.*, **11**, 188 (1943).
(5) W. A. Noyes, Jr., D. Harter, and W. A. Mulac, *J. Chem. Phys.*, **44**, 2100 (1966).
(6) H. Ishikawa and W. A. Noyes, Jr., *J. Chem. Phys.*, **37**, 583 (1962).
(7) A. M. Halpern and W. R. Ware, *J. Chem. Phys.*, **53**, 1969 (1970).
(8) A. Gandini, D. A. Whytock, and K. O. Kutschke, *Proc. Roy. Soc., Sec. A*, **306**, 529 (1968).
(9) A. Albrecht, *J. Chem. Phys.*, **33**, 156 (1960).
(10) A. M Halpern and W. R. Ware, *J. Chem. Phys.*, **54**, 1271 (1971).
(11) G. R. Fleming, O. L. J. Gijzeman, and S. H. Lin, *Chem. Phys. Lett.*, 21, 527 (1973).
(12) R. B. Bowles, J. R. Majer, and J. C. Robb, *Trans. Faraday Soc.*, **58**, 2394 (1962).
(13) P. A. Hackett and D. Phillips, *J. Chem. Soc., Faraday Trans. 1*, **68**, 329 (1972).
(14) P. A. Hackett and D. Phillips, *J. Chem. Soc., Faraday Trans. 1*, **68**, 335 (1972).
(15) J. R. Majer, C. Olavesen, and J. C. Robb, *J. Chem. Soc. A*, 893 (1969); *J. Chem. Soc. B*, 48 (1971).
(16) P. G. Bowers, *Can. J. Chem.*, **46**, 307 (1968).

Photochemistry of Halogenated Acetones. III. Vibrational Relaxation in Singlet States

Peter A. Hackett and David Phillips*[1]

Department of Chemistry, The University, Southampton SO9 5NH, England *(Received June 19, 1973; Revised Manuscript Received January 14, 1973)*

Single-step and two-step mechanisms for vibrational relaxation in the first excited singlet state manifold of CPFA and DCTFA are tested. Results are not unambiguous, but better agreement is obtained for a two-step mechanism, in agreement with that proposed for HFA. Rate constants are given.

Introduction

Investigations into the gas-phase photochemistry of carbonyl compounds can be performed in two ideal pressure conditions. In the first case the experimental pressure is high enough to ensure complete vibrational relaxation of the optically formed excited state. In this high-pressure region only the photochemistry of the Boltzmann distribution of vibrational levels is observed. In the second ideal case the experimental pressure is low enough that molecular collisions become unimportant during the lifetime of the excited state produced optically. In this low-pressure region the photochemistry of the vibronic state formed by optical excitation, modified only by any intramolecular vibrational redistribution, is observed. It has been shown in the preceding paper that the rates of primary processes are dependent upon the internal energy of the excited state. This is implied by the increase in Φ_F with ketone pressure following excitation with short wavelength radiation.

In practice most experiments are performed utilizing an excitation energy greater than the energy of the 0–0 transition, and an intermediate experimental pressure. The first condition is often imposed by the use of mercury vapour lamps or polychromatic radiation, the second because of the necessity of obtaining measurable yields of products, which thus necessitates having significant absorption (high pressure), but negligible relaxation (low pressure). The results of these nonideal experimental conditions is that the experimental observations are made upon an unknown distribution of vibrational levels between those formed optically and the Boltzmann distribution. Given these observations it becomes important to know the mechanism of the relaxation of the optically formed vibrational distribution into the Boltzmann distribution of vibrational levels. This paper presents an attempt to clarify this mechanism for chloropentafluoroacetone (CPFA) and 1,3-dichlorotetrafluoroacetone (DCTFA), and compares this with the available data on vibrational relaxation in hexafluoroacetone (HFA).

Results

Many of the experimental results discussed here have been presented in the preceding paper. They are the pressure dependence of the fluorescence quantum yield of CPFA and DCTFA following excitation at 340, 325, 310, 300 and 280 nm, and the zero pressure radiative and nonradiative rate constants measured at the same excitation wavelengths.

Additional results given here are the fluorescence decay curves of CPFA and DCTFA measured at pressures between 2 and 12 Torr, following excitation at 300 nm. These decay curves were nonexponential. A typical curve is shown in Figure 1. Figure 2 shows the effect of octafluorocyclobutane upon the fluorescence quantum yield of DCTFA.

Discussion

Two mechanisms for vibrational relaxation were tested. In the first mechanism it was assumed every collisional deactivation encounter removed all the excess vibrational energy of the excited state. This mechanism is the equivalent of the "hard-sphere" collisional deactivation often used as a first approximation. This mechanism is shown below.

$A + h\nu \longrightarrow {}^1A_n$	absorption	
${}^1A_n \xrightarrow{k_1} A + h\nu_F$	fluorescence	(1)
${}^1A_n \xrightarrow{k_2} D$	nonradiative decay	(2)
${}^1A_n + A \xrightarrow{k_3} {}^1A_0 + A$	vibrational relaxation	(3)
${}^1A_0 \xrightarrow{k_4} A + h\nu_F$	fluorescence	(4)
${}^1A_0 \xrightarrow{k_5} D$	nonradiative process	(5)

where A is the ketone, subscripts refer to vibrational energy content and superscripts to multiplicity of excited states.

A solution of these equations in the steady-state approximation is

$$\Phi_F = \frac{k_1}{k_1 + k_2 + k_3[A]} + \frac{k_4 k_3[A]}{(k_1 + k_2 + k_3[A])(k_4 + k_5)} \quad (6)$$

or

$$k_3 = \frac{\Phi_F(k_1 + k_2) - k_1}{[A](\Phi_{F_\infty} - \Phi_F)} \quad (7)$$

where $\Phi_{F_\infty} = k_4/(k_4 + k_5)$ is the fluorescence yield of the Boltzmann distribution of vibrational levels.

k_3 was calculated from eq 7 for experimental values of Φ_F at excitation wavelengths of 325, 310, 300, and 280 nm at varying pressures of CPFA and DCTFA. The variation in k_3 with the experimental pressure is shown in Figure 3A (CPFA) and 3B (DCTFA).

The second mechanism tested is shown below

$A + h\nu \longrightarrow {}^1A_n$	absorption	
${}^1A_n \xrightarrow{k_8} A + h\nu_F$		(8)
${}^1A_n \xrightarrow{k_9} D$		(9)

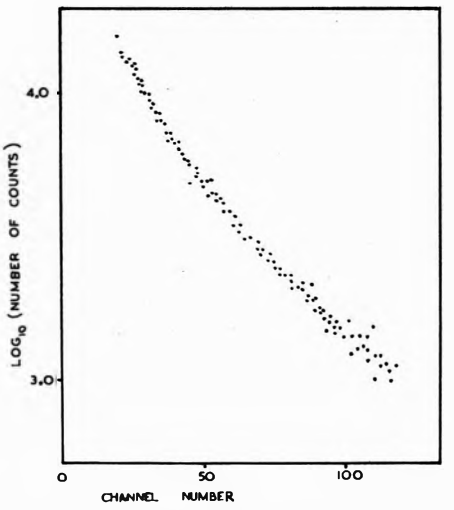

Figure 1. Typical nonexponential decay curve. Fluorescence decay of 4 Torr of CPFA excited at 300 nm (0.64 nsec per channel).

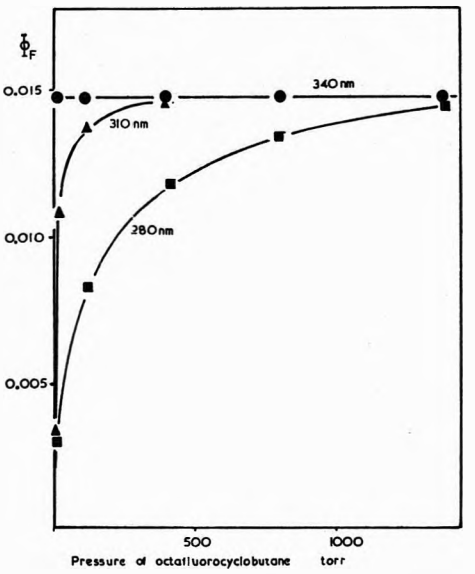

Figure 2. Effect of pressure of octafluorocyclobutane on the fluorescence quantum yield of DCTFA at 20°: circles, 340-nm excitation; triangles, 310-nm excitation; squares, 280-nm excitation.

$$^1A_n + A \xrightarrow{k_{10}} {}^1A_m + A \quad (10)$$

$$^1A_m \xrightarrow{k_{11}} A + h\nu_F \quad (11)$$

$$^1A_m \xrightarrow{k_{12}} D \quad (12)$$

$$^1A_m + A \xrightarrow{k_{10}} {}^1A_0 + A \quad (10)$$

$$A_0 \xrightarrow{k_{13}} {}^1A_0 + h\nu_F \quad (13)$$

$$^1A_0 \xrightarrow{k_{14}} D \quad (14)$$

Solution for Φ_F gives

$$\Phi_F = \frac{k_8}{k_8 + k_9 + k_{10}[A]} + \frac{k_{11}}{(k_{11} + k_{12} + k_{10}[A])} \frac{k_{10}[A]}{(k_8 + k_9 + k_{10}[A])} + \frac{k_{13}}{(k_{13} + k_{14})} \frac{k_{10}[A]}{(k_{11} + k_{12} + k_{10}[A])} \frac{k_{10}[A]}{(k_8 + k_9 + k_{10}[A])} \quad (16)$$

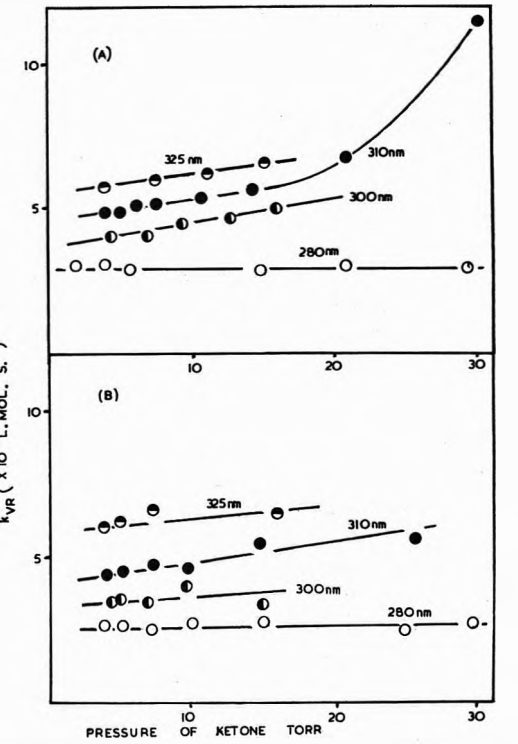

Figure 3. Rate constants for vibrational relaxation from quantum yield data assuming one-step deactivation: (A) CPFA, (B) DCTFA. For successful model, computed value of rate constant should be invariant with pressure.

or

$$0 = (\Phi_{F\infty} - \Phi_F)y^2 + (k_8 + k_{11} - \Phi_F(k_{12} + k_9))y + k_8k_{12} - \Phi_Fk_{12}k_9 \quad (17)$$

where $\Phi_{F\infty} = k_{13}/(k_{13} + k_{14})$ is the fluorescence quantum yield of the Boltzmann distribution of vibrational levels, and $y = k_{10}[A]$.

The derivation of eq 17 uses the valid approximation that $k_8 + k_9 \simeq k_9$ and that $k_{11} + k_{12} \simeq k_{12}$. The mechanism further assumes that all deactivation steps have the same rate constant, k_{10}. Equation 17 was solved for k_{10} at experimental values of Φ_F at excitation wavelengths of 310, 300, and 280 nm. The intermediate level (^1A_m) was arbitrarily assigned to be midway between ^1A_n and $^1A_0$ in energy. Thus zero pressure rates following optical excitation at 325 nm were used to test Φ values at 310 and 300 nm, and zero pressure rates following optical excitation at 300 nm were used to test the data obtained at 280 nm. Values of k_{10} deduced from this treatment are shown in Figure 4A (CPFA) and 4B (DCTFA).

The two mechanisms were tested further by analysis of the nonexponential fluorescence decay curves. Inspection of the first mechanism yields

$$I_f(t) \propto \left[k_1 + \frac{k_4k_3[A]}{\tau_2^{-1} - \tau_1^{-1}}\right] \exp(-t/\tau_1) - \left[\frac{k_4k_3[A]}{\tau_2^{-1} - \tau_1^{-1}}\right] \exp(-t/\tau_2) \quad (18)$$

where $\tau_2^{-1} = k_4 + k_5$, and $\tau_1^{-1} = k_1 + k_2 + k_3[A]$, and $I_f(t)$ is the time-resolved fluorescence intensity. This equation with one adjustable parameter k_3 was used to fit each decay curve by the method of least squares, using the computer. The variation in k_3 with experimental pressure is shown in Figure 5.

Inspection of the second mechanism yields

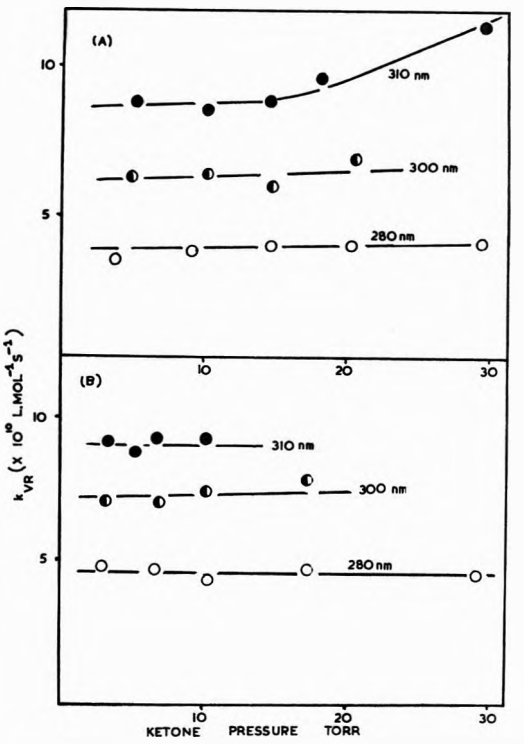

Figure 4. Rate constants for vibrational relaxation from quantum yield data assuming two-step deactivation: (A) CPFA, (B) DCTFA. Successful model would show k_{VR} invariant with pressure.

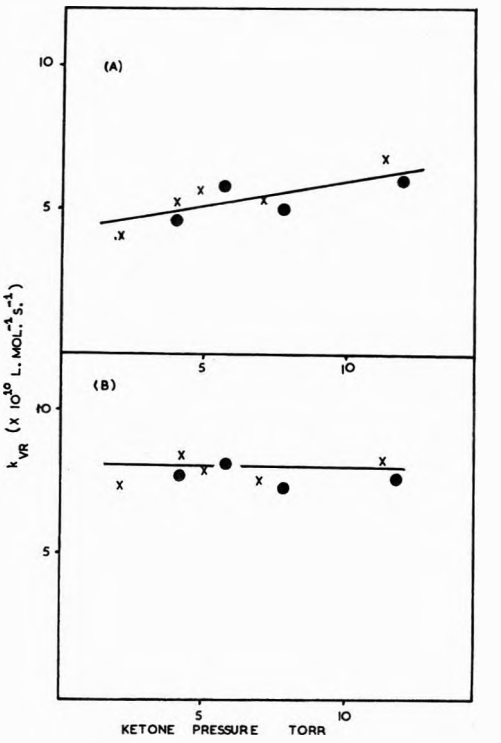

Figure 5. Rate constants for vibrational relaxation from decay time data at 300-nm excitation assuming (A) one-step and (B) two-step deactivation: circles, DCTFA; crosses, CPFA. Mechanism B clearly leads to values of k_{VR} invariant over the pressure range studied, and is thus to be preferred.

$$I_f(t) \propto \left[\frac{k_{10}^2 k_{13}[A]^2}{(\tau_3^{-1} - \tau_2^{-1})(\tau_2^{-1} - \tau_2^{-1})}\right] \exp(-t/\tau_1) - \left[\frac{k_{10}k_{11}[A]}{(\tau_2^{-1} - \tau_3^{-1})} + \frac{k_{10}^2 k_{13}[A]^2}{(\tau_2^{-1} - \tau_3^{-1})(\tau_1^{-1} - \tau_2^{-1})}\right] \exp(-t/\tau_2) + \left[\frac{k_8 k_{10} k_{11}[A]}{(\tau_2^{-1} - \tau_3^{-1})} + \frac{k_{10}^2 k_{13}[A]^2}{(\tau_2^{-1} - \tau_3^{-1})(\tau_1^{-1} - \tau_3^{-1})}\right] \exp(-t/\tau_3) \quad (19)$$

where $\tau_1^{-1} = k_{13} + k_{14}$, $\tau_2^{-1} = k_{10} + k_{11} + k_{12}$, $\tau_3^{-1} = k_8 + k_9 + k_{10}[A]$. Analysis of the nonexponential decay curves was then made using eq 19.

Figure 5 shows the values of k_3 deduced from this treatment.

This approach is exactly that of Halpern and Ware[2] in their treatment of the nonexponential decay curves from hexafluoroacetone (HFA). These authors found that k_3 increased linearly with pressure over a pressure range from 1 to 15 Torr, as has been found in this study. They presented k_{10} values determined at three pressures between 2 and 6 Torr (ignoring much more data at higher pressures) and concluded that because these values are constant within experimental uncertainty that the second mechanism is validated over the first. However, the scatter in the three points presented would allow k_{10} to be a quantity increasing with pressure with the same magnitude as k_3. Hence we feel that the analysis by Halpern and Ware[2] cannot be accepted as proof or disproof of either mechanism.

Kutschke[3-6] has presented various graphical tests which support the weak multistep mechanism of collisional deactivation. However, these tests involved the assumption that the phosphorescence yield was proportional to the fluorescence yield of the Boltzmann distribution, *i.e.*, that phosphorescent triplet state HFA molecules are only produced by intersystem crossing from the Boltzmann distribution of singlet vibrational levels. Ware[2] has shown that this approximation is invalid and hence the results presented by Kutschke are no longer rigorously correct.

TABLE I: Rate Constants (k_{VR}) for Vibrational Relaxation of DCTFA[a] by Octafluorocyclobutane (OFCB)

Excitation wavelength, nm	OFCB pressure, Torr	$k_{20} \times 10^{-10}$, M^{-1} sec^{-1} [b]	$k_{22} \times 10^{-10}$, M^{-1} sec^{-1} [b]
280	100	2.7	2.7
280	400	2.6	2.9
280	800	2.6	2.8
280	1400	7.0	8.2
310	100	5.3	8.5

[a] DCTFA pressure = 30 Torr. [b] Explanation in text.

The data presented here make a distinction between the two mechanisms no less difficult. The increase in k_3 and k_{10} at high ketone pressures probably points to the failure of both mechanisms to explain the observed results. However k_{10} varies less with pressure than k_3 at low ketone pressures (Figure 3) and hence the two-step mechanism is a better approximation than the one-step collisional deactivation mechanism. This could also be inferred from the fact that k_{10} is closer to the gas kinetic collisional rate constant (2.2×10^{11} M^{-1} sec^{-1}) than k_3. The decrease in k_3 and k_{10} with decreasing wavelength of excitation implies that more deactivation steps should be invoked at high internal energies of the optically formed state. It would be a simple matter to test multistep collisional deactivation mechanisms, using computations based upon radiative and nonradiative rates interpolated from the zero pressure rates already measured. However,

it is felt that such computations would require more precise data to give meaningful results.

When an inert gas is present it is necessary to add the following step to the first mechanism

$$^1A_n + M \xrightarrow{k_{20}} {}^1A_0 + M \quad (20)$$

which yields

$$k_3[A] + k_{20}[M] = \frac{\Phi_F(k_1 + k_2) - k_1}{(\Phi_{F_\infty} - \Phi_F)} \quad (21)$$

The following steps are added to the second mechanism

$$^1A_n + M \xrightarrow{k_{22}} {}^1A_m + M \quad (22)$$

$$^1A_m + M \xrightarrow{k_{23}} {}^1A_0 + M \quad (23)$$

and eq 17 is only changed by the fact that y is now equal to $k_{10}[A] + k_{22}[M]$. The values of k_{20} and k_{22} deduced from eq 21 and 17 for the vibrational relaxation of DCTFA by octafluorocyclobutane at excitation wavelengths of 310 and 280 nm are shown in Table I.

Here it is more difficult to determine which scheme is the closest approximation to reality, since values obtained are similar, and both increase at very high pressures of added gas. Either mechanism would give a rate constant smaller than that obtained for relaxation by the ketone itself. This result is expected since there will be better matching of vibrational frequencies in the ketone.

References and Notes

(1) Author to whom correspondence should be addressed.
(2) A. M. Halpern and W. R. Ware, *J. Chem. Phys.*, **53**, 1969 (1970).
(3) (a) D. A. Whytock and K. O. Kutschke, *Proc. Roy. Soc., Ser. A*, **306**, 503 (1968); (b) A. Gandini and K. O. Kutschke, *ibid.*, 511 (1968).
(4) A. Gandini, D. A. Whytock, and K. O. Kutschke, *Proc. Roy. Soc., Ser. A*, **306**, 529 (1968).
(5) A. Gandini, D. A. Whytock, and K. O. Kutschke, *Proc. Roy. Soc., Ser. A*, **306**, 537 (1968).
(6) A. Gandini, D. A. Whytock, and K. O. Kutschke, *Proc. Roy. Soc., Ser. A*, **306**, 541 (1968).

Photochemistry of Halogenated Acetones. IV. Quenching of the Excited States

Peter A. Hackett and David Phillips*

Department of Chemistry, The University, Southampton SO9 5NH, England *(Received June 19, 1973; Revised Manuscript Received January 14, 1974)*

The quenching of the relaxed excited singlet states of DCTFA and TCTFA by a variety of unsaturated and saturated hydrocarbons has been investigated. For unsaturated quenchers a good inverse correlation between ionization potential of quencher and quenching rate constant was found suggesting the initial formation of a charge transfer complex, as has been proposed for HFA and CPFA. Triplet quenching data for DCTFA was reevaluated, and mechanisms of quenching are discussed.

Introduction

During the course of a study of abstraction reactions of CF_2Cl radicals it was observed that the decomposition of 1,3-dichlorotetrafluoroacetone (DCTFA) was quenched by added cyclopentane, perfluorocyclopentane,[1] and benzene.[2] It has also been shown that DCTFA will form stable oxetane adducts with perfluoro olefins upon liquid-phase photolysis[3] at −78°. It was the purpose of this part of the work to determine the role of the singlet and triplet excited states of the ketones in these and other interesting reactions.

The singlet and triplet state quenching of hexafluoroacetone (HFA) has been investigated[4-7] and more recently the quenching of singlet state chloropentafluoroacetone (CPFA) by alkanes[8] and alkenes[9] has been reported.

Results

Addition of up to 200 Torr of molecular oxygen had no effect upon the fluorescence yield of DCTFA or TCTFA. The effect of addition of inert gases such as octafluorocyclobutane and perfluoro-2-butene has been discussed in the earlier papers.

Biacetyl, benzene, cyclohexane, butadiene, *cis*- and *trans*-2-butene quenched the fluorescence of DCTFA, the last three compounds with the same efficiency. Results for the quenching of DCTFA by these molecules and also by a variety of olefins were given in an earlier paper.[10]

Stern–Volmer plots (ϕ_{F0}/ϕ_F) for the fluorescence quenching of TCTFA by butadiene, *cis*-2-butene and *trans*-2-butene are shown in Figure 1. Similar plots for quenching of the fluorescence of CPFA, DCTFA, and TCTFA by biacetyl are given in Figure 2.

The fluorescence quenching behavior upon excitation at 340 nm may be discussed using the following mechanism

$$A \xrightarrow{I_A} {}^1A_0 \quad \text{excitation} \quad (1)$$

$$^1A_0 \xrightarrow{k_{NR}} D \quad \text{radiationless transition} \quad (2)$$

$$^1A_0 \xrightarrow{k_R} A + h\nu \quad \text{fluorescence} \quad (3)$$

$$^1A_0 + M \xrightarrow{k_Q} Q \quad \text{singlet quenching} \quad (4)$$

where A refers to HFA, CPFA, DCTFA, or TCTFA and M refers to the additive.

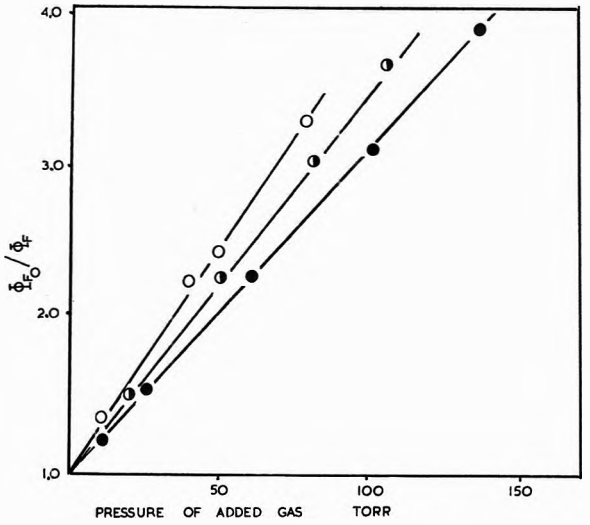

Figure 1. Stern–Volmer plots for quenching of the singlet state of TCTFA by olefins (excitation wavelength, 340 nm; 20°): open circles, 1,3-butadiene; half-filled circles, *trans*-2-butene; filled circles, *cis*-2-butene.

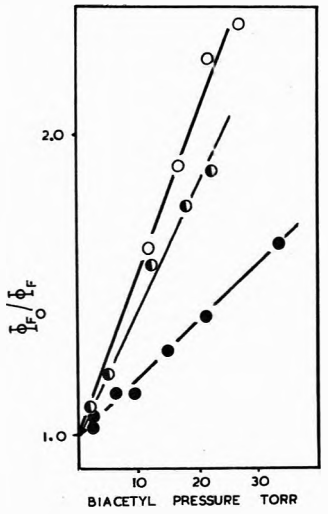

Figure 2. Stern–Volmer plots for quenching of singlet states of ketones by biacetyl (excitation wavelength, 340 nm; 20°): open circles, DCTFA; half-filled circles, CPFA; filled circles, TCTFA.

A consideration of the mechanism shows that

$$\phi_{F_0}/\phi_F = 1 + \frac{k_Q[M]}{k_R + k_{NR}} = 1 + k_Q[M]\tau_D \qquad (5)$$

where τ_D is the fluorescence decay time in seconds at zero pressure of additive.

If $P_{1/2}$ is the pressure of additive in Torr such that $\phi_{F0}/\phi_F = 2$ it follows that at 25°

$$k_Q = 1/((5.382P_{1/2} \times 10^{-\xi})(\tau_D))\ M^{-1}\ \text{sec}^{-1} \qquad (6)$$

Values of $P_{1/2}$ and k_Q deduced from the above procedure are shown in Table I. (τ_D values were obtained from earlier papers.)

The 2-butenes, benzene, cyclohexane, and perfluoro-2-butene all quenched the phosphorescence of biacetyl sensitized by DCTFA at 340 nm. Except for butadiene, addition of quencher had no effect upon the phosphorescence of biacetyl excited directly at 404.7 nm. Thus, any quenching observed was associated with the precursor of the biacetyl triplet state, which must be the excited state of the ketone. 1,3-Butadiene, however, quenches the triplet state of biacetyl, and thus competitive quenching experiments with this additive were not performed. Since the singlet state of DCTFA is quenched by some of these compounds, the quenching of the sensitized phosphorescence may be due to this cause, or to real triplet quenching, or both. Plots of ϕ_F/ϕ_S (where ϕ_F is the fluorescence quantum yield of DCTFA at any pressure of additive and ϕ_S is the corresponding yield of emission sensitized by biacetyl) against pressure of additive compensate for the singlet quenching and reveal the extent of true triplet quenching. Such plots are shown in Figure 3. These data were given in an earlier paper,[10] but in that case the value of ϕ_F had been determined incorrectly, leading to incorrect rate constants. It is thus worthwhile including the correct data here.

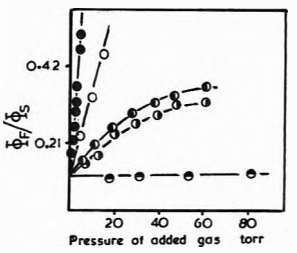

Figure 3. Quenching of DCTFA triplet state by hydrocarbons. Plots of ϕ_F/ϕ_S against pressure (see text). Figure taken from Figure 4, ref 10, normalized to corrected value of ϕ_F.

Quenching of the sensitized phosphorescence of biacetyl may be discussed using the following additional steps

$$^1A + B \xrightarrow{k_7} A + {}^1B \qquad (7)$$

$$^3A_m + B \xrightarrow{k_8} A + {}^3B \qquad (8)$$

$$^3A_m \xrightarrow{k_9} D \qquad (9)$$

$$^1B \xrightarrow{k_{10}} {}^3B \qquad (10)$$

$$^3B \xrightarrow{k_{11}} B + h\nu_p \qquad (11)$$

$$^3B \xrightarrow{k_{12}} B \qquad (12)$$

$$^3A_m + M \xrightarrow{k_{13}} Q \quad \text{triplet quenching} \qquad (13)$$

where B = biacetyl.

Assuming quenching of the excited singlet state DCTFA by biacetyl to be small under the conditions used in the competitive quenching experiments, then

$$\frac{\phi_F}{\phi_S} = \frac{k_{14} + k_{12}}{k_{11}} \frac{k_R}{k_{NR}} \frac{k_8[B] + k_9 + k_{13}[M]}{k_8[B]} \qquad (14)$$

Ratios of slope to intercept of such plots yield values of the rate constant ratio $k_{13}/(k_8[B] + k_9) = k_{13}\tau_{T,B}^{-1}$ where $\tau_{T,B}$ is the triplet state DCTFA lifetime in the presence of the experimental pressure of biacetyl. Values of this ratio are shown in Table II.

Discussion

The mechanism of DCTFA and TCTFA fluorescence quenching by olefin molecules will be considered first. Singlet–singlet energy transfer between olefin and ketone may be discounted as the first excited $\pi\pi^*$ singlet states of the olefins are at much higher energies than the $n\pi^*$ singlet states of the ketones. A collisionally induced intersystem crossing may be similarly discarded since not all the olefins are efficient quenchers of the ketone singlet state.

TABLE I: Quenching Parameters of Excited Singlet State CPFA,[a] DCTFA,[b] and TCTFA[c] at 25° Excited at 340 nm

Compd	Compound pressure, Torr	Quenching additive	Pressure range covered, Torr	Half-quenching pressure, Torr	$k_Q \times 10^{-10}$, M^{-1} sec^{-1}	IP, eV
DCTFA	80	*cis*-2-Butene	0–63	16.0	3.87	9.14
DCTFA	80	*trans*-2-Butene	0–67	16.0	3.87	9.12
DCTFA	80	1,3-Butadiene	0–43	16.0	3.87	9.07
DCTFA	80	Benzene	0–40	38.0	1.63	9.25
DCTFA	80	Ethylene	0–250	198	0.31	10.51
DCTFA	80	Vinyl fluoride	0–240	299	0.21	10.25
DCTFA	80	1,1-Difluoroethylene	0–200	326	0.19	10.31
DCTFA	80	Perfluoro-2-butene	0–300		0.01[d]	11.25
DCTFA	80	Cyclohexane	0–70	200	0.31	
DCTFA	80	Biacetyl	0–30	21.0	2.95	
CPFA	60	Biacetyl	0–35	23.8	2.23	
TCTFA	60	Biacetyl	0–35	52	2.86	
TCTFA	60	*cis*-2-Butene	0–140	47.5	3.13	9.12
TCTFA	60	*trans*-2-Butene	0–105	41.0	3.63	9.12
TCTFA	60	1,3-Butadiene	0–80	34.0	4.37	9.07
TCTFA	60	Cyclohexane	0–80		0.01[d]	
TCTFA	60	Perfluoro-2-butene	0–310		0.01[d]	11.25

[a] τ_D = 35 nsec. [b] τ_D = 30 nsec. [c] τ_D = 12.5 nsec. [d] Maximum values.

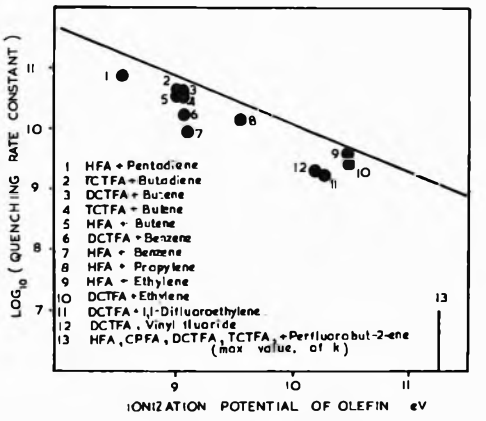

Figure 4. Correlation of efficiency of quenching of singlet states of ketones with ionization potential of olefin quenchers: solid line, correlation found for quenching of CPFA by 14 olefins (ref 9).

Hence it is more likely that the ketone molecule interacts chemically with the olefins, with the possible formation of a stable product. A notable correlation here, shown in Table I, is between the quenching rate constant of an olefin and its ionization potential. As the ionization potential of the quencher molecule decreases, its quenching rate constant is found to increase. A correlation of this type was noted for HFA fluorescence quenching by piperylene, 2-butene, propylene, benzene, and ethylene.[6] The measured quenching rate constants were 8×10^{10}, 3.5×10^{10}, 1.6×10^{10}, 8.2×10^{10}, and 4.1×10^{9} M^{-1} sec^{-1}, respectively. Perfluoropropylene was shown to have a negligible quenching effect. Another study of HFA fluorescence quenching gave k_Q for *cis*-2-butene and isobutene as 2.4×10^{10} and 2.7×10^{10}, respectively.[5]

The quenching of CPFA by 14 olefins has been recently reported[9] and it has been shown that the data fit the equation

$$\log k_Q = 18.0 - 0.79(\mathrm{IP}) \qquad (15)$$

where IP is the olefin ionization potential in electron volts and k_Q is the olefin bimolecular quenching rate constant.

Figure 4 shows this line plus the quenching data for HFA, DCTFA, and TCTFA fluorescence. It can be seen that the correlation holds for the four ketone molecules, with the provision that rates of CPFA fluorescence quenching seem in general to be greater than for the other molecules. This may be a reflection of the electron deficiency of the carbonyl oxygen. Thus $^1n\pi^*$ acetone is not quenched by olefins, dienes, or benzene in the gas phase or in solution,[11,12] but hexafluoroacetone obviously is. This is due to the electron-withdrawing effect of the CF_3 groups, which make the carbonyl oxygen more electron deficient in the $n\pi^*$ singlet and triplet excited states. This effect may be seen in the ground-state ionization potentials of these molecules: acetone (9.68 eV) and hexafluoroacetone (11.68 eV). Such values are not available for CPFA, DCTFA, or TCTFA, but may be reflected in the rate of fluorescence quenching of these molecules by *cis*-2-butene. The measured rates are 3.5×10^{10},[6] 5.6×10^{10},[5] 3.9×10^{10}, and 3.1×10^{10} M^{-1} sec^{-1} for HFA, CPFA, DCTFA, and TCTFA, respectively.

The correlation between ionization potential and quenching rate constant does not hold when the olefin is substituted with strongly electron-withdrawing groups on the double bond. Thus vinyl fluoride, vinylidene fluoride, and perfluoro-2-butene have lower quenching rate constants than would be expected on the basis of their ionization potentials. A similar effect has been noted in the fluorescence quenching of CPFA by chloroethylenes.[9]

Thus it has been shown that the excited singlet states of HFA interact with olefins *via* a charge transfer mechanism; the charge is transferred from the olefin to the carbonyl oxygen to give a complex which may dissociate to

TABLE II: Quenching Parameters of Triplet DCTFA[a] at 25° Excited at 340 nm

Compound	Pressure range studied, Torr	$k_{13}/(k_8([B] + k_9)$,[b] $M^{-1} \times 10^3$
cis-2-Butene	0–3.15	16.2
trans-2-Butene	0–3.08	16.2
Benzene	0–15	5.16
Cyclohexane	0–60	1.51
Perfluoro-2-butene	0–87	0.10

[a] Pressure of DCTFA = 80 Torr. [b] Pressure of biacetyl = 1.2 Torr.

give ground-state molecules, excited singlet ketone, or chemical reaction may occur

$$A^1 + Q \underset{k_2}{\overset{k_1}{\rightleftharpoons}} [AQ] \xrightarrow{k_3} [A^{\delta-} \cdots\cdots {}^{\delta+}Q] \xrightarrow{k_4} A + Q \quad (16)$$

$$\downarrow k_5$$

quenching product

The correlation implies that there are only small changes in the preexponential factors for the different quenching molecules. It also implies that the activation energy of the quenching reaction is linearly related to the ionization potential of the quenching molecule. If it is assumed that process k_1 is governed by the gas-kinetic collision rate ($k = \sigma_{AB}^2(8\pi kT/\mu)^{1/2}$ with values of σ_{AB} from ref 13 we find that $k_1 \approx 1.5 \times 10^{11}\ M^{-1}\ \text{sec}^{-1}$ for $\sigma_{AB}^2 = 20$ Å,[2] hence it would seem that one collision in every five is effective in producing the charge transfer intermediate. The nature of the collisional complex AQ and the difficulty in describing its lifetime have been discussed.[14]

Stable oxetanes have been detected in the liquid-phase photolysis of HFA and DCTFA with perfluoro-2-butene[3] and in the gas-phase photolysis of HFA and DCTFA with perfluoropropylene.[7] It is not, therefore, inconceivable that the charge transfer complex postulated reacts to form the closed ring oxetane; however, such an assertion would be dependent upon product identification. This was not attempted, although the formation of oxetanes from excited singlet $n\pi^*$ states has been postulated[15,16] and these systems might be worthy of further study.

Biacetyl quenches the fluorescence of CPFA, DCTFA, and TCTFA with rates of 2.2×10^{10}, 2.95×10^{10}, and 2.86×10^{10}. The rate constant of quenching of HFA fluorescence by biacetyl has been measured as $3.1 \times 10^{10}\ M^{-1}\ \text{sec}^{-1}$ by other workers using a technique similar to ours.[5] In view of the excellent overlap of the ketone emission spectra with the biacetyl absorption spectra, this interaction probably occurs by singlet–singlet energy transfer. Such an interaction would result in formation of a biacetyl molecule with sufficient energy to make decomposition inevitable. Obviously this energy transfer process occurs with a rate which is less than collisional and hence resonance energy transfer may be excluded. This observation is verified by a consideration of the k_R values for the four ketones: HFA, 2.2×10^5; CPFA, 5.65×10^5; DCTFA, 5×10^5; and TCTFA $3.4 \times 10^5\ \text{sec}^{-1}$. There is no apparent dependence of k_Q on k_R, as has been noted for energy transfer from aromatic compounds to cyclopentanone, 2-pentanone, and pyrazoline[17] and thus the energy transfer probably occurs by the exchange energy transfer mechanism.

Cyclohexane quenches the fluorescence of DCTFA with a rate constant of $3.1 \times 10^9\ M^{-1}\ \text{sec}^{-1}$. The formation of adducts between DCTFA and cyclopentane in gas-phase photolysis has been demonstrated[18] by the identification of reaction products due to the hydrogen abstraction reaction

$$(CF_2Cl)_2CO^* + \bigcirc \longrightarrow (CF_2Cl)_2\dot{C}OH + \bigcirc\cdot \quad (17)$$

$$(CF_2Cl)_2\dot{C}OH + \bigcirc \longrightarrow (CF_2Cl)_2CHOH + \bigcirc\cdot \quad (18)$$

It thus seems reasonable to explain the observed fluorescence quenching on the basis of the above mechanism. This proposition is supported by the observation that photolysis of DCTFA in cyclohexane solution[19] gives hydrogen abstraction products

$$(CF_2Cl_2)CO^* + \bigcirc \longrightarrow (CF_2Cl)_2\dot{C}OH + \bigcirc\cdot \longrightarrow (CF_2Cl)_2(C_6H_{11})OH \quad (19)$$

It has also been noted that cyclopentane quenches CPFA with rate constant 3.7×10^9 which is of the same order as that reported here between DCTFA and cyclohexane.

The quenching of HFA triplet has been investigated by phosphorescence decay time studies.[4] Since the phosphorescence decay time of HFA in the absence of quencher was known it was possible to extract absolute rate constants for triplet state quenching. When these rate constants were compared with the fluorescence quenching rate constants it was seen that a parallelism existed[6] for quenching rates of olefins. If we assume such a parallelism exists for all ketone molecules, which is reasonable since the carbonyl oxygen will be as electron deficient in triplet and singlet excited states, we can assign the rate of DCTFA triplet quenching by biacetyl to be $3 \times 10^{10}\ M^{-1}\ \text{sec}^{-1}$. We then obtain $k_8(\text{BiA}) + k_9 = 1.92 \times 10^6\ \text{sec}^{-1}$ and rate constants for quenching of DCTFA triplet by *cis*-2-butene, benzene, cyclohexane, and perfluoro-2-butene of 3.1×10^{10}, 9.8×10^9, 2.9×10^9, and $1.9 \times 10^8\ M^{-1}\ \text{sec}^{-1}$, respectively. These rates parallel the DCTFA fluorescence quenching rates, which lends support to the original hypothesis.

The triplet energies of HFA, CPFA, DCTFA, and TCTFA have been determined as 26,250,[20] 26,000,[21] 26,000, and 26,000 cm^{-1}, respectively. The triplet energies of 2-butene and benzene are 27,400[22] and 29,500 cm^{-1},[23] the former value measured by the oxygen perturbation method and the latter value from phosphorescence emission studies. It would not therefore be expected that these two compounds could quench ketone triplets by an energy transfer mechanism. However, it has been shown that acetone[24] and HFA[25] both of which have lower lying triplet levels than the olefin, cause the cis–trans isomerization of *cis*-2-butene. It was shown that the isomerization was not caused by the methyl, acetyl,[24] and trifluoromethyl radicals[25] present, and hence an endothermic triplet–triplet energy transfer from the ketones to the butene seemed to be indicated. Thus the energy transfer process involves a nonspectroscopic olefin triplet state, as has been suggested to account for energy transfer from ketones to ethylenes.[26]

It has been demonstrated that mercury quenches the triplet states of hexafluoroacetone and trifluoroacetone, and a charge-transfer interaction was proposed.[27] The effect of mercury on DCTFA and TCTFA triplets was investigated by determining the biacetyl-sensitized emission yields on a system containing mercury and one with mercury absent. There was no observed difference in the maximum or the slope of these plots on either system and hence it is concluded that any effect of mercury on the triplet states of DCTFA or TCTFA must be minimal. This may merely be a reflection of the short lifetimes of DCTFA and TCTFA triplets compared to HFA triplet.

Acknowledgments. We are grateful to The Science Research Council, The Royal Society, and Monsanto Chemicals Ltd. for financial support.

References and Notes

(1) J. R. Majer, D. Phillips, and J. C. Robb, *Trans. Faraday Soc.*, **61**, 122 (1965).
(2) J. R. Majer, D. Phillips, and J. C. Robb, *Trans. Faraday Soc.*, **61**, 110 (1965).

(3) J. F. Harris and D. D. Coffmann, *J. Amer. Chem. Soc.*, **84**, 1153 (1962).
(4) A. Gandini and K. O. Kutschke, *Can. J. Chem.*, **44**, 1720 (1966).
(5) A. Gandini, D. D. Whytock, and K. O. Kutschke, *Proc. Roy. Soc., Ser. A*, **306**, 537 (1968).
(6) W. R. Ware and S. K. Lee, *J. Chem. Phys.*, **49**, 217 (1968).
(7) R. H. Knipe, A. S. Gordon, and W. R. Ware, *J. Chem. Phys.*, **51**, 840 (1967).
(8) A. J. Yarwood, *Can. J. Chem.*, **50**, 1429 (1972).
(9) H. S. Samant and A. J. Yarwood, *Can. J. Chem.*, **49**, 2053 (1971).
(10) P. A. Hackett and D. Phillips, *J. Chem. Soc., Faraday Trans. 1*, **68**, 335 (1972).
(11) R. F. Borkman and D. R. Kearns, *J. Amer. Chem. Soc.*, **88**, 3467 (1966).
(12) R. E. Rebbert and P. Ausloos, *J. Amer. Chem. Soc.*, **87**, 5569 (1965).
(13) J. V. Hirschfelder, C. F. Curtiss, and R. B. Bird in "Molecular Theory of Gases and Liquids," Wiley, New York, N. Y., 1954.
(14) M. W. Schmidt and E. K. C. Lee, *J. Amer. Chem. Soc.*, **92**, 3579 (1970).
(15) P. Dowd and A. Gold, *J. Amer. Chem Soc.*, **92**, 5725 (1970).
(16) N. J. Turro, P. Wriede, J. C. Patton, D. Arnold, and A. Glick, *J. Amer. Chem. Soc.*, **89**, 3950 (1967).
(17) G. M. Breuer and E. K. C. Lee, *Chem. Phys. Lett.*, **14**, 407 (1972).
(18) J. R. Majer, C. Olavesen, and J. C. Robb, *J. Chem. Soc. B*, 48 (1971).
(19) E. G. Howard, P. B. Sergeant, and C. G. Krespass, *J. Amer. Chem. Soc.*, **89**, 1422 (1967).
(20) A. Gandini and K. O. Kutschke, *Proc. Roy. Soc., Ser. A*, **306**, 511 (1968).
(21) J. P. Simons and A. J. Yarwood, *Nature (London)*, **187**, 316 (1960).
(22) K. F. Banhoeffer and L. Farkos, *Z. Phys. Chem.*, **A134**, 337 (1927).
(23) J. B. Birks in "Photophysics of Aromatic Molecules," Wiley-Interscience, London, 1970.
(24) R. B. Cundall and A. S. Davies, *Trans. Faraday Soc.*, **82**, 2444 (1966).
(25) A. Gandini, D. A. Whytock, and K. O. Kutschke, *Proc. Roy. Soc., Ser. A*, **306**, 529 (1968).
(26) G. S. Hammond and J. B. Saltiel, *J. Amer. Chem. Soc.*, **85**, 2516 (1963).
(27) A. Gandini, D. A. Whytock, and K. O. Kutschke, *Ber. Bunsenges. Phys. Chem.*, **72**, 296 (1968).

Generation of Radicals in the Charge-Transfer Photochemistry of Coordination Complexes of Cobalt(III) in Aqueous Solution[1]

Deborah D. Campano,[2] Evan R. Kantrowitz, Morton Z. Hoffman,* and Marc S. Weinberg

Department of Chemistry, Boston University, Boston, Massachusetts 02215 *(Received October 1, 1973)*

The quantum yields of Co^{2+} formation, $\phi(Co^{2+})$, were determined for the 254-nm irradiation of 24 Co(III) complexes of the general form $Co(NH_3)_5O_2CR^{2+}$ at pH 1 in N_2- and O_2-purged solutions. The values of $\phi(Co^{2+})$ in N_2 were in the range 0.15–0.25 with no obvious correlation with the pK_a or redox potential of the free carboxylic acid ligand. Quantum yield values significantly out of that range were rationalized in terms of secondary radical attack on the complex or alternative photochemical pathways originating from the initial charge-transfer excitation. Secondary radical attack was evaluated through the use of O_2 as a scavenger. Where determined, the stoichiometric ratio of Co^{2+}:CO_2:R· radical was 1:1:1. The flash photolysis of $Co(NH_3)_5O_2CCH_2CO_2H^{2+}$ and $Co(NH_3)_5O_2CCH_2Ph^{2+}$ yielded transient absorptions due to the $\cdot CH_2CO_2H$ and $PhCH_2\cdot$ radicals, respectively. The $\cdot CH_2OH$ radical, generated from $Co(NH_3)_5O_2CCH_2OH^{2+}$ or the γ-radiolysis of methanolic aqueous acid solution, did not give evidence of reduction of that complex or $Co(NH_3)_6^{3+}$. In contrast, the $(CH_3)_2\dot{C}OH$ radical reduces Co(III) complexes. Finally, the CH_3 radical was detected by esr from the photolysis of $Co(NH_3)_5O_2CCH_3^{2+}$.

Introduction

Irradiation of simple ammine complexes of Co(III) in their intense ligand-to-metal charge transfer (CTTM) band generates Co^{2+} and a free radical derived from the one-electron oxidation of a ligand.[3]

$$Co^{III}(NH_3)_5X \xrightarrow[CTTM]{h\nu} Co^{2+} + 5NH_4 + X\cdot \quad (1)$$

Flash photolysis and radical scavenger experiments have established the nature of X· unequivocally for $Co(NH_3)_5Br^{2+}$,[4] $Co(NH_3)_5I^{2+}$,[4,5] $Co(NH_3)_5N_3^{2+}$,[6,7] $Co(NH_3)_5NO_2^{2+}$,[8] and $Co(NH_3)_5CO_3^{+}$.[9] Less certain are the cases where the ligand X = NH_3,[10,11] H_2O,[10] and Cl^-,[12] for example. For the carboxylatopentaammine complexes $Co(NH_3)_5O_2CH^{2+}$, $Co(NH_3)_5O_2CCH_3^{2+}$, and $Co(NH_3)_5O_2CCO_2H^{2+}$, the formation of H atoms,[13] CH_3 radicals,[14] and $C_2O_4^-$ (or CO_2^-) radicals,[15] respectively, has been demonstrated. In fact, the 1:1:1 stoichiometry of Co^{2+}, CO_2, and the radical has shown that the photoreduction of these complexes of the form $Co(NH_3)_5O_2CR^{2+}$ can be described simply as

$$Co(NH_3)_5O_2CR^{2+} \xrightarrow[CTTM]{h\nu} Co^{2+} + CO_2 + R\cdot + 5NH_3 \quad (2)$$

although it has not been established whether the precursor radical, $RCO_2\cdot$, is actually released free into solution. The convenient photochemical generation of CH_3 radicals in aqueous solution *via* reaction 2 has been employed in the synthesis of macrocyclic complexes containing Co(III)–alkyl bonds.[16]

Although the 254-nm photolysis[13] of $Co(NH_3)_5O_2CCH_3^{2+}$ can be represented entirely by reaction 2, $Co(NH_3)_5O_2CH^{2+}$ and $Co(NH_3)_5O_2CCO_2H^{2+}$ demonstrate other processes that ultimately lead to Co^{2+}, specifically ligand decomposition and linkage isomerization.[14,15] In addition, further reaction of the R· radicals with the parent complex can lead

to an enhanced yield of Co^{2+} through electron transfer or hydrogen abstraction.

$$R\cdot + Co(III) \longrightarrow Co^{2+} + \text{stable product derived from } R\cdot \quad (3)$$

Values of k_3 are $\sim 10^7$, $\sim 10^3$, and $\leq 10^7\ M^{-1}\ sec^{-1}$ for R = -H, $-CH_3$, and $-CO_2H$, respectively.[13-15] Despite these other processes, the values of the quantum yield of Co^{2+} production (and thus of R· production) from reaction 2 for these complexes are very similar: 0.15, 0.19, and 0.1–0.2 for R = -H, $-CH_3$, and $-CO_2H$, respectively.[13-15]

This paper reports the results of continuous and flash photolysis studies of complexes of the form $Co(NH_3)_5O_2CR^{2+}$ in which the R group is varied systematically so as to cause a change in the basicity of the ligand, acid-base properties of the complex, and the nature of the resultant R· radical. Of particular interest is the effect of R- on the quantum yield of product formation, the identification of the R· radical and its subsequent behavior, and the implications for the understanding of the primary processes in Co(III) photochemistry.

Experimental Section

Preparation of Complexes. In general. the complexes were prepared as the perchlorate salts following the method of Gould and Taube[17] in which the parent carboxylic acid is allowed to react with $Co(NH_3)_5OH_2^{3+}$. In the cases where the yields were poor, alternative preparative methods were used. $Co(NH_3)_5O_2CH_2CH_3^{2+}$ was prepared by the method of Jackman, Scott, and Portman[18] in which propionic anhydride was allowed to react with $Co(NH_3)_5OH_2^{3+}$. The method of Olson and Taube[19] was used for complexes containing dicarboxylic acids: $Co(NH_3)_5O_2C(CH_2)_{1-3}CO_2H^{2+}$ and *cis*- and *trans*-$Co(NH_3)_5O_2CCH{=}CHCO_2H^{2+}$. The method of Dockal, Everhart, and Gould[20] was found to be most appropriate for $Co(NH_3)_5O_2CC_6H_{10}CO_2H^{2+}$ and $Co(NH_3)_5O_2CC{\equiv}C-CO_2H^{2+}$. All the complexes were recrystallized at least once and their absorption spectra compared with the literature value, if known. If no reference to a previous preparation of a specific compound could be found, recrystallization was continued until the measured molar absorptivity remained unchanged. Continued recrystallization generally removed the parent carboxylic acid as an impurity and caused ϵ to increase. The purity of such a compound was deemed acceptable when ϵ_{503} had a value in the 65–75 $M^{-1}\ cm^{-1}$ range.

Photochemical Apparatus and Procedures. The 254-nm photolysis units and the Xenon Corp. flash photolysis apparatus have been described in detail previously.[15] The quantum yield of Co^{2+} formation was determined from the continuous photolysis relative to $Co(NH_3)_5O_2CCH_3^{2+}$ in 0.1 M $HClO_4$ for which $\phi(Co^{2+}) = 0.19$.[14] Co^{2+} was determined by complexation with SCN^- in an acetone–water solution according to Kitson's method.[21] Spectra were recorded on a Cary 14 spectrophotometer. Solutions prepared from triply distilled water were purged of oxygen by passage of Cr^{2+}-scrubbed nitrogen through the solution for 20 min prior to photolysis and during the photolysis period in the case of the 254-nm irradiations. In the latter photolyses, the concentration of the complex was chosen so that $OD_{254} > 7$ and all the incident light would be absorbed. In the flash experiments, solutions were discarded after the first flash.

The analysis for CO_2 was performed by quantitative absorption of the gas on Ascarite. The scrubbed N_2 was passed through a U-tube containing Ascarite and then into the solution to be photolyzed. The exit gas from the photolysis cell was passed through a tube of Drierite to remove the water and then into a carefully weighed U-tube containing Ascarite in the first half and Anhydrone, $Mg(ClO_4)_2$, in the second half. Any CO_2 trapped by the Ascarite displaces H_2O which is trapped by the Anhydrone. The scrubbed N_2 (or, alternatively, tank O_2) was allowed to flow through the photolysis cell for 30 min before photolysis, during, and for 90 min after photolysis. The gain in weight of the Ascarite–Anhydrone tube was attributed to absorbed CO_2; no weight gain was observed in the absence of photolysis. The analytical method was standardized against the CO_2 released in the photolysis cell upon the acidification by $HClO_4$ of a $NaHCO_3$ solution.

Acetone was determined quantitatively by reaction with hypoiodite to produce iodoform which was determined spectrophotometrically.[22]

Radiolysis Procedures. γ-Ray irradiations were conducted in a well-type ^{60}Co source with a dose rate of about 5.0×10^{16} eV $ml^{-1}\ min^{-1}$. Solutions were prepared from triply distilled water that had been irradiated and photolyzed and were contained in sealed Pyrex vessels that had provision for a preirradiation N_2 purge. After irradiation for a measured length of time, analysis for Co^{2+} was performed as above from which was calculated the G value of Co^{2+} formation.

Esr Detection of Radicals. Solutions of complexes were exposed to an unfiltered 1000-W Hg–Xe source (Hanovia) within the optical transmission cavity of a Varian V-4560 esr spectrometer. The N_2-purged solutions were flowed slowly ($\sim$1 ml min^{-1}) through the standard Varian aqueous solution quartz flat cell (path length 0.03 mm) while a scan was made of the radical resonance spectral region. These experiments were conducted at the University of Western Ontario in collaboration with Professor J. R. Bolton.

Results and Discussion

Spectra and Complexes. The spectra of all the complexes showed the general features common to Co(III)–amine complexes with an oxygen-bonded carboxylate ligand: ligand-field (d-d) bands at 503 and 360 nm (ϵ <100 $M^{-1}\ cm^{-1}$) and the intense (ϵ >$10^3\ M^{-1}\ cm^{-1}$) charge-transfer bands in the ultraviolet. The different complexes showed subtle variations in the position of the steep ultraviolet absorption envelope which resulted in a range of values of ϵ_{254} from 2×10^3 to $6 \times 10^3\ M^{-1}\ cm^{-1}$. The only obvious correlation between the nature of the R group on the carboxylate ligand and ϵ_{254} was seen for the complexes possessing electron-withdrawing functions ($-CCl_3$, $-CF_3$, $-CH_2CN$) or unsaturated systems ($-C{\equiv}CH$, $-C{\equiv}CCO_2H$) where ϵ_{254} was up to a factor of 5 lower than for R = $-CH_3$ (ϵ_{254} $3.4 \times 10^3\ M^{-1}\ cm^{-1}$).

Inasmuch as the absorption spectra of complexes that do not possess an acidic moiety are not affected by pH (*e.g.*, R = -H, $-CH_3$; $Co(NH_3)_4C_2O_4^+$),[13-15] no examination of this point was made for complexes of monocarboxylate ligands. On the other hand, it is known[15,23] that the ultraviolet charge-transfer bands of $Co(NH_3)_5O_2CCO_2H^{2+}$ are affected by pH indicating that the free end of the oxalato ligand can be deprotonated with pK_a = 2.2. Coordination of $^-O_2CCO_2H$ (pK_a = 4.14) to the tripositive metal center has the effect of withdrawing electrons from the ligand, weakening the O–H bond, and promoting the acidity of the free end. This same effect was observed

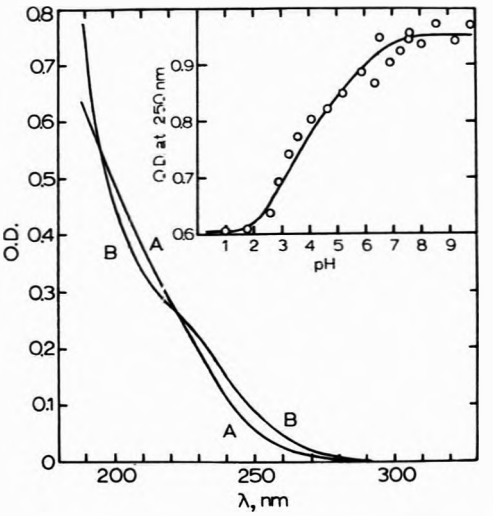

Figure 1. Uv spectrum of $Co(NH_3)_5O_2CCH_2CO_2H^{2+}$; [complex] = 2.5×10^{-5} *M*: (A) the acidic form in 0.1 *M* $HClO_4$; (B) the basic form at pH 7. The insert shows OD at 250 nm as a function of pH for [complex] = 2.5×10^{-4} *M*.

(Figure 1) for $Co(NH_3)_5O_2CCH_2CO_2H^{2+}$ (pK_a = 4.0 compared to pK_a = 5.69 for $^-O_2CCH_2CO_2H$) indicating that the influence of the metal center is somewhat lessened due to the increase in the number of intervening bonds. A spectrophotometric titration of other dicarboxylate complexes was not attempted although a pH effect on the spectrum was found for R = $-(CH_2)_3CO_2H$ and $-CH{=}CHCO_2H$ (cis and trans). It is to be noted that the pK_a for $Co(NH_3)_5O_2C(CH_2)_2CO_2H^{2+}$ has been determined[24] to be ~4 compared to the pK_a (4.6, 5.9) of succinic acid.

In general, the molar absorptivities of the complexes at 254 nm were $\sim 10^3$ times that of the free ligands in either the protonated or deprotonated forms. Only for the unsaturated dicarboxylic acids (R = $-CH{=}CHCO_2H$ (cis and trans); $-C{\equiv}CCO_2H$) did the free ligand show appreciable absorption ($\epsilon_{254} > 10^2$ M^{-1} cm^{-1}). Even here, however, the absorptivity of the complex at 254 nm was at least ten times that of the free ligand. Thus, making the reasonable assumption that strictly intraligand transitions are relatively unaffected by coordination, it can be concluded that irradiation of the complex at 254 nm causes excitation of CTTM states and not direct excitation of the ligand.

Quantum Yields. The quantum yields of Co^{2+} formation in 0.1 *M* $HClO_4$ at 25° are presented in Table I for solutions purged with N_2 or with O_2. Also included for reference are the pK_a values of the free carboxylic acid ligands. Examination of the table reveals that with certain exceptions which will be discussed separately, the values of $\phi(Co^{2+})$ for the 254-nm photolysis of $Co(NH_3)_5O_2CR^{2+}$ complexes in N_2-purged solutions are in the rather narrow range of 0.15–0.25. The constancy of the values Table I is highlighted by the relatively wide range of acidities of the free carboxylic acids (and the corresponding basicities of the coordinating carboxylate anions) and the variations in the redox potentials of the free ligands.[25] These results indicate that the Co^{2+} arises from a common mechanistic pathway with similar yields for all the complexes. These yields are apparently less a matter of the nature of the ground-state molecule than they are reflective of the behavior of the excited states from whence they arise.

The generation of the C-bonded formato isomer in the photochemistry of the formato- and oxalato-amine complexes was attributed[13,15] to the presence of alternative photochemical pathways which permitted excitation of the ligand. A similar proposal can be advanced to explain the sharply reduced $\phi(Co^{2+})$ values for the maleato and fumarato (R = $-CH{=}CHCO_2H$) complexes. It is well established[26] that both maleic and fumaric acids undergo wavelength-independent isomerization when irradiated in the ultraviolet and that the process proceeds *via* low-lying triplet states.[27] Irradiation of the maleato and fumarato complexes could result in the excitation of the ligand-localized triplet state in competition with the generation of the charge-transfer triplet which appears to be the precursor of the Co^{2+}.[28] Such a ligand excitation may be expected to cause isomerization although no attempt to detect that process was made in the research reported here. Lest it be thought that the reduction in $\phi(Co^{2+})$ is a result of the direct absorption of radiation by the ligand, note should be made of the "normal" value of $\phi(Co^{2+})$ shown by the acetylenedicarboxylato complex (R = $-C{\equiv}CCO_2H$) which also possesses a strongly absorbing ligand. The somewhat diminished quantum yield exhibited by the cyclopropylcarboxylato complex may also be reflective of the availability of low-lying triplet states and alternative excitation pathways; apparently, the photochemistry of cyclopropanes resembles that of olefins in many ways.[27] On the other hand, the cyclohexylcarboxylato complexes show "normal" behavior. In this regard, it should be mentioned that $\phi(Co^{2+})$ values from pentaammine complexes containing an aromatic carboxylate ligand, such as R = $-Ph$, are also quite low (~0.04).[29] However, the methylene group in the phenylacetato complex apparently insulates the charge-transfer and ligand-localized excited states from each other sufficiently so that the value of $\phi(Co^{2+})$ is the same as that of the other substituted acetato complexes. The somewhat lower value for the trifluoroacetato complex may be the result of a dependence of ϕ on the nature of the spectral band irradiated. The charge-transfer bands of this complex are somewhat shifted to higher energies (compared to $Co(NH_3)_5O_2CCH_3^{2+}$, for example) which results in a low value (665 M^{-1} cm^{-1}) for ϵ_{254}. Thus, inasmuch as the quantum yield for photoreduction in Co(III) complexes generally diminishes as irradiation is performed on the low-energy tail of the CTTM absorption,[3] tail irradiation in $Co(NH_3)_5O_2CCF_3^{2+}$ could produce the observed result.

Examination of Table I reveals further that, in general, $\phi(Co^{2+})$ in O_2-saturated solutions is the same as $\phi(Co^{2+})$ in N_2-purged solutions. This is a common property of Co(III) complexes in which the generated radical R· does not cause the reduction of the substrate in a secondary step. It is also indicative of the lack of quenching of the excited states by O_2. On the cases where there is an O_2 effect, specifically where R = $-H$,[13] $-CO_2H$,[15] and $-C(CH_3)_2OH$, the quantum yield in N_2 is virtually twice that in O_2 due to the inclusion of reaction 3 into the mechanism. The 2-hydroxy-2-propyl radical, $(CH_3)_2\dot{C}OH$, which would be the resultant radical from the photolysis of the α-hydroxyisobutyrato complex, is well established as a good reducing agent[30] with rate constants in the order of 10^7–10^9 M^{-1} sec^{-1} [31,32] for reaction with Co(III) complexes.

$$(CH_3)_2\dot{C}OH + Co(III) \longrightarrow Co^{2+} + (CH_3)_2CO \qquad (4)$$

In the presence of O_2, $(CH_3)_2\dot{C}OH$ radicals would be scav-

enged rapidly ($k_5 > 10^9\ M^{-1}\ sec^{-1}$) to generate the peroxy radical which leads eventually to the formation of acetone.[33]

$$(CH_3)_2\dot{C}OH + O_2 \longrightarrow (CH_3)_2C(\dot{O}_2)OH \longrightarrow \text{acetone} \quad (5)$$

Thus, while in N_2-purged solutions $Co^{2+}/CO_2 = 1.7$ and $Co^{2+}/(CH_3)_2CO = 2.1$, in O_2-saturated solution, these ratios have values of 0.97 and 1.1, respectively.

Scavenging of an R· radical by 2-propanol *via* H-atom abstraction also results in the formation of $(CH_3)_2\dot{C}OH$. $\phi(Co^{2+})$ for the malonato (R = $-CH_2CO_2H$) complex is approximately doubled in the presence of 2-propanol indicating that reactions 6 and 4 are operative.

$$\cdot CH_2CO_2H + (CH_3)_2CHOH \longrightarrow CH_3CO_2H + (CH_3)_2\dot{C}OH \quad (6)$$

A similar effect of the presence of 2-propanol had been seen previously in the cases of $Co(NH_3)_5O_2CCH_3^{2+}$ [13] and $Co(NH_3)_4CO_3^+$.[34] In N_2-purged solution of the malonato complex in the absence of alcohol, $Co^{2+}/CO_2 = 1.0$.

Flash Photolysis. The flash photolysis of N_2-purged solutions of $Co(NH_3)_5O_2CCH_2CO_2H^{2+}$ ($1 \times 10^{-4}\ M$) gave rise to pH-dependent transient spectra as shown in Figure 2. These spectra are very similar to those of the $\cdot CH_2CO_2H$ and $\cdot CH_2CO_2^-$ radicals and the pH dependence (insert to Figure 2) shows that the radicals exist in an acid–base equilibrium with $pK_a \sim 4.5$.[35] The decay of the transient spectra was *via* second-order kinetics (Figure 3) demonstrating that at that concentration of substrate, any reaction of the radical with the complex must be negligible. From the slope of the graph in Figure 3, a value of $2k/\epsilon = 1.4 \times 10^6$ is obtained. Taking $\epsilon_{350} = 880\ M^{-1}\ cm^{-1}$,[36] a value of $2k = 1.2 \times 10^9\ M^{-1}\ sec^{-1}$ at pH 6.5 is obtained, in very good agreement with previous results.[35,36] The generation of the $\cdot CH_2CO_2H$ radical from the flash photolysis of malonic acid has recently been reported although it is interesting to note that the ionization of the acid causes no observable transient absorption to be generated.[37] In this regard, the formation of the R· radical from the CTTM excitation of the complex *via* reaction 2 does not mirror the photochemistry of the free aliphatic carboxylate anions where photoionization and charge transfer does not appear to occur.[37] There is no indication in the continuous and flash photolysis of the malonato complex that any ligand decomposition or linkage isomerization occurs in comparison with the behavior of the oxalato complex.[15]

The photochemistry of the malonato complex can be summarized by the following scheme.

$$\left.\begin{array}{l}(NH_3)_5CoO_2CCH_2CO_2H^{2+} \\ \quad pK_a\ 4.0 \updownarrow H^+ \\ (NH_3)_5CoO_2CCH_2CO_2^+\end{array}\right\} \xrightarrow{h\nu}$$

$$Co^{2+} + 5NH_3 + CO_2 + \cdot CH_2CO_2H \quad \lambda_{max}\ 320\ nm$$

$$pK_a\ 4.5 \updownarrow H^+$$

$$\cdot CH_2CO_2^- \quad \lambda_{max}\ 350\ nm$$

The flash photolysis of a number of other complexes (R = $-(CH_2)_2CO_2H$, $-(CH_2)_3CO_2H$, $-CH{=}CHCO_2H$ (cis and trans), $-C{\equiv}CCO_2H$, and $-C_6H_{10}CO_2H$) resulted only in weak tail absorptions at $\lambda < 320$ nm consistent with the unstructured spectra known for β- and γ-carboxy radicals.[35]

The flash photolysis of the phenylacetato complex gives rise to the characteristic absorption spectrum of the benzyl ($PhCH_2\cdot$) radical (Figure 4) which decays *via* second-order kinetics (Figure 5) with a value of $2k/\epsilon = 2.2 \times 10^5$. Owing to the disagreement about the value of ϵ for the benzyl radical,[36,38-40] a reliable value for $2k$ could not be

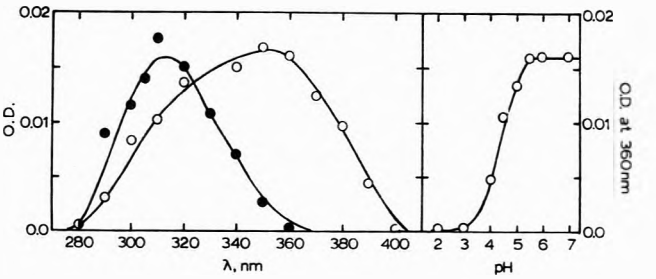

Figure 2. Transient spectra from the flash photolysis of $1 \times 10^{-4}\ M$ $Co(NH_3)_5O_2CCH_2CO_2H^{2+}$ in N_2-purged solution; OD read 50 μsec after the initiation of the flash: ●, pH 2.0; ○, pH 6.8. The insert shows the variation of the OD at 360 nm as a function of pH.

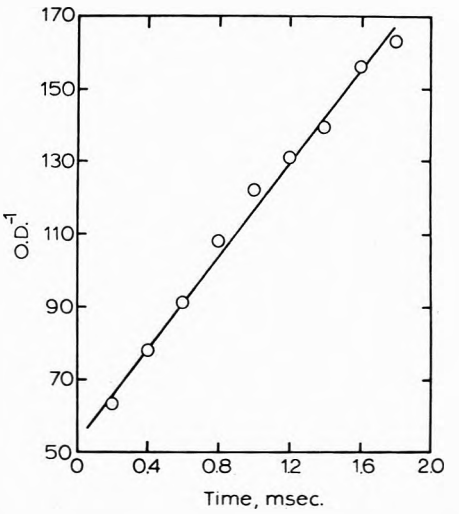

Figure 3. Second-order plot of the decay of the transient absorption from the flash photolysis of $1 \times 10^{-4}\ M$ $Co(NH_3)_5O_2CCH_2CO_2H^{2+}$ at pH 6.5 in N_2-purged solution: monitoring wavelength = 350 nm.

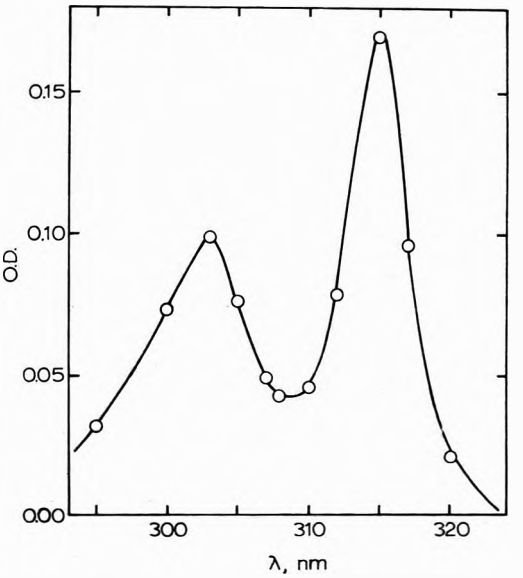

Figure 4. Transient spectrum from the flash photolysis of $1 \times 10^{-5}\ M$ $Co(NH_3)_5O_2CCH_2Ph^{2+}$ at pH 7.0 in N_2-purged solution; OD read 50 μsec after the initiation of the flash.

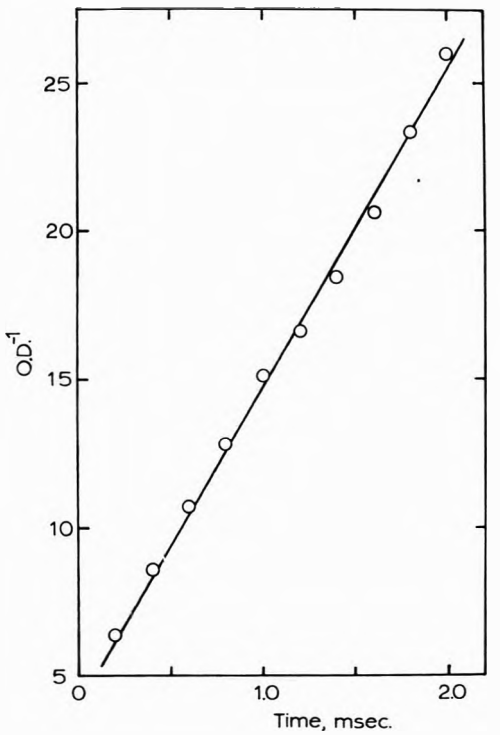

Figure 5. Second-order plot of the decay of the benzyl radical from the flash photolysis of 1×10^{-5} *M* $Co(NH_3)_5O_2CCH_2Ph^{2+}$ at pH 7.0 in N_2-purged solution: monitoring wavelength = 315 nm.

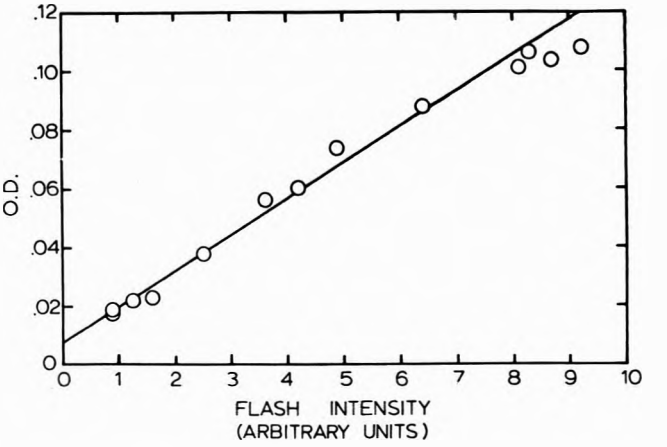

Figure 6. Dependence of the "initial" absorbance of the benzyl radical (read 50 μsec after the initiation of the flash) from the flash photolysis of $Co(NH_3)_5O_2CCH_2Ph^{2+}$ on the flash lamp intensity.

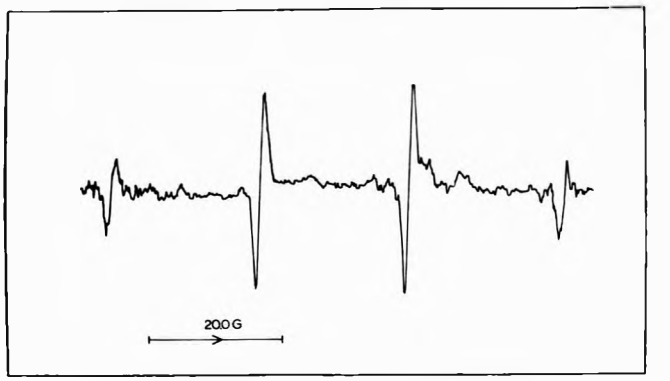

Figure 7. Esr spectrum of the CH_3 radical formed from the photolysis of 1×10^{-2} *M* $Co(NH_3)_5O_2CCH_3^{2+}$ at pH 1 in N_2-purged solution. Flow rate of solution through the cell ~1 ml min^{-1}. The esr spectrometer (100-kHz modulation frequency) was operated with a modulation amplitude of 1.25 G and a microwave power of 10 mW.

calculated except that all the possible values would be $>10^9\ M^{-1}\ sec^{-1}$ which is reasonable for this radical.

In a recent paper on the flash photolysis of aromatic carboxylic acids in aqueous solution, Mittal, *et al.*,[41] noted that the formation of the benzyl radical from phenylacetic acid and phenylacetate occurs *via* a biphotonic process. They speculated that a second quantum of light is required to excite the long-lived triplet state to the dissociative state that undergoes loss of $\cdot CO_2H$ or e_{aq}^-, depending upon the pH of the solution. In order to test if the benzyl radical arose from similar ligand-localized states in the phenylacetato complex, the concentration of radical (as measured by its absorbance) was determined as a function of the intensity of the flash.[42] Figure 6 shows that the benzyl radical is formed in a monophotonic process as represented by reaction 2.

$\cdot CH_2OH$ Radical Reactions. The $\cdot CH_2OH$ radical is a good reducing agent[30] and has been shown to react fairly rapidly with $Co(NH_3)_5^{3+}$ ($k = 1.4 \times 10^8\ M^{-1}\ sec^{-1}$ at pH 6) to yield Co^{2+} quantitatively,[32] presumably *via* an electron-transfer reaction[43] analogous to reaction 4.

$$\cdot CH_2OH + Co(III) \longrightarrow Co^{2+} + H_2CO \qquad (7)$$

One might anticipate, therefore, that a diminution of $\phi(Co^{2+})$ by a factor of 2 in O_2-saturated solution should be observed for R = $-CH_2OH$ as has been seen for R = $-C(CH_3)_2OH$ inasmuch as the $\cdot CH_2OH$ radical is also efficiently scavenged by O_2.[44] Such an effect is not observed for R = $-CH_2OH$ at pH 1 which leads to the conclusion that the $\cdot CH_2OH$ radical in acidic solution does not reduce the Co(III) parent complex. We had noted this same nonreactive behavior earlier in the case of the photolysis of the acetato complex[14] where the presence of up to 10 *M* CH_3OH did not measurably alter $\phi(Co^{2+})$ despite the fact that CH_3OH is an efficient scavenger for CH_3 radicals producing $\cdot CH_2OH$. In order to check this point independently, we generated $\cdot CH_2OH$ radicals *via* the γ-radiolysis of aqueous solutions of CH_3OH.

$$H_2O \longrightarrow e_{aq}^-(2.8),\ OH(2.8),\ H(0.6)^{45} \qquad (8)$$

$$H + CH_3OH \longrightarrow \cdot CH_2OH + H_2 \quad (k = 1.6 \times 10^6\ M^{-1}\ sec^{-1})^{46} \qquad (9)$$

$$OH + CH_3OH \longrightarrow \cdot CH_2OH + H_2O \quad (k = 5.0 \times 10^8\ M^{-1}\ sec^{-1})^{46} \qquad (10)$$

$$e_{aq}^- + CH_3OH \longrightarrow CH_3OH^- \quad (k < 10^5\ M^{-1}\ sec^{-1})^{46} \qquad (11)$$

In acidic solution, e_{aq}^- is converted efficiently to H atoms.

$$e_{aq}^- + H^+ \longrightarrow H \quad (k = 2.2 \times 10^{10}\ M^{-1}\ sec^{-1})^{46} \qquad (12)$$

The radiolysis of a 1×10^{-3} *M* solution of $Co(NH_3)_5O_2CCH_2OH^{2+}$ in 0.5 *M* $HClO_4$ and 0.2 *M* CH_3OH resulted in $G(Co^{2+}) = 0.6$ which is a factor of 10 lower than that expected from reactions 8–10, 12, and 7. Similarly low yields of Co^{2+} ($G = 0.4$) were obtained from the radiolysis of $Co(NH_3)_6^{3+}$ under identical conditions. It is quite apparent that reaction 7 is pH dependent. Inasmuch as there does not appear to be any evidence that the $\cdot CH_2OH$ radical undergoes protonation at pH <6, the lack of an ap-

TABLE I: Quantum Yields of Co^{2+} Formation from the 254-nm Photolysis of $Co(NH_3)_5O_2CR^{2+}$ Complexes[a]

R	pK_a of RCO_2H[b]	$\phi(Co^{2+})$ N_2 purge	$\phi(Co^{2+})$ O_2 purge
	Carboxylic Acids		
-H	3.77	0.30[c]	0.15[c]
$-CH_3$	4.76	0.19[d]	0.19[d]
$-CH_2Cl$	2.86	0.22[d]	0.20
$-CH_2Br$	2.86	0.22	0.20
$-CCl_3$	0.65	0.24[d]	0.22
$-CF_3$	0.23	0.11	0.10
$-CH_2OH$	3.83	0.27	0.28
$-CH_2CN$	2.46	0.17	0.18
$-CH_2CH_3$	4.88	0.24	0.25
$-C(CH_3)_3$	5.01	0.25	0.27
$-C(CH_3)_2OH$	~4	0.56	0.29
$-CH=CH_2$	4.25	0.14	0.12
$-C\equiv CH$	~4	0.12	0.09
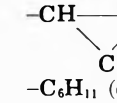	4.83	0.10	0.08
$-C_6H_{11}$ (cyclo)	4.90	0.15	
$-CH_2Ph$	4.28	0.22	0.19
	Dicarboxylic Acids		
$-CO_2H$	1.25, 4.14	0.65[e]	0.33[e]
$-CH_2CO_2H$	2.83, 5.69	0.15	0.16
		0.26[f]	
$-(CH_2)_2CO_2H$	4.20, 5.64	0.18	0.18
$-(CH_2)_3CO_2H$	4.34, 5.41	0.20	
$-CH=CHCO_2H$ (cis)	1.92, 6.23	0.07	0.06
$-CH=CHCO_2H$ (trans)	3.02, 4.38	0.05	0.04
$-C\equiv CCO_2H$	1.73, 4.40	0.15	
$-C_6H_{10}CO_2H$ (1,4-*cyclo*)	4.18, 5.42	0.16	

[a] 0.1 *M* $HClO_4$; 25°. $\phi(Co^{2+})$ values known to ±15%. [b] "Handbook of Biochemistry," 2nd ed, Chemical Rubber Publishing Co., Cleveland, Ohio, 1970; G. Kortüm, W. Vogel, and K. Andrussow, "Dissociation Constants of Organic Acids in Aqueous Solution," Butterworths, London, 1961. [c] Disregarding the Co^{2+} yield arising from the C-bonded formato isomer; ref 13. [d] Values taken from ref 14. [e] Total Co^{2+} yield; ref 15. Subtraction of the Co^{2+} yield from the C-bonded formato isomer makes $\phi(Co^{2+})$ in N_2 = 0.1–0.2. [f] Solution contains 1 *M* 2-propanol.

preciable Co^{2+} yield in acidic solution must be due to the mechanism of the interaction of the radical with the Co(III) complexes. This matter is currently under investigation.

Esr Detection. The continuous photolysis of 1×10^{-2} *M* $Co(NH_3)_5O_2CCH_3^{2+}$ at pH 1 within the esr cavity resulted in the resonance spectrum shown in Figure 7 where the quartet has an intensity distribution 1:3:3:1 with a^H = 22.7 ± 0.1 G. This spectrum can be unambiguously attributed to the CH_3 radical.[47] Attempts to resolve radical resonance spectra from other complexes failed: $Co(NH_3)_6^{3+}$, $Co(NH_3)_4C_2O_4^+$, $Co(NH_3)_4CO_3^+$, $Co(NH_3)_5O_2CPh^{2+}$, $Co(NH_3)_5O_2CCH_2Ph^{2+}$, and $Co(C_2O_4)_3^{3-}$. These failures can be rationalized in terms of the quantum yields of radical production, the absorption spectra of the complexes, and the lifetimes of the radicals due to their reactivity with the substrates and themselves.

Acknowledgment. The authors thank Dr. S. -N. Chen and Mr. K. R. Olson for assistance in some aspects of this research.

References and Notes

(1) This research was supported by the National Science Foundation through Grant No. GP 11213 and the Undergraduate Research Participation Program. Presented in part at the 10th Informal Conference on Photochemistry, Oklahoma State University, Stillwater, Okla., May 1972 and at the Symposium on Photochemistry of Inorganic and Organometallic Compounds, 164th National Meeting of the American Chemical Society, New York, N. Y., Aug 1972, INOR 23.
(2) Participant in the NSF–URP Program at Boston University, summer 1971.
(3) V. Balzani and V. Carassiti, "Photochemistry of Coordination Compounds," Academic Press, New York, N. Y., 1970.
(4) S. A. Penkett and A. W. Adamson, *J. Amer. Chem. Soc.*, **87**, 2514 (1965).
(5) S. D. Malone and J. F. Endicott, *J. Phys. Chem.*, **76**, 2223 (1972).
(6) A. W. Adamson, *Discuss. Faraday Soc.*, **29**, 163 (1960).
(7) J. F. Endicott, M. Z. Hoffman, and L. S. Beres, *J. Phys. Chem.*, **74**, 1021 (1970).
(8) V. Balzani, R. Ballardini, N. Sabbatini, and L. Moggi, *Inorg. Chem.*, **7**, 1398 (1968).
(9) S. -N. Chen, V. W. Cope, and M. Z. Hoffman, *J. Phys. Chem.*, **77**, 1111 (1973).
(10) J. F. Endicott and M. Z. Hoffman, *J. Amer. Chem. Soc.*, **87**, 3348 (1965).
(11) M. F. Manfrin, G. Varani, L. Moggi, and V. Balzani, *Mol. Photochem.*, **1**, 387 (1969).
(12) G. Caspari, R. G. Hughes, J. F. Endicott, and M. Z. Hoffman, *J. Amer. Chem. Soc.*, **92**, 6801 (1970).
(13) E. R. Kantrowitz, M. Z. Hoffman, and K. M. Schilling, *J. Phys. Chem.*, **76**, 2492 (1972).
(14) E. R. Kantrowitz, M. Z. Hoffman, and J. F. Endicott, *J. Phys. Chem.*, **75**, 1914 (1971).
(15) A. F. Vaudo, E. R. Kantrowitz, M. Z. Hoffman, E. Papaconstantinou, and J. F. Endicott, *J. Amer. Chem. Soc.*, **94**, 6655 (1972).
(16) T. S. Roche and J. F. Endicott, *J. Amer. Chem. Soc.*, **94**, 8622 (1972).
(17) E. S. Gould and H. Taube, *J. Amer. Chem. Soc.*, **86**, 1319 (1964).
(18) L. M. Jackman, R. M. Scott, and R. H. Portman, *Chem. Commun.*, 1338 (1968).
(19) M. V. Olson and H. Taube, *Inorg. Chem.*, **9**, 2073 (1970).
(20) E. R. Dockal, E. T. Everhart, and E. S. Gould, *J. Amer. Chem. Soc.*, **93**, 5662 (1971).
(21) R. E. Kitson, *Anal. Chem.*, **22**, 664 (1950).
(22) S. D. Nogare, T. O. Norris, and J. Mitchell, Jr., *Anal. Chem.*, **23**, 1473 (1951).
(23) C. Andrade and H. Taube, *Inorg. Chem.*, **5**, 1087 (1966).
(24) Unpublished observations by D. Bearcroft quoted in ref 23.
(25) L. Meites, "Polarographic Techniques," 2nd ed, Interscience, New York, N. Y., 1965.
(26) J. G. Calvert and J. N. Pitts, Jr., "Photochemistry," Wiley, New York, N. Y., 1966, p 431.
(27) P. J. Wagner and G. S. Hammond, *Advan. Photochem.*, **5**, 21 (1968).
(28) P. Natarajan and J. F. Endicott, *J. Amer. Chem. Soc.*, **94**, 3635 (1972).
(29) D. D. Campano, E. R. Kantrowitz, and M. Z. Hoffman, unpublished results.
(30) J. Lilie, G. Beck, and A. Henglein, *Ber. Bunsenges. Phys. Chem.*, **75**, 458 (1971).
(31) M. Z. Hoffman and M. Simic, *J. Amer. Chem. Soc.*, **94**, 1757 (1972).
(32) H. Cohen and D. Meyerstein, *J. Amer. Chem. Soc.*, **94**, 6944 (1972).
(33) R. Stockhausen, A. Henglein, and G. Beck, *Ber. Bunsenges. Phys. Chem.*, **73**, 567 (1969).
(34) V. W. Cope, S. -N. Chen, and M. Z. Hoffman, *J. Amer. Chem. Soc.*, **95**, 3116 (1973).
(35) P. Neta, M. Simic, and E. Hayon, *J. Phys. Chem.*, **73**, 4207 (1969).
(36) M. Z. Hoffman and E. Hayon, *J. Phys. Chem.*, **77**, 990 (1973).
(37) L. J. Mittal, J. P. Mittal, and E. Hayon, *J. Phys. Chem.*, **77**, 1482 (1973).
(38) For example, H. C. Christensen, K. Sehested, and E. J. Hart, *J. Phys. Chem.*, **77**, 983 (1973), and references quoted therein.
(39) J. P. Mittal and E. Hayon, *Nature (London), Phys. Sci.*, **240**, 21 (1972).
(40) T. O. Meiggs, L. I. Grossweiner, and S. I. Miller, *J. Amer. Chem. Soc.*, **94**, 7981 (1972).
(41) L. J. Mittal, J. P. Mittal, and E. Hayon, *J. Phys. Chem.*, **77**, 2267 (1973).
(42) The intensity of the flash, taken as proportional to $CV^2/2$, was varied through variation of the discharge voltage and charging capacitance.
(43) J. H. Baxendale and R. S. Dixon, *Z. Phys. Chem. (Frankfurt am Main)*, **43**, 161 (1964).
(44) G. E. Adams, B. D. Michael, and R. L. Willson, *Advan. Chem. Ser.*, **No. 81**, 289 (1968).
(45) The numbers in parentheses represent the G values of the primary radicals from the γ-radiolysis of water; G = number of radicals produced per 100 eV of radiation energy absorbed.
(46) M. Anbar and P. Neta, *Int. J. Appl. Radiat. Isotopes*, **18**, 493 (1967).
(47) D. Greatorex and T. J. Kemp, *Trans. Faraday Soc.*, **67**, 1576 (1971).

Electron Paramagnetic Resonance Absorption in Oriented Phosphorescent 2,3-Benzocarbazole and 1,2,3,4-Tetrahydroanthracene at Magnetic Fields below 65 G[1]

Roger E. Gerkin* and Arthur M. Winer[2]

Department of Chemistry, The Ohio State University, Columbus, Ohio 43210 *(Received November 12, 1973)*

Electron paramagnetic resonance absorptions have been observed from phosphorescent 2,3-benzocarbazole, an impurity which is ubiquitous in commercial chrysenes, and from phosphorescent 1,2,3,4-tetrahydroanthracene (THA), an impurity which was identified in symmetric octahydroanthracene (OHA). Triplet-state zero-field splittings for 2,3-benzocarbazole oriented in single-crystal *p*-terphenyl and in single-crystal chrysene at ~85 K, and for THA oriented in single-crystal OHA at ~85 and ~273 K, have been determined using data obtained at magnetic fields below ~65 G. Multiple resonance absorptions (five for each of the two transitions studied) were observed for 2,3-benzocarbazole in *p*-terphenyl whereas only single signals were observed for each of the corresponding transitions for 2,3-benzocarbazole in the chrysene host structure. Only single signals were observed from THA in single-crystal OHA, and its zero-field splittings and spin Hamiltonian parameters were found to be quite similar to those of naphthalene, the largest aromatic substructure of THA.

Introduction

In the course of an extensive low-field electron paramagnetic resonance study of triplet chrysene oriented in *p*-terphenyl or symmetric octahydroanthracene (OHA),[3-5] two tenacious impurities were encountered in sample materials used in the preparation of chrysene mixed crystals. The first of these two impurities, 2,3-benzocarbazole, occurs in the guest material, chrysene, in concentrations as high as 10% even in nominally very pure commercial samples.[6,7] The second impurity, identified as 1,2,3,4-tetrahydroanthracene (THA), was found to occur persistently in OHA, even after this host material had been zone-refined, chromatographed, or recrystallized. In order to remove any doubt concerning the possible origin from impurity triplet states of multiple resonance absorptions observed for chrysene in *p*-terphenyl or OHA,[3-5] it was deemed desirable to investigate the low-field resonance spectra of 2,3-benzocarbazole and THA. We here report the results of these brief investigations of phosphorescent 2,3-benzocarbazole oriented in single crystals of *p*-terphenyl and chrysene, and of phosphorescent 1,2,3,4-tetrahydroanthracene oriented in single crystals of symmetric octahydroanthracene.

Experimental Section

Apparatus and Methods. The basic low-field spectrometer and the experimental methods employed have been described in detail elsewhere.[4,8,9] Optical spectra obtained for purposes of identification of species were taken on a Turner spectrofluorophosphorimeter described previously.[4] Precision determinations of zero-field splittings were made for crystal samples in brass resonant cavities immersed either in liquid nitrogen boiling at ambient pressure, or in distilled water–ice slush baths.

Sample Preparation. 2,3-Benzocarbazole employed as a guest material in mixed crystals with *p*-terphenyl or chrysene was obtained from Chemical Procurement Laboratories Inc. and was purified by vacuum sublimation. The wavelength of the fluorescence maximum observed for this purified material in EPA glass was 4030 Å, a value in good agreement with a previously reported value of 4070 Å obtained for 2,3-benzocarbazole in *N,N*-dimethylformamide.[7]

Chrysene-d_{12} of nominal isotopic purity 98% was obtained from Merck Sharp and Dohme, Ltd. (MSD. Lot No. AD-024), and was subjected to column chromatography on Woelm neutral alumina, the only purification procedure shown to be effective in removing essentially all of the 2,3-benzocarbazole impurity. The removal was demonstrated by the absence, visually determined, of the characteristic orange phosphorescence of 2,3-benzocarbazole in single crystals of chrysene photoexcited at ~85 K. (Four additional impurity bands were resolved on the column and were also separated from the chrysene-d_{12}.) Some chrysene-d_{12} was used unpurified as a "source" of 2,3-benzocarbazole in an unknown state of deuteration in mixed crystals of chrysene-d_{12} in *p*-terphenyl.

Scintillation grade *p*-terphenyl was obtained from Arapahoe Chemicals Inc. and was used without further purification, since no (impurity) phosphorescence was detected visually from single crystals photoexcited at ~85 K, nor was magnetic resonance observed from such crystals.

1,2,3,4-Tetrahydroanthracene (THA) was synthesized from 9,10-dihydroanthracene according to the procedure of Orchin.[10] The THA obtained was chromatographed on Woelm neutral alumina using benzene eluant and was recrystallized from ethanol.

Symmetric octahydroanthracene (OHA) obtained from Chemical Procurement Laboratories, Inc., was zone-refined 50 passes, chromatographed, or recrystallized twice from ethanol. Further discussion concerning the use of OHA is given below.

Mixed Crystals. Single crystals were grown, cleaved, and mounted in resonant cavities as described previously.[8] The temperature of crystals illuminated by the unfiltered radiation of the A-H6 source and contained in cavities immersed in liquid nitrogen was taken to be 85 ± 3 K on the basis of previous measurements made in this laboratory. Such temperatures are designated canonically as ~85 K in the text.

The compositions and nominal guest concentrations of mixed crystals employed in these studies are shown in Table I.

TABLE I: Composition and Nominal Guest Concentrations of Mixed Crystals Employed in This Study

Boule no.	Host material	Host purification	Guest material(s)	Mode of occurrence of guest	Nominal guest concn, mol %
199	*p*-Terphenyl	None[a]	Chrysene-d_{12}[b]	Added	0.1
169	*p*-Terphenyl	None[a]	Chrysene-d_{12}[c]	Added	0.9
			1,2-Benzocarbazole	Added incidentally as an impurity in the chrysene-d_{12}	~0.1[d]
266	*p*-Terphenyl	None[a]	2,3-Benzocarbazole	Added	1.1
252	*p*-Terphenyl	None[a]	2,3-Benzocarbazole	Added	0.08
104	Chrysene	None	2,3-Benzocarbazole	Host impurity	10[d]
254	Chrysene	None	2,3-Benzocarbazole	Host impurity	10[d]
226	OHA	None	THA	Host impurity	*e*
241	OHA	None	THA	Host impurity	*e*
347	OHA	Recrystalled twice from ethanol	THA	Added	2.0
348	OHA	Recrystalled twice from ethanol	None[f]		

[a] No phosphorescent impurities were detectable in this material (see text). [b] Purified by column chromatography to remove essentially all 2,3-benzocarbazole (see text). [c] Unpurified. [d] Estimate based on nominal 10–12 mol % of 2,3-benzocarbazole found in commercial chrysenes. See ref 6 and 7. [e] Not determined. [f] Impurities reduced but not completely removed (see text).

Treatment of Data

The spin Hamiltonian chosen to interpret the magnetic resonance data is

$$\mathcal{H} = \mathbf{H}\cdot g|\beta|\cdot\mathbf{S} + DS_C^2 + E(S_A^2 - S_B^2) \qquad (1)$$

consistent with our previous usage.[8]

The field dependence of the associated energy levels and the method of least-squares fitting of the resonance data have been presented previously.[8]

Magnetic Resonance Observations for 2,3-Benzocarbazole

p-Terphenyl Host. Assignments to chrysene-d_{12} triplet states (oriented in *p*-terphenyl single crystals) of multiplet patterns of resonance absorptions associated with sets of slightly different zero-field splittings at ~0.116, ~0.062, and ~0.053 cm^{-1} were made in detailed analyses given in ref 4 and 5. The component signals in the multiplet patterns were interpreted as arising from sets of differently oriented chrysene-d_{12} triplets which occupy several kinds of sites of substitution at which there are significantly different molecular crystal fields giving rise to the observed differences in the zero-field splittings of the component signals. In addition to these three well-characterized multiplets containing a total of 20 resonance absorptions, two other sets of multiple resonance absorptions were observed from mixed crystals of chrysene-d_{12} in *p*-terphenyl. For one set of signals the corresponding zero-field splittings were shown to range between 0.0847 and 0.0858 cm^{-1}, while zero-field splittings corresponding to absorptions in the other multiplet ranged in value from 0.0636 to 0.0644 cm^{-1}. At least five resonance absorptions were observed in each of these patterns, and each absorption within a multiplet was shown to be associated with a slightly different zero-field splitting by changing the microwave frequency by small increments so that the centers of the individual resonance signals were moved successively to zero magnetic field.

When an authentic sample of 2,3-benzocarbazole (Figure 1a) was used as the sole guest in *p*-terphenyl mixed crystals, multiplet structure patterns were observed at

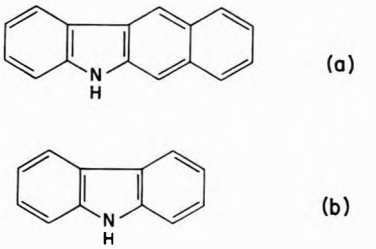

Figure 1. Structure of (a) 2,3-benzocarbazole and (b) carbazole.

~0.085 and at ~0.064 cm^{-1} from such crystals, and component signals in these patterns were shown to correspond one-to-one with components of the multiplet patterns observed at ~0.085 and ~0.064 cm^{-1} from impure chrysene in *p*-terphenyl mixed crystals. No absorption patterns were observed, however, at the three energies corresponding to the chrysene-d_{12} zero-field splittings. Conversely, when *p*-terphenyl mixed crystals prepared with chromatographed chrysene-d_{12} were studied, the three absorption patterns attributed to chrysene-d_{12} were observed but the two patterns attributed to 2,3-benzocarbazole were not. These results confirm that 2,3-benzocarbazole was indeed not the source of any of the resonance absorptions attributed to chrysene in our previous analyses[4,5] but was the origin of the ~0.085- and ~0.064-cm^{-1} multiplets observed in those studies.

The correspondence between multiplet signals observed from authentic 2,3-benzocarbazole in *p*-terphenyl, and those observed from 2,3-benzocarbazole incorporated in *p*-terphenyl *via* its occurrence as a contaminant in chrysene-d_{12} suggests the following self-consistent alternatives: (a) that the 2,3-benzocarbazole present as an impurity underwent little or no deuteration during the perdeuteration of its chrysene carrier with the consequence that the present experiments give no information about a possible deuterium isotope effect in 2,3-benzocarbazole; (b) that the 2,3-benzocarbazole was perdeuterated during the predeuteration of its chrysene carrier with the consequence that the present experiments establish that phosphorescent 2,3-benzocarbazole, in contrast to most other triplet

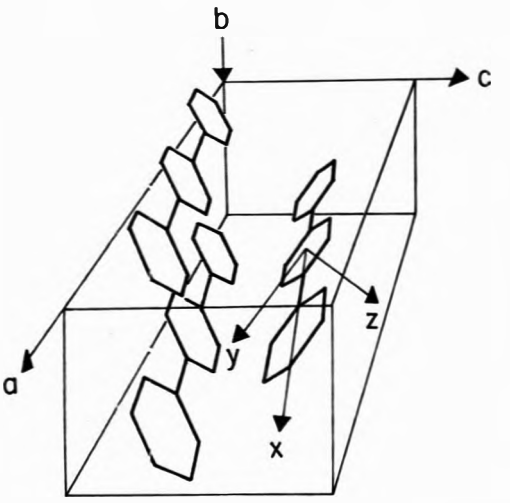

Figure 2. *p*-Terphenyl crystal structure.

states studied in this laboratory,[11,12] manifests essentially no deuterium isotope effect in its zero-field splittings at ~85 K.

Chrysene Host. Single crystals of unpurified chrysene-h_{12} grown by the Bridgman method were of very poor quality. Nonetheless, when photoexcited at ~85 K such crystals manifested intense orange phosphorescence, as did single crystals of 2,3-benzocarbazole in *p*-terphenyl. Two weak resonance absorptions were observed from the (2,3-benzocarbazole in) chrysene crystals. The zero-field splittings associated with the absorptions were determined and found to be 0.08594 cm^{-1} with standard deviation 0.00003 cm^{-1} and 0.06372 cm^{-1} with standard deviation 0.00002 cm^{-1}, respectively. Thus, the approximate values found for the (multiple) zero-field splittings of 2,3-benzocarbazole in *p*-terphenyl host are very similar to these more precise values determined for the two individual signals observed from the chrysene host structure. A quite small host-structure shift in zero-field splittings[3,4] is indicated by a comparison of the average values of the multiple 2,3-benzocarbazole splittings observed for *p*-terphenyl host with the single values obtained for chrysene host.

The observation of multiple resonance absorptions from phosphorescent 2,3-benzocarbazole in *p*-terphenyl, but only single absorptions at corresponding energies for the chrysene host structure, parallels results we have obtained for other triplet states studied in at least two host structures of which one was *p*-terphenyl. For example, chrysene-d_{12} in *p*-terphenyl manifests at least seven resonance absorptions corresponding to the $|D - E|/hc$ zero-field transition but only two absorptions for the same transition when oriented in the OHA host structure.[4] A comparable reduction in number of signals was obtained for chrysene-d_{12} on going from *p*-terphenyl to biphenyl host.[4] We interpret these observations in terms of the propensity of a guest triplet state to adopt a unique orientation at a substitutional site in a given host structure, *e.g.*, 2,3-benzocarbazole in chrysene, or conversely to adopt multiple stable orientations, as is the case for every guest which we have studied in *p*-terphenyl.

If 2,3-benzocarbazole occupies substitutional sites in the *p*-terphenyl host structure (Figure 2) so that its fine structure axes are approximately parallel to the molecular axes of *p*-terphenyl, then provisionally (on the basis of satisfaction of the zero-field selection rules)[4] the zero-field splittings at ~0.085 cm^{-1} may be associated with $|D - E|/hc$ and those at ~0.064 cm^{-1} may be associated with $|D + E|/hc$.

Consistent with this assignment, the values of the spin Hamiltonian parameters for 2,3-benzocarbazole in chrysene at ~85 K are $|D|/hc$ = 0.07483 cm^{-1} and $|E|/hc$ = 0.01111 cm^{-1}, each with standard deviation 0.00003 cm^{-1}. We are not aware of any previous experimental determinations of the spin Hamiltonian parameters of 2,3-benzocarbazole, either for glass or mixed single-crystal systems. However, $|D|/hc$ and $|E|/hc$ for carbazole (Figure 1b) in glassy ether have been measured as 0.102 and 0.007 cm^{-1}, respectively.[13]

Magnetic Resonance Observations for 1,2,3,4-Tetrahydroanthracene (THA) in Symmetric Octahydroanthracene (OHA)

As discussed in a previous paper,[4] extensive purification of OHA, including zone-refining and chromatography, failed to remove an impurity which gave rise to a yellow-green phosphorescence emission from photoexcited single crystals of OHA, both at ~85 and at ~273 K. Only for OHA recrystallized several times from ethanol was significant reduction in the impurity, as evidenced by reduced phosphorescence intensity, obtained.

Two magnetic resonance absorptions were detected from photoexcited single crystals of unpurified OHA and the zero-field splittings associated with the absorptions were determined at ~85 K to be 0.111420 and 0.083237 cm^{-1}, respectively, with estimated uncertainties for replicate determinations ~1 × 10^{-5} cm^{-1}. Magnetic resonance lifetimes measured in experiments at ~0.111 and ~0.083 cm^{-1} were found to be approximately 1 sec at ~85 K. The absorption line width for the signal near ~0.111 cm^{-1} was approximately 15 G.

In an experiment in which the resonant cavity was immersed in a distilled water–ice slush and a bandpass filter[4] for A-H6 excitation was employed, the resonance absorption associated with the zero-field splitting value 0.11142 cm^{-1} at ~85 K was determined semiquantitatively to have a corresponding zero-field splitting at 273 K of 0.1097 cm^{-1}. Thus, an approximate zero-field splitting temperature coefficient of -9×10^{-6} cm^{-1} K^{-1} was observed for the transition at ~0.111 cm^{-1}.

The similarity of the magnitudes of the triplet energy (as evidenced by the observed phosphorescence), zero-field splittings, magnetic resonance lifetime, and temperature coefficient of the $(D - E)$ zero-field splitting of the impurity to the values of these properties for naphthalene suggested that the impurity might be THA, shown in Figure 3a. An additional basis for this suggestion was that in the catalytic hydrogenation of anthracene both THA and OHA (Figure 3b) are produced.

Further verification of the identity of the impurity was made difficult, however, by the behavior of OHA boules grown by the Bridgman method[14] from OHA recrystallized twice from ethanol and then doped with authentic samples of THA. Such boules consistently shattered violently, after exerting sufficient force to break the crystal-growing tubes some hours after they emerged from the heated region of the air-core furnace. In contrast, undoped boules of recrystallized OHA remained ice-clear and retained definite cleavage planes months after being grown. Two groups of investigators have described phase transformations in OHA similar to those observed in the present research, but neither group discussed the role of impuri-

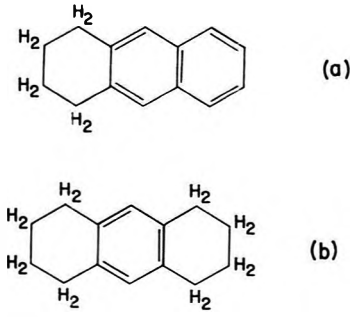

Figure 3. Structure of (a) 1,2,3,4-tetrahydroanthracene and (b) symmetric octahydroanthracene.

ties in the processes.[15,16] A thorough investigation of this problem lay outside the scope of this research.

Inasmuch as whole boules of authentic THA in recrystallized OHA could not be produced, the best single crystal pieces which could be salvaged from shattered boules were employed in double-crystal experiments. A special double-window resonant cavity was constructed and then divided by an opaque partition.[8] A single-crystal of THA in recrystallized OHA was placed behind one window, and a crystal from a boule grown from the same recrystallized OHA (but not doped with THA) was placed behind the other window. Rotation of the resonant cavity by π permitted alternately photoexciting one, but not the other, crystal piece.

In such two-crystal experiments no signals were observed from single crystals of undoped recrystallized OHA whereas for the same host material which had been doped with THA, resonance absorptions were observed at $\sim$0.111 and $\sim$0.083 cm^{-1}. Precision zero-field splitting determinations for the two observed signals at $\sim$85 K yielded values of 0.111424 and 0.083228 cm^{-1} which may be compared with values of 0.111420 and 0.083236 cm^{-1}, respectively, determined (as discussed above) for the resonance absorptions observed at $\sim$85 K from the impurity in unpurified OHA. These precision determinations of zero-field splittings establish the identity of the OHA impurity to be THA.

Due to the comparatively poor quality of OHA crystals obtained in these studies and the lack of a detailed crystal structure determination for OHA it was not possible to assign the observed zero-field energies for THA to corresponding zero-field transitions on the basis of a rigorous investigation of satisfaction of the zero-field selection rules as a function of orientation. By analogy to naphthalene, however, it is plausible to assign the 0.11142- and 0.08323-cm^{-1} splittings to $|D - E|/hc$ and $|D + E|/hc$, respectively. This leads to values of $|D|/hc$ and $|E|/hc$ for THA in OHA of 0.09733 and 0.01410 cm^{-1}, respectively, at $\sim$85 K. (For naphthalene in biphenyl the corresponding values are approximately 0.0993 and 0.0155 cm^{-1}, respectively.) To our knowledge the precision zero-field splittings and spin Hamiltonian parameters presented here for THA are the first such data reported for a partially hydrogenated aromatic hydrocarbon.

References and Notes

(1) This work was supported in part by the National Science Foundation.
(2) Statewide Air Pollution Research Center, University of California, Riverside, Calif. 92502.
(3) R. E. Gerkin and A. M. Winer, *J. Chem. Phys.*, **47**, 2504 (1967).
(4) R. E. Gerkin and A. M. Winer, *J. Chem. Phys.*, **56**, 1359 (1972).
(5) R. E. Gerkin and A. M. Winer, *J. Chem. Phys.*, **58**, 1360 (1973).
(6) P. Mabille and N. P. Buu-Hoi, *J. Org. Chem.*, **25**, 1937 (1950).
(7) D. F. Bender, E. Sawicki, and R. M. Wilson, *Anal. Chem.*, **36**, 1011 (1964).
(8) R. E. Gerkin and P. Szerenyi, *J. Chem. Phys.*, **50**, 4095 (1969).
(9) A. M. Winer, Ph.D. Dissertation, The Ohio State University, 1969.
(10) M. Orchin, *J. Chem. Soc.*, **66**, 535 (1944).
(11) R. E. Gerkin and A. M. Winer, *J. Chem. Phys.*, **50**, 3114 (1969).
(12) A. S. Cullick, R. E. Gerkin, D. L. Thorsell, and A. M. Winer, to be submitted for publication.
(13) S. Siegel and H. S. Judeikis, *J. Phys. Chem.*, **70**, 2201 (1966).
(14) J. N. Sherwood and S. J. Thompson, *J. Sci. Instrum.*, **34**, 42 (1965).
(15) V. N. Vatulev and A. F. Prikhot'ko, *Fiz. Tverd. Tela*, **7**, 42 (1965).
(16) Yu. V. Mnyukh and M. A. Tseneva, *Dokl. Akad. Nauk SSSR*, **162**, 326 (1965).

Radicals Formed after Electron Attachment to 5-Halouracils in Aqueous Glasses[1]

M. D. Sevilla,* R. Failor, and G. Zorman

Department of Chemistry, Oakland University Rochester, Michigan 48063 *(Received October 11, 1973)*

Publication costs assisted by the Atomic Energy Commission and Oakland University

Radicals produced after electron attachment to 5-bromo-6-methyluracil and the 5-halouracils at 77°K in neutral (12 *M* LiCl) and alkaline (8 *M* NaOH) aqueous glasses have been investigated by esr spectroscopy. Electron attachment to 5-bromo-6-methyluracil in 12 *M* LiCl at 77°K results in an anion radical. The anion dehalogenates upon warming at 150°K to form the 6-methyluracil-5-yl radical. Esr spectra indicate that upon further warming this second species undergoes hydrolysis to form the 5-hydroxy-6-methyl-5,6-dihydrouracil-6-yl radical. The results for the halouracils in 12 *M* LiCl suggest stable anions for bromo-, chloro- and fluorouracil at 77°K. Warming the bromouracil anion to 155°K results in a spectrum attributed to the uracilyl radical. Warming to 165°K results in the hydrolysis of the uracilyl radical to form a radical analogous to that found for 5-bromo-6-methyluracil. The fluorouracil and chlorouracil radical anions remained stable throughout the temperature range investigated. In 8 *M* NaOD the π anions were found to be somewhat less stable. The π anions of 5-bromouracil and 5-bromo-6-methyluracil were not observed at 77°K; however, those of chloro- and fluorouracil were observed. The difference in stability of the anions in the two glasses is attributed to the fact that the nitrogens are protonated in the neutral glass whereas they are not in the alkaline glass. In addition protonation of the anion at an oxygen in the neutral glass is also likely. This would produce a neutral radical and result in further stabilization.

Introduction

The radiation sensistivity of 5-bromouracil containing DNA has produced considerable interest in the radiation chemistry of 5-halouracils.[2] This sensitivity has been attributed to the dehalogenation of bromine after attack by radiolytic intermediates.[2] A number of studies employing differing techniques have shown that one of these radiolytic intermediates, the electron, induces reductive dehalogenation in 5-halouracils.[3-5] The primary intermediates, the anion radicals, have been observed in pulse radiolytic experiments in the cases of fluoro- and chlorouracil.[4] The bromouracil anion has not been observed in pulse radiolytic experiments.

Several esr studies have been performed on the halouracils. In an esr investigation employing steady-state radiolysis to generate electrons in aqueous solution it was found that the lifetimes of the halouracil anions were too short to be observed.[5] Esr studies on γ-irradiated single crystals of 5-halouracils have given evidence for radicals which could be interpreted as protonated anions; however no evidence for dehalogenation was found.[6,7]

Esr studies in alkaline aqueous glasses at low temperature have resulted in conflicting reports that the anion radicals of the 5-halouracils are stable at 77°K[8] and that they are unstable toward dehalogenation at this temperature.[9] In order to resolve this apparent discrepancy as well as to further elucidate the mechanisms of reaction after electron attachment to 5-halouracils, we have investigated the reaction of electrons with these compounds in neutral and alkaline aqueous glasses.

Experimental Section

5-Halouracils were obtained from Calbiochem (A grade) and used without further purification. 5-Bromo-6-methyluracil was synthesized from 6-methyluracil by the method of Sasaki and Ardo.[10] The product was recrystallized from ethanol.

The experimental procedure was essentially that used in our previous work in 8 *M* NaOD and 12 *M* LiCl.[9,11,12] In this technique a solution of 12 *M* LiCl-H_2O, 12 *M* LiCl-D_2O (98% D), or 8 *M* NaOD (*ca.* 92% D) containing 10 m*M* $K_4Fe(CN)_6$ and *ca.* 1 m*M* of the halouracil is cooled to 77°K. The glass formed is photolyzed with 254-nm light at 77°K for times usually less than 1 min. Trapped electrons formed in the photolysis are photobleached with *filtered* light from an incandescent lamp. The filter used (a mixed solution of $K_4Fe(CN)_6$ and $K_3Fe(CN)_6$) filtered uv and blue light. This was necessary as several of the anion radicals formed dehalogenated when exposed to unfiltered light.

The *g* values and hyperfine splittings in this work are measured relative to potassium peroxylamine disulfonate (A_N = 13.0 G and *g* = 2.0056). The *g* values are measured from the center of the spectrum and are reproducible to ±0.0003.

Results and Discussion

I. 5-Bromo-6-methyluracil. 5-Bromo-6-methyluracil in a Neutral Glass. 5-Bromo-6-methyluracil (BrMeU) was investigated to aid our interpretation of the results found for the halouracils which follow. The substitution of a methyl group at position 6 allows for a clear distinction between the various radicals formed after electron attachment.

The reaction of electrons with BrMeU in 12 *M* LiCl-D_2O at 77°K resulted in the spectrum in Figure 1A. Analysis of the *ca.* 1:3:3:1 quartet yields a 16.8-G methyl group splitting with *g* = 2.0026. This initial spectrum could be due to the anion radical or the 6-methyluracil-5-yl radical (radical II) produced by debromination of the anion. The following evidence strongly supports the anion as the initial species. First, the methyl group splitting is nearly identical with that found for the methyl group in the 6-methyluracil anion.[8] Next resolution of the methyl proton splittings would not be expected for the 6-methyluracil-5-

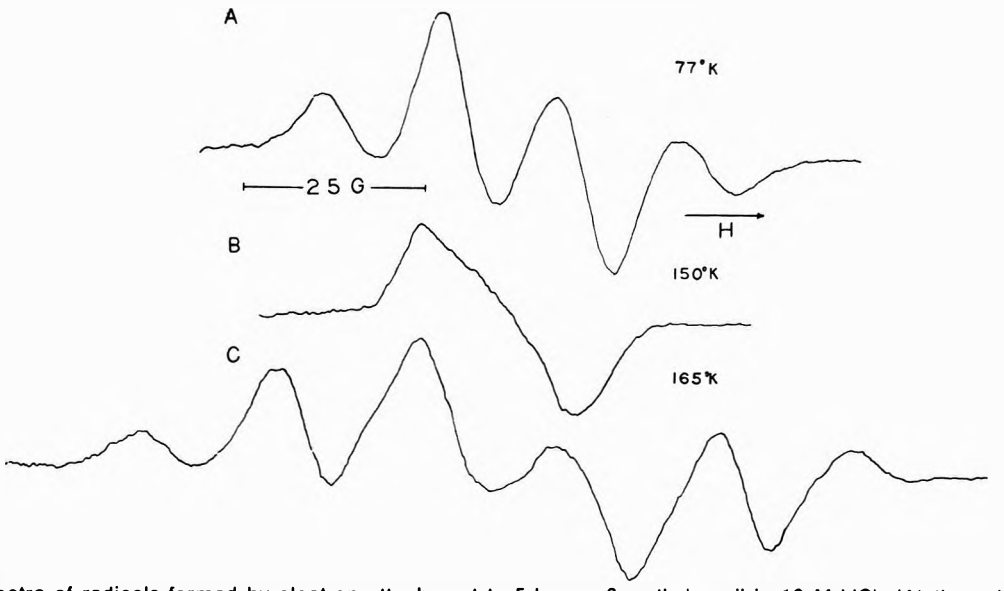

Figure 1. Esr spectra of radicals formed by electron attachment to 5-bromo-6-methyluracil in 12 *M* LiCl: (A) the anion radical (I) or its protonated analog in D_2O at 77°K; (B) the 6-methyluracil-5-yl radical (II) in D_2O after warming to 150°K; (C) the 5-hydroxy-6-methyl-5,6-dihydrouracil-6-yl radical (III) after further warming to 165°K in H_2O.

yl radical due to the nature of the interaction in σ radicals. Finally the observed splitting is in agreement with π-electron spin density calculations which indicate a large spin density ($\rho \cong 0.5$) at position 6 in all uracil and halouracil anions.[8,13,14] Warming the anion to 140°K or irradiating with unfiltered light from an incandescent lamp gave the 24-G singlet shown in Figure 1B. This spectrum is attributed to radical II produced by debromination as shown in reaction 1. Resolution of the methyl proton splittings is not found for this radical as expected.

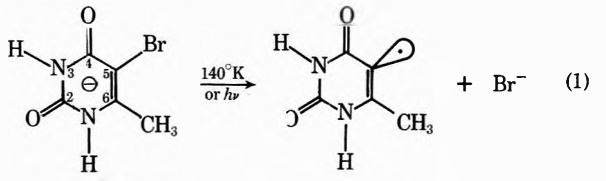

I II

Further warming of radical II in LiCl–H_2O to 160°K resulted in the spectrum shown in Figure 1C. The spectrum consists of six lines in the approximate ratio of intensities 1:3:4:4:3:1. Interpretation of the spectrum yields a 19.5-G splitting due to three equivalent protons and a 42-G splitting due to a single proton. The only radical consistent with such splittings is a radical with one β proton at the 5 position and a radical site at position 6. This strongly suggests that the hydration reaction (reaction 2) takes

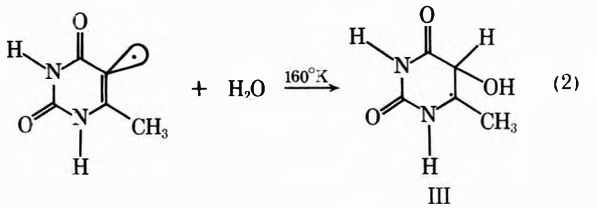

III

place on warming to form the 5-hydroxy-6-methyl-5,6-dihydrouracil-6-yl radical (III). This is confirmed by the fact that a quartet of 20 G is observed in LiCl–D_2O after warming to 170°K. Due to the wide line widths the β deuteron splitting is not resolved. To eliminate the possibility that a bimolecular reaction of the radical with the parent compound was occurring, experiments were performed where the original concentration of BrMeU was varied over tenfold in LiCl–H_2O. The results showed no change in the rate of production of the third radical species with concentration as would be expected for a hydration reaction.

5-Bromo-6-methyluracil in a Alkaline Glass. Electron attachment to BrMeU in 8 *M* NaOD at 77°K resulted in an esr spectrum consisting of a 8-G wide singlet at g = 2.0022. Since a quartet spectrum is expected for the π anion,[15] the results suggest the π-anion radical is not stable in 8 *M* NaOD. The observed spectrum is associated with the 6-methyluracil-5-yl radical (radical IV).

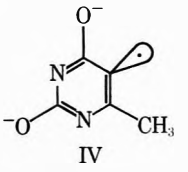

IV

Although radical IV shows no more resolution than the very similar radical II, the line width for radical IV is considerably less than that found for II. This may be due to the structural differences in the two radicals. Warming radical IV to 160°K resulted is a second radical perhaps due to a hydration reaction. However this spectrum has not yet yielded to interpretation.

The greater stability of the anion in the neutral glass over that found in the alkaline glass may be due in part to the fact that the nitrogens are protonated in the neutral glass. In addition the production of a neutral radical by protonation of an oxygen is likely. This would further stabilize the radical. Such oxygen protonated radicals have been suggested from studies of the γ irradiation of 5-halouracil single crystals[6] and the pulse radiolysis of thymine in aqueous solution.[16]

2. 5-Halouracils in a Neutral Glass. 5-Bromouracil. Electron attachment to 5-bromouracil (BrU) at 77°K in 12 *M* LiCl–D_2O or –H_2O results in a 13-G doublet spectrum at g = 2.0025 as shown in Figure 2A. Warming to 155°K results in a irreversible conversion to a broad 31-G singlet in D_2O (Figure 2B). In H_2O the singlet is somewhat more broad. In light of the results found for MeBrU, where the

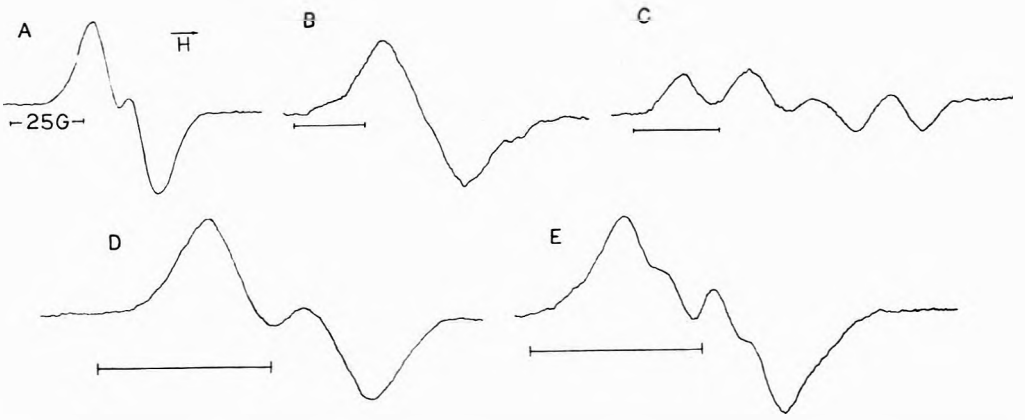

Figure 2. Esr spectra of radicals formed by electron attachment to 5-halouracils in 12 *M* LiCl: (A) the 5-bromouracil anion or its protonated analog at 77°K in D_2O; (B) the uracil-5-yl radical (V) produced by warming the bromouracil anion to 155°K in D_2O; (C) the 5-hydroxy-5,6-dihydrouracil-6-yl radical (VI) produced by warming V to 160°K in H_2O; (D) the chlorouracil anion or protonated analog at 77°K in D_2O; (E) the fluorouracil anion or protonated analog at 140°K in D_2O.

well-resolved anion converts to a broad singlet, a reasonable explanation of these results is that the initial spectrum is due to the anion or protonated anion and the second broadened spectrum is due to the uracil-5-yl radical (V). We therefore tentatively assign the initial species to the anion radical and the second species to the uracilyl radical. Upon warming the second species to 160°K in $LiCl-H_2O$ a quartet spectrum shown in Figure 2C is found. Interpretation of this spectrum results in a 41-G (β proton) splitting and a 20.5-G (α proton) coupling. In D_2O only a 19-G doublet is observed. These results are excellent evidence for the hydration of the uracilyl radical to produce radical VI as in reaction 3. If samples are warmed

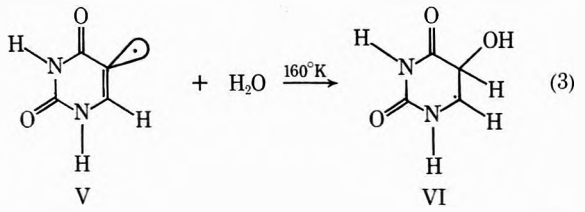

V VI

directly to 165°K where the glass softens to allow radical migration the quartet spectrum appears in much lessened intensity. This is attributed to radical–radical recombination which competes with the hydration reaction at these temperatures.

5-Chlorouracil. Electron attachment to 5-chlorouracil (ClU) in 12 *M* $LiCl-D_2O$ or $-H_2O$ results in an esr spectrum consisting of a 15-G doublet splitting at $g = 2.0029$ (Figure 2D). The radical remained stable to 165°K where the glass softens. The g value, hyperfine splitting, and temperature stability of this radical strongly suggest that it is the anion or protonated anion. No evidence is found for a broad singlet spectrum expected for a uracilyl radical; however, a partial conversion to a quartet identical with that found for BrU is found to appear at 165°K in some experiments. This may be due to partial dehalogenation of the anion caused by the warming or more likely by light during photobleaching and transfer.

5-Fluorouracil. Electron attachment to 5-fluorouracil (FU) at 77°K results in evidence for an exceptionally stable anion. Over the temperature range 77–170°K a spectrum is found consisting of a 13-G doublet further split by a second doublet of 5.3 G with $g = 2.0033$ (Figure 2E). This second splitting is likely due to interaction with the fluorine atom in the anion. This is reasonable in light of the nuclear spin of ½ for fluorine and the fact that even a

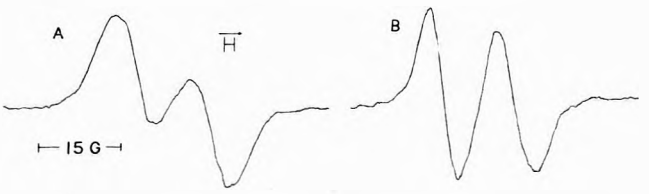

Figure 3. Esr spectra of radicals formed by electron attachment to 5-chlorouracil in 8 *M* NaOD: (A) the π anion radical at 77°K; (B) the uracil-5-yl radical at 110°K formed by photolyzing the radical in A with unfiltered visible light.

small spin density on a fluorine can result in a relatively large hyperfine splitting.[17] No temperature dependence in hyperfine splitting or g value was observed.

3. 5-Halouracils in an Alkaline Glass. Reaction of electrons with the 5-halouracils in 8 *M* NaOD resulted in stable π anions in two cases. Electron attachment to FU at 77°K resulted in an esr spectrum whose analysis yielded at 12-G splitting at $g = 2.0033$. The g value is the same as found in LiCl and is good evidence for an π-anion radical. No further reaction was noted upon photobleaching with unfiltered light or warming. At 77°K electron attachment to ClU resulted in an initial spectrum indicative of the π anion. The spectrum consists of a 14-G doublet and $g = 2.0028$ (Figure 3A). The π anion was light sensitive and upon irradiation with unfiltered light from an incandescent lamp for 10 min converted to a much more well-resolved 13.1-G doublet splitting at $g = 2.0022$ (Figure 3B). Irradiation for intermediate time periods resulted in spectra which showed an overlap of both the π anion and the second radical. Electron attachment to BrU at 77°K resulted in a spectrum identical in hyperfine splitting, g value and line shape with the second radical found for ClU. In addition both the second radical from ClU and the BrU radical power saturated readily; thus, low microwave power levels were utilized in the recording of their spectra. These spectra are likely due to the uracil-5-yl

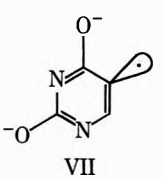

VII

radical (radical VII) produced by dehalogenation of the π anions of ClU and BrU. Several findings support this con-

clusion. The low g value is indicative of a σ radical.[18] The 13-G splitting observed for this radical is in the range expected for σ radicals of aromatic systems. For example, the phenyl radical has an ortho splitting of 18 G whereas the 2-pyridyl radical has an ortho hydrogen splitting of 8 G.[19] The fact that BrU and ClU give identical spectra is also good evidence for dehalogenation. Finally the improved resolution of the uracilyl radical in NaOD over that found in LiCl-D_2O is in agreement with the results found for 6-methyluracil-5-yl in the two media.

In light of these results we must correct our previous work where we reported stable anions for all halouracils in 8 M NaOD at $-160°$.[8] In our present work we have shown that the BrU π anion is unstable in 8 M NaOD even at 77°K; whereas, the FU and ClU π anions are found to be stable at 77°K. Since in the previous work samples were photobleached with unfiltered light the ClU π anion was likely predominantly converted to the uracilyl radical. The report by Simpson and Zimbrick that all halouracil anions are unstable toward dehalogenation at 77°K in 8 M NaOD is also in disagreement with the results of this work. These workers do not report photobleaching with filtered light. This would explain the lack of observance of the ClU π anion. Since the BrU π anion is unstable it would also not be observed; however, the FU π anion is stable to visible light and should be observed.

An explanation for the difficulty in the identification of the radicals observed in 8 M NaOD in our work and other work is that the halouracil π anions and the uracilyl radical have very similar spectra in the alkaline glass. However as we have indicated these radicals can be distinguished by differences in g value, line shape, and power saturation behavior.

Comparison to Other Work and Conclusions. A comparison of our results with some recent work is of interest. Patterson and Bansal report in a pulse radiolysis study that the stabilities of the halouracil anions are in the order FU > ClU ≫ BrU.[4] We find the same order of stabilities in the neutral and alkaline glasses. In a conductometric pulse radiolysis study Bhatia and Schuler have reported that the protonation of ClU anion at pH 5.2 effectively competes with dehalogenation, and that this competition is pH dependent.[3b] In agreement with these results we find that the ClU anion is much more stable in a neutral aqueous glass than in an alkaline glass. We attribute this to protonation of the anion at an oxygen resulting in a more stable neutral radical. Bhatia and Schuler did not find evidence for a protonated BrU anion even at low pH, whereas our results suggest this species may be stable at low temperature in a neutral glass. Patterson and Bansal report that the uracilyl radical gave a hydrolysis intermediate.[4] This finding is in good agreement with the results found here. However, we have been able to identify the hydrolysis intermediate as radical VI.

Zimbrick, Ward, and Myers have hypothesized a mechanism for radiation sensitization of BrU-DNA.[2] They suggest that electron attachment to BrU in BrU-DNA results in the uracilyl radical and that this species subsequently abstracts from an adjacent deoxyribose group. The final step leads to single strand breakage. This mechanism is quite plausible. However, we can suggest that the hydration of the uracilyl radical is a possible competing reaction with the abstraction reaction. This is reasonable is light of the fact that the uracilyl radical would have restricted movement in the DNA structure. The hydrated radical if formed could of course also abstract from the ribose group; although, this would be less favored energetically than abstraction by the uracilyl radical.

Acknowledgment. The authors would like to thank Virginia Brooks for synthesis of 5-bromo-6-methyluracil.

References and Notes

(1) This research was supported in part by the Division of Biomedical and Environmental Research of the U. S. Atomic Energy Commission.
(2) J. E. Zimbrick, J. F. Ward, and L. S. Myers, Jr., *Int. J. Radiat. Biol.*, **16**, 505 (1969); **16**, 525 (1969).
(3) (a) K. M. Bansal, L. K. Patterson, and R. H. Schuler, *J. Phys. Chem.*, **76**, 2386 (1972); (b) K. Bhatia and R. H. Schuler, *ibid.*, **77**, 1888 (1973).
(4) L. K. Patterson and K. M. Bansal, *J. Phys. Chem.*, **76**, 2392 (1972).
(5) P. Neta, *J. Phys. Chem.*, **76**, 2399 (1972).
(6) J. Hüttermann and A. Müller, *Int. J. Radiat. Biol.*, **15**, 297 (1969).
(7) E. G. Nice and D. Rorke, *Int. J. Radiat. Biol.*, **15**, 197 (1969).
(8) M. D. Sevilla and C. Van Paemel, *Photochem. Photobiol.*, **15**, 407 (1972).
(9) L. D. Simpson and J. D. Zimbrick, *Radiat. Res.*, **51**, 459 (1972).
(10) T. Sasaki and M. Ando, *Bull. Chem. Soc. Jap.*, **41**, 2215 (1968).
(11) M. D. Sevilla, *J. Phys. Chem.*, **74**, 669 (1970).
(12) M. D. Sevilla, C. Van Paemel, and G. Zorman, *J. Phys. Chem.*, **76**, 3577 (1972).
(13) J. Baudet, G. Berthier, and B. Pullman, *C. R. Acad. Sci.*, **254**, 762 (1962).
(14) M. D. Sevilla, *J. Phys. Chem.*, **75**, 626 (1971).
(15) Due to the fact that the nitrogens of the parent compound are deprotonated in this alkaline matrix, this species is likely a trianion radical. To emphasize the fact that it is the π-electron system which has gained the electron the radical is designated a π-anion radical.
(16) L. M. Theard, F. C. Peterson, and L. S. Myers, Jr., *J. Amer. Chem. Soc.*, **75**, 3815 (1971).
(17) A. Carrington and A. D. McLachlan, "Introduction to Magnetic Resonance," Harper and Row, New York, N. Y., 1967, p 112.
(18) R. W. Fessenden and R. H. Schuler, *J. Chem. Phys.*, **39**, 2147 (1963).
(19) J. E. Bennett and B. Mile, *J. Phys. Chem.*, **75**, 3432 (1971).

Electron Paramagnetic Resonance of Ruthenium(III) Halopentaammines in Single Crystals

Doron Kaplan and Gil Navon*

Department of Chemistry, Tel-Aviv University, Tel-Aviv, Israel *(Received June 25, 1973; Revised Manuscript Received January 7, 1974)*

The epr of $[Ru(NH_3)_5Cl]^{2+}$ and $[Ru(NH_3)_5Br]^{2+}$ imbedded in single crystals of $[Co(NH_3)_5Cl]Cl_2$ has been investigated. The tetragonal and rhombic splittings and the orbital reduction factors were calculated from the experimental g tensors. The corrected orbital reduction factor $k_{\pi\pi}$ was estimated as 0.81 in both complexes. It was found that $E(xz,yz) > E(xy)$, and that the tetragonal splitting is larger when the axial ligand is the chloride ion, while the rhombic is the same in both complexes. A discussion of the energy levels in terms of the π antibonding interaction is given.

Introduction

The effect of various ligands on the energy levels in tetragonal complexes has drawn a considerable interest,[1] and has been formulated in terms of the crystal field and molecular orbital theories.[2-5] Most of the experimental data were taken from optical spectroscopy measurements. However, both σ and π interactions contribute to the observed optical transition energies, and the separation of these two factors is not straightforward. Electron paramagnetic resonance parameters, on the other hand, are determined by the properties of the ground state almost exclusively, and can thus be used for the evaluation of either σ or π interaction in those cases where the unpaired electron occupies a t_{2g} or an e_g orbital, respectively. Since chemical properties are usually ground-state properties, epr parameters become very useful for correlations of electronic structure with chemical behavior.

In the case of low-spin d^5 complexes, the unpaired electron occupies the t_{2g} orbitals which are split under the combined effect of noncubic ligand fields and spin–orbit coupling. It is the purpose of the present work to investigate the effect of halide ligands on the energy levels and on the covalency in ruthenium(III)–ammine complexes.

Experimental Section

$[Ru(NH_3)_5Cl]Cl_2$, $[Ru(NH_3)_5Br]Br_2$, and $[Co(NH_3)_5Cl]Cl_2$ were prepared as described earlier.[6-8] All compounds were recrystallized twice from water. Absorption spectra of the aqueous solutions of the compounds were found to be identical with spectra published in the literature.[9,10]

Single crystals for the epr measurements were prepared from mixed aqueous solutions of the cobalt and the ruthenium complexes. About 20 ml of a saturated $[Co(NH_3)_5Cl]Cl_2$ solution, containing 4–5% of the ruthenium salt, was left in an evaporating dish, at room temperature, under a mild air stream. Crystallization was thus effected before the complexes were appreciably hydrolyzed. Crystals formed within 48 hr and were about 1 mm in length.

Epr spectra were obtained with a Varian V-4502 X-band spectrometer. The crystal was mounted on a goniometer head, aligned by X-ray oscillation and precession photographs, and transferred to a quartz rod by means of a double-micrometer device. The final crystal orientation in the cavity was found to be correct within ±2° as proved by Lauë photographs of the transferred crystals. Cooling to 77°K was achieved by immersing the crystal in liquid nitrogen contained in a "finger" type dewar, which was inserted into the cavity. Lower temperatures were obtained in a special tubular dewar passing through the cavity. The crystal was mounted inside the dewar and cooled by a stream of helium gas.

Calibration of the g factors was done using a sample of DPPH which was mounted near the crystal.

Experimental Results

The crystal structure of $[Co(NH_3)_5Cl]Cl_2$ has been determined.[11] The crystals are orthorhombic with the Co–Cl bond axis in the cation lying in a crystallographic ac plane. The unit cell in a ruthenium-doped crystal contains two pairs of magnetically nonequivalent complex ions, and hence the epr spectrum of a crystal in an arbitrary direction is expected to be composed of two signals. The two signals should coincide when the magnetic field is parallel to either of the crystallographic planes ab and bc. The largest magnetic anistropy should be found in the bc plane. We found that the epr spectra of the crystals doped with ruthenium complex ions behave according to crystal structure (Figure 1). The measurements of the angular behavior of the epr signals have been performed at 77°K.

The g tensors were calculated from these measurements according to Schonland.[12] We define the g tensor principal axes in terms of the angles θ and φ, which are the polar angles of the z direction of the g tensor in the crystallographic coordinate system. The g tensors and their principal axes are given in Table I.[13]

Our measured values of θ and φ of 48 and 0° respectively should be compared with the values 49 and 0° which can be calculated from the crystallographic data of ref 11.

At 77°K the epr line widths of both the chloropentaammine and the bromopentaammine complexes are of the order of 100 G. The resonance lines of the $[Ru(NH_3)_5Br]^{2+}$ spectra were also quite distorted at this temperature. On cooling the crystals below 60°K, a hyperfine structure in the form of four equally spaced, equally intense lines per each magnetic site was resolved in the $[Ru(NH_3)_5Br]^{2+}$ spectrum. We assign this structure to an interaction of the unpaired electron spin with the bromine nuclear spin ($I = 3/2$). The resonance line width of the $[Ru(NH_3)_5Cl]^{2+}$ ion was narrowed upon cooling, but no ligand hyperfine structure was observed even at 7°K.

The resonance line width of both complexes was also

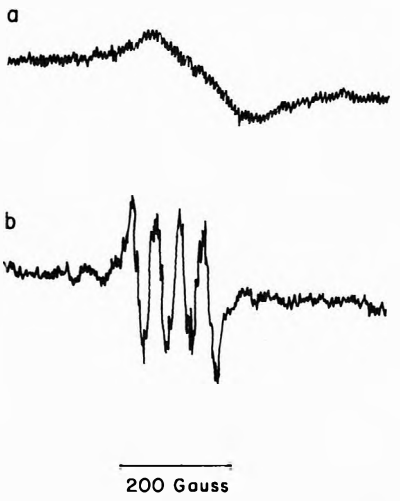

Figure 1. Epr spectra of $[Ru(NH_3)_5Br]^{2+}$ in $[Co(NH_3)_5Cl]Cl_2$ at (a) 77, and (b) 16°K. Only the lower field signal is shown.

TABLE I: *g* Tensors and Magnetic Principal Axes in Ruthenium Halopentaammines

	$[Ru(NH_3)_5Cl]Cl_2$	$[Ru(NH_3)_5Br]Br_2$
$\|g_x\|$	0.987 ± 0.008	1.13 ± 0.01
$\|g_y\|$	1.513 ± 0.005	1.634 ± 0.008
$\|g_z\|$	2.983 ± 0.003	2.798 ± 0.004
θ_1	0.0 ± 0.1°	0.0 ± 0.2°
φ_1	48.0 ± 0.1°	48.0 ± 0.2°
θ_2	0.0 ± 0.1°	0.0 ± 0.2°
φ_2	132.0 ± 0.1°	132.0 ± 0.2°

found to depend on the orientation of the crystal in the magnetic field. Further investigation of these phenomena is planned.

Analysis of the *g* Tensors

The theory of low-spin d^5 complexes has been formulated by Bleaney and O'Brien[14] and by Griffith.[15] In principle, the system is treated as a one-hole t_{2g} configuration. The real functions *xz*, *yz*, and *xy*, which are the π-antibonding molecular orbitals, are split under the combined effect of noncubic ligand fields and the spin–orbit coupling. The diagonal elements of the ligand field perturbation are $-1/2\ v$, $1/2\ v$, and Δ for the *xz*, *yz*, and *xy* orbitals, respectively, while the off-diagonal elements are assumed to vanish. On application of the perturbation hamiltonians an energy matrix[14,15] is obtained, the eigenvalue of which are three Kramers doublets.

We write the ground state in the form[14,15]

$$|+\rangle = A|\zeta^+\rangle + B|-1^-\rangle + C|1^-\rangle$$
$$|-\rangle = -A|\zeta^-\rangle + B|1^+\rangle + C|-1^+\rangle \quad (1)$$

where $|1\rangle = -(1/\sqrt{2})(xz + iyz)$, $|-1\rangle = (1/\sqrt{2})(xz - iyz)$, $|\zeta\rangle = ixy$, and the superscripts plus or minus indicate the spin state.

Next, one diagonalizes the usual Zeeman perturbation within the ground-state doublet, arriving at a set of equations

$$g_z = 2A^2 - 2(k+1)B^2 + 2(k-1)C^2$$
$$(1/2)(g_x + g_y) = -2(A^2 + \sqrt{2}kAB) \quad (2)$$
$$(1/2)(g_x - g_y) = 2(2BC + \sqrt{2}kAC)$$

where k is the orbital reduction factor. This formulation implies that g_x and g_y have similar signs.[14]

$$A^2 + B^2 + C^2 = 1 \quad (3)$$

is the normalization condition.

In the above treatment, the interactions of the t_{2g}^5 with excited configurations were neglected. However, they are taken into account later in the corrections of k.

A computer program was written in order to evaluate the various parameters appearing in eq 1 and the ligand field energy levels. In order to do this, the sign of the g factors should be known. We have tried to solve eq 1, substituting all the possible sign combinations of g_x, g_y, and g_z, within the limitation that the signs of g_x and g_y are equal. This procedure yielded only two possible solutions for each of the ruthenium halopentaammines. However, one solution of the two contained an internal inconsistency, namely, the expected "ground" state lying between the other two energy levels. In the same solutions, the k values were not physically acceptable, being 1.47 for the $[Ru(NH_3)_5Cl]^{2+}$ and 1.63 for the $[Ru(NH_3)_5Br]^{2+}$ complex. These solutions were thus discarded. The two acceptable solutions are presented in Table II. They correspond to negative signs of the three elements of the g tensors in both complexes. We also include in Table II the energy differences, ΔE_1 and ΔE_2, between the two excited levels and the ground-state Kramers doublet.

TABLE II: Ground-State Wave Function Parameters, Orbital Reduction Factors, and Energy Level Splittings in Ruthenium Halopentaammines

	$[Ru(NH_3)_5Cl]Cl_2$	$[Ru(NH_3)_5Br]Br_2$
A	0.388	0.426
B	0.920	0.903
C	0.056	0.053
k	0.939	0.936
Δ/λ	−0.873	−0.663
V/λ	−0.158	−0.158
$\Delta E_1/\lambda$	−1.306	−1.340
$\Delta E_2/\lambda$	−1.977	−1.837

It can be seen from Table II that the rhombic potentials obtained for both complexes are identical within the experimental error. This is understandable as the same host crystal was used for the epr measurements of both compounds. Since the rhombic potential is small in comparison to the tetragonal, a simplified calculation can be made by assuming an entirely tetragonal distortion. Setting $v = 0$, $g_\parallel = g_z$, $g_\perp = (1/2)(g_x + g_y)$, one obtains from eq 1[16]

$$g_\parallel = -2[(1+k)\cos^2\alpha - \sin^2\alpha]$$
$$g_\perp = -2[\sqrt{2}k\cos\alpha\sin\alpha + \sin^2\alpha]$$

where

$$\tan 2\alpha = \sqrt{2}\left(\frac{1}{2} - \frac{\Delta}{\lambda}\right)$$

The results for k and for Δ/λ are then respectively 0.935 and −0.877 for the $[Ru(NH_3)_5Cl]^{2+}$ ion, and 0.932 and −0.670 for the $[Ru(NH_3)_5Br]^{2+}$ ion.

A comparison of these values with those appearing in Table II shows that the rhombic distortion, although largely affecting the g tensor, has practically no effect on either k or Δ.

Discussion

It is interesting to compare the $[Ru(NH_3)_5X]^{2+}$ cation, where X is a halide ion, to the $[Ru(NH_3)_6]^{3+}$ ion. The epr

TABLE III: An Analysis of the g Tensors Obtained in Ref 17 for $[Ru(NH_3)_6]Cl_3$ in $[Co(NH_3)_6Cl_3]$

g_x	g_y	g_z	k	Δ/λ	V/λ	$\Delta E_1/\lambda$	$\Delta E_2/\lambda$
−2.06	−2.02	−1.72	0 95	0.12	−0.02	−1.54	−1.46
−1.80	−1.90	−2.06	0 94	−0.08	0.04	−1.47	−1.53
−1.15	−1.84	−2.66	0 95	−0.51	0.22	−1.37	−1.75

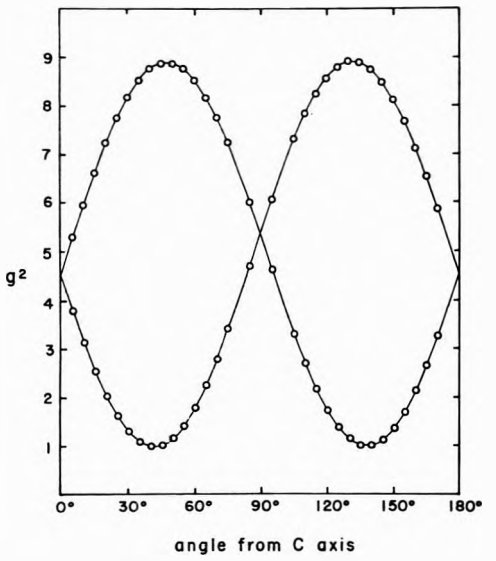

Figure 2. Angular dependence of g^2 in the ac plane for $[Ru(NH_3)_5Cl]^{2+}$ in $[Co(NH_3)_5Cl]Cl_2$ at 77°K.

spectrum of $[Ru(NH_3)_6]Cl_3$ in single crystals of $[Co(NH_3)_6]Cl_3$ has been investigated by Griffiths, Owen, and Ward.[17] These authors observed three different g tensors, which were assigned to different crystal field environments. We made use of their results, feeding the experimental g values in our programs, and using all the possible sign combinations as before. The resulting parameters are given in Table III.

One should note that k is not greatly changed upon going from the hexaammineruthenium complex to the halopentaammineruthenium complexes. We should recall that any possible anisotropy in k has been ignored in our calculation. The lack of dependence of k on the nature of the axial ligand (*i.e.*, when this ligand is NH_3, Cl^-, or Br^-) indicates that k may indeed be isotropic in this case.

Thornley[18] has shown that the factor k is not a pure π orbital reduction factor when the t_{2g}^5 configuration in the ground state is mixed with low-lying $t_{2g}^{5-n}e_g^n$ excited states. In that case, k is a combination of two factors, $k^6_{\pi\pi}$ and $k_{\sigma\pi}$. This point has been further discussed by Griffith[19] who considered also the interaction between the two terms $^2T_{2g}'$ and $^2T_{2g}''$ of the $t_{2g}^4e_g$ configuration. To first order, only these two terms are mixed with the $^2T_{2g}$ of t_{2g}^5 under the electrostatic interaction. Interactions due to spin-orbit coupling were found to be small[18] and were neglected. The energy levels of the mixed $^2T_{2g}'$ and $^2T_{2g}''$ are

$$E_1 = 10Dq + (7 + \sqrt{34})B - C$$
$$E_2 = 10Dq + (7 - \sqrt{34})B - C \qquad (4)$$

B and C are the Racah parameters. Then[19]

$$k = k_{\pi\pi} + k_{\sigma\pi}B(13.2E_1^{-1} - 1.2E_2^{-1}) \qquad (5)$$

For simplicity, one may assume $k_{\sigma\pi} = k_{\pi\pi}$, while $10Dq$, B, and C are usually known from the d–d transitions in the optical specturm of the complex. However, the absorption spectra of ruthenium–ammine complexes are dominated by charge transfer bands[10] which render the evaluation of energy parameters very difficult. Only for $[Ru(NH_3)_6]^{3+}$ approximate values of $10Dq$ and B could be estimated from the spectrum (assuming $C = 4B$, G. Navon, unpublished results). These values are 3.4×10^4 and 580 cm^{-1}, respectively. We then find from eq 4 and 5 $k_{\pi\pi} = 0.81$ for the ruthenium–hexammine complex.

It has been reported[5] that in the acidopentaammines of cobalt and chromium, the Racah parameter C is unaffected by the nature of the acido ligand. If we assume that this is also true for the acidopentaammines of ruthenium, then $k_{\pi\pi} = 0.81$ also for chloro- and bromopentaammineruthenium. This value may be compared with the results obtained for other d^5 metal complexes. For example, the corrected $k_{\pi\pi}$ is in the range of 0.72–0.87 for various covalent iron(III) complexes, such as, $[Fe(CN)_6]^{3-}$, $Fe(S_2COC_2H_5)_3$, and $[Fe(phen)_3]^{3+}$ [20] and 0.72 in $[IrCl_6]^{2-}$.[18] Thus the covalency of ruthenium(III)–ammine complexes is comparable to that of strongly covalent complexes of iron(III) and smaller than that of hexachloroiridium(IV). Uncorrected orbital reduction factors in several ruthenium complexes have been reported by Hudson and Kennedy.[21] Most of their values are close to 1.00 but correcting those k values according to the above procedure should lead to lower results as well.

The magnetic susceptibilities of ruthenium–ammine complexes have been measured and the results were used for the evaluation of k.[22] The values of k, found by this method, were 0.95 and 1.00 (±0.05) in $[Ru(NH_3)_5Cl]Cl_2$ and $[Ru(NH_3)_6]Cl_3$, respectively. These values are in agreement with our (uncorrected) value of 0.94–0.95 and correspond to a practically ionic metal–ligand bond. Taking account of the contribution of excited states leads, however, to $k_{\pi\pi}$ values which are more acceptable from a chemical point of view.

The orbital reduction factor is related to the covalency parameter used in the molecular orbital formulation. The π molecular orbital in the complex may be written as

$$|t_{2g}\rangle = N_\pi(d_{t_{2g}} - \lambda_\pi\chi)$$

Here λ_π is the covalency parameter and χ is the appropriate linear combination of the ammonia π orbitals. It can be shown that[16,23]

$$k_{\pi\pi} = 1 - \frac{1}{2}N_\pi^2\lambda_\pi^2 \qquad (6)$$

Neglecting the overlap integral, we have

$$N_\pi^2 = (1 + \lambda_\pi^2)^{-1} \qquad (7)$$

and substituting our value of $k_{\pi\pi}$, we obtain $\lambda_\pi = 0.78$. This value is significantly higher than the value of $\lambda_\pi = 0.28$, calculated from nmr paramagnetic shifts of the ammine proton of the $[Ru(NH_3)_6]^{3+}$.[24] Also it may be pointed out that using eq 6 and 7, a "perfect" covalency with $\lambda_\pi = 1$ gives $k_{\pi\pi} = 0.75$, while a value of $k_{\pi\pi} = 0.72$ has been calculated for both $IrCl_6^{2-}$ [18] and $[Fe(CN)_6]^{3-}$.[20]

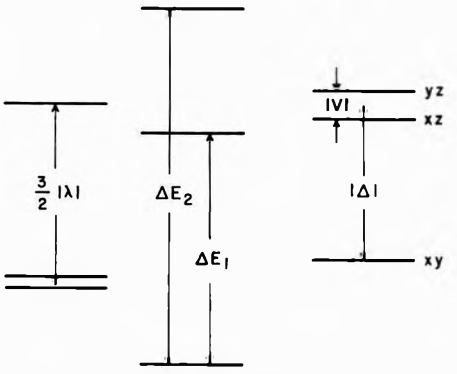

Figure 3. One-electron energy level scheme, drawn to scale for the $[Ru(NH_3)_5Cl]^{2+}$ ion: left, spin-orbit coupling only; right, tetragonal and rhombic splittings only; middle, actual energy levels.

An uncorrected k value of 0.74 for $[Mn(CN)_6]^{4-}$ has been reported.[14] This indicates that the evaluation of the covalency parameter λ_π from the orbital reduction factor is unsatisfactory and should be further elaborated. We note here that the incorporation of ligand-ligand overlap integrals in the relation between $k_{\pi\pi}$ and λ_π[25] does lead to a reduced value of λ_π. The correction obtained, however, seems to be insignificant.

We next discuss the energy level splitting. In Table II the values of Δ/λ found for the ruthenium-halopentammine complexes are listed. In order to calculate the absolute magnitude of Δ in each complex, the spin-orbit coupling constant in that complex should be known. The spin-orbit coupling constant in the Ru^{3+} free ion has been reported to be -1180 cm^{-1},[26] and we should expect the same parameter in the complex to be smaller. We assume that λ in $[Ru(NH_3)_6]^{3+}$ and in $[Ru(NH_3)_5X]^{2+}$ (X = Cl^-,Br^-) ions is about -1000 cm^{-1}. In that case, the tetragonal splitting would be -870 and -660 cm^{-1}, respectively.

Earlier in this paper Δ was defined as

$$\Delta = E(xy) - \frac{1}{2}[E(xz) + E(yz)]$$

so that Δ is positive when the xz, yz doublet lies lower than xy in the energy scale. By working in the one-hole scheme, we obtained negative values of Δ/λ. Coming back to the complementary d^5 configuration, the signs of the tetragonal splitting and of the spin-orbit coupling constants are simultaneously reversed, so that the sign of their ratio remains unchanged. Since the one-electron spin-orbit coupling constant is always positive, a negative value of Δ/λ means that the xz, yz orbitals are higher in energy relative to the xy orbital (see Figure 3). Since the halide ion wave functions are admixed in the xz, yz molecular orbitals, it is clear that the halide ligand has a destabilizing effect on these orbitals. This conclusion can be rationalized in terms of the ligand contribution to the π antibonding character of the molecular orbitals. Considering the ammonia molecule, the π orbitals e_x and e_y are combinations of the nitrogen $2p_x$, $2p_y$ and the hydrogen 1s atomic orbitals. The e_x, e_y orbitals are not as available for π bonding as are the lone pair orbitals of the halide ion, for two reasons: (1) the overlap of the e orbitals with the metal ion d orbitals is relatively small, and (2) the ionization potential of the e orbital is expected to be greater than that of the halide p orbital, making the latter closer in energy to the metal d orbital. Hence the π interaction with the halide ion is stronger than that with ammonia, and the xz and yz molecular orbitals become less stable than the xy orbital.

The magnitude of the tetragonal splitting was found here to depend on the halide ligand, the order being $|\Delta(Cl^-)| > |\Delta(Br^-)|$. Upon going from Cl^- to Br^-, the polarizability of the ligand π orbitals increases while, on the other hand, the distance between the centers of the metal ion and the ligand also increases. These two phenomena are expected to have opposing effects on the extent of the π bonding. In addition, the distance increase may result in a reduced electrostatic repulsion between the ligand and the metal d orbitals. Apparently the resultant of these effects is a slight overall reduction of the tetragonal splitting in the $[Ru(NH_3)_5Br^-]^{2+}$ complex.

It has been pointed out by Taube[27] that the rates of reduction of $[Ru(NH_3)_5X]^{2+}$ ions by Cr^{2+} can be arranged in the order $k_{Cl^-} > k_{Br^-} > k_{I^-}$. This is the opposite of the order known for the reduction rates of the corresponding cobalt(III) and chromium(III) complexes. This effect may have some relation on the order of the tetragonal splittings obtained in the present work. Since a larger tetragonal splitting is indicative of a stronger π interaction, the chloride ligand in the chloropentaammineruthenium complex may be expected to conduct electrons more easily.

Acknowledgment. We would like to thank Dr. U. Shmueli for his help with the X-ray photographs and the alignments of the crystals.

References and Notes

(1) See, *e.g.*, D. A. Rowley and R. S. Drago, *Inorg. Chem.*, **7**, 795 (1968), and references therein.
(2) W. Moffitt and C. J. Ballhausen, *J. Inorg. Nucl. Chem.*, **3**, 178 (1956).
(3) H. Yamatera, *Bull. Chem. Soc. Jap.*, **31**, 95 (1958).
(4) D. S. McClure in "Advances in the Chemistry of Coordination Compounds," S. Kirschner, Ed., Macmillan, New York, N. Y., 1961, p 498.
(5) R. A. D. Wentworth and T. S. Piper, *Inorg. Chem.*, **4**, 709 (1965).
(6) L. H. Vogt, J. L. Katz, and S. E. Wiberly, *Inorg. Chem.*, **4**, 1157 (1965).
(7) K. Gleu and K. Rehm, *Z. Anorg. Allg. Chem.*, **227**, 237 (1936).
(8) W. A. Hynes, L. K. Yanowski, and M. Shiller, *J. Amer. Chem. Soc.*, **50**, 3053 (1938).
(9) M. Linhard and M. Weigel, *Z. Phys. Chem.*, **11**, 308 (1957).
(10) H. Hartmann and C. Bushbeck, *Z. Phys. Chem.*, **11**, 120 (1957).
(11) G. G Messmer and E. L. Amma, *Acta Crystallogr., Sect. B*, **24**, 417 (1968).
(12) D. S. Schonland, *Proc. Phys. Soc. (London)*, **73**, 788 (1958).
(13) Stanko (J. A. Stanko, Ph.D. Thesis, University of Illinois, 1966) observed the epr spectra of $Ru(NH_3)_5Cl^{2+}$ and $Ru(NH_3)_5I^{2+}$ in $[Rh(NH_3)_5Cl]Cl_2$ and $[Ir(NH_3)_5Cl]Cl_2$ single crystals, respectively, and reported $g_\parallel = 2.92$ and $g_\perp = 0.92$ for the chloro complex and $g_\parallel = 2.72$ and $g_\perp = 1.20$ for the iodo complex. However, it is difficult to compare these results with ours, since his data were calculated from spectral angular dependence in one crystallographic plane only, and his $g_\perp$ values are therefore unknown combinations of g_x and g_y.
(14) B. Bleaney and M. C. M. O'Brien, *Proc. Phys. Soc. (London)*, **69**, 1216 (1956).
(15) J. S. Griffith, "The Theory of Transition Metal Ions," Cambridge University Press, New York, N. Y., 1964.
(16) K. W. H. Stevens, *Proc. Roy. Soc., Ser. A*, **219**, 542 (1953).
(17) J. H. E. Griffiths, J. Owen, and I. M. Ward, *Proc. Roy. Soc., Ser. A*, **219**, 526 (1953).
(18) J. H. M. Thornley, *J. Phys. C.*, **1**, 1024 (1968).
(19) J. S. Griffith, *Mol. Phys.*, **21**, 135 (1971).
(20) S. A. Cotton and J. F. Gibson, *J. Chem. Soc. A*, 803 (1971).
(21) A. Hudson and M. J. Kennedy, *J. Chem. Soc. A*, 1116 (1969).
(22) B. N. Figgis, J. Lewis, F. E. Mabbs, and G. A. Webb, *J. Chem. Soc. A*, 422 (1966).
(23) J. Owen and J. H. M. Thornley, *Rep. Progr. Phys.*, **29**, 675 (1966).
(24) D. Waysbort and G. Navon, *J. Chem. Phys.*, **59**, 5685 (1973).
(25) M. Gerloch and J. R. Miller, *Progr. Inorg. Chem.*, **10**, 1 (1968).
(26) T. M. Dunn, *Trans. Faraday Soc.*, **57**, 1441 (1961).
(27) H. Taube, "Electron Transfer Reactions of Complex Ions in Solution," Academic Press, New York, N. Y., 1970.

Infrared Spectra of *n*-Butylamine Adsorbed on Silica–Alumina

Tetsuo Morimoto,* Junichiro Imai, and Mahiko Nagao

Department of Chemistry, Faculty of Science, Okayama University, Okayama, Japan *(Received October 17, 1973)*

Infrared spectra of *n*-butylamine adsorbed on silica–alumina were measured to investigate the character and properties of the acid sites on the surface. The silica–alumina samples were prepared by mixing silica and alumina, both of which were ion-free samples produced by the hydrolysis of each metal alcoholate. The results show that pure silica outgassed at 500° has no acid sites on the surface, while 100° treated silica in air has very weak protonic acid sites which react with *n*-butylamine but are inert toward pyridine. The outgassed pure alumina surface has aprotonic acid sites, which are able to change to protonic acid sites by adsorbing water molecules. On silica–alumina, strong protonic type of acid sites appear that are not found on the individual oxides; the strength of the acid sites increases with decreasing content of alumina in silica–alumina.

Introduction

The properties of acid sites on solid surfaces have been studied by means of such techniques as titration of the acid sites with basic molecules in the presence of Hammett indicators,[1,2] infrared spectroscopy of the molecules adsorbed on the surfaces,[3,4] and vapor-phase adsorption of molecules such as ammonia.[5-8] Of these techniques, infrared spectroscopy of adsorbed molecules can distinguish two types of acid sites on the surface, *i.e.*, Lewis and Brönsted acid types. For this purpose, ammonia (pK_b = 4.75) or pyridine (pK_b = 8.75) has been frequently used as an adsorbate,[9-14] while the application of *n*-butylamine (pK_b = 3.38) to the same purpose has only been described by Fripiat, *et al.*[15] On the contrary, the latter has been often employed for the titration method.[16-18] Since *n*-butylamine is a stronger base than the other two, it will react with weaker acid sites than pyridine. The authors have measured infrared spectra of *n*-butylamine adsorbed on silica–alumina in order to examine the applicability of the adsorbate to the determination of the acid type on a surface. The present paper includes results that demonstrate the usefulness of *n*-butylamine for this purpose, and that the strength of the protonic acid sites measured by this method on silica–alumina varies with alumina content.

Experimental Section

Materials. The silica–alumina samples used are the same as reported previously.[19] Ethylsilicate of reagent grade was purified by redistillation (bp 164–165°) and then hydrolyzed at 100° in a large amount (20 times) of water to form silica gel (S). Alumina (A) was also prepared by the hydrolysis of aluminum isopropoxide, the latter being synthesized from pure metallic aluminum and 2-propanol. For the hydrolysis, 100 g of aluminum isopropoxide was stirred in a mixed solution containing 180 ml of 2-propanol and 60 ml of water at room temperature. Each precipitate was washed sufficiently with distilled water, dried at 100°, and then calcined at 500° for 10 hr. A definite amount of each precipitate was mixed in aqueous gel state, and then subjected to the same treatments as in the case of the individual oxides. Thus, four kinds of silica–alumina were prepared, differing in composition, *i.e.*, of 13, 25, 50, and 75 wt % of alumina (SA-13, SA-25, SA-50, and SA-75). X-Ray analysis showed the crystal form of alumina to be η form, but that of silica amorphous.

The surface area of these solid samples, determined by applying the BET theory to the nitrogen adsorption data obtained at −196°, was found to be 628, 201, 573, 472, 408, and 397 m^2/g for S, A, SA-13, SA-25, SA-50, and SA-75, respectively.

The adsorbates, *n*-butylamine (bp 76–78°) and pyridine (bp 116°), were purified by redistillation from reagent grade material in the presence of sodium hydroxide

Cell. The cell used for infrared absorption spectroscopy was an *in-situ* cell substantially similar to that used by Peri and Hannan.[20] Rock salt plates were fitted to the cell windows using silicon grease. The sample disk could be heated after moving to a position in an electric oven by the use of a magnet from the outside. The extent of vacuum attainable in the cell was 1×10^{-4} Torr. The spectrometer used was of the type IR-G manufactured by Nippon Bunko Co.

Measurement of Infrared Absorption Spectrum. About 15–30 mg of a powdered sample was pressed under a pressure of 2 ton/cm^2 to produce a disk of 2 cm in diameter. The disk mounted in the cell was outgassed at 500° for 4 hr, exposed to *n*-butylamine vapor of 40 Torr for 24 hr at room temperature, pumped off for 4 hr at room temperature, and then subjected to the measurements of infrared absorption spectrum in the ranges of wave number 1300–1800 and 2500–4000 cm^{-1}. After that, the spectroscopic measurements and outgassing at elevated temperatures were repeated successively.

Results and Discussion

Infrared Spectra of n-Butylamine. Infrared absorption spectra of *n*-butylamine were illustrated in Figure 1. Here, *n*-butylamine was used in three states, *i.e.*, (a) in pure liquid, (b) in chloroform solution, and (c) in the form of *n*-butylamine hydrochloride dispersed in Nujol. The assignment of the infrared absorption bands of *n*-butylamine has been carried out by several authors.[15,21]

As is shown in Figure 1a, liquid *n*-butylamine exhibits the absorption band at 1605 cm^{-1}, which can be assigned to the NH_2 bending vibration,[21] while in chloroform solution the band shifts to 1580 cm^{-1} (Figure 1b). This shift will possibly depend on the strength of hydrogen bond.

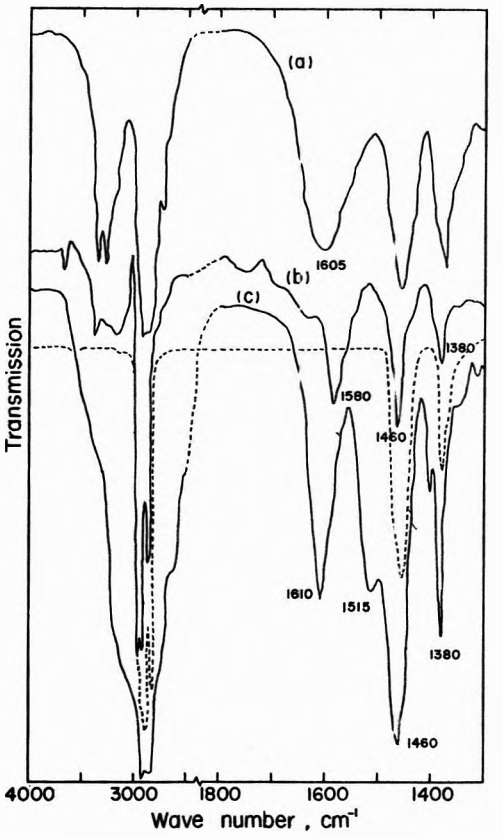

Figure 1. Infrared spectra of *n*-butylamine: (a) pure liquid; (b) in chloroform solution; (c) *n*-butylam ne hydrochloride dispersed in Nujol. The dotted line represents the spectrum of Nujol.

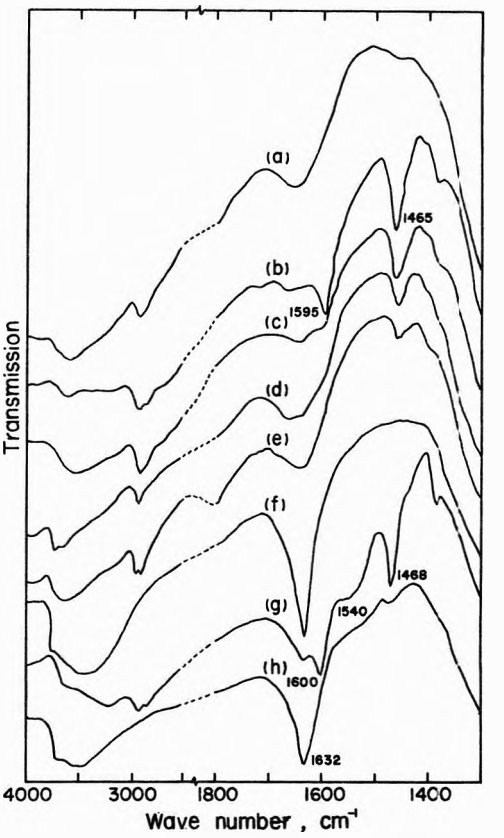

Figure 2. Infrared spectra of *n*-butylamine adsorbed on silica gel: (a) background spectrum obtained after pretreatment at 500°; after *n*-butylamine adsorption, spectra were recorded after pumping off at (b) room temperature; (c) 100°; (d) 200°; (e) 300°. On 100° treated silica, spectra were recorded as follows: (f) background; after immersion in *n*-butylamine, dried at 100° for (g) 10 min; (h) several hours.

The bands observed at 1460 and 1380 cm^{-1} clearly come from the CH_2 bending vibration, as can be seen also in the spectrum of Nujol itself.

In the spectrum of *n*-butylamine hydrochloride two bands are observed at 1610 and 1515 cm^{-1}, both of which are absent in the spectrum of liquid *n*-butylamine (Figure 1c). Silverstein and Bassler[21] cite that the NH_3^+ groups exhibit the symmetrical and asymmetrical bending vibration bands in the regions of 1550–1504 and 1600–1575 cm^{-1}, respectively. Undoubtedly, the bands observed on the spectrum of *n*-butylamine hydrochloride agree with these two bands. Of the two, the band due to asymmetrical NH_3^+ bending vibration appears in the same region as that of the NH_2 bending vibration, and consequently this band is not applicable to ascertain whether the NH_3^+ species are present or not on the surface. On the contrary, the band at 1550–1504 cm^{-1} due to symmetrical NH_3^+ bending vibration seems to be of great advantage to the same purpose, because it is in the region independent from the NH_2 bending vibration.

Adsorption of n-Butylamine on Silica Gel. The infrared spectra of *n*-butylamine adsorbed on silica are recorded in Figure 2. After the adsorption of *n*-butylamine on the silica sample pretreated at 500°, the band at 1595 cm^{-1} appears strongly, the intensity of which decreases markedly with pumping off at elevated temperatures and extinguishes after pumping off at 300°. That the spectra exhibit no band at 1550–1504 cm^{-1} manifests the absence of the Brönsted acid sites on 500° treated silica. These results suggest that adsorbed *n*-butylamine molecules are mostly bonded on the surface through hydrogen bonding. The spectra of pyridine adsorbed on silica pretreated at 500° show the ring stretching vibration bands at 1590 and 1440 cm^{-1} in accordance with the results reported by Parry,[11] and they disappear almost completely after pumping off at 100° for 4 hr, as illustrated in Figure 3.[22] Pyridine can thus be desorbed more easily from the silica surface than *n*-butylamine. Van Cauwelaert, *et al.*,[23] have recently reported that the band at 3750 cm^{-1} due to stretching vibration of free hydroxyl groups on silica surfaces shifts to 2890 cm^{-1} by the adsorption of *n*-butylamine through hydrogen bonding. The absorption in this range, however, overlaps with that of CH stretching vibration, which makes difficult the identification of the formation of hydrogen bonding between *n*-butylamine and hydroxyl groups.

A preliminary test indicated that dimethylaminoazobenzene adsorbed on the silica surface from a benzene solution could assume acidic color (red), which proves that the silica surface has very weak acid sites. Another test was carried out by using the silica sample pretreated at 100° for 24 hr in air; it was immersed in liquid *n*-butylamine, dried at 100° for several hours in air, and then applied to the measurement of the infrared spectra (Figure 2f–h). The results showed that, after immersing in liquid *n*-butylamine, the intensity of the H_2O deformation band near 1630 cm^{-1} diminishes slightly, and at the same time new bands appear at 1600, 1545, 1468, and 1385 cm^{-1}; the former two may be assigned to the NH_3^+ bending vibration and the latter two to CH bending. This suggests that part of water physisorbed on the 100° treated silica are displaced by *n*-butylamine. In addition, Figure 2h shows

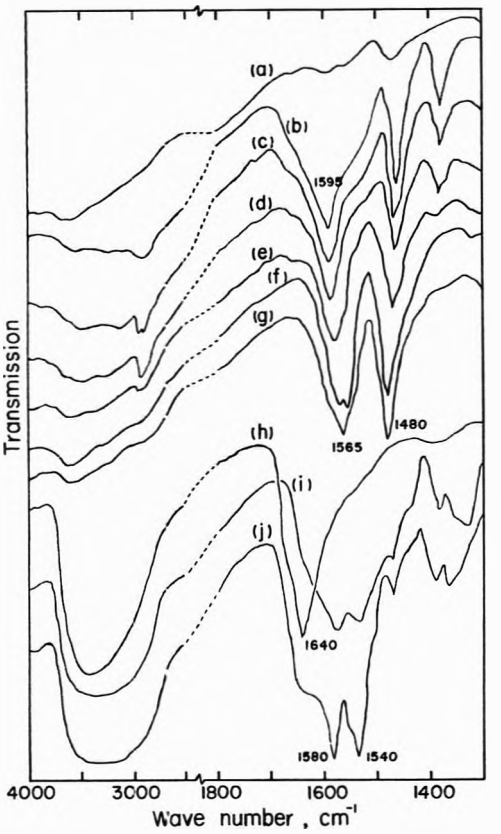

Figure 4. Infrared spectra of *n*-butylamine adsorbed on alumina: (a) background spectrum obtained after pretreatment at 500°; after *n*-butylamine adsorption, spectra were recorded after pumping off at (b) room temperature; (c) 100°; (d) 200°; (e) 300°; (f) 400°; (g) 500°. On 100° treated alumina, spectra were recorded as follows: (h) background; after immersion in *n*-butylamine, dried at 100° for (i) 10 min; (j) several hours.

that evacuation of this sample at 100° for 4 hr leads to almost complete desorption of adsorbed *n*-butylamine, but it leaves the undisplaced water as it stands. This result, together with the coloration of dimethylaminoazobenzene, indicates the presence of very weak protonic sites on the silica surface, as do the results obtained by Fripiat, *et al.*,[24] from infrared spectroscopic studies, that NH_4^+ species are formed by the adsorption of NH_3 on 120 and 200° treated silica gels.

Here, one may suspect the possibility of NH_3^+ formation by the reaction of *n*-butylamine with water, because an appreciable amount of physisorbed water can be expected to be present on the 100° treated silica surface. A spectroscopic test carried out on the mixture of liquid water and *n*-butylamine, however, demonstrated the absence of the NH_3^+ species. We can thus conclude that weak acid sites detected by the *n*-butylamine adsorption on the 100° treated silica originate from the reaction of *n*-butylamine with the surface, and not with physisorbed water. On the other hand, the same experiment carried out on 100° treated silica using pyridine as an adsorbate did not show a band at 1540 cm^{-1} indicating the presence of pyridinium ions[11] (Figure 3).[22] These findings give evidence that protonic acid sites on silica surface are so weak that they are insensitive to pyridine but sensitive to *n*-butylamine.

Adsorption of n-Butylamine on Alumina. Infrared spectra of *n*-butylamine adsorbed on alumina pretreated at 500° *in vacuo* are represented in Figure 4. These spectra have no band near 1540 cm^{-1}, which manifests the absence of protonic acid sites. On the contrary, the strong band of the NH_2 bending vibration appears near 1600 cm^{-1}, which shifts gradually from 1595 to 1565 cm^{-1} when the sample disk is heated at elevated temperatures. Furthermore, it is to be noted that this band remains even after treating the disk at 500° *in vacuo* (Figure 4g). For comparison, adsorption of pyridine was carried out on the same alumina sample. In accordance with the result obtained by Parry,[11] the spectra exhibit a strong band at 1450 cm^{-1} showing evidence of aprotonic acid sites, and the band remains after pumping off the sample at 500° (Figure 5).[22] If *n*-butylamine molecules are adsorbed on Lewis acid sites, the NH_2 bending vibration should still remain. By comparing the desorbabilities of two kinds of basic molecules adsorbed on alumina, it may reasonably be considered that the band at 1595–1565 cm^{-1} is attributed to *n*-butylamine strongly adsorbed on aprotonic acid sites of alumina. The *n*-butylamine adsorption was carried out also on the alumina sample pretreated at 100° in air, on which a considerably large amount of water would remain possibly physisorbed. The spectra obtained have two sharp bands at 1540 and 1580 cm^{-1} (Figure 4i); the former demonstrates the existence of the Brönsted acid sites, while the latter corresponds to the NH_2 bending vibration. This indicates that part of the Lewis acid sites would be converted to the Brönsted acid sites through reaction with water, as described by Parry.[11] It may therefore be concluded that the band at 1595–1565 cm^{-1} originated from the NH_2 bending vibration of *n*-butylamine adsorbed on the Lewis acid sites on alumina. Additionally, it has been reported that the protonic acid sites on the alumina surface are so weak that they can protonate ammonia[11] but not pyridine.[11,25,26] A consistent result has been obtained by the present investigation; the protonic acid sites on the 100° treated alumina can react with *n*-butylamine to produce the NH_3^+ species (Figure 4h–j), but not with pyridine (Figure 5).[22]

Adsorption of n-Butylamine on Silica–Alumina. The adsorption of *n*-butylamine was carried out on four kinds of silica–alumina pretreated at 500° *in vacuo*. The data presented in Figures 6 and 7 refer to the samples of SA-13 and SA-50. The spectra of *n*-butylamine adsorbed on SA-13 have the band at 1520–1503 cm^{-1} composed of more than two constituents, which is considered to come from the symmetrical NH_3^+ bending vibration as stated above. By pumping off the sample disk at elevated temperatures, the intensity of this band decreases and at the same time the frequencies of the band shift to lower wave number in the sense that constituents of higher frequencies in the band diminish more rapidly than those of lower frequencies. Similar tendencies are observed on every sample of silica–alumina, *e.g.*, as shown in SA-50 in Figure 7. These findings indicate that there are more than two kinds of NH_3^+ species adsorbed on silica–alumina surfaces differing in acid site strength, and that *n*-butylamine adsorbed on the stronger sites persists up to higher temperatures. Furthermore, it should be pointed out that this band moves gradually to lower wave number with decreasing content of alumina in silica–alumina.

In Table I, the frequency of the most intensive absorption in the range of the symmetrical NH_3^+ bending vibration is listed as a function of pumping-off temperature and alumina content. It can be seen clearly from Table I that the frequency shifts to lower wave number with increasing temperature of pumping off as well as with decreasing amount of alumina in silica–alumina. Admitted-

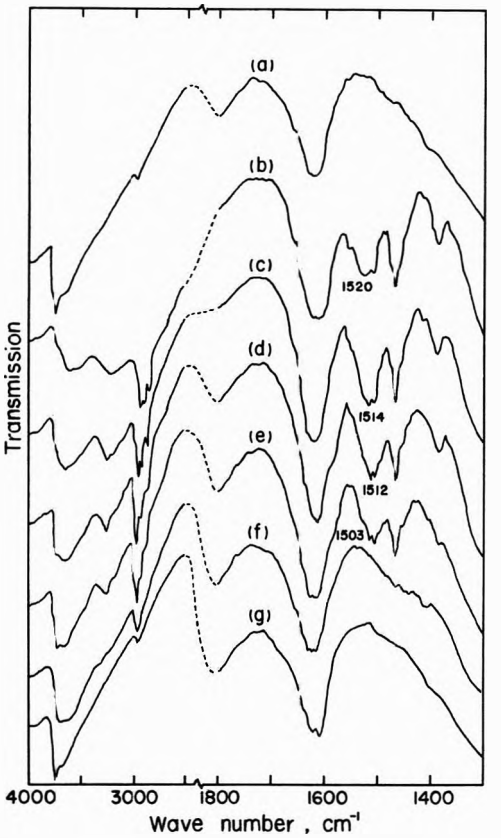

Figure 6. Infrared spectra of *n*-butylamine adsorbed on silica–alumina (SA-13): (a) background spectrum obtained after pretreatment at 500°; after *n*-butylamine adsorption, spectra were recorded after pumping off at (b) room temperature; (c) 100°; (d) 200°; (e) 300°; (f) 400°; (g) 500°.

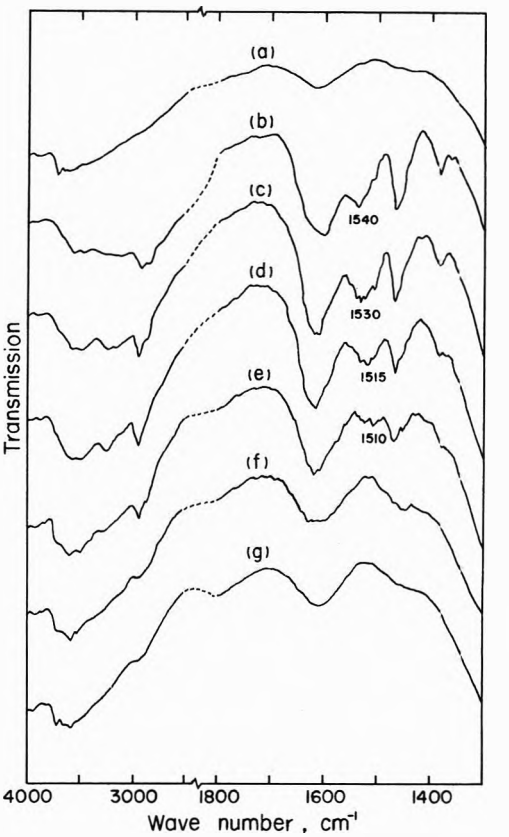

Figure 7. Infrared spectra of *n*-butylamine adsorbed on silica–alumina (SA-50): (a) background spectrum obtained after pretreatment at 500°; after *n*-butylamine adsorption, spectra were recorded after pumping off at (b) room temperature; (c) 100°; (d) 200°; (e) 300°; (f) 400°; (g) 500°.

TABLE I: Frequency Shift of Symmetrical NH_3^+ Bending Vibration (cm^{-1})

Sample	Pumping-off temperature			
	Room temp	100°	200°	300°
SA-13	1520	1514	1512	1503
SA-25	1520	1515	1514	1510
SA-50	1540	1530	1515	1510
SA-75	1540	1540	1522	1520

ly, it may be considered that *n*-butylamine adsorbed on weaker acid sites is desorbable more easily than that on stronger acid sites. These discussions will lead to an important conclusion that the strength of the protonic acid sites decreases with increasing amount of alumina in silica-alumina.

Furthermore, the background band in the vicinity of 1620 cm^{-1} in Figures 6 and 7 seems to be due to the Si–O overtone for the following reasons. The absence of molecular water on the 500° treated silica-alumina samples will not permit the appearance of the H_2O bending vibration near 1600 cm^{-1}. As described above, on adsorption of *n*-butylamine, the absorption band appears in the same region either by the bending vibration of NH_2 species adsorbed on the Lewis acid sites or of NH_3^+ species formed by adsorption on the Brönsted acid sites. Also, Figures 6 and 7 indicate that the absorption band in this region shifts to lower wave numbers by pumping off the samples with adsorbed *n*-butylamine at increasingly elevated temperatures; the larger the alumina content, the greater the shift. On the other hand, the adsorption experiment of pyridine on the 500° treated silica-alumina samples testifies to the presence of the Brönsted as well as the Lewis acid sites (Figures 8 and 9).[22] It is also evident that the pyridine adsorbed on the Brönsted acid sites can be removed by pumping off at 100–200°, whereas that on the Lewis acid sites remains even after treatment at 500°. Thus, it is suggested that the shift of the background absorption stated above is due to the change in perturbation of Si–O vibration which is caused by the strong adsorption of *n*-butylamine on the Lewis acid sites probably located about aluminum atoms in Si–O–Al bondings.

The possibility of dissociative adsorption of *n*-butylamine should be considered on these samples. If it occurs, the surface hydroxyl groups and the secondary amine adsorbed on the surfaces should be produced. Silverstein and Bassler[21] and Bellamy[27] report that the absorption band due to the bending vibration of the secondary amine appears in the range 1650–1550 cm^{-1} which approximates to the absorption due to the bending vibration of the primary amine, and that the former is very weak compared to the latter. Thus, the absorption of the secondary amine is possibly hidden in that of the primary amine if the both are present. The actual data demonstrate a fairly strong absorption in this region (Figures 6 and 7), which gives evidence of the primary amine but makes the presence of the secondary amine obscure. On the other hand, the band due to the OH stretching vibration near 3600–3700 cm^{-1} shifts slightly to lower wave number by the adsorption of *n*-butylamine, and it recovers completely by pumping off at 500°; this seems to verify a small possibility of dissociative adsorption of *n*-butylamine.

The existence of protonic acid sites on silica-alumina has been reported by many authors[9-14] using ammonia and pyridine, but they did not examine the variation of the strength of the acid sites with the content of alumina in silica-alumina. In the previous paper,[19] it has been suggested that on silica-alumina there appear a new type of physisorption sites for water molecules which are absent on the surfaces of individual oxides. According to the mechanism postulated on the formation of the new sites, the sites should have the character of protonic acid. An analogous assumption has been made by Léonard, *et al.*,[28] on the origin of the Brönsted acid sites on silica-alumina; such structural defects as aluminum atoms substituting silicon in tetrahedral coordination are responsible for it. The present investigation on the infrared spectra of adsorbed *n*-butylamine seems to support these postulations.

Supplementary Material Available. Figures 3, 5, 8, and 9, showing the ir spectra of pyridine adsorbed on S, A, SA-13, and SA-50, respectively, will appear following these pages in the microfilm edition of this volume of the journal. Photocopies of the supplementary material from this paper only or microfiche (105 × 148 mm, 24× reduction, negatives) containing all of the supplementary material for the papers in this issue may be obtained from the Journals Department, American Chemical Society, 1155 16th St., N.W., Washington, D. C. 20036. Remit check or money order for $3.00 for photocopy or $2.00 for microfiche, referring to code number JPC-74-704.

References and Notes

(1) C. Walling, *J. Amer. Chem. Soc.*, **72**, 1164 (1950).
(2) H. A. Benesi, *J. Amer. Chem. Soc.*, **78**, 5490 (1956).
(3) L. H. Little, "Infrared Spectra of Adsorbec Species," Academic Press, London, 1966.
(4) M. L. Hair, "Infrared Spectroscopy in Surface Chemistry," Marcel Dekker, New York, N. Y., 1967.
(5) A. Clark, V. C. F. Holm, and D. M. Blackburn, *J. Catal.*, **1**, 244 (1962).
(6) V. C. F. Holm and A. Clark, *J. Catal.*, **2**, 16 (1963).
(7) A. E. Hirschler, *J. Catal.*, **6**, 1 (1966).
(8) F. S. Stone and L. Whalley, *J. Catal.*, **8**, 173 (1967).
(9) J. E. Mapes and R. P. Eischens, *J. Phys. Chem.*, **58**, 1059 (1954).
(10) D. E. Nicholson, *Nature (London)*, **186**, 630 (1960).
(11) E. P. Parry, *J. Catal.*, **2**, 371 (1963).
(12) J. J. Fripiat, A. Léonard, and J. B. Uytterhoeven, *J. Phys. Chem.*, **69**, 3274 (1965).
(13) N. W. Cant and L. H. Little, *Nature (London)*, **211**, 69 (1966).
(14) M. R. Basila and T. R. Kantner, *J. Phys. Chem.*, **71**, 467 (1967).
(15) J. J. Fripiat, A. Servais, and A. Léonard, *Bull. Soc. Chim. Fr.*, 635 (1962).
(16) M. W. Tamele, *Discuss. Faraday Soc.*, **8**, 270 (1950).
(17) O. Johnson, *J. Phys. Chem.*, **59**, 827 (1955).
(18) H. A. Benesi, *J. Phys. Chem.*, **61**, 970 (1957).
(19) T. Morimoto, M. Nagao, and J. Imai, *Bull. Chem. Soc. Jap.*, **44**, 1282 (1971).
(20) J. B. Peri and R. B. Hannan, *J. Phys. Chem.*, **64**, 1526 (1960).
(21) R. M. Silverstein and G. C. Bassler, "Spectrometric Identification of Organic Compounds," 2nd ed, Wiley, New York, N. Y., 1967.
(22) See paragraph at end of paper regarding supplementary material.
(23) F. H. Van Cauwelaert, F. Vermoortele, and J. B. Uytterhoeven, *Discuss. Faraday Soc.*, **52**, 66 (1971).
(24) J. J. Fripiat, C. Van der Meersche, R. Touillaux, and A. Jelli, *J. Phys. Chem.*, **74**, 382 (1970).
(25) M. R. Basila, T. R. Kantner, and K. H. Rhee, *J. Phys. Chem.*, **68**, 3197 (1964).
(26) H. Knozinger and H. Stolz, *Fortschr. Koll. Polym.*, 55, 16 (1971).
(27) L. J. Bellamy, "The Infra-red Spectra of Complex Molecules," 2nd ed, Methuen, London, 1958.
(28) A. J. Léonard, P. Ratnasamy, F. D. Declerck, and J. J. Fripiat, *Discuss. Faraday Soc.*, 52, 98 (1971).

Liquid Ammonia Solutions. XII. A Raman Study of Nitrates and Thiocyanates

A. T. Lemley and J. J. Lagowski*

Department of Chemistry, University of Texas at Austin, Austin, Texas 78712

(*Received August 6, 1973*)

The results of a Raman spectrophotometric investigation of liquid ammonia solutions of $NaNO_3$, NaSCN, NH_4NO_3, NH_4SCN, $LiNO_3$, and LiSCN suggest that the anions dominate interaction with the solvent in the sodium and ammonium salts, while the cation competes with the anion for solvent interaction in the case of the lithium salts. The vibrational spectra of the nitrate and thiocyanate ions imply that the former exhibits a weak interaction with the solvent while strong interactions occur through the sulfur end of the SCN^- ion.

Introduction

The results of recent vibrational studies[1,2] from this laboratory have dealt with the structure of ammonia in the liquid state. A model was proposed for the pure liquid based on its Raman spectrum, particularly in the 3300-cm^{-1} region, which contains the N-H stretching fundamentals. The present work continues these studies, on liquid ammonia solutions of soluble salts, using Raman spectroscopy.

The nitrate ion exhibits a Raman spectrum which, in solution, is sensitive to its environment. It has been used as a probe in aqueous solutions to characterize anion-water and anion-cation interactions.[3-5] Since only one ammonia fundamental mode is obscured by the Raman spectrum of NO_3^-, solutions of nitrate salts in ammonia are amenable for study. The thiocyanate ion also exhibits a Raman spectrum and none of its fundamental modes interfere with those of ammonia. The spectrum of SCN^- is sensitive to interactions through either the sulfur or nitrogen end of the ion.[6]

Sodium, ammonium, and lithium nitrates and thiocyanates were chosen for this study of their high solubilities in liquid ammonia. The purpose of the present Raman study is to elucidate anion-solvent and anion-cation interactions in liquid ammonia solutions of these salts.

Experimental Section

All solutions were prepared using reagent grade chemicals; NH_4NO_3 was recrystallized from methanol and NH_4SCN was recrystallized from absolute ethanol to dry the commercial salt. Sodium nitrate was obtained as the anhydrous salt and was dried at 110° before use; NaSCN, $LiNO_3$, and LiSCN were each recrystallized from NH_3 several times; the solid was then subjected to high vacuum for 12–24 hr. Samples of the anhydrous salts were placed in the Raman cell in an inert atmosphere. The ammonia used to prepare the solutions was distilled from, and stored over, sodium. Just before use it was condensed onto sodium again and then distilled into the sample cell. The Raman cell has been described previously.[2]

Raman spectra were measured with a Cary 82 Raman spectrophotometer. The exciting source was the 5145-Å line of a Coherent Radiation Laboratories Model 53A argon-ion laser. Computer resolution of experimental envelopes was accomplished by a non-linear least-squares fit of symmetric bands, a technique described completely elsewhere.[2]

Results

Raman spectra of solutions of $NaNO_3$, NaSCN, NH_4NO_3, NH_4SCN, $LiNO_3$, and LiSCN in liquid ammonia were measured under pressure at 25°. The concentrations of the solutions varied in general from an NH_3/salt molar ratio of 6/1 to *ca.* 40/1. Some salts ($LiNO_3$, NH_4NO_3, and NH_4SCN) form stable solutions, *i.e.*, vapor pressure less than 1 atm at ambient temperature, at molar ratios of 3/1 or less and their spectra were also recorded. The N–H stretching regions of all spectra were resolved by means of computer methods into four bands. The positions of these bands, and of the other ammonia fundamentals are reported in Table I for a representative concentration of each salt solution, *i.e.*, *ca.* 6/1 molar ratio. The uncertainties in the positions of these bands are the rigorous statistical uncertainties which come out of the non-linear least-squares method of resolution. Uncertainties in half-width and intensity are greater than those in position. The uncertainties reflect the best fit within a cluster of fits and for the frequency positions these are within experimental error. The symmetric bending mode, ν_2, of NH_3 is not reported for nitrate solutions because it is obscured by the very strong ν_1 symmetric stretching mode of the nitrate ion. A new band grew in at 1120 cm^{-1} in each spectrum of the sodium and ammonium thiocyanate solutions, becoming more intense as the concentration increased. In the spectrum of an 8.6/1 NH_4SCN solution this new band was as intense as the band at 1060 cm^{-1}. The two bands also showed similar intensities at approximately the same concentration of a NaSCN solution. The band labeled ν' has been shown to be sensitive to the hydrogen bonding interaction of one hydrogen atom of an NH_3 molecule.[2] For a given cation, *e.g.*, Na^+, the position of this band changed with salt concentration. Figure 1 shows how the frequency of the ν' band shifted in solutions of $NaNO_3$ and NaSCN. As the solutions became dilute, the band position approached the frequency of this band in the pure solvent. Similar results were not seen in spectra of the lithium or the ammonium salt solutions. The profile of the N–H stretching region changed with concentration in a regular way regardless of the nature of the salt. The $2\nu_4$ band became sharper and more intense relative to the ν_1 band on dilution, while the ν_3 band became broader and less intense.

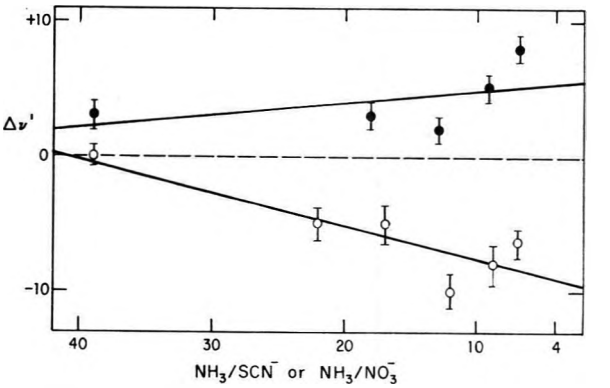

Figure 1. Change in position of ν' from 3271 cm^{-1} (pure NH_3) in $NaNO_3$ and NaSCN solutions *vs.* concentration: (●) $NaNO_3$; (O) NaSCN. Lines drawn are least-squares fit to the data.

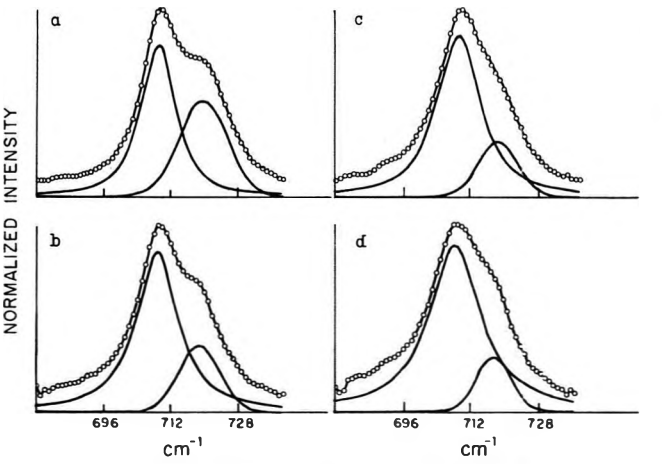

Figure 2. Computer resolutions of ν_4 in-plane bending mode of NO_3^- in $NaNO_3$ solutions: NH_3/NO_3^- (a) 5.8/1, (b) 9.3/1, (c) 18/1, (d) 38/1.

Bands in the Raman spectra characteristic of the nitrate ions have also been studied. Positions of the nitrate ion fundamentals for the $NaNO_3$, NH_4NO_3, and $LiNO_3$ solutions are reported in Table II. The frequencies given are the maxima of resolved bands in the case of the ν_3 and ν_4 modes. Band positions of the nitrate ion fundamentals were constant over the concentration range for all modes except the ν_3 asymmetric stretching mode in the $LiNO_3$ solutions. The two bands in this region were separated by 59 cm^{-1} in the 3/1 $LiNO_3$ solution and the separation decreased to 33 cm^{-1} in the 16/1 $LiNO_3$ solution. The intermediate solutions had intermediate separations.

Changes occurred in the relative intensities of the two bands in the ν_4 in-plane bending region of the $NaNO_3$ and $LiNO_3$ spectra. Computer resolutions of this envelope for the $NaNO_3$ solutions are pictured in Figure 2. The profile of the asymmetric stretching region of the nitrate ion is shown for these same $NaNO_3$ solutions in Figure 3. Figure 4 shows the ν_4 envelope in several $LiNO_3$ solutions. The band assigned to the symmetric stretching mode of the nitrate ion in the 3/1 $LiNO_3$ solution is pictured in Figure 5. The asymmetry observed in this band was also observed (although to a lesser extent) in the spectrum of the 6/1 $LiNO_3$ solution.

The thiocyanate ion has three fundamental modes. Only two, which are ascribed to the C–N and C–S stretching modes, were observed in the Raman spectra of the thiocyanate solutions. The third mode, which is a bending

TABLE I: Raman Frequencies[a] and Assignments of NH_3 Fundamental Modes

	Concn	ν_4	ν_2	$2\nu_4$	ν'	ν_1	ν_3
NH_3		1648	1046	3214	3271	3300	3385
$NaNO_3$	5.8/1			3224 ± 0.2	3279 ± 1	3305 ± 0.1	3387 ± 0.2
NH_4NO_3	7/1			3221 ± 0.1	3285 ± 1	3305 ± 0.1	3385 ± 0.1
NaSCN	7/1		1060, 1120	3220 ± 0.2	3265 ± 1	3299 ± 0.1	3382 ± 0.2
NH_4SCN	6.9/1		1060, 1120	3216 ± 0.2	3278 ± 1	3297 ± 0.2	3378 ± 0.3
$LiNO_3$	6.1/1			3221 ± 0.2	3280 ± 2	3303 ± 0.2	3382 ± 0.2
LiSCN	5.9/1			3215 ± 0.2	3281 ± 1	3297 ± 0.1	3374 ± 0.2

[a] In cm^{-1}.

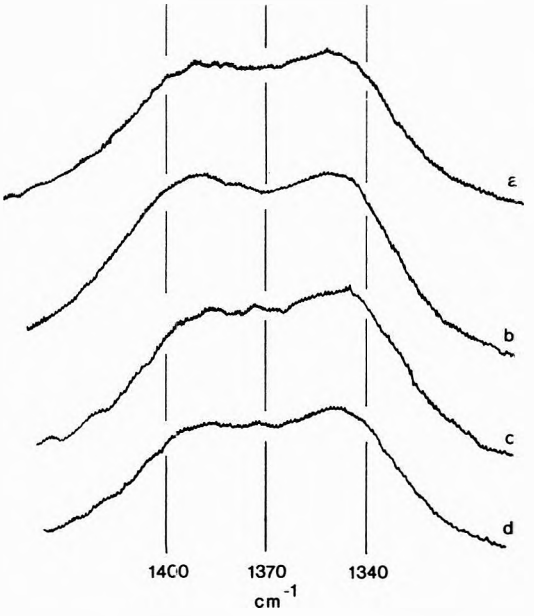

Figure 3. Raman spectra of ν_3 antisymmetric stretching mode for $NaNO_3$ solutions: NH_3/NO_3^- (a) 5.8/1, (b) 9.3/1, (c) 18/1, (d) 38/1.

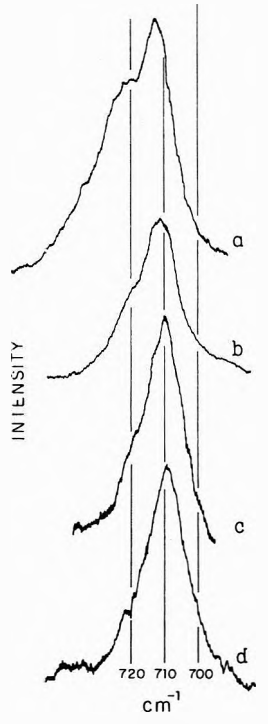

Figure 4. Raman spectra of ν_4 in-plane bending mode of NO_3^- in $LiNO_3$ solutions: NH_3/NO_3^- (a) 3/1, (b) 6/1, (c) 11/1, (d) 16/1.

TABLE II: Raman Frequencies[a] and Assignments of NO_3^- Fundamental Modes

D_{3h}	$NaNO_3$	NH_4NO_3	$LiNO_3$
ν_4	709	712	709
	719		719
ν_1	1046	1046	1046
ν_3	1348	1332	1348[b]
	1392	1381	1396[b]

[a] In cm^{-1}. [b] Values for 6/1 $LiNO_3$ solution.

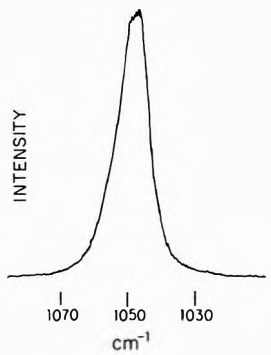

Figure 5. Raman spectrum of ν_1 symmetric stretching mode in $LiNO_3$ solution: NH_3/NO_3^- 3/1. Spectral band width is 1.5 cm^{-1}.

mode, would be expected between 450 and 500 cm^{-1}. The positions of the observed bands are reported for NaSCN, NH_4SCN, and LiSCN in Table III. The relative intensities of these bands changed with concentration of the salt but their positions did not. Computer-resolved bands of the C-S region of NaSCN solutions appear in Figure 6. The C-S region for NH_4SCN solutions was very similar to that for the NaSCN solutions. The band at 740 cm^{-1} increased in intensity relative to the band at 750 cm^{-1} as the NH_3/salt molar ratio increased, *i.e.*, as the solution became more dilute. While the C-N stretching mode appeared to be a single band in NaSCN and NH_4SCN solutions, it changed in half-width with concentration. The band was widest for the most concentrated solutions and became narrower on dilution. The widths at half-height are reported in Table IV for NaSCN solutions. Both the C-S and the C-N stretching regions of the LiSCN in ammonia solution are somewhat different from that of the thiocyanate ion in other salt solutions. In the C-S stretching region a new band was seen at 765 cm^{-1} and no band was present at 750 cm^{-1}. A new band was present at 2075 cm^{-1} in the C-N stretching region; it decreased in intensity with dilution relative to the band at 2063 cm^{-1} paralleling the intensity changes observed in the C-S stretching region. These regions of a representative spectrum are shown in Figure 7.

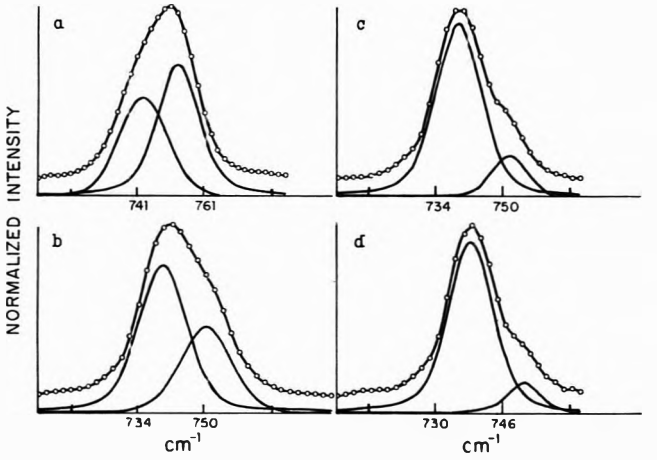

Figure 6. Computer resolutions of C–S stretching mode in NaSCN solutions: NH_3/SCN^- (a) 5/1, (b) 7/1, (c) 12/1, (d) 22/1.

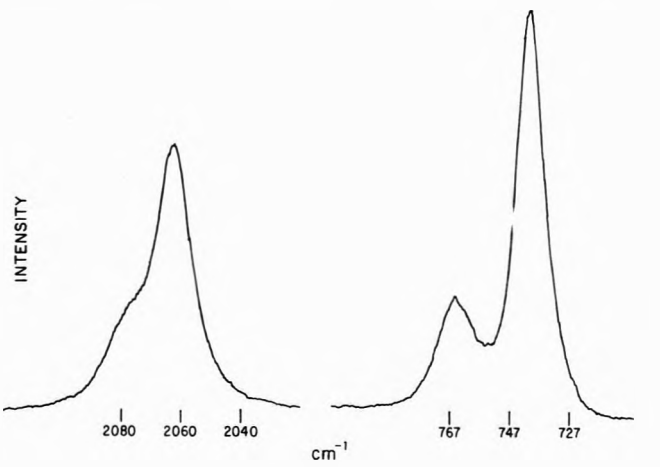

Figure 7. Raman spectrum of 6/1 LiSCN solutions, C–S and C–N stretching regions.

TABLE III: Raman Frequencies[a] and Assignments of SCN^- Fundamental Modes

$C_{\infty v}$	NaSCN	NH_4SCN	LiSCN
ν_3	740	740	740
	750	750	765
ν_1	2063	2063	2063
			2075

[a] In cm^{-1}.

TABLE IV: Half-Widths[a] of the C–N Stretching Mode in NaSCN Solutions

NH_3/NaSCN	Half-width, cm^{-1}	NH_3/NaSCN	Half-width, cm^{-1}
4.9	24	17	13
7.0	17	22	11
8.7	15	39	11
12	13		

[a] Width at half-height.

Discussion

Ammonia Bands. A recent report[2] postulated a linear model for the arrangement of ammonia molecules in the liquid state, partially based on the four band resolution of the N–H stretching region of the Raman spectrum. It was suggested that some of the NH_3 molecules in the liquid have unperturbed C_{3v} symmetry (*i.e.*, the end molecules of a hydrogen bonded dimer or trimer which have all three hydrogen atoms unassociated) while others have perturbed C_{3v} symmetry such that the stretching modes are split and bands due to an ammonia species of C_s symmetry are evident. This species has one hydrogen atom of a molecule associated with another NH_3 molecule through the nitrogen atom, *i.e.*, $H_3N\cdots HNH_2$. The band which is primarily due to the N–H stretching mode of hydrogen atoms associated in this manner is broad, occurring at 3271 cm^{-1}. It was shown that when sodium iodide and sodium perchlorate are added to liquid NH_3 the position of this band is anion dependent. The N–H stretching modes of NH_3 molecules in several environments, all involving some type of association or hydrogen bonding, would contribute to the Raman intensity of this band. In addition, the position of ν_2, the symmetric bending mode, shifted to a higher frequency in NaI spectrum, and while not resolved, could have been due to two bands, the original at 1050 cm^{-1}, and a second one at a higher frequency. In the current work, there is some shift in the position of the 3271-cm^{-1} band for the sodium salt solutions, which, while not a large shift, is anion and concentration dependent. At low concentrations of salt the band is close to the frequency in pure NH_3 and as concentration is increased the anion has more effect on the hydrogen bonding structure in NH_3. The slight shift to higher frequency for the nitrate salt implies that the nitrate ion interacts with NH_3 in a manner similar to solvent molecules interacting with each other. In contrast, the band shifts to lower frequency in the thiocyanate solutions implying a strong NH_3–SCN interaction.

However, the frequency shifts observed for this resolved band, even with the uncertainty limits imposed by the method of resolution, are not sufficiently significant to confirm a picture of anion interaction with ammonia through the hydrogen atoms. But the presence of the second band in the ν_2 region at 1120 cm^{-1} for the thiocyanate solutions can be attributed to the symmetric bend of ammonia molecules which are not the same as the bulk solvent. Since it is negative ions which bring about this new band, interaction would be expected to occur through the hydrogen end of the ammonia molecule. Iodide and bromide salts also affect ν_2 of ammonia in the same way.[1] Although part of this region is obscured for the nitrate salt solutions by the symmetric stretching mode of the nitrate ion, this band is sufficiently narrow in all the solutions to show that no new bands grow in with increased salt concentration at a frequency far from 1050 cm^{-1}. The nitrate ion thus seems to have little effect on the bulk solvent, which the slope of the line for the nitrate solutions (Figure 1) confirms. However, the greater negative slope of the line for the thiocyanate solutions is in agreement with the strong NH_3–SCN interaction implied by the band at 1120 cm^{-1}. Analysis of thiocyanate bands (*vide infra*) confirms this model.

Neither the NH_4^+ nor Li^+ salt solutions exhibit changes in ν' as do the Na^+ salt solutions. The NH_4^+ ion is similar to the solvent molecule and must fit into the solvent structure to some extent, possibly affecting the N–H stretching modes of NH_3 so that they do not reflect the strong SCN^- interaction as does the bending mode. Concurrent work in this laboratory[7] has established an electrostatic model for the $[Li(NH_3)_4]^+$ species in lithium salt solutions. The experimental symmetric stretching mode of this species indicates a solvation energy which is

30 kcal/mol higher than that predicted for Na^+ in NH_3. Therefore, in a lithium salt solution of 6/1 molar ratio, most of the ammonia molecules are associated with the lithium ion, and the SCN^- interaction with this species is not apparent in the spectrum of the ammonia bands.

The amount of Fermi resonance interaction in NH_3 solutions appears to decrease with increasing salt concentration, *i.e.*, as the amount of bulk solvent decreases, as is evidenced by the broadening and decreasing intensity of the solvent band assigned to $2\nu_4$. It appears that Fermi resonance occurs mainly in solvent molecules which interact with each other since the $2\nu_4$ band increases and sharpens not only with dilution, but also when the temperature is lowered and the solvent is more ordered.[2] The antisymmetric stretching mode, ν_3, of the NH_3 species becomes sharper in concentrated salt solutions. It has been suggested[8] that this band broadens due to rotational freedom in bulk solvent and that solute interactions restrict this freedom; the results obtained here are in agreement.

The model developed thus far for dilute salt solutions involves bulk solvent molecules interacting with each other, giving rise to a stretching mode at 3271 cm^{-1} and a bending mode at 1046 cm^{-1} which are sensitive to hydrogen bonding between solvent molecules. When the concentration of the sodium salt is increased sufficiently the anion interaction dominates. In the concentrated lithium salt solutions most of the solvent molecules are not free to interact with the anions because they strongly solvate the lithium ion.

Nitrate Bands. The nitrate ion, if unperturbed, has D_{3h} symmetry. The modes which are Raman active are ν_1 (A_1) the symmetric stretching mode, ν_3 (E) the antisymmetric stretching mode, and ν_4 (E) the in-plane bending mode. The degenerate ν_3 mode is split in aqueous solutions due to the hydrogen bonding effect of the solvent.[3] It can be further split due to outer-sphere or inner-sphere ion pairing.[4] A new band in the region of the degenerate ν_4 mode usually indicates contact ion pairing.[5] The ν_3 antisymmetric stretching mode was split in all of the nitrate solutions reported here. The fact that ν_3 is split in NH_4NO_3 solutions implies that the splitting is due to hydrogen bonding interaction with the solvent. The ν_4 bending mode is symmetrical in the NH_4NO_3 solutions so contact ion pairing is not evident. However, the ν_4 bending mode is a doublet in the $NaNO_3$ solutions, even in the 39/1 molar ratio sample. The high-frequency band at 719 cm^{-1} grows with increasing concentration, and since it is depolarized, as is the band at 709 cm^{-1}, it probably arises from a nitrate ion species which has formed an inner-sphere ion pair with the sodium ion. Inner-sphere ion pairing has been observed in aqueous solutions of $NaNO_3$.[8] If the new band at 719 cm^{-1} is characteristic of an ion pair, a contribution might be expected in the ν_3 region. However, computer resolution of the spectra pictured in Figure 3 give two bands with constant separation within the epxerimental error. Ion pairing occurs in even the most dilute solution for which the spectrum is shown and this region does not appear to be sensitive to an increase in ion pairing

As would be expected from the evidence based on the NH_3 fundamental modes, the nitrate ion bands in the lithium nitrate solutions give results different from those for the sodium nitrate solutions. The ν_4 bending mode of NO_3^- does not show asymmetry until a molar ratio of 11/1 is reached. The lithium ion is strongly solvated with ammonia and does not form inner-sphere ion pairs easily. Gardiner, *et al.*,[9] have claimed that ν_4 does not exhibit doublet character in ammonia until a molar ratio of 4/1 is reached. The spectrum in Figure 4 shows that there are clearly two bands in an ammonia $LiNO_3$ solution with 11/1 molar ratio. The change in splitting with concentration of the ν_3 asymmetric stretching mode in the lithium solutions correlates with the changes in the ν_4 bending region. In dilute $LiNO_3$ solutions the splitting in the ν_3 mode is due to solvent interactions, and the ν_4 region reveals no doublet. In the more concentrated solutions a new band arises near ν_4 and the amount of splitting in ν_3 increases as inner sphere ion pairs are formed. In the solution with a 3/1 molar ratio, there is sufficient inner-sphere ion pairing to cause a second ν_1 symmetric stretching mode to appear on the high-frequency side of the 1048-cm^{-1} band. Asymmetry on the low-frequency side has been noted in concentrated aqueous solutions of nitrates[4,10] and in molten nitrates.[11] The high-frequency asymmetry in the lithium nitrate solution is not unique; aqueous calcium nitrate also exhibits a spectrum with asymmetry on the high-frequency side.[10]

Thiocyanate Bands. The thiocyanate ion is a linear species whose vibrational spectrum can be analyzed under the point group $C_{\infty v}$ leading to three fundamental modes: $\nu_1(\Sigma)$, the C-N stretch, $\nu_3(\Sigma)$, the C-S stretch, and $\nu_2(\pi)$ the bending mode. The increase of thiocyanate salt concentration in ammonia causes the appearance of a new band on the high-frequency side of the ν_2 symmetric bending mode of ammonia (1120 cm^{-1}). This high-frequency bending mode implies a strong interaction between SCN^- and NH_3. Previous studies[12] of sulfur-containing species in liquid ammonia suggest that hydrogen bonding exists between sulfur and the hydrogen atoms of NH_3. The position of the C-S stretching bands in all of the solutions studied suggests that it is the sulfur end of the thiocyanate ion which interacts strongly with the solvent and perhaps with the cations. If there were no strong interaction with the sulfur end of SCN^- the C-S stretching mode would be expected close to 950 cm^{-1}.[13] The position of the observed C-N stretching mode is reasonable for a SCN^- species which is loosely solvated at the nitrogen end.[6] Two bands are evident in the C-S stretching region of all salt solutions. The results for the NaSCN and the NH_4SCN ammonia solutions are the same, so they will be treated together. In these solutions two bands are observed at 740 and 750 cm^{-1}. In the LiSCN solutions the two bands appear at 740 and 765 cm^{-1}. The 740-cm^{-1} band is easily assigned to NH_3-SCN^- interaction since it is common to all solutions and because it becomes less intense in concentrated solutions where anion-cation interactions would be expected. At the same time, the 2063-cm^{-1} band is common to all solutions and must be the C-N stretch of a SCN^- species which is loosely solvated probably at the nitrogen end of the molecule. There is only one band in the C-N stretching region of the NaSCN and NH_4SCN solutions while the two bands in the C-S region which change in relative intensity with changing concentration imply two SCN^- species, perhaps in equilibrium with each other and interacting with the solvent through their sulfur ends. However, in the most concentrated solutions when the two bands in the C-S region are of about equal intensity, the half-width of the band in the C-N region is widest. As the solutions become less concentrated one band (or species) dominates in the C-S region and the C-N band gets narrower. The C-N stretching mode is thus sensitive to the interactions at the sulfur

end of the molecule, but not enough to give rise to two resolvable bands.

While it has been suggested that the 740-cm^{-1} band is due to an NH_3-SCN^- interaction, the 750-cm^{-1} band of the sodium and ammonium salts and the 765-cm^{-1} band of the LiSCN solutions have not been accounted for. The fact that both these bands are of higher frequency than the 740-cm^{-1} band implies that they are due to a SCN^- species with a C-S stretching mode which has a stronger force constant and a weaker or perhaps less covalent interaction of the sulfur end of the molecule with another species. If the Na^+ ion and the NH_4^+ ion are considered in terms of their electrostatic properties, they would be expected to act alike. If a $M^+ \cdots {}^-S-C{\equiv}N$ interaction occurs in these solutions, it would be reasonable to suggest that the C-S stretching mode of SCN^- would occur at a slightly higher frequency than it would in a species of the type $H_2NH \cdots {}^-S-C{\equiv}N$ since the metal-sulfur interaction might be weaker than the ammonia-sulfur interaction making the C-S bond stronger. The fact that this second band occurs at an even higher frequency in LiSCN solutions can be explained by the strong solvation of the lithium ion. The polarizing power of Li^+ is shielded by the solvation shell of NH_3 molecules and any lithium-sulfur interactions are thus weaker than sodium-sulfur interactions, resulting in a stronger C-S bond and a C-S stretching mode at higher frequency.

The second band in the C-N stretching region in the LiSCN solutions is $\sim$10 cm^{-1} higher than the 2063-cm^{-1} band. It could be associated with the same species which gives rise to the 765-cm^{-1} C-S stretching mode. However, there is no apparent reason why it should be so far removed from the 2063-cm^{-1} band when only one C-N stretching mode is seen in the NaSCN and NH_4SCN solutions. The lithium ion solvates a considerable number of the available molecules. If the 2063-cm^{-1} band is due to SCN^- which has considerable solvation at the nitrogen as well as at the sulfur end of the molecule, the 2074-cm^{-1} band which grows with increasing concentration in the LiSCN solutions could be due to SCN^- which is desolvated to a large extent. This desolvation would not be expected to occur in the NaSCN and NH_4SCN solutions because these cations allow anion-solvent interactions to dominate in concentrated solutions.

Summary

The cations Na^+ and NH_4^+ do not appear to interfere with the structure of bulk ammonia, and Na^+ appears to form ion pairs with NO_3^- at lower concentrations in NH_3 than in H_2O. The cation Li^+ appears to have an ordering effect on liquid ammonia, which prevents it from interacting with anions. The nitrate ion exhibits a hydrogen bonding interaction with NH_3 which appears to be similar to its interaction with H_2O, but in the presence of loosely solvated Na^+ it forms ion pairs. The thiocyanate ion exhibits a strong interaction with NH_3 and with Na^+, NH_4^+, and Li^+. There appears to be an equilibrium between the anion-solvent species and the anion-cation species but quantitative measurements on this point are not available. The vibrational spectrum of the thiocyanate ion is quite sensitive to its environment and reflects the strong interaction with NH_3.

Acknowledgment. We wish to thank the Robert A. Welch Foundation and the National Science Foundation for financial support.

References and Notes

(1) J. H. Roberts, A. T. Lemley, and J. J. Lagowski, *Spectrosc. Lett.*, **5**, 271 (1972).
(2) A. T. Lemley, J. H. Roberts, K. R. Plowman, and J. J. Lagowski, *J. Phys. Chem.*, **77**, 2185 (1973).
(3) A. R. Davis, J. W. Macklin, and R. A. Plane, *J. Chem. Phys.*, **50**, 1478 (1969).
(4) A. T. Lemley and R. A. Plane, *J. Chem. Phys.*, **57**, 1648 (1972).
(5) D. E. Irish, A. R. Davis, and R. A. Plane, *J. Chem. Phys.*, **50**, 2262 (1969).
(6) A. Tramer, *J. Chim. Phys.*, **59**, 232 (1962).
(7) K. R. Plowman and J. J. Lagowski, *J. Phys. Chem.*, **78**, 143 (1974).
(8) J. D. Riddell, D. J. Lockwood, and D. E. Irish, *Can. J. Chem.*, **50**, 2951 (1972).
(9) D. J. Gardiner, R. E. Hester, and W. E. L. Grossman, *J. Chem. Phys.*, **59**, 175 (1973).
(10) G. J. Janz, K. Balasubrahmanyam, and B. G. Oliver, *J. Chem. Phys.*, **51**, 5723 (1969).
(11) K. Balasubrahamanyam and G. J. Janz, *J. Chem. Phys.*, **57**, 4084 (1972).
(12) J. T. Nelson and J. J. Lagowski, *Inorg. Chem.*, **6**, 862 (1967).
(13) G. Herzberg and C. Reid, *Discuss. Faraday Soc.*, **9**, 92 (1959).

Volumetric and Isentropic Compressibility Behavior of Aqueous Amine Solutions. I

M. V. Kaulgud* and K. J. Patil

Department of Chemistry, Nagpur University, Nagpur-10, India *(Received September 14, 1973)*

Partial molal volumes ($\bar{V}_2$) and apparent molal adiabatic compressibilities (ϕ_k) at 20° have been obtained at low concentrations (0–25 mol %) for the following amines from measurements of density and sound velocity: $MeNH_2$, $EtNH_2$, n-$PrNH_2$, n-$BuNH_2$, $(Me)_2NH$, $(Et)_2NH$, $Et(NH_2)_2$, and $BzNH_2$. The $\bar{V}_2(x_2)$ curves exhibit minima for all amines but $BzNH_2$, and are analogous to the behavior of alcohol–water systems. The ϕ_k values are generally negative at low concentrations but assume positive values at higher concentrations. For $MeNH_2$, $(Me)_2NH$, and (possibly) $EtNH_2$ the apparent adiabatic compressibility goes through a minimum. The results are shown to be consistent with the stabilizing influence of the amines on the water structure. The $\phi_k(x_2)$ curves indicate a possible distinction of the way amine molecules exert their stabilizing influence. The lower members seem to dissolve substitutionally, whereas the higher members occupy the cavities forcing water into an ordered arrangement (hydrophobic hydration).

Introduction

In recent years there has been considerable interest in the studies in dilute aqueous solutions of nonelectrolytes and a special class of electrolytes (tetraalkylammonium halides) because these solutes exhibit abnormal behavior at low concentrations. Thus, the work of Glew[1] showed enhanced stabilization of water structure around the solute molecules in the form of clusters or cages for ethylene oxide–water system from partial molar volume and pmr studies. Anomalies in many thermodynamic properties of alcohol–water systems, including the behavior of partial molal volume, have been explained by Franks and Ives[2] on the basis of flickering cluster model of Frank and Wen.[3] Partial molal volumes of some tetraalkylammonium salts go through a minimum at a particular concentration indicating the enclosure of these ions in water cages.[4] These conclusions have been confirmed by Kay, *et al.*,[5] who studied the variation of the viscosity B coefficient and its' temperature variation for these alkyl ions. Depending upon the size of the alkylammonium ion, the B values are large, positive, and decrease with increasing temperature. Thus, information available in dilute solutions of many nonelectrolytes indicates (Franks[6]) formation of clathrate hydrate-like structure in solution.

In a recent communication[7] from this laboratory, it was shown that sound velocity in some aqueous-aliphatic amine solutions go through a pronounced maximum at a certain low concentration, which is mainly governed by the geometry of the molecules. Measurements[8] of the viscosity B coefficient for some of these amines in solution and their temperature variation showed a behavior, similar to those of tetraalkylammonium ions in water, indicating that a similar ordering effect on water molecules must be exerted by the amine molecules as well. Additional evidence for this behavior of amines is derived from the work of Jeffrey, *et al.*,[9] who have obtained solid hydrates of some of the amines and have also established their structure by X-ray study.

In order to throw more light on the interaction of aliphatic amines with water, we have undertaken a detailed study of partial molal volumes as well as apparent compressibility of the following amines in water at different concentrations and at 20°: methyl-, ethyl-, dimethyl-, diethyl-, n-propyl-, and n-butylamine. To this list were added ethylenediamine and benzylamine, to see if the presence of an additional interacting $-NH_2$ group or the presence of a benzene ring in the amine molecule has any significant influence on the interactions.

Experimental Section

Methylamine (Fluka, 40% in water), ethylamine (Fluka, 70% in water), and dimethylamine (Riedel-de-Haen, 40% in water) were directly used. The strength of these solutions were obtained by titrating them with standard hydrochloric acid solutions volumetrically as well as by pH titrations. Dilutions were made by adding a weighed amount of water to weighed amount of solutions and the concentrations were obtained in terms of mole fraction (x_2) of amine.

n-Butylamine (Fluka, purum), n-propylamine (Fluka, practical), and benzylamine (Riedel-de-Haen) were dried over potassium hydroxide pellets and distilled twice. Ethylenediamine (CP grade) was purified by the standard method. The refractive indices and densities of these purified liquids agreed well with literature values.

All solutions were prepared fresh before experiment with double distilled water in stoppered conical flasks. The densities at constant temperature (20 ± 0.02°) were found by using a calibrated 10-ml density bottle suspended in a U-10 ultrathermostat. The densities are considered to be accurate to ±5 units in the fifth decimal place. Sound velocity measurements for these systems were reported previously.[7]

Results and Discussion

Results of densities and sound velocities measurements for all the amines studied between 0 and 100 mol % (except methyl-, ethyl-, and dimethylamine, where the measurements could not be done at higher concentrations) are available as supplementary material. The plots of density *vs.* weight fraction of amine result in curves which are convex upward indicating a contraction in volume after mixing in all cases.

From the density data, the apparent molal volumes (ϕ_v) were calculated using the expression

$$\phi_v = \frac{1000(d_0 - d)}{cd_0} + \frac{M_2}{d_0} \quad (1)$$

where c is the concentration in molarity, M_2 is the molecular weight of solute, and d_0 and d are the densities of solvent and solution, respectively. The corresponding partial molal volumes ($\bar{V}_2$) were evaluated by plotting ϕ_v *vs.* molality (m), finding the slopes $\partial\phi_v/\partial m$, and using the expression

$$\bar{V}_2 = \phi_v + m(\partial\phi_v/\partial m) \quad (2)$$

The estimated error in ϕ_v and $\bar{V}_2$ at the lowest concentration is about ±0.2 ml, but is much smaller at higher concentrations. The apparent molal compressibility of solute were determined from

$$\phi_k = \frac{1000(\beta - \beta_0)}{c} + \beta_0\phi_v \quad (3)$$

where β and β_0 are the adiabatic compressibilities of solution and solvent, respectively. The estimated error in ϕ_k at the lowest concentration is $\pm 1 \times 10^{-10}$ cm^2 dyn^{-1}.

In Figure 1 we have plotted $\bar{V}_2$ and the excess partial molal volume (inserts) $\bar{V}_2^E = \bar{V}_2 - V_2$ (V_2 = molar volume of the pure solute) *vs.* the mole per cent of amine. Figure 2 shows the variation of the apparent molal adiabatic compressibility ϕ_k with concentration for all the amines. As the concentrations are sufficiently low and the temperature (20°) not very high, the difference between the isothermal and adiabatic compressibility is thought to be small enough to be ignored (*cf.* results of ϕ_k at 20° for *n*-PrOH of Alexander and Hill[10]). Smooth extrapolations of the curves in Figures 1 and 2 yielded $\bar{V}_2^0$ and ϕ_k^0, the corresponding property at infinite dilution. In view of the work of Franks and Smith[11] on the extrapolation of ϕ_v curves to zero concentration in order to obtain $\bar{V}_2^0$ values, the procedure followed by us might be questioned. In order to test the correctness of our procedure, the $\bar{V}_1(x_2)$ values for methyl- and dimethylamine (where sufficient data points below the mimimum in $\bar{V}_2$ are available) were examined for their dependence on x_2^2 and x_2^3 (x_2 = mole fraction of amine). It was found that $\bar{V}_1(x_2)$ exhibited a satisfactory dependence on x_2^2 rather than x_2^3 indicating the absence of an inflection point in the $\bar{V}_2(x_2)$ curves,[11] thus justifying smooth extrapolation. It was assumed that other amines also possess no inflection points in the $\bar{V}_2(x_2)$ curves. This assumption is not wholly unjustified as the difference in $\bar{V}_2^0$ for the homologous amines, which represents the limiting partial molal volume of a $-CH_2$ group, turn out in our case to be 17.1, 16, and 14.8 ml for the monoamines respectively (*cf.* Table I) in fair agreement with the value of 15.0 ml obtained by Alexander[12] from measurements on alcohols. From Figures 1 and 2 the following observations can be made. (1) $\bar{V}_2$ and hence $\bar{V}_2^E$ ($= \bar{V}_2 - V_2$) go through a minimum in all the amines except benzylamine. (2) The concentration at minimum in $\bar{V}_2$ and $\bar{V}_2^E$ decreases as the chain length of the amine molecule increases. (3) The limiting partial molal volumes are smaller than the molar volumes of the pure solutes suggesting loss in volume of amine in solution. Again the limiting partial molal excess volumes $\bar{V}_2^{0E}$ is governed by the chain length, being more negative for longer chains. Introduction of a second amine group in $EtNH_2$ to form $Et(NH_2)_2$ reduces $\bar{V}_2^{0E}$. Similar observations were also made for the partial molal volumes of *n*-alcohols and glycols by Alexander[12] and Nakanishi[13] and seem to be a common feature of monosubstituted

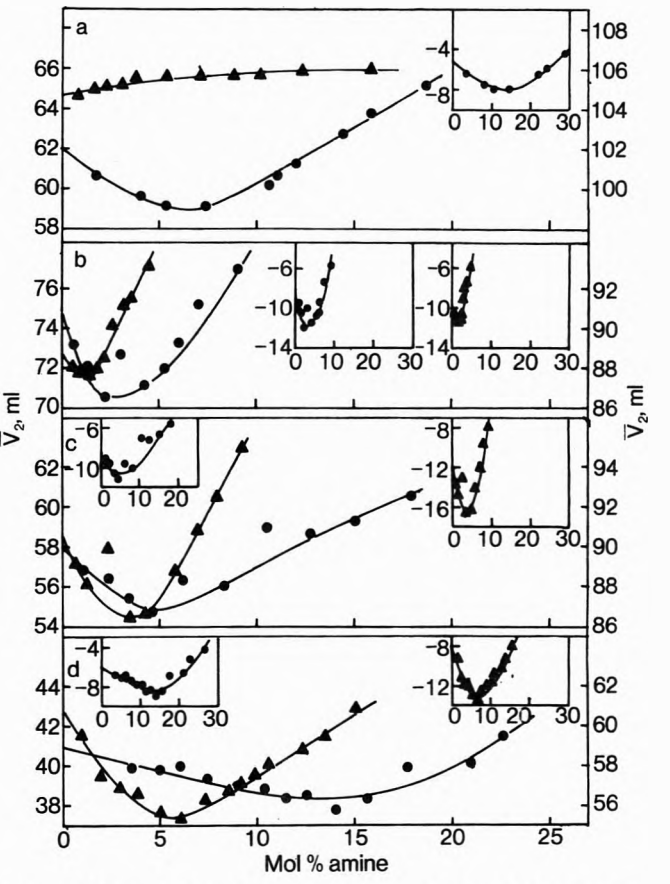

Figure 1. Partial molal volume ($\bar{V}_2$) and excess partial molal volume (inserts) $\bar{V}_2^E$ ($= \bar{V}_2 - V_2$) at 20° as a function of mole per cent of amine for the aqueous solutions of: (a) (the concentration axis for this frame is from 0 to 50 mol %) ethylenediamine (●) and benzylamine (▲, right-hand scale), (b) *n*-propylamine (●) and *n*-butylamine (▲, right-hand scale), (c) ethylamine (●) and diethylamine (▲, right-hand scale), (d) methylamine (●) and dimethylamine (▲, right-hand scale).

alkyl derivatives. (4) The apparent molal compressibility ϕ_k are generally negative at low concentration but become positive at higher concentration after passing through zero. The concentration at which ϕ_k passes through zero is about the same as that at which $\bar{V}_2$ goes through minimum. Remarkably in methyl- and dimethylamine (and probably in ethylamine) the ϕ_k's are weakly positive at low concentration and undergo minima before assuming more positive values at higher concentrations. The magnitude of the limiting apparent molal compressibility ϕ_k^0 also appears to be governed by chain length, becoming more negative for longer amines. For benzylamine the ϕ_k values are positive throughout the concentration range. (5) The slope $\partial\bar{V}_2/\partial x_2$ of the $\bar{V}_2(x_2)$ curves before minima is least for methyl amine and highest for *n*-butylamine, other amines having intermediate values. Slopes of apparent compressibility $\partial\phi_k/\partial x_2$ also show similar characteristic differences.

In Table I are collected values of $\bar{V}_2^0$, $\bar{V}_2^{0E}$, ϕ_k^0, $\partial\bar{V}_2/\partial x_2$, and $\partial\phi_k/\partial x_2$ at 20° as also the viscosity B coefficients at 25°[8] for all the amines.

Examination of Figures 1 and 2 shows at the outset that benzylamine behaves like a normal solute with both $\bar{V}_2$ and (positive) ϕ_k increasing monotonously with concentration. The abnormal behavior of $\bar{V}_2$ and $\bar{V}_2^E$ for the amines is similar to those of alcohols[2] and tetraalkylammonium halides[4] indicating a similarity in the solute-solvent interactions in the case of these classes of solutes. The negative

TABLE I

Solute	Mole fraction of amine at minimum ϕ_V	$\bar{V}_2^0$, ml	$\bar{V}_2^{0E}$, ml	$(\phi_K^0) \times 10^{10}$, cm² dyn⁻¹	$\partial\bar{V}_2/\partial x_2$, ml	$(\partial\phi_K/\partial x_2) \times 10^{10}$, cm² dyn⁻¹	Viscosity B coefficient (at 25°), M^{-1}
Methylamine	0.18	40.9	−5.90[a]	+4.5	−20	48	0.11
Ethylamine	0.083	58.0	−8.0[a]	−2.5	−69	200	0.23
n-Propylamine	0.05	74.0	−8.5	−9.5	−159	357	0.27
n-Butylamine	0.02	88.8	−10.1	−16.0	−163	1150	0.35
Dimethylamine	0.085	60.8	−8.0[a]	+2.5	−102	181	0.19
Diethylamine	0.045	90.8	−12.1	−10.0	−153	416	0.51
Ethylenediamine	0.22	62.1	−5.0	−6.5	−30	45	
Benzylamine		104.7	−4.2	+8.5	*b*		

[a] The molar volume (V_2) for these solutes have been obtained from the density data taken from ref 14. [b] Positive.

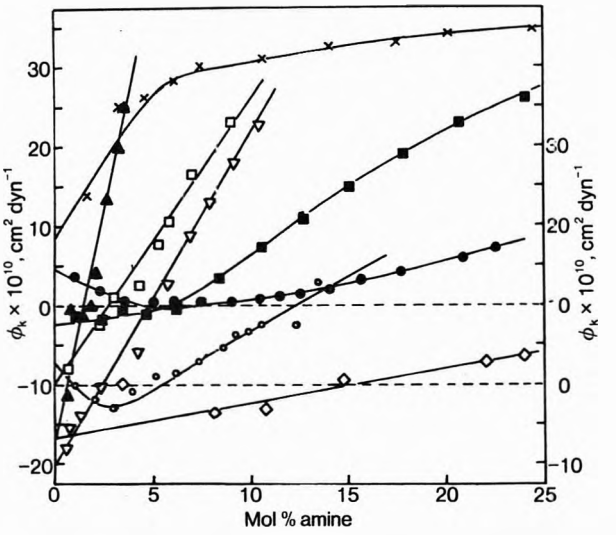

Figure 2. Apparent molal compressibility ϕ_K at 20° as a function of mole per cent amine for the aqueous solutions of: methylamine (●), ethylamine (■), *n*-propylamine (□), *n*-butylamine (▲), dimethylamine (○, right-hand scale), diethylamine (▽, right-hand scale), ethylenediamine (◇, right-hand scale), benzylamine (×).

values of ϕ_K for some amines at lower concentrations are similar to those for *n*-PrOH observed by Alexander and Hill[10] at infinite dilution and at temperatures lower than 30°. This was interpreted by them as being due to the loss of structural compressibility of water on account of the increase in the population of four bonded water molecules in the vicinity of the solute molecules. Critical evaluation of all the available physicochemical data for alcohol-water systems led Franks and Ives[2] to the conclusion that there must be reinforcement of water structure in the neighborhood of alcohol molecules in dilute solutions. Results of $\bar{V}_2(x_2)$, ϕ_K, and viscosity B coefficients for amines[8] also seem to be consistent with this view of structure-forming effect by the solute. Additional support for this view comes from the analysis of the entropies of hydration (ΔS_h) values for some dialkylamines by Franks and Watson,[15] who have shown that ΔS_h values are negative even after making allowance for the loss of rotational entropy on dissolving. Negative entropies of hydration must of necessity arise out of an ordering effect exerted by the amines on the neighboring water molecules.

The relative magnitudes of $\bar{V}_2^{0E}$, ϕ_K, and the B coefficients throw interesting light on the differences. Thus $\bar{V}_2^{0E}$ for methyl to butyl alcohol are of the order of −2 to −6 ml,[16] the corresponding amines show higher values of −5.9 to −12 ml (Table I). Although no reliable estimate can be made for this quantity for alkylammonium ion, these are presumably much larger than for amines.[17] Likewise, ϕ_K^0 for tetramethyl- to tetrabutylammonium ion shows maximum negative values of −9.1 to -25.5×10^{-10} cm² dyn⁻¹ (obtained by subtracting ϕ_K^0 for $Br^- = +2 \times 10^{-10}$ from that of salt[18]), while those for amines are little less negative (Table I), and those for alcohols are least negative: *e.g.*, ϕ_K^0 for *n*-PrOH in water is -3×10^{-10} cm² dyn⁻¹ [10] and for EtOH -2×10^{-10} cm² dyn⁻¹.[19] A more negative ϕ_K^0 means a greater loss of structural compressibility of water implying a greater ordering effect by the solute on the solvent. Values of viscosity B coefficients for amines (Table I, column 8) are generally higher than for alcohols (0.087 to 0.3 M^{-1} [20]) but lower than those for tetraalkylammonium ions[5] (~1.4 M^{-1} for $(n\text{-}C_4H_9)_4N^+$). It can thus be inferred from these observations that amines have a stronger ordering effect on water structure than alcohols but less than the alkylammonium ions.

The slopes $-\partial\bar{V}_2^E/\partial x_2$ show revealing differences similar to those for alcohols in water,[2,21] increasing with the hydrophobic character of the solute. Higher slopes mean that the interactions causing negative $\bar{V}_2^{0E}$ become dominate as more solute molecules dissolve in water. Following Franks, *et al.*,[10,22,23] it appears to be reasonable to conclude that for *n*-$PrNH_2$, *n*-$BuNH_2$, and $(Et)_2NH$ the stronger solute-solute interactions are responsible for high slopes $-\partial\bar{V}_2^E/\partial x_2$. Conversely, the smaller slopes for other amines, especially $MeNH_2$ and $EtNH_2$, would indicate that the solute-solute interactions are much weaker, which would amount to stronger solute-solvent interactions. Substitution of one more amine group in $EtNH_2$ to give $Et(NH_2)_2$ should cause stronger solute-solvent interaction lowering $-\partial\bar{V}_2^E/\partial x_2$, as is also observed.

The slopes $\partial\phi_K/\partial x_2$ are also revealing. *n*-$BuNH_2$, *n*-$PrNH_2$, and $(Et)_2NH$ show very high values. If a strong solute-solute interaction for these solutes is accepted, rapid increase in ϕ_K to positive values can be understood as resulting from a superposition on the negative structural contribution (resulting from structural stabilization of water) a rapidly increasing positive contribution due to solute-solute interaction (pure amines possess much higher compressibility than water). The steeper the increase, the stronger the assumed interaction. Higher values of $-\partial\bar{V}_2/\partial x_2$ should thus result in higher values of $\partial\phi_K/\partial x_2$, which is acutally found to be the case (Table I).

The concentration dependence of ϕ_K for $MeNH_2$ and $(Me)_2NH$ is rather startling and appears to be the first cases of ϕ_K showing extrema at low concentrations.[24] $EtNH_2$ also shows signs of a possible minimum, but the same cannot be established for want of sufficient data at

TABLE II

Solute	Activity coefficient	Free energy of solution ΔG, cal/mol
Methylamine	0.186	−1023
Ethylamine	0.494	−296
n-Propylamine	2.07	+431
n-Butylamine	7.70	+1158
Dimethylamine	0.505	−250
Diethylamine	4.70	+1150

lower concentrations. A possible clue to understanding these features can be had from the activity coefficients and free energy of solution obtained by Christie and Crisp[25] in dilute solutions of a number of amines at 25°, which are given in Table II.

It is noteworthy that only $MeNH_2$, $EtNH_2$, and $(Me)_2NH$, which have activity coefficients less than unity (negative deviations from Raoult's law) and negative free energies of solution (indicating affinity for water molecules), exhibit minima in ϕ_k. Whereas other amines showing activity coefficients greater than unity have no minimum in ϕ_k and, moreover, the ϕ_k values are large and negative at low concentrations. It is helpful at this point to invoke the hypothesis of substitutional dissolution for the lower amines ($MeNH_2$, $EtNH_2$, and $(Me)_2NH$) and interstitial dissolution for others (an idea proposed by Franks and Ives[2] in their review). Accordingly, the interstitially dissolved amines can be thought of as occupying either the cavities existing in the open water structure, or else such suitable cavities are "created on demand" (Franks and Ives) to suit the size and shape of the solute. The latter case will lead to strengthening of water structure in the vicinity of solute molecules giving negative values of ϕ_k.

In substitutional dissolution, an amine molecule at infinite dilution occupies one of the so called "framework sites" (Franks and Ives), displacing one water molecule into the interstitial site (Frank and Wen). Formation of one or two hydrogen bonds with amines thus leads to breakdown of a few others formed originally by the oxygen atom of the displaced water molecule. This leads to an incipient breakdown of water structure leading to small positive values of ϕ_k. Addition of further amine molecules can then be thought of as undergoing preferentially hydrogen bonding with the displaced water molecules, thus creating a fresh lattice site. This would decrease ϕ_k. This decrease in ϕ_k with increasing concentration may continue to a point, where accommodation of the solute on the framework site is compatible with the native structure of pure water. Any addition of solute beyond this point must lead to a gradual break down of the lattice leading to an increase in ϕ_k again. $MeNH_2$ which shows a broad flat minimum at a comparatively higher concentration happens to be the most compatible with the water structure because of its small size. The bulky $(Me)_2NH$ with a sharp minimum at lower concentration appears to be less so. The minimum in ϕ_k for the longer $EtNH_2$ molecules lies probably at concentration below 1 mol %. Such an explanation based upon substitutional dissolution would be in conformity with the magnitude of activity coefficients, smaller slopes for $\partial \bar{V}_2^E/\partial x_2$ and smaller values for viscosity B coefficients.

In conclusion, we can say that the volumetric and compressibility properties of amines, which in dilute aqueous solution show a strong similarity to those of alcohols and other monofunctional nonelectrolytes, are consistent with amine molecules having a stabilizing influence on water structure. Results of apparent compressibility measurements further indicate a possible distinction of the way amine molecules exert their stabilizing influence. The lower members of the homologous series appear to dissolve predominantly substitutionally and thus strengthen the native water structure whereas the higher members dissolve by occupying cavities and forcing water into an ordered arrangement (hydrophobic hydration).

Acknowledgments. We thank Professor R. H. Sahasrabudhey for his keen interest in this work. One of us (K. J. P.) is thankful to the University Grants Commission, India, for the award of a Junior Research Fellowship.

Supplementary Materials Available. Tables of concentrations, densities, sound velocities, partial molal volumes, and apparent molal isentropic compressibilities data for all the eight amines at 20° will appear following these pages in the microfilm edition of this volume of the journal. Photocopies of the supplementary material from this paper only or microfiche (105 × 148 mm, 24× reduction, negatives) containing all of the supplementary material for the papers in this issue may be obtained from the Journals Department, American Chemical Society, 1155 16th St., N.W., Washington, D. C. 20036. Remit check or money order for $3.00 for photocopy or $2.00 for microfiche, referring to code number JPC-74-714.

References and Notes

(1) D. N. Glew and N. S. Rath, *Can. J. Chem.*, **45**, 3058 (1967).
(2) F. Franks and D. J. G. Ives, *Quart. Rev., Chem. Soc.*, **20**, 1 (1966).
(3) H. S. Frank and W. Y. Wen, *Discuss. Faraday Soc.*, **24**, 133 (1957).
(4) W. Y. Wen and S. Saito, *J. Phys. Chem.*, **68**, 2639 (1964).
(5) R. L. Kay, T. Vituccio, C. Zawoyski, and D. F. Evans, *J. Phys. Chem.*, **70**, 2336 (1966).
(6) F. Franks in "Physico-Chemical Processes in Mixed Aqueous Solvents," F. Franks, Ed., Heinemann, London, 1967.
(7) M. V. Kaulgud and K. J. Patil, *Acustica*, **28**, 130 (1973).
(8) R. I. Patel, K. J. Patil, and M. V. Kaulgud, *Z. Phys. Chem. (Frankfurt am Main)*, **86**, 67 (1973).
(9) R. K. McMullan, J. H. Jorden, and G. A. Jeffrey, *J. Chem. Phys.*, **47**, 1218 (1967).
(10) D. M. Alexander and D. J. T. Hill, *Aust. J. Chem.*, **18**, 605 (1965).
(11) F. Franks and H. T. Smith, *Trans. Faraday Soc.*, **64**, 2962 (1968).
(12) D. M. Alexander, *J. Chem. Eng. Data*, **4**, 252 (1959).
(13) K. Nakanishi, N. Kato, and M. Maruyama, *J. Phys. Chem.*, **71**, 814 (1967).
(14) J. Timmermans, "Physico-Chemical Constants of Pure Organic Compounds," Elsevier, Amsterdam, 1950.
(15) F. Franks and B. Watson, *Trans. Faraday Soc.*, **65**, 2339 (1969).
(16) L. Benjamine, *J. Phys. Chem.*, **70**, 3731 (1966).
(17) F. Franks and H. T. Smith, *Trans. Faraday Soc.*, **63**, 2589 (1967).
(18) B. E. Conway and R. E. Verrall, *J. Phys. Chem.*, **70**, 3953 (1966).
(19) Obtained by analyzing the sound velocity data of R. Kuhnkies, Dissertation No. D-83, Technical University, Berlin, 1962.
(20) T. Herskovits and T. M. Kelly, *J. Phys. Chem.*, **77**, 381 (1973).
(21) K. Nakanishi, *Bull. Chem. Soc. Jap.*, **33**, 793 (1960).
(22) F. Franks and M. A. J. Quickenden, *Chem. Commun.*, 338 (1968).
(23) F. Franks, M. A. J. Quickenden, D. S. Reid, and B. Watson, *Trans. Faraday Soc.*, **66**, 583 (1970).
(24) We are grateful to Dr. F. Franks for drawing our attention to this point.
(25) A. O. Christie and D. J. Crisp, *J. Appl. Chem.*, **17**, 11 (1967).

Digital Simulation of Tubular Electrode Response in Stationary and Flowing Solution

James B. Flanagan and Lynn Marcoux*

Department of Chemistry, Texas Tech University, Lubbock, Texas 79409 *(Received March 26, 1973; Revised Manuscript Received November 27, 1973)*

Publication costs assisted by The Robert A. Welch Foundation

The various approximations made by Levich in order to calculate electrochemical responses at tubular electrodes have been tested using digital simulation. Specifically Levich assumed steady-state conditions, linear rather than cylindrical diffusion, no axial diffusion, and a linear rather than parabolic velocity profile. Using digital simulation a model for tubular electrodes was developed which makes possible the calculation of electrochemical response without these assumptions. These calculations quantitatively define the limits of the approximations as well as predict response beyond those limits. Transient response both under potentiostatic and galvanostatic conditions is obtained *via* this model. In addition to this the effect of potential scan rate upon voltammograms produced at flowing tubes is presented.

Hydrodynamic voltammetry is an extremely popular electrochemical experiment because it offers to the student of electrode reactions controlled and reproducible mass transfer conditions under which steady-state measurements may be accomplished. To the analytical chemist the convective component of mass transfer offers increased analytical sensitivity. It is an unfortunate fact of electrochemical life that this same very useful convective component also greatly complicates the derivation of those equations which describe electrode response.

Convective diffusion systems are described mathematically by combining the diffusion and convection terms in an equation of the form

$$\frac{\partial C}{\partial t} = D\nabla^2 C - \left(u_x\frac{\partial C}{\partial x} + u_y\frac{\partial C}{\partial y} + u_z\frac{\partial C}{\partial z}\right) \qquad (1)$$

where C is the concentration of the electroactive species; D, the diffusion coefficient; and u_x, u_y, u_z are the components of the flow velocity. Clearly it is necessary to have available hydrodynamic expressions for the various flow velocities and it is this complication which is largely responsible for the limited development of hydrodynamic voltammetry. Although plate[1,2] and conical[3] electrodes situated in flowing solutions have been given some attention, most hydrodynamic voltammetry has been carried out at rotating disk electrodes[4,5] simply because of the availability of solutions for the hydrodynamic equations. The rotating disk electrode and its variant, the rotating ring-disk electrode, have been fully developed as tools by which to investigate both charge transfer at the electrode and chemical reactions following charge transfer. The extent of their usefulness is best demonstrated by the extensive special bibliography devoted to rotating electrodes which appeared in a recent monograph.[6] Another hydrodynamic electrode system, the tubular electrode, has received some attention but in view of its great potentialities, its usefulness is largely unexplored.

The few existing papers which describe tubular electrode experiments may be divided into two categories, namely, those which are principally hydrodynamic in nature and those which are more directly concerned with electrochemical results. Studies in the first category use the electrode reaction principally as an indicator of the flow conditions. Studies of this sort were stimulated by earlier experiments involving planar electrodes fixed in flowing solutions,[2,7] and are represented by the work of Bazán and Arvía[8,9] and Ross and Wragg.[10] Electrochemically oriented experiments have been carried out almost entirely by Blaedel and his past and present coworkers. This work began with the construction of a simple gravity flow tubular platinum electrode which was used to verify Levich's theoretical analysis of convective diffusion to the surface of a tube.[11] This was followed by a more complete derivation of the expressions for steady-state current–voltage curves for reversible[12] as well as quasireversible and irreversible electrode reactions.[13] The only homogeneous reaction studied at a tubular electrode has been the classical catalytic case.[14]

$$O + ne \rightleftharpoons R \qquad (2)$$

$$R + Z \xrightarrow{k} O \qquad (3)$$

With the exception of the theoretical treatment of current–time curves at tubular electrodes in quiet solution[15] all other studies have been involved with either the development of new electrode materials[16,17] or with the application of tubular electrodes to actual analyses.[18-21]

Thus far all theoretical analyses of tubular electrode response have relied upon Levich's treatment of the mass transfer problem.[22] By necessity this treatment contained several approximations and limitations. The finite difference method as developed and extensively used by Feldberg[23,24] has proved extremely helpful in the past for the solution of complicated electrochemical problems. This has been especially true in the case of convective diffusion[25-28] and for difficult geometries.[29-32] In order to fully explore current–potential–time relationships at tubular electrodes we have utilized this technique and developed a finite difference model for tubular electrode calculations.

The equation describing mass transfer to the inner surface of a tube through which a solution is flowing in a laminar regime is

$$\frac{\partial C}{\partial t} = D\left\{\frac{\partial^2 C}{\partial r^2} + \frac{1}{r}\frac{\partial C}{\partial r} + \frac{\partial^2 C}{\partial z^2}\right\} + V_0\left\{1 - \frac{r^2}{R^2}\right\}\frac{\partial C}{\partial Z} \qquad (4)$$

where $C = C(r,Z,t)$ is the concentration at any point within the tube, D is the diffusion coefficient, r is the ra-

dial coordinate, Z is the axial coordinate, R is the inside radius of the tube, and V_0 is the axial flow rate. The use of the Poiseuille velocity profile

$$V = V_0\left\{1 - \frac{r^2}{R^2}\right\} \tag{5}$$

in the above expression requires that a sufficiently long inlet region exist in order for this parabolic profile to establish itself. It is also to be carefully noted that eq 4 is valid only in the case of laminar flow and that this restriction will be imposed throughout this discussion.

It is obvious from eq 4 that the analytical solution of the mass transfer problem with appropriate electrochemical boundary and initial conditions is a difficult task. In order to simplify this problem several approximations have been made. The solutions obtained under these approximations were of course limited to a very restricted set of conditions. The best known set of approximations are probably those used by Levich.[33]

Levich solved the equation

$$\frac{\partial C}{\partial t} = 0 = D\frac{\partial^2 C}{\partial r^2} + 2V_0\left\{\frac{R - r}{R}\right\}\frac{\partial C}{\partial Z} \tag{6}$$

using the boundary conditions appropriate to constant applied potential in the region of convective-diffusion control. These are

$$C(Z,r,0) = C^b \tag{7}$$

$$C(Z,r,t) = 0 \quad 0 < Z < X, t > 0 \tag{8}$$

$$r \xrightarrow{\lim} \infty \; C(Z,r,t) = C^b \tag{9}$$

Here X is the electrode length, t is the time after the boundary condition is imposed, and C^b is the concentration of the electroactive species in the solution bulk. Comparison of eq 6 with eq 4 reveals that the following approximations were made in order to facilitate solution.

(1) $\partial C/\partial t = 0$. This is of course the steady-state assumption which although it permits the useful calculation of steady-state currents, precludes the possibility of studying transient phenomena.

(2) $(1/r)(\partial C/\partial r) = 0$. This assumes that the diffusion process may be approximated by linear diffusion which is tantamount to saying that the diffusion layer is much smaller than the tube radius. This places a physical limit on the tube geometry and flow rate.

(3) $\partial^2 C/\partial Z^2 = 0$. The neglect of axial diffusion places a restriction on the lower end of flow rates which may be utilized, because this assumption requires axial mass transport to be due predominantly to flow.

(4) $V_0[1 - (r^2/R^2)] \cong 2V_0[(R - r)/r]$. The approximation of the Poiseuille velocity profile by a linear one also limits the tube size to large tubes since it again requires that the diffusion layer be small in comparison to the tube radius. Using these assumptions and the above boundary conditions (7-9) an expression (10) was obtained for the steady-state current at a tubular electrode.

$$i = 2.01nF\pi C^b D^{2/3} R^{2/3} X^{2/3} V_0^{1/3} \tag{10}$$

More recently a similar problem has been treated and extensively discussed using a different set of assumptions and boundary conditions.[34] In the present notation the equation which was solved was

$$0 = D\left\{\frac{\partial^2 C}{\partial r^2} + \frac{1}{r}\frac{\partial C}{\partial r} + \frac{\partial^2 C}{\partial Z^2}\right\} + V\frac{\partial C}{\partial Z} \tag{11}$$

and the boundary conditions used were

$$C(Z,R) = C_1 \quad 0 < Z < X \tag{12}$$

$$C(Z,R) = C_2 \quad Z < 0, Z > X \tag{13}$$

$$Z \xrightarrow{\lim} \infty \; \partial C/\partial Z = 0 \tag{14}$$

The flow field, V, is assumed to be constant. The inclusion of axial diffusion as well as the use of the cylindrical Laplacian certainly increases the rigor of this solution; however, the assumption of a uniform flow field which is independent of radius is questionable. This assumption is probably not as good as the linear gradient employed by Levich. It must also be noted that the boundary condition described by eq 13 is not strictly speaking the case for a tubular electrode surrounded by insulating surfaces since the surface concentration on the upstream side should not be the same as that on the downstream side.

Method

The computational method used was the digital simulation technique which has been applied to a variety of electrochemical problems. This technique is mathematically equivalent to the explicit difference method which has been used to solve the boundary value problems of diffusion. The mathematical considerations are fully discussed in several standard numerical analysis texts.[35,36] The methodology for the application of this procedure has been thoroughly described by Feldberg.[24]

The electrode model consists of a net of points in a coordinate system of proper symmetry. For tubular electrodes two-dimensional circular cylindrical coordinates constitute the appropriate system. This same geometry was recently used in a theoretical discussion of finite planar disk electrodes.[29] A model of the simulation grid is shown in Figure 1. The model electrode is L units in length and P units in radius. There are $P + 1$ radial divisions. The surface of the electrode is taken to be at the points where $\rho = 1$, $0 < \zeta \leq L$ where ρ and ζ are the radial and axial coordinates, respectively. The tube surface corresponding to net points $\zeta \leq 0$ or $\zeta > L$ was taken to be nonelectroactive. In this model solution resistive drops have been ignored. This assumption was made in order to remain consistent with previous treatments so as to facilitate comparison. These effects will depend markedly on geometry and will certainly be important in the case of nonaqueous electrolytes.

The finite difference formalism for cylindrical diffusion has been discussed in detail.[29] Very briefly the finite difference equations for diffusion used in this work are given below. Linear diffusion was necessary to model the assumptions made by Levich, and the difference equation for one-dimensional diffusion is given by

$$F_{\rho,\zeta,\kappa+1} = F_{\rho,\zeta,\kappa} + \delta(F_{\rho-1,\zeta,\kappa} - 2F_{\rho,\zeta,\kappa} + F_{\rho+1,\zeta,\kappa}) \tag{15}$$

where κ is the iteration counter, δ is the dimensionless diffusion coefficient

$$\delta = D\Delta t/(\Delta r)^2 \tag{16}$$

and $F_{\rho,\zeta,\kappa}$ is the dimensionless concentration at the point (ρ,ζ) and at time κ

$$F_{\rho,\zeta,\kappa} = C_{\rho,\zeta,\kappa}/C^b \tag{17}$$

For one-dimensional circular radial diffusion the diffusion equation becomes for $1 < \rho < P + 1$

$$F_{\rho,\zeta,\kappa+1} = F_{\rho,\zeta,\kappa} + \delta(F_{\rho-1,\zeta,\kappa} - 2F_{\rho,\zeta,\kappa} + F_{\rho+1,\zeta,\kappa}) + \frac{\delta}{2(P - \rho + 1)}\{F_{\rho-1,\zeta,\kappa} - F_{\rho+1,\zeta,\kappa}\} \tag{18}$$

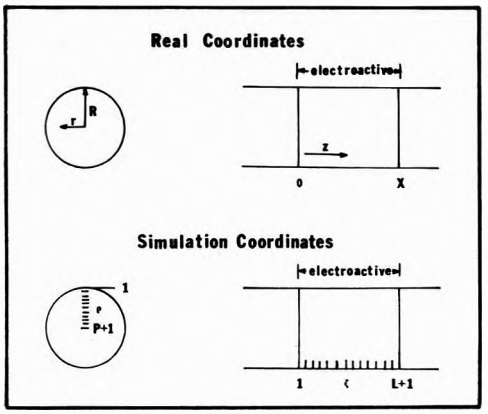

Figure 1. Electrode coordinate systems: (a) real coordinates, (b) simulation coordinates.

and for the central element where $\rho = P + 1$, it is

$$F_{P+1,\zeta,\kappa+1} = F_{P+1,\zeta,\kappa} + 4\delta(F_{P,\zeta,\kappa} - F_{P+1,\zeta,\kappa}) \quad (19)$$

Clearly the concentration of the $\rho = 1$ element is established by the boundary conditions of the experiment to be simulated. Several possible treatments exist for two-dimensional cylindrical diffusion, and in this work the simplest approach was chosen. The equations were for $1 < \rho < P + 1$

$$F_{\rho,\zeta,\kappa+1} = F_{\rho,\zeta,\kappa} + \delta(F_{\rho+1,\zeta,\kappa} + F_{\rho-1,\zeta,\kappa} + F_{\rho,\zeta-1,\kappa} - 4F_{\rho,\zeta,\kappa} + F_{\rho,\zeta+1,\kappa}) + \frac{\delta}{2(P - \rho + 1)}\{F_{\rho-1,\zeta,\kappa} - F_{\rho,\zeta,\kappa}\} \quad (20)$$

and for $\rho = P + 1$

$$F_{P+1,\zeta,\kappa+1} = F_{P+1,\zeta,\kappa} + 4\delta(F_{P,\zeta,\kappa} - F_{P+1,\zeta,\kappa}) + \delta(F_{P,\zeta-1,\kappa} - 2F_{P,\zeta,\kappa} + F_{P,\zeta+1,\kappa}) \quad (21)$$

The proper boundary conditions are imposed on the "electroactive" elements: $\rho = 1$, and $1 \leq \zeta \leq L + 1$.

Since there is a convective component in only one direction the convection problem at a flowing tubular electrode is quite simple. The only complication is that the viscosity of the fluid is responsible for a parabolic velocity profile. The expression used to calculate solution displacement due to convection was

$$\Delta\zeta = W_0\left(1 - \frac{(P - \rho + 1)^2}{P^2}\right) \quad (22)$$

where W_0 is the maximum axial velocity in units of ζ per time step. The linear gradient used by Levich is expressed by

$$\Delta\zeta = W_0\left\{\frac{2(\rho - 1)}{P}\right\} \quad (23)$$

In eq 22 and 23, $\Delta\zeta_\rho$ is the number of axial units that the solution is displaced in lamina ρ per time step κ. This means that the concentration originally at point (ρ,ζ) becomes the concentration at point $(\rho,\zeta + \Delta\zeta)$. Since the net points must be indexed by integers and $\Delta\zeta$ is not necessarily integral, a weighted average of two upstream concentrations must be used in order to obtain the new concentration. Taking the notation $\|X\|$ to mean the greatest integer less than or equal to X, the concentration may be calculated from

$$F_{\rho,\zeta}' = (1 + \|\Delta\zeta\| - \Delta\zeta)F_{\rho,\zeta-\|\Delta\zeta\|} + (\Delta\zeta - \|\Delta\zeta\|)F_{\rho,\zeta-\|\Delta\zeta\|+1} \quad (24)$$

where $F_{\rho,\zeta}$ is the old dimensionless concentration and $F_{\rho,\zeta}'$ is the new dimensionless concentration brought about by convection. A similar approach has been used to treat convection at the rotating ring–disk electrode.[37]

The boundary conditions used depended upon the electrochemical experiment being simulated and were established at the beginning of each time step. For voltammetry the electrode reaction was taken to be rapid and the surface concentrations for a given potential were calculated *via* the Nernst equation. For potentiostatic transients and steady-state currents in the region of convective-diffusion control, the surface concentration of the electroactive species was set equal to zero. The boundary conditions for the galvanostatic experiment were more complicated since although the total current flowing at the electrode is a preset constant, the flux along the electrode varies; therefore, the current at each annulus must vary. This case is completely analogous to similar conditions at the finite planar disk and has been discussed in detail.[29]

Certain dimensionless parameters have proved useful when interconverting between real and simulation space. By analogy to the real current which is given by eq 10 the simulation current is calculated from

$$Z_{\lim} = 1.018\delta^{-1/3}P^{-1/3}L^{2/3}W_0^{1/3} \quad (25)$$

Often for convenience currents are normalized with respect to the limiting current. Another very useful tubular electrode parameter has been derived by intersecting the Cottrell equation

$$i = nFAD^{1/2}C^b/\pi^{1/2}t^{1/2} \quad (26)$$

with the limiting current expression, eq 10. This yields a time-like parameter known as the equivalent time and denoted t'. It may be easily shown that the equivalent time is given by

$$t' = 0.3152R^{2/3}X^{2/3}D^{-1/3}V_0^{-2/3} \quad (27)$$

or if the volume flow rate, V_f, is used[11]

$$V_f = \pi R^2 V_0/2 \quad (28)$$

the expression becomes

$$t' = 0.4259R^2X^{2/3}D^{-1/3}V_f^{-2/3} \quad (29)$$

The simulation counterpart of this quantity is

$$\theta' = t'D/R^2 = 0.3152L^{2/3}P^{-4/3}\delta^{2/3}W_0^{2/3} \quad (30)$$

Normalizing the time axis by dividing by the equivalent time permits the presentation of the time-dependent behavior of whole families of electrodes by a single curve. It will also be seen that this quantity is useful in defining other experimental parameters such as the scan rate in voltammetry. The notation used is summarized in Appendix I.

Results and Discussion

Zero Flow Limit. In order to establish the lower limit of response as well as to compare simulation results with known analytical solutions the zero flow limit was investigated. The problem of radial diffusion in an infinite tube has been discussed.[15,38,39] Since the assumption of an infinite tube eliminates axial diffusion, Fick's second law is given by

$$\frac{\partial C(r,t)}{\partial t} = D\frac{\partial^2 C(r,t)}{\partial r^2} + \frac{1}{r}\frac{\partial C(r,t)}{\partial r} \quad (31)$$

and the boundary conditions have already been stated. The solution to this equation is[38,39]

$$C(r,t) = \frac{2C^b}{R}\sum_1^\infty \left(\frac{1}{\alpha_n}\right)\frac{J_0(\alpha_n r)}{J_1(\alpha_n r)} \exp\{-D\alpha_n^2 t\} \quad (32)$$

where α_n is the nth root of the equation

$$J_0(\alpha_n r) = 0 \quad (33)$$

and $J_i(y)$ is a Bessel function of order i. From this expression the flux of the electroactive species at the electrode surface, hence the current, may be determined. The current-time behavior is expressed by[15]

$$i = 4\pi nFXC^bD\sum_1^\infty \exp\{D\alpha_n^2 t\} \quad (34)$$

This situation was simulated and it was determined that for $P > 30$ the simulation approached the analytical solution within 0.4%. Since we were interested in the effects of axial diffusion it seemed worthwhile to repeat this calculation including this term. This amounts to an evaluation of the importance of edge effects at tubular electrodes and is to some extent comparable to previous discussions of edge effects at planar electrodes.[29,40,41] The results of this calculation are shown in Figure 2. The geometry used for this calculation was the same as that employed experimentally by Oesterling and Olson,[15] $X/R = 16.7$. The current including axial diffusion is normalized with respect to the current calculated from eq 34 and plotted *vs.* tD/R^2. From this plot it is clear that there is a substantial current due to axial diffusion under these conditions. In the interest of comparison some of the experimental data of Oesterling and Olson[15] have also been plotted in Figure 2. The calculation confirms the general tendency of their points taken at longer times to depart from simple theory. There are several possible explanations for the failure of the simulation to completely explain their data. The electrode was a mercury coated platinum tube; consequently, some departure from the assumed geometry due to the surface tension of mercury would be expected. In order to make the comparison one must know the diffusion coefficient for the ion in question and uncertainty is often present in these values. The best explanation, however, is probably the existence of a small convective component which would become important at longer times. This convection could be due to vibration or in the case of ion–ion reductions it could be due to density differences between oxidation states. One unfortunate aspect of tubular electrodes is that because of their geometry, no means exists to compensate for this latter source of convection. This, of course, is not the case for planar electrodes.[42] The importance of axial diffusion may be experimentally minimized by increasing the X/R ratio.

The Levich Assumptions. The first simulation done with a flowing solution was a calculation using the Levich assumptions, and boundary conditions, eq 6–9. For values of $L > 50$ and diffusion layer thickness greater than 30, the simulation converged within 0.2% of the values calculated by Levich. This confirmed the validity of our approach, gave some idea of the number of volume elements necessary to obtain convergence, and also provided us with an estimate of our probable error. The latter point is an important one since probable error in this technique is often difficult to establish.

Potentiostatic and Galvanostatic Transients. The time-dependent response of a convective system to a current or potential step has been considered in the past as a problem in its own right.[43-45] Here transient response is considered because it leads to an understanding of the significance of t' which in turn is useful in explicating the importance of cylindrical diffusion. Thus the current transient which occurs when the potential is stepped from a value at which no Faradaic process takes place to one at which the Faradaic current is convective-diffusion controlled was simulated. The calculation was carried out using the Levich assumptions, and the result is shown in Figure 3. In this figure the time axis is normalized by dividing by t', and the current axis is normalized with respect to the limiting current. Not surprisingly the current-time behavior is very Cottrell-like in the region $t/t' < 0.4$, and it reaches the steady-state value at $t/t' > 2.0$.

The time-dependent response of a flowing tubular electrode to a current step is shown in Figure 4. Because the flux at the electrode surface is not constant along the length of the tube the calculations involved were rather lengthy. In the interest of conserving computer time the Levich assumptions were made for this calculation. A reversible electron transfer was assumed so the magnitude of the current step may be related to the ordinate of Fig-

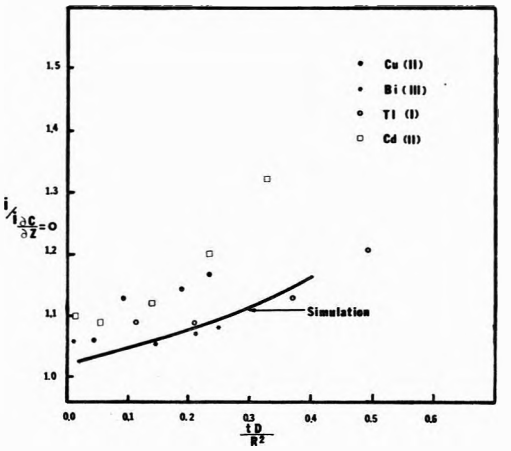

Figure 2. Departures from eq 34 due to axial diffusion. Data points taken from ref 15.

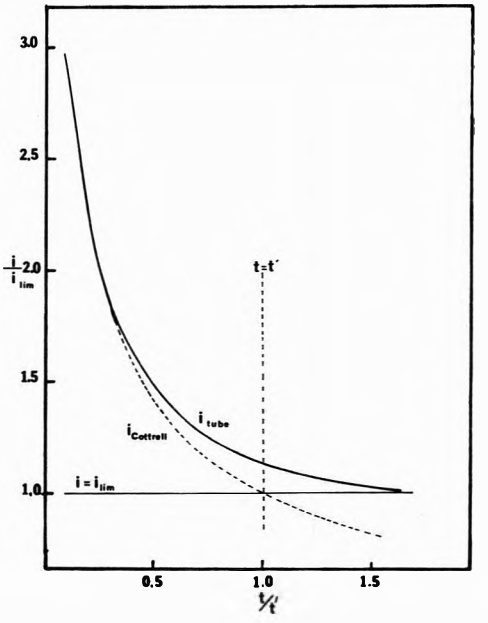

Figure 3. Current transient when a potential step is applied to a flowing solution.

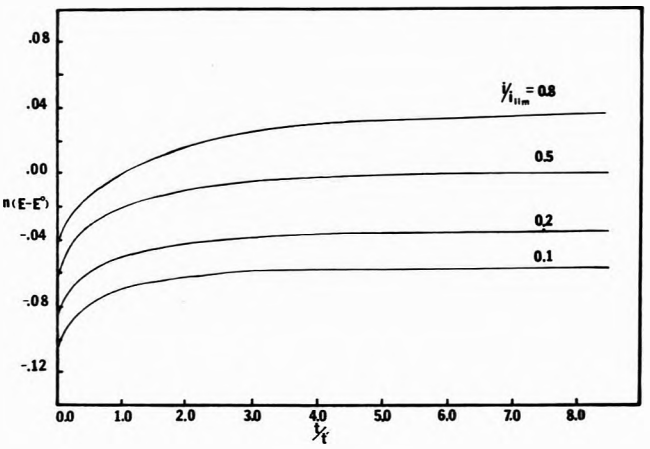

Figure 4. Potential transient when a current step is applied to a flowing solution.

ure 4 by means of Blaedel and Klatt's[12] equation for a reversible voltammogram at a flowing tube

$$E = E^\circ - \frac{RT}{nF} \ln \left(\frac{D_{ox}}{D_{red}}\right)^{2/3} - \frac{RT}{nF} \ln \frac{i}{i_D - i} \quad (35)$$

From Figure 4 it is apparent that the steady-state potential is reached when $t/t' > 4.0$.

Cylindrical Diffusion. Figure 3 makes it quite apparent that the equivalent time, t' defined by eq 29, very nearly describes a condition of the diffusion layer at a flowing tube which corresponds to that for a stationary electrode at time t'. This suggests that it might be profitable to substitute t' into eq 34 and thereby estimate the change in steady-state current due to the cylindrical geometry. Figure 5 shows the results of such an experiment. The lower curve represents a simulation including cylindrical diffusion and the upper curve is the result of the above approximation. This makes clear the region in which cylindrical geometry must be taken into account and provides a good approximation for much of this region. Additionally the difference between the two curves provides an estimate of the departures expected when Poiseuille flow is neglected. Clearly linear diffusion may be safely used whenever $t'D/R^2 < 10^{-4}$. In terms of experimental variables this requires that $XD/V_f < 10^{-6}$ and if we take the conventional value of 1×10^{-5} cm^2/sec for D then one would expect Levich theory to be perfectly adequate when X/V_f is less than 0.1 sec/cm^2.

Axial Diffusion. Axial diffusion was seen to be important in the zero flow limit; however, its significance in the case of flowing solution will depend upon flow rate and geometry. Figure 6 shows the simulation for an electrode with an X/R ratio of 1/1. The lower curve in this figure is for an X/R ratio of infinity, *i.e.*, no possible axial diffusion. The departure of the lower curve is due entirely to cylindrical diffusion and parabolic flow. The geometry chosen is an extreme one and even here the influence of axial diffusion is slight. In fact it is even somewhat compensatory. For electrode and flow rates for which the other Levich assumptions held it was impossible to produce an axial diffusion effect. Not surprisingly the neglect of axial diffusion is seen to be the best of the Levich assumptions.

Scan Rate. The derivation of the equation of the current-voltage curve for a tubular electrode with flowing solution is relatively easy if one makes the steady-state assumption.[12,13] From an experimental point of view it would be useful to know at what potential scan rate the steady-state assumption becomes valid. Figure 7 shows the results of the simulation of this problem. The assumptions used were identical with those used for the treatment of galvanostatic transients. Various voltammograms shown as a function of nVt' where V is the voltage scan rate in mV/sec. Both the current and potential axes have been normalized. This calculation demonstrates that the steady-state assumption is valid for cases in which $nVt' < 5$. Perhaps more important is the fact that one might

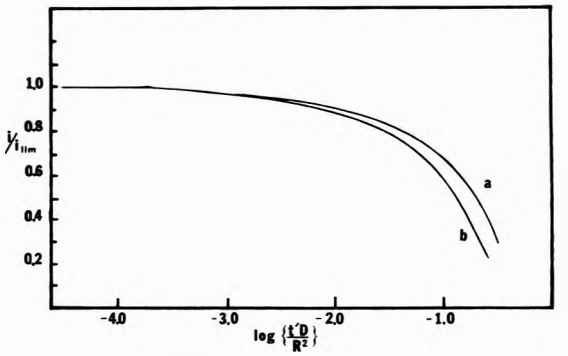

Figure 5. Departures from Levich equation due to cylindrical diffusion. Curve a is calculated from eq 39 and curve b is the simulation.

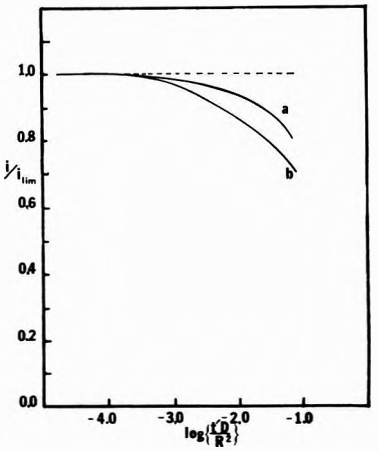

Figure 6. Departures from Levich equation due to axial diffusion. Curve a is for an electrode with $X/R = 1/1$ and curve b represents the limiting case $X/R = \infty$.

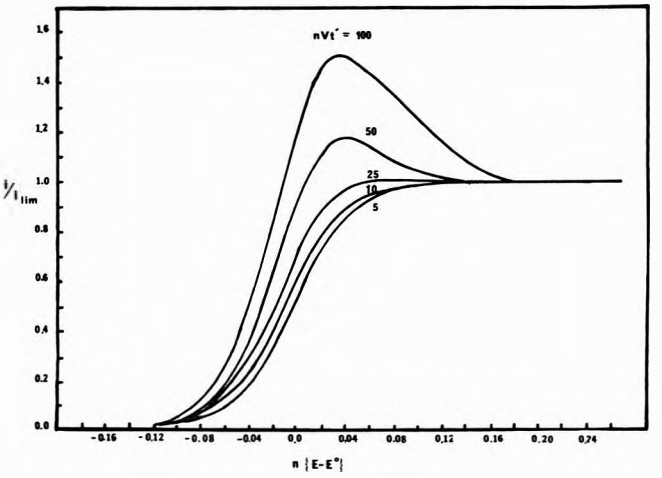

Figure 7. Voltammograms of a reversible system at a flowing tube electrode as a function of scan rate.

naively assume that the absence of a current maximum would experimentally confirm steady-state behavior when this, in fact, is not the case. The voltammogram obtained in the case $nVt' = 25$ has no maximum but the value of $E_{1/2}$ obtained from this curve would be in error by $20/n$ mV. With respect to this parameter it should be recalled that for a tubular electrode $E_{1/2}$ differs from the polarographic $E_{1/2}$ by $(RT/6nF) \ln (D_{ox}/D_{red})^{1/2}$.

Acknowledgment. The support of the Robert A. Welch Foundation (Grant No. D-511) is gratefully acknowledged.

Appendix I. Explanation of Notation

r = actual radial coordinate
ρ = radial coordinate of model
R = inside tube radius
Z = actual axial coordinate
S = axial coordinate of model
X = electrode length
D = actual diffusion coefficient
δ = dimensionless diffusion coefficient
V_0 = axial flow rate
V_f = volume flow rate
W_0 = maximum axial velocity in units of ζ per time step
L = number of length units of model
P = number of radial units of model
κ = iteration counter
θ = dimensionless time
$F_{\rho,\zeta,\kappa}$ = dimensionless concentration
Z = dimensionless current parameter
t' = equivalent time (see eq 27 and 29)
θ' = dimensionless equivalent time

References and Notes

(1) V. G. Levich, *Discuss. Faraday Soc.*, **1**, 37 (1947).
(2) G. Wranglen and O. Nilsson, *Electrochim. Acta*, **7**, 121 (1962).
(3) J. Jordan, R. A. Javick, and W. E. Ranz, *J. Amer. Chem. Soc.*, **80**, 3846 (1958).
(4) R. N. Adams, "Electrochemistry at Solid Electrodes," Marcel Dekker, New York, N. Y., 1969.
(5) V. G. Levich, "Physicochemical Hydrodynamics," Prentice-Hall, Englewood Cliffs, N. J., 1962.
(6) Reference 4, pp 110–114.
(7) C. S. Lin, E. B. Denton, H. S. Gaskill, and G. L. Putnam, *Ind. Eng. Chem.*, **43**, 2136 (1951).
(8) J. C. Bazán and A. J. Arvía, *Electrochim. Acta*, **9**, 17 (1964).
(9) J. C. Bazán and A. J. Arvía, *Electrochim. Acta*, **9**, 667 (1964).
(10) T. K. Ross and A. A. Wragg, *Electrochim. Acta*, **10**, 1093 (1965).
(11) W. J. Blaedel, C. L. Olson, and L. R. Sharma, *Anal. Chem.*, **35**, 2101 (1963).
(12) W. J. Blaedel and L. N. Klatt, *Anal. Chem.*, **38**, 879 (1966).
(13) L. N. Klatt and W. J. Blaedel, *Anal. Chem.*, **39**, 1065 (1967).
(14) L. N. Klatt and W. J. Blaedel, *Anal. Chem.*, **40**, 512 (1968).
(15) T. O. Oesterling and C. L. Olson, *Anal. Chem.*, **39**, 1546 (1967).
(16) T. O. Oesterling and C. L. Olson, *Anal. Chem.*, **39**, 1543 (1967).
(17) W. D. Mason and C. L. Olson, *Anal. Chem.*, **42**, 548 (1970).
(18) W. J. Blaedel and C. L. Olson, *Anal. Chem.*, **36**, 343 (1964).
(19) W. D. Mason and C. L. Olson, *Anal. Chem.*, **42**, 488 (1970).
(20) D. B. Easty, W. J. Blaedel, and C. Anderson, *Anal. Chem.*, **43**, 509 (1971).
(21) W. J. Blaedel and S. C. Boyer, *Anal. Chem.*, **43**, 1538 (1971).
(22) Reference 5, p 112.
(23) S. W. Feldberg and C. Auerbach, *Anal. Chem.*, **36**, 505 (1964).
(24) S. W. Feldberg in "Electroanalytical Chemistry—A Series of Advances," Vol. III, A. J. Bard, Ed., Marcel Dekker, New York, N. Y., 1969.
(25) L. S. Marcoux, R. N. Adams, and S. W. Feldberg, *J. Phys. Chem.*, **73**, 2611 (1969).
(26) K. B. Prater and A. J. Bard, *J. Electrochem. Soc.*, **117**, 207 (1970).
(27) K. B. Prater and A. J. Bard, *J. Electrochem. Soc.*, **117**, 335 (1970).
(28) K. B. Prater and A. J. Bard, *J. Electrochem. Soc.*, **117**, 1517 (1970).
(29) J. B. Flanagan and L. Marcoux, *J. Phys. Chem.*, **77**, 1051 (1973).
(30) I. B. Goldberg and A. J. Bard, *J. Electroanal. Chem.*, **38**, 313 (1972).
(31) I. B. Goldberg and A. J. Bard, *J. Phys. Chem.*, **75**, 3281 (1971).
(32) I. B. Goldberg, A. J. Bard, and S. W. Feldberg, *J. Phys. Chem.*, **76**, 2550 (1972).
(33) Reference 5, pp 112–113.
(34) H. E. Wilhelm, *Z. Angew. Phys.*, **30**, 376 (1971).
(35) B. Carnahan, H. A. Luther, and J. O. Wilkes, "Applied Numerical Methods," Wiley, New York, N. Y., 1969, p 429.
(36) C.-E. Froberg, "Introduction to Numerical Analysis," 2nd ed, Addison-Wesley, Reading, Mass., 1965, p 294.
(37) K. B. Prater in "Applications of Computers to Chemical Instrumentation," J. S. Mattson, H. B. Mark, Jr., and J. C. MacDonald, Jr., Ed., Marcel Dekker, New York, N. Y., 1972.
(38) R. M. Barrer, "Diffusion In and Through Solids," Macmillan, New York, N. Y., 1941, p 34.
(39) W. Jost, "Diffusion in Solids, Liquids, and Gases," Academic Press, New York, N. Y., 1960, p 52.
(40) P. J. Lingane, *Anal. Chem.*, **36**, 1723 (1964).
(41) Z. G. Soos and P. J. Lingane, *J. Phys. Chem.*, **68**, 3821 (1964).
(42) M. von Stackelberg, M. Pilgram, and V. Toome, *Z. Elektrochem.*, **57**, 342 (1953).
(43) J. M. Hale, *J. Electroanal. Chem.*, **6**, 187 (1963).
(44) J. M. Hale, *J. Electroanal. Chem.*, **8**, 332 (1964).
(45) R. P. Buck and H. E. Keller, *Anal. Chem.*, **35**, 900 (1963).

Ion Association between Naphtho[b]cyclobutene Radical Anion and Alkali Metal Ions[1]

Reuben D. Rieke*[2] and Stephen E. Bales

William Rand Kenan, Jr. Laboratories of Chemistry, University of North Carolina, Chapel Hill, North Carolina 27514
(Received August 11, 1972)

Alkali metal reduction of naphtho[b]cyclobutene has been carried out in a variety of ethereal solvents in order to study ion-pairing effects. The methylene protons of naphtho[b]cyclobutene were found to be equivalent under all conditions involving tight ion pairs. The origin of this equivalency is discussed.

Interest in the detailed structure of ion pairs has been considerable.[3] Of particular interest has been the study of the kinetics and equilibria between structurally different ion pairs.[3c-e] Esr studies of pyracene[4] and acenaphthene[5] radical anions have provided examples of line-width alternation and nonequivalency of methylene protons as a re-

sult of ion pairing. Our studies[6] of benzocyclobutene (BCB) radical anion provided a further example of these phenomena caused by ion pairing. For these systems, the common feature is an ethylene bridge in the 1 and 8 positions for pyracene and acenaphthene and in the 2 and 3 positions for BCB. As a result of these studies, the naphthalene analog of BCB, naphtho[*b*]cyclobutene (I), was of

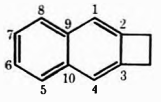

I

interest due to its ethylene bridge at the 2 and 3 positions. In this paper we would like to present our results of a study of the various ion pairs of the radical anion of I. All hyperfine splitting constants (hfsc) are given in gauss.

Results

Table I gives the results for this ion-pairing study of compound I. Reduction of I with potassium in dimethoxyethane (DME)[7] or a mixture of DME and hexamethylphosphoramide (HMPA) gave virtually identical, temperature-independent esr spectra. Methylene nonequivalency, alternating line widths, and ion pairing were not observed using these conditions. It was decided to try other combinations of metal and solvent to see if these phenomena could be produced from I.

Sodium Reductions. Reduction of I with sodium in DME gave reversible, temperature-independent spectra from −20 to −80° that were essentially the same as those obtained from reductions using potassium in DME and DME-HMPA. The hfsc for the methylenes was slightly smaller, having a value of 5.80.

When sodium and tetrahydrofuran (THF) were used, the spectra obtained from −100 to −65° were the same as observed using potassium and DME, except the hfsc for the 1 and 4 protons was slightly smaller, having a value of 5.35. At −60 and −50° a large increase in line width was noted from 0.15 G at −65° to approximately 0.50 G at −60 and −50°. At −45° metal splittings due to the sodium cation were observed, A_{Na} at −45° being 0.50. The sodium splitting increased with temperature giving a value of 1.10 at room temperature. Despite the ion-pair formation, the methylene protons remained equivalent over the range where metal splittings were observed: −45° to room temperature. The spectra were reversible with temperature and could be simulated quite well over the entire temperature range. Experimental and calculated spectra for −60 and −30° are shown in Figure 1. The −60° spectra had hfsc of $A_{1,4}$ = 5.35, $A_{5,8}$ = 4.23, $A_{6,7}$ = 1.60, and A_{CH_2} = 5.80, while the −30° spectra had hfsc of $A_{1,4}$ = 5.10, $A_{5,8}$ = 4.20, $A_{6,7}$ = 1.55, A_{CH_2} = 5.75, and A_{Na} = 0.75.

Finally, I was reduced with sodium in diethyl ether (DEE). Spectra were obtained at −100 and −120° and decayed rapidly at higher temperatures. Also, the spectra exhibited metal splittings which increased with temperature. Calculated spectra gave good fits as far as the number and positions of lines, but the relative intensities did not agree with the experimental results, probably as a result of modulation of the Na hfsc. This might arise by interconversion of ion pairs of different solvation number.[3c]

Potassium Reductions. When potassium and THF were used the hfsc showed slight perturbations compared to the free ion case, with $A_{1,4}$ = 5.10, $A_{5,8}$ = 4.40, $A_{6,7}$ = 1.65, and A_{CH_2} = 5.70. However, the methylene protons were

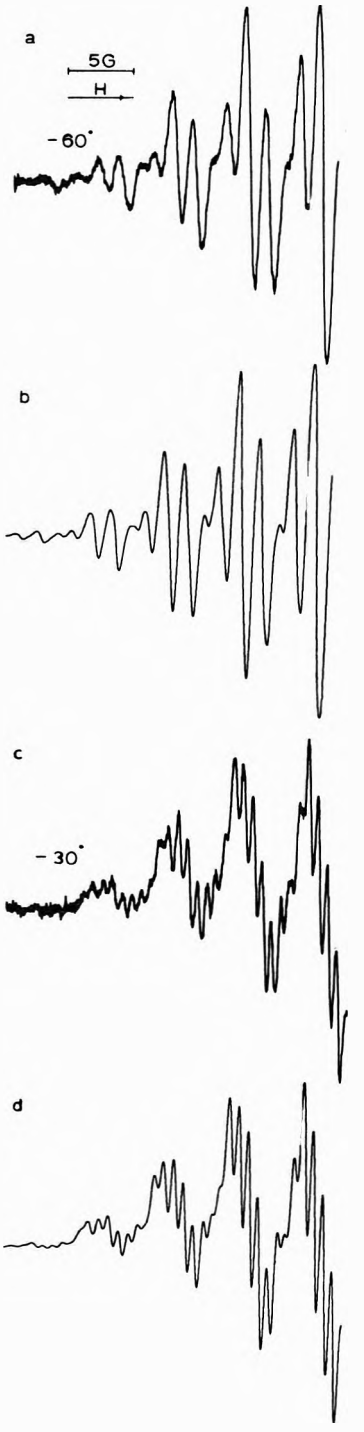

Figure 1. Esr spectra of the radical anion of I prepared using sodium and THF: (a) experimental spectrum at −60°; (b) calculated −60° spectrum using hfsc given in text and a line width of 0.500 G; (c) experimental spectrum at −30°; (d) calculated −30° spectrum using line width of 0.500 G.

equivalent and the spectra exhibited little change from −120 to −30°. Calculated and experimental spectra at −70° are shown in Figure 2.

Finally, I was reduced with potassium in DEE. Unusual spectra were obtained from −100° to room temperature having a large center peak flanked by narrower hyperfine lines. The spectra were weak but appeared to be independent of temperature. A good spectrum was obtained at room temperature and the hyperfine portion could be simulated quite well using $A_{1,4}$ = 5.00, $A_{5,8}$ = 4.45, $A_{6,7}$ =

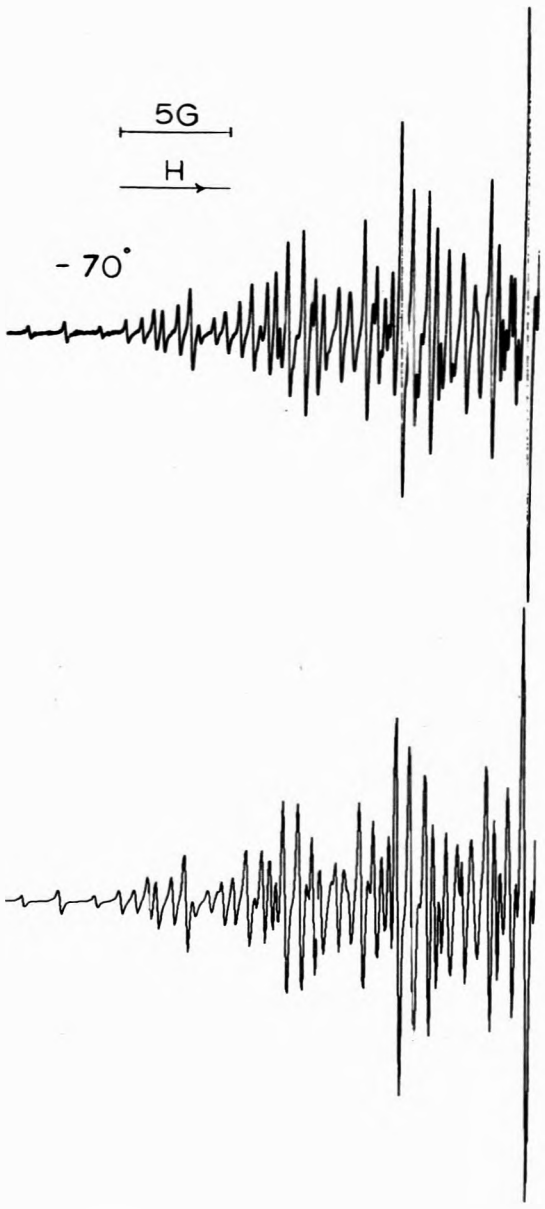

Figure 2. Esr spectrum of the radical anion of I prepared using potassium and THF: upper, experimental spectrum at −70°; lower, calculated −70° spectrum using hfsc given in text and a line width of 0.125 G.

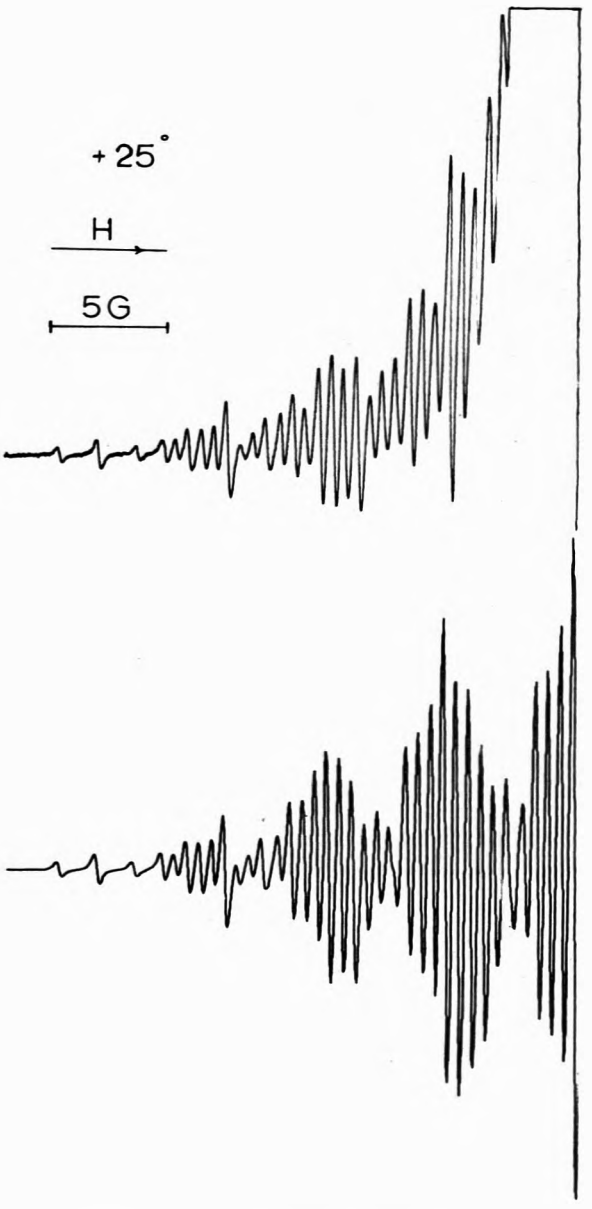

Figure 3. Esr spectrum of the radical anion of I prepared using potassium and DEE: upper, experimental spectrum at +25°; lower, calculated +25° spectrum using hfsc given in text and a line width of 0.200 G.

1.60, and A_{CH_2} = 5.50. The methylene protons appeared to be equivalent over the temperature range studied; calculated spectra using two sets of two gave poorer fits than those using one set of four. The origin of the large center peak was not determined. One possibility was that the center peak was due to solvated electrons but this was not considered likely in DEE. As the concentrations were always 5×10^{-3} M or less, a rapid electron exchange process between anion or anions and the neutral species seemingly can be ruled out. One possible explanation is that it arises from a decomposition product. It is interesting to note that upon reduction with sodium in DEE the large center peak was not observed, so the solvent does not appear to be the determining factor. The calculated and experimental spectra for +25° are shown in Figure 3.

Other Attempted Reductions. It was suggested that ion-pair formation and thus the probability of making the methylenes nonequivalent would be most favored using lithium and THF.[8] Reduction of I under these conditions was very slow. The spectra obtained consisted of one broad line which could not be resolved. Finally, I was added to lithium in 2-methyltetrahydrofuran (MTHF), but no color change was observed and as far as we could tell no reduction of I occurred.

Discussion of Results

The results for this ion-pairing study of I are given in Table I. The values for the hfsc are considered good to ±0.05 G. The temperatures are good to ±0.1°. The table shows that reduction with potassium in DME or DME-HMPA and sodium in DME produced the free ion, with ion pairing being negligible. However, in sodium and THF or DEE ion pairs were formed, as evidenced by the metal splittings. The perturbations of the hfsc (compared to the free ion case) for potassium in THF and DEE may also be

TABLE I: Hfsc Obtained for I Using Various Conditions of Metal and Solvent

Solvent	Metal	$A_{1,4}$	$A_{5,8}$	$A_{6,7}$	A_{CH_2}	A_M	Temp, °C
DME	K	5.40	4.20	1.58	5.85		−50 to +25
DME–HMPA	K	5.40	4.20	1.60	5.82		−88 to 0
DME	Na	5.40	4.20	1.60	5.80		−80 to −20
THF	K	5.10	4.40	1.65	5.70		−120 to −30
THF	Na	5.35	4.23	1.60	5.80		−100 to −50
		5.10	4.20	1.55	5.75	0.75	−30
		5.00	4.00	1.50	5.50	1.10	+25
DEE	K	5.00	4.45	1.60	5.50		+25
DEE	Na	5.50	4.35	1.65	5.80	0.20	−120
		5.47	4.30	1.62	5.72	0.25	−100

attributed to ion pairing, though metal splittings were not observed for these reductions. However, the methylenes remained equivalent and alternating line widths were not observed for any of the reduction conditions shown in Table I. This observation was quite unexpected as formally I is very similar to acenaphthene and pyracene. In all these molecules the methylene protons are situated about the same distance from the center of the 9–10 bond. There are three possible explanations for this observation. First, under all the conditions studied, we could have been in a region of fast exchange. A second possibility is that the metal ion is located in the plane of the NBCB molecule in a symmetrical position with respect to the methylene protons either close to the methylene protons or close to atoms 6 and 7. A third possibility is that the metal ion is above the π cloud but for steric reasons is located over the ring involving atoms 5–10. We tend to rule out the second view. This stems partially from our work with benzocyclobutene[6] but also from the finding that the metal ion is located above the plane in the case of pyracene.[9] Also calculations on acenaphthene radical anion ion pair indicated that the preferred positions of the metal cation would be above the 9–10 bond.[5] This was also predicted for naphthalene by Goldberg and Bolton.[3a] We also feel that the third possibility is unlikely for the following reasons. Reduction of I under a variety of conditions which surely yielded a variety of ion pairs showed negligible temperature dependency of the aromatic hfsc. It would seem that this could be explained in one of two ways. One possibility is that the cation is not fixed in a potential well over either ring and is jumping rapidly back and forth. Thus the observed hfsc are a weighted time average of a large number of possible values. The second possibility is that the solvated cation is in a single potential well over the ring involving atoms 5–10 due to steric repulsion of the methylene groups attached to positions 2 and 3.[10] We feel that the second explanation is not likely. First of all, the methylene groups attached to the 2 and 3 position are sterically about the smallest alkyl substituent one can attach to the naphthalene ring system. Far larger substituents have been placed on the naphthalene system and these have not prevented tight ion pairs from forming with large metal hfsc. For example, the 2,6-di-*tert*-butylnaphthalenide system shows a large sodium hyperfine splitting in MTHF.[3c] Thus even with a large *tert*-butyl group on each ring tight ion pairs can be formed. Finally, the reduction of 2,3-dimethylnaphthalene in DME with potassium shows a very large temperature dependence of the aromatic hfsc in contrast to I.[7] Sterically two methyl groups are larger than the fused four-membered ring and now the potential wells over each ring appear to be different in energy or else now the cation is essentially over the ring involving atoms 5–10 and it is in equilibrium with a loose ion pair or the free ion.

From these observations, it would appear that in I the cation is rapidly jumping back and forth from over one ring to over the other on one side of the molecule. If this is so, it would seem that the only logical explanation for the equivalency of the methylene protons is that we are also in a region of fast exchange for the movement of the cation from one side of the naphthalene molecule to the other side. The reason for the lower barrier of interconversion of the two ion pairs of I compared to pyracene or acenaphthene is not readily apparent. It is interesting to note, however, that any interconversion process that can be described as resulting from rotation about the long axis of I relative to the metal cation should be more facile than for either pyracene or acenaphthene due to the positioning of the alkyl substituents.

One other interesting observation pointed out by Goldberg[11] is that the sodium splitting in DEE is about 0.2 G at −120° while for naphthalene radical anion it is 0.80 G. In THF, both I and naphthalene have a metal splitting of about 1.0 G. This would suggest that the methylene protons do affect the potential well over the substituted ring. In the case of the tighter ion pair (DEE) at low temperatures, the sodium ion may be spending more time over the 9–10 bond which has low spin density. This could be a result of the potential well over the substituted ring being displaced toward the unsubstituted ring due to steric interaction with the methylene protons.

In order to gain some additional evidence on this point, HMO calculations were carried out. The effect of the metal cation was taken into account by making those positions near the cation more electronegative. HMO calculations employing different coulomb integral variations were run for three possible ion pairs: the cation above the 9–10 bond, near the 6–7 bond, and above the center of the ring containing carbon atoms 5 through 10. The calculations indicated that the best correlation was obtained when the cation was located over the center of the ring farthest from the ethylene bridge. This configuration was calculated by making the coulomb integrals for carbons 5 through 10 more electronegative by $-0.05|\beta_0|$ ($h_{5,10} = -0.05$) and using the coulomb integrals for carbons 1 through 4 which gave the best fits for the free ion case ($h_{1,4} = -0.2$, $h_{2,3} = 0.1$). The calculated hfsc were $A_{1,4} = 5.00$, $A_{5,8} = 4.37$, $A_{6,7} = 1.72$, and $A_{CH_2} = 4.54$. Inspection of Table I shows that these values agree quite well with the trends observed for NBCB as ion pairing increased.

Experimental Section

Usual high-vacuum techniques using alkali metals and ethereal solvents were employed to prepare the radical anions studied. The initial hydrocarbon concentration was approximately 5×10^{-3} *M*. Dimethoxyethane (Aldrich), tetrahydrofuran (MCB), and diethyl ether (Allied) were dried by several distillations from lithium aluminum hy-

dride (Alfa), degassed on the vacuum line using the freeze–pump–thaw technique, and distilled under vacuum to solvent bumpers containing sodium–potassium alloy (Unified Science Associates). Hexamethylphosphoramide (Aldrich) was dried by several vacuum distillations from Linde 13X molecular sieves (Union Carbide) followed by degassings on the vacuum line prior to use.

Epr spectra were recorded on a Varian E-3 spectrometer with X-band frequencies and an E-3 variable temperature accessory. Temperatures were checked using a Honeywell Model 2746 potentiometer and copper–constantan thermocouple, and are considered good to at least ±2°. Gas chromatographic analyses were performed on a Hewlett-Packard 5750 research chromatograph using an 8 ft × 1.4 in. column of 10% SE-30 on Chromosorb P. Computer simulations of theoretical esr spectra were done using a Fortran Version IV program for mixtures employing Lorentzian line shapes written by Griffin.[12] Melting points were taken on a Fisher–Johns hot-block apparatus and are uncorrected.

Naphtho[b]cyclobutene was prepared by the procedure of Cava and Shirley;[13] it was purified by gc to give mp 86.5–87.5, lit.[13] mp 86.5; mass spectrum *m/e* 154.

Acknowledgment. Helpful discussions with Ira B. Goldberg and E. de Boer are gratefully acknowledged. Financial support of this investigation by the National Science Foundation is gratefully acknowledged.

References and Notes

(1) A preliminary communication on part of this material has appeared: R. D. Rieke and S. E. Bales, *Tetrahedron Lett.*, 2439 (1972).
(2) Alfred P. Sloan Fellow, 1973–1975.
(3) (a) I. B. Goldberg and J. R. Bolton, *J. Phys. Chem.*, **74**, 1965 (1970); (b) N. M. Atherton and S. I. Weissman, *J. Amer. Chem. Soc.*, **83**, 1330 (1961); (c) N. Hirota, *J. Phys. Chem.*, **71**, 127 (1967); (d) A. Crowley, N. Hirota, and R. Kreilick, *J. Chem. Phys.*, **46**, 4815 (1967); (e) N. Hirota, *J. Amer. Chem. Soc.*, **90**, 3603 (1968); (f) B. J. McClelland, *Trans. Faraday Soc.*, **57**, 1458 (1961); *Chem. Rev.*, **64**, 301 (1964).
(4) E. de Boer and E. L. Mackor, *Proc. Chem. Soc., London*, 23 (1963); *J. Amer. Chem. Soc.*, **86**, 1513 (1964); E. de Boer, *Recl. Trav. Chim. Pays-Bas*, **84**, 609 (1965).
(5) M. Iwaizumi, M. Suzuki, T. Isobe, and H. Azumi, *Bull. Chem. Soc. Jap.*, **40**, 2754 (1967).
(6) R. D. Rieke, S. E. Bales, P. M. Hudnall, and C. F. Meares, *J. Amer. Chem. Soc.*, **93**, 697 (1971); R. D. Rieke and S. E. Bales, *Chem. Phys. Lett.*, **12**, 631 (1972).
(7) R. D. Rieke, C. F. Meares, and L. I. Rieke, *Tetrahedron Lett.*, 5275 (1968).
(8) E. de Boer, private discussion.
(9) Reference 8. See also A. H. Reddoch, *Collog. Int. Cent. Nat. Rech. Sci.*, **No. 164**, 419 (1966).
(10) One can also invoke rapid exchange with loose and free ions and not affect the argument.
(11) I. B. Goldberg, private communication.
(12) R. G. Griffin, Ph.D. Thesis, Washington University, St. Louis, Mo., 1968.
(13) M. P. Cava and R. L. Shirley, *J. Amer. Chem. Soc.*, **82**, 654 (1960).

Electrochemistry of Rhodium–Dipyridyl Complexes[1]

Gregory Kew, Keith DeArmond,* and Kenneth Hanck

Department of Chemistry, North Carolina State University, Raleigh, North Carolina 27607 *(Received August 6, 1973)*

Voltammetric data have been obtained for 2,2′-dipyridyl (dip) complexes of rhodium in acetonitrile. A reaction sequence is proposed based on analysis of electrochemical and luminescence data. For $[Rh(dip)_3]^{3+}$, the first one-electron reduction is followed by moderately fast elimination of one dip ligand. A second, apparently reversible, one-electron transfer which produces a Rh(I) species is also followed by a chemical reaction. Two more stepwise, reversible one-electron transfers yield $[Rh(dip)_2]^0$ and $[Rh(dip)_2]^-$ successively. Reactions for $[Rh(dip)_2Cl_2]^+$ exactly parallel those found for the tris dip complex except chloride is eliminated following the first electron transfer. Preparation and cyclic voltammetry of $(dipH)[Rh(dip)Cl_3(OH)]\cdot H_2O$, $[Rh(dip)_2]ClO_4\cdot 3H_2O$, and $[Rh(dip)_2Cl]_2(ClO_4)_2\cdot 4H_2O$ confirm the above sequence

Introduction

A combination of electrolysis and electron spin resonance (esr) spectroscopy was first used to study light atom π-radical systems.[2] The esr hyperfine and electrochemical data obtained can be useful in describing highest filled and lowest empty π orbitals[3] and often may be correlated with the corresponding spectral transitions.[4,5] This general method has been extended to a number of transition metal complexes involving π-type and other ligands. These include the dithiolato complexes of Ni, V, Co, and Rh,[6] the dipyridyl chelates of Cr and V,[7,8] and organometallic compounds involving the metals Mo, Mn, Fe, Co, Ni, Rh, Cr, W, and Ir bonded to π-type ligands as well as to a carbonyl carbon.[9]

Nonaqueous solvents such as acetonitrile (AN) and *N,N*-dimethylformamide (DMF) have proved superior to H_2O for stabilization of reduced species due to their lower oxidizing power and lower proton availability. Examples of this are seen in the reduction sequences of $[Cr(dip)_3]^{3+}$, $[Mn(dip)_3]^{2+}$, $[Fe(dip)_3]^{2+}$, and $[Co(dip)_3]^{2+}$ in H_2O[10] *vs.* their reduction in AN.[11,12]

Redox and kinetic properties of metal–dipyridyl complexes have been frequently studied, mostly in aqueous solution. Several general reviews are available.[13] Polarog-

raphy of Rh-amine complexes in aqueous solution has been reported by Gillard, Osborn, and Wilkinson.[14] In all cases the first reduction process involved two electrons. This was also true for reduction of $[Rh(Sacac)_3]$ in acetone,[15] the only reported nonaqueous study. Of the various Rh diimines, only the reduction of $[Rh(dip)_2Cl_2]^+$ has been attempted. This work, also by Gillard, *et al.*, in aqueous solution,[14] was inconclusive. Recently Bard, *et al.*, studied the chemiluminescence and electrochemistry of $[Ru(dip)_3]^{2+}$, isoelectronic to $[Rh(dip)_3]^{3+}$, in AN.[16]

Attempts to produce paramagnetic species from $[Rh(dip)_3]^{3+}$ and $[Rh(dip)_2Cl_2]^+$ (by electrochemical reduction in AN) stable enough to detect by esr have not been successful to date. Consequently a more general electrochemical study of the reduction sequence for these complexes was initiated.

Experimental Section

Reagents. The acetonitrile (AN) was Fisher reagent grade further purified by stirring with CaH_2 and decanting onto P_2O_5 from which it was distilled. It was refluxed over CaH_2 and redistilled discarding the first 20% and last 15–20%. *N,N*-Dimethylformamide (DMF) used was Matheson Coleman and Bell reagent grade further dried with type 4A molecular sieve for several days and redistilled at reduced pressure.[17] Tetraethylammonium perchlorate (TEAP) used as a base electrolyte was Eastman White Label further purified by three recrystallizations from distilled H_2O. It was dried in a vacuum oven at 100° overnight and stored under dry N_2. The complexes were synthesized using $RhCl_3 \cdot 3H_2O$ from Engelhard Industries and 2,2′-dipyridyl (dip) from Aldrich Chemical Co Both were used without further purification.

Synthesis. Preparation of $[Rh(dip)_3]Cl_3 \cdot 5H_2O$, $[Rh(dip)_2Cl_2]Cl \cdot 2H_2O$, $[Rh(dip)_3](ClO_4)_3 \cdot 2H_2O$, and $[Rh(dip)_2Cl_2]ClO_4$ has been described previously.[18] The complex $(dipH)[Rh(dip)Cl_3(OH)] \cdot H_2O$ was synthesized by a procedure described by Kulasingam, McWhinnie, and Miller for preparation of $(phenH)[Rh(phen)Cl_4]$.[19] The product was recrystallized from a water–acetone (1:1 by volume) mixture rather than from water due to the tendency of $(dipH)[Rh(dip)Cl_3(OH)] \cdot H_2O$ to undergo further ligand exchange in H_2O yielding $[Rh(dip)_2Cl_2]Cl \cdot 2H_2O$. $[Rh(dip)_2]ClO_4 \cdot 3H_2O$ was prepared by $NaBH_4$ reduction of $[Rh(dip)_3](ClO_4)_3 \cdot 2H_2O$ as described by Martin, McWhinnie, and Waind.[20] $[Rh(dip)_2Cl]_2(ClO_4)_2 \cdot 4H_2O$ was prepared by reduction of $[Rh(dip)_2Cl_2]ClO_4$ according to a general scheme reported by the same authors. Products were used immediately after purification and drying or were stored under dry N_2. Those previously reported were characterized by comparison with published spectra. Spectral properties of $(dipH)[Rh(dip)Cl_3(OH)] \cdot H_2O$ are to be published separately. *Anal.* (Atlantic Microlab, Inc., Atlanta, Ga.) Calcd for $(dipH)[Rh(dip)Cl_3(OH)] \cdot H_2O$: C, 43.08; N, 10.05; Cl, 19.10; H, 3.62. Found: C, 43.72; N, 9.93; Cl, 18.33; H, 3.75.

Apparatus. Optical spectra were obtained with a Cary Model 14 spectrometer (uv-visible), Perkin-Elmer Model 521 spectrometer (ir), or an Aminco-Bowman spectrophotofluorometer (uv-visible emission).

The drybox used was obtained from S. Blickman, Inc. (Model ILE with Vacuum Atmospheres Corp. Dri-Train Model He-373-BI for H_2O and O_2 removal).

Electrochemical measurements were made with a Princeton Applied Research (PAR) Model 174 polarographic analyzer, a conventional, three-electrode instrument, and a Hewlett-Packard-Moseley Model 7001A recorder. Cyclic voltammetry above 0.2 V/sec potential scan rate involved use of a triangle wave generator based on a circuit design by Bull and Bull[21] interfaced to the PAR Model 174. Rise time of the Model 174 potentiostat is not precisely known but voltammetric curves taken above 80 V/sec are slightly distorted. Since positive feedback *iR* compensation was not available, some additional distortion results from uncompensated resistance. A voltage "sweep and hold" capability was not available, consequently residual current curves for runs faster than 0.2 V/sec could not be obtained except in the case of the least cathodic reduction.

A Tektronix Model 502A oscilloscope and a Tektronix Model C-12 oscilloscope camera were used to record fast voltammograms. The electrochemical cell used was of a conventional H-type design with an isolation compartment separated from the test and reference compartments by fine porosity frits.

All data reported here were obtained at a vertical platinum wire electrode whose geometric area was 0.335 cm^2. (At various times a vertical Pt foil electrode and horizontal Pt "button" disk electrode, Beckman No. 39273, were also used. No qualitative differences in voltammetric curve shape were noted using these.)

Techniques. Platinum electrodes were cleaned between experiments with hot 15 *M* nitric acid, rinsed six times in deionized water (>5 megohm cm), and finally rinsed with electronics grade methanol. They were then "dried" in a nitrogen stream and introduced into a dry, nitrogen filled glove bag or box at least 1 hr before use. At least two preliminary, single-cycle scans were performed in the test solution at approximately 10 V/sec to condition the working electrode before recording the data. In order to assure an oxide-free platinum surface the anodic limit of each scan was equal to or less than 0.1 V *vs.* sce.

In practice both the isolation and reference compartments of the electrochemical cell described above were filled with AN 0.10 *M* in TEAP. A large diameter agar–4% KCl salt bridge extending to an sce was inserted into the reference compartment only during an individual experimental measurement. No difficutly with frit plugging due to $KClO_4$ precipitation was observed; no attempt was made to obtain an accurate estimate of liquid junction potential resulting but voltammetric peaks were reproduced within ±10 mV.

Data were obtained with the above cell assembly contained either within a drybox or in a glove bag flushed with nitrogen of less than 20 ppm total impurity content. Nitrogen used for deaerating or blanketing test solutions was passed through a bed of Ridox (room temperature O_2 removal catalyst)[22] and through a solvent saturation bubbler.

Results

All complexes were dissolved in AN 0.10 *M* in TEAP. Redox couples observed in this study are designated by increasing roman numerals, I through V, proceeding toward more negative potentials. For example, see Table I.

Cyclic voltammograms of $[Rh(dip)_3]^{3+}$ at two sweep rates at a platinum electrode are shown in Figure 1. The solution was colorless initially. While observing experiments at moderate potential scan rates (*e.g.*, 0.02–0.10 V/sec), a red-violet colored material was observed at the

TABLE I: Examples of Variation in E_{pc} and $[E_{pc} - E_{(p/2)c}]$ or $[E_{pa} - E_{pc}]$ with Change in v[a,b]

	I + II		I		II		III		IV	
v	E_{pc}	$[E_{pc} - E_{(p/2)c}]$	E_{pc}	$[E_{pa} - E_{pc}]$	E_{pc}	$[E_{pa} - E_{pc}]$	E_{pc}	$[E_{pa} - E_{pc}]$	E_{pc}	$[E_{pa} - E_{pc}]$
				A. $[Rh(dip)_3]^{3+}$, 6.02×10^{-4} M						
0.10	0.83	70					1.46	58	1.67	60
9.52			0.83		0.96		1.48	90	1.69	95
31.8			0.86	120	1.00		1.49	120	1.71	130
89.8			0.93	195	1.06		1.53	200	1.75	210
				B. $[Rh(dip)_2Cl_2]^{+}$, 5.16×10^{-4} M						
0.10	0.84	54					1.46	64	1.67	66
1.50	0.92	65								
10.5	0.97	80					1.47	80	1.68	90
32.2	1.01	130					1.49	120	1.70	130
87.1	1.05	125								

	I			II			III		
v	E_{pc}	i_{pc}	$[E_{pc} - E_{(p/2)c}]$	E_{pc}	i_{pc}	$[E_{pc} - E_{(p/2)c}]$	E_{pc}	i_{pc}	$[E_{pc} - E_{(p/2)c}]$
			C. $[Rh(dip)Cl_3(OH)]^{-}$, 1.60×10^{-4} M						
0.02	0.83	24.8	148	1.28	20.6	67			
0.10	0.83	34.4	145	1.27	35.5	66			
0.20	0.83	94.4	146	1.28	105.2	66	2.21	549	79

[a] Results for Rh(III) dip complexes in 0.10 M TEAP/AN solutions at a Pt electrode. [b] v in V/sec, E_{pc} in $-$V *vs.* sce, $[E_{pa} - E_{pc}]$ in mV, i_{pc} in μA.

electrode surface shortly after passing the potential corresponding to the least negative cathodic peak, $(E_{pc})_{I+II}$. On removing the applied potential, the colored product moved away from the electrode changing in color to a shade of yellow before diffusing into the bulk of solution. Prolonged electrolysis at potentials slightly more negative than $(E_{pc})_{I+II}$ led to a pale-yellow colored solution.

Cyclic voltammograms of $[Rh(dip)_2Cl_2]^{+}$ and $[Rh(dip)Cl_3(OH)]^{-}$ are presented in Figures 2 and 3. Note the similarity between the voltammograms for the tris and bis complexes at 0.10 V/sec scan rate. At a scan rate of 31.2 V/sec an additional wave is resolved in the vicinity of -0.8 V for $[Rh(dip)_3]^{3+}$ (Figure 1b) but not for the bis or mono dip complexes.

A red-violet colored material is also formed at the working electrode during electrolysis of $[Rh(dip)_2Cl_2]^{+}$. The sequence of events for the red-violet product parallels that seen in the $[Rh(dip)_3]^{3+}$ solutions except the color change from red-violet to yellow is not clearly observed since the bis complex solution is initially a pale yellow.

$(dipH)[Rh(dip)Cl_3(OH)]\cdot H_2O$ dissolves in acetonitrile to form a pale, dull orange-colored solution. No color change is seen at the electrode-solution interface on electrolysis. In addition to the waves shown in Figures 1–3, another is found peaking at approximately -2.20 V *vs.* sce for all three complexes. This wave is much larger for $[Rh(dip)_3]^{3-}$ than for $[Rh(dip)_2Cl_2]^{+}$ or $[Rh(dip)Cl_3(OH)]^{-}$ and arises from reduction of uncomplexed 2,2′-dipyridyl. An irreversible wave may also be seen at approximately +1.4 V in solutions where the counterion is chloride. This wave is due to oxidation of chloride.[16]

Figure 4 shows cyclic voltammograms of $[Rh(dip)_3]^{3+}$ in which the potential scan was reversed shortly after $(E_{pc})_I$ to check for reoxidation of the reduction products. No similar oxidation wave was observed for the other two complexes. Data derived from voltammograms of the tris, bis, and mono dip Rh(III) complexes are found in Table I.

Figure 5 shows a cyclic voltammogram of $[Rh(dip)_2]^{+}$. The waves in the region from -1.3 to -1.7 V for this complex are identical to those in the same region for

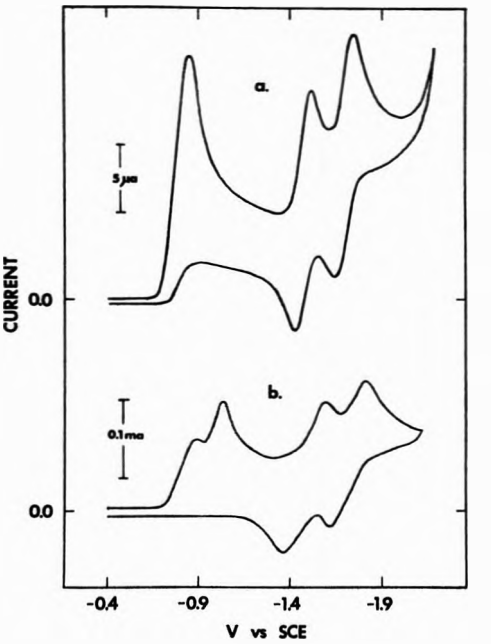

Figure 1. Cyclic voltammograms of $[Rh(dip)_3]^{3+}$, 1.08×10^{-4} *M*: (a) $v = 0.10$ V/sec; (b) $v = 31.2$ V/sec.

$[Rh(dip)_3]^{3+}$ and $[Rh(dip)_2Cl_2]^{+}$ indicating $[Rh(dip)_2]^{+}$ is also the species present at these potentials when one starts with the Rh(III) tris and bis complexes.

$[Rh(dip)_2]ClO_4\cdot 3H_2O$ is prepared by reduction of $[Rh(dip)_3](ClO_4)_3\cdot 2H_2O$ suspended in water.[20] Addition of $NaBH_4$ produces an immediate color change and a deep red-violet solid settles out. This dried material dissolves slowly when added to AN-containing 0.10 *M* TEAP. Solution within 1–2 mm of the undissolved crystals on the bottom of the container is purple-tinted but changes to yellow as it diffuses away. Final color of the solution is a rich golden yellow, markedly darker than the pale yellow hue characteristic of $[Rh(dip)_2Cl_2]^{+}$. The color difference does not seem to be due to concentration differences alone

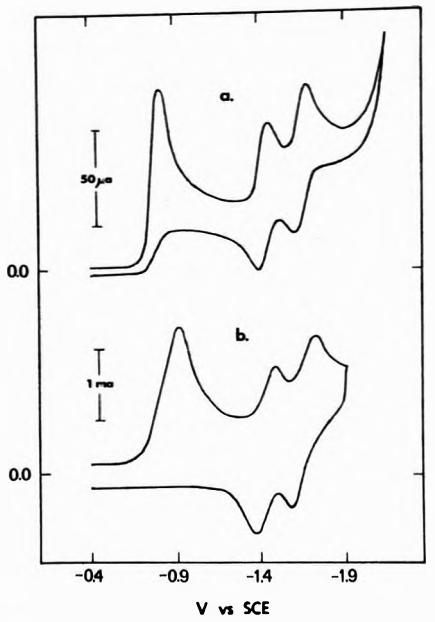

Figure 2. Cyclic voltammograms of $[Rh(dip)_2Cl_2]^+$, 5.16 × 10^{-4} *M*: (a) v = 0.10 V/sec; (b) v = 32.2 V/sec.

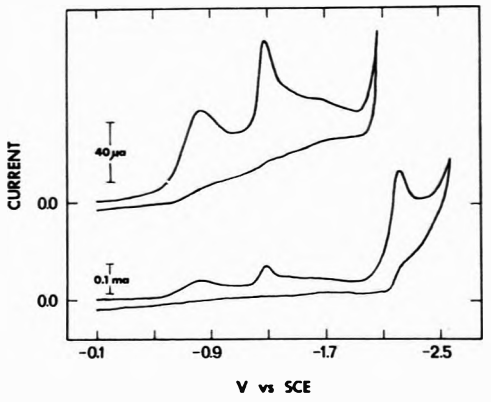

Figure 3. Cyclic voltammograms of $[Rh(dip)Cl_3(OH)]^-$, 1.60 × 10^{-4} *M*: v = 0.10 V/sec.

since the solubility limit of both complexes is similar (below 10^{-3} *M*).

Figure 6 is the cyclic voltammogram of $[Rh(dip)_2Cl]_2^{2+}$ obtained by chemical reduction of $[Rh(dip)_2Cl_2]ClO_4$. On dissolving the solid in AN, red-violet solution is observed in the vicinity of remaining undissolved crystals. The coloration persists considerably longer in this case, until the solution diffuses at least 1 cm away from the crystals, but the final color of the solution is yellow, intermediate in shade between that observed for $[Rh(dip)_2]^+$ and that for $[Rh(dip)_2Cl_2]^+$.

No red-violet material was visible at the working electrode during voltammetry of $[Rh(dip)_2]^+$ while some was observed during voltammetry of $[Rh(dip)_2Cl]_2^{2+}$. In both cases the bulk of solution was a shade of yellow before, during, and after electrolysis. Data obtained from voltammograms of $[Rh(dip)_2]^+$ and $[Rh(dip)_2Cl]_2^{2+}$ may be found in Table II.

No change was observed in the voltammetric peaks associated with any of these complex ions when free 2,2′-dipyridyl was added, within experimental error. A trend suggesting concentration dependence in rate at which $(E_{pc})_I$ and $(E_{pc})_{II}$ shifted with changing scan rate was noted[23] but could not be more closely characterized due to low solubility of the complexes and the estimated experimental error in potential measurement.

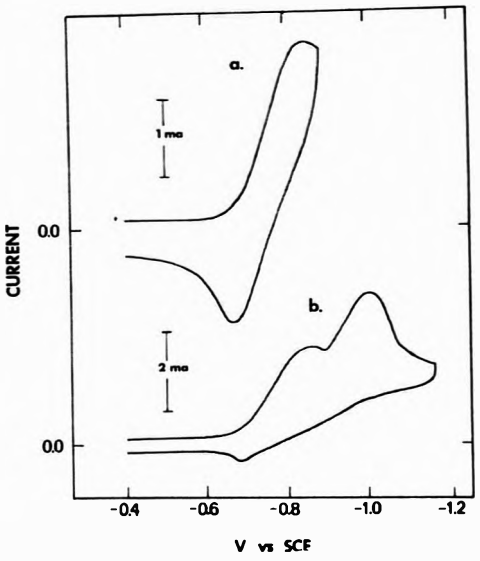

Figure 4. Cyclic voltammograms of $[Rh(dip)_3]^{3+}$, 1.08 × 10^{-4} *M*: (a) v = 46.1 V/sec; (b) v = 46.3 V/sec.

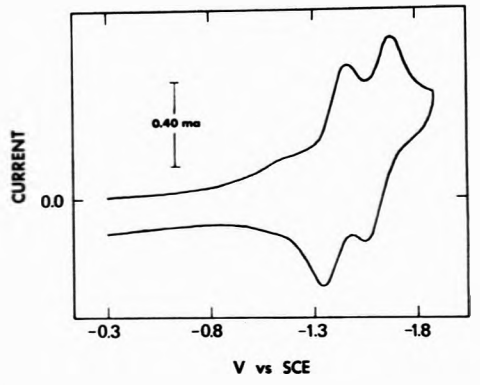

Figure 5. Cyclic voltammograms of $[Rh(dip)_2]^+$, 5.15 × 10^{-4} *M*: v = 9.65 V/sec.

TABLE II: Examples of Variation in E_{pc} and $[E_{pc} - E_{(p/2)c}]$ or $[E_{pa} - E_{pc}]$ with v[a,b]

	I + II		III		IV	
v	E_{pc}	$[E_{pc} - E_{(p/2)c}]$	E_{pc}	$[E_{pa} - E_{pc}]$	E_{pc}	$[E_{pa} - E_{pc}]$
	A. $[Rh(dip)_2Cl]_2^{2+}$, 6.50 × 10^{-4} *M*					
0.10	0.83	55	1.46		1.66	
1.72	0.90	60	1.49	120	1.68	110
9.56	1.00	70	1.52	180	1.70	150
32.0	1.03	90	1.57	280	1.74	240
91.8	1.06					
	B. $[Rh(dip)_2]^+$, 5.15 × 10^{-4} *M*					
0.10			1.46	60	1.67	70
9.64			1.49	110	1.69	110
32.4			1.51	160	1.72	170
91.7			1.56	250	1.76	250

[a] Results for Rh(I) and Rh(II) dip complexes in 0.10 *M* TEAP/AN solutions at a Pt electrode. [b] E_{pc} in −V *vs.* sce, $[E_{pc} - E_{(p/2)c}]$ and $[E_{pa} - E_{pc}]$ in mV.

Discussion

Electron Transfer Sequence. Reduction sequences are proposed (Figure 7) which are consistent with the voltam-

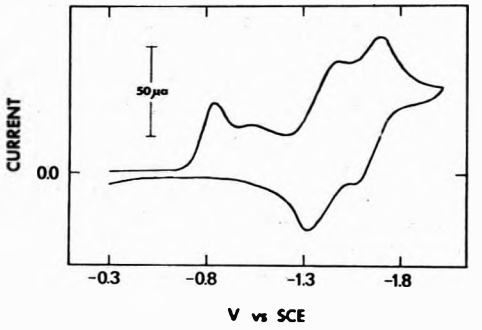

Figure 6. Cyclic voltammograms of $[Rh(dip)_2Cl]_2^{2+}$, 6.50×10^{-4} *M*: $v = 1.72$ V/sec.

metric results obtained for $[Rh(dip)_3]^{3+}$, $[Rh(dip)_2Cl_2]^+$, $[Rh(dip)_2Cl]_2^{2+}$, and $[Rh(dip)_2]^+$. Comparison of the first two steps for the Rh(III) species is particularly important.

Waves I and II. a. General. The single large wave observed at $(E_{pc}) = -0.83$ V *vs.* sce for a $[Rh(dip)_3]^{3+}$ solution scanned at 0.10 V/sec is in fact a composite wave (Figure 1). The resolution of a second wave at higher sweep rates clearly establishes that it results from more than one discrete electron transfer process. Unless the potential scan is reversed shortly after passing $(E_{pc})_I$ (Figure 4a), no corresponding oxidation wave is observed (*e.g.*, Figure 1b). Presence of oxidation wave I indicates that a moderately fast chemical reaction is interposed between the first electron transfer and the second electron transfer. The voltammogram in Figure 4b shows potential scan reversal after passing $(E_{pc})_{II}$. That portion of the second reduction wave which is visible has a slope identical with the slope of the first wave suggesting that the second electron transfer process itself may be fast enough to produce a corresponding oxidation wave if not followed by a very fast chemical reaction. The chemical reaction following reduction wave II seems considerably faster than the one which follows reduction wave I since no oxidation wave II may be observed at the maximum scan rate of our instrumentation.

Theory for a variety of ECE mechanisms has been worked out by Nicholson and Shain.[24] For an ECE mechanism with both electron transfers reversible, the flux of reactants for the two separate electron transfers are independent for any conceivable type of intervening chemical reaction, *i.e.*, $(i)_{a+b} = (i)_a + (i)_b$. Plots of E *vs.* log $[i/(i_d - i)]$ from dc polarographic data indicate $n = 1.00 \pm 0.05$ for the composite wave as do values of $[E_{pc} - E_{(p/2)c}]$ from stationary electrode voltammograms at scan rates <0.5 V/sec (for solution concentrations $>5 \times 10^{-4}$ *M*). This suggests that the difference in E° between the two charge transfers, $\Delta E^\circ \equiv (E_{II}^\circ - E_I^\circ)$, must be small but negative. If instead $\Delta E^\circ > 0$, the slope and/or $[E_{pc} - E_{(p/2)c}]$ for the composite wave should approach that expected for a reversible two electron transfer process. If ΔE° were $\ll 0$, two reduction waves should be observed, even at slow sweep rates.

Voltammetric peak potential shifts of reduction waves I and II appear due to kinetic influence from the following chemical reactions and the effect of uncompensated resistance.

The fact that an oxidation peak may be observed associated with redox couple I and the lack of a similar peak for couple II supports the view that $(k_f)_{II} \gg (k_f)_I$. Influence of the "kinetic parameter," k_f/a, on the shape of a voltammetric curve for an EC mechanism has been explored.[25] ($k_f/a = (k_f RT)/(nFv)$, since $a \equiv (nFv)/(RT)$.) If scan rate, v, increases, k_f/a decreases, producing a cathodic shift. Extended to the present situation, if $(k_f)_{II} \gg (k_f)_I$, as v increases, the absolute value of $(k_f)_{II}/a$ decreases more rapidly than does $(k_f)_I/a$. Thus the difference in reaction rates could cause reduction wave II to shift further cathodically than does reduction wave I for a given increase in scan rate. Consequently the composite wave may be resolved into two waves.

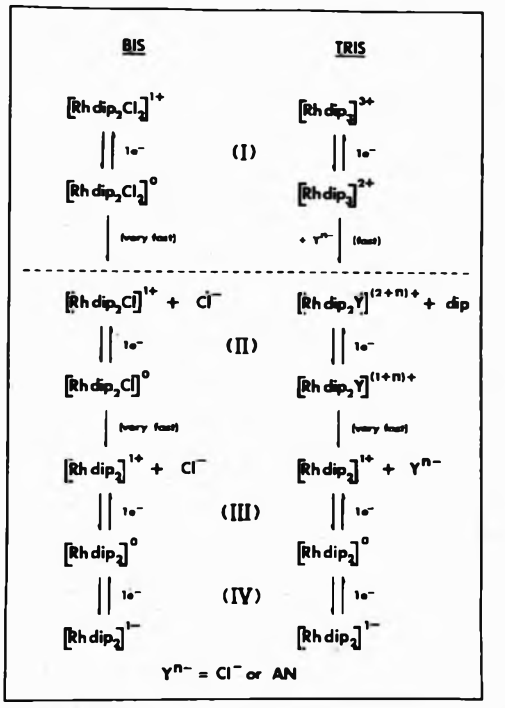

Figure 7. Proposed reaction sequence for tris and bis dip rhodium complexes.[29]

In the limit of very large k_f for a following chemical reaction, a reduction peak undergoes a cathodic shift of $30/n$ mV per decade increase in potential scan rate, according to theory.[25] However, in the present case (Table I.A) a threefold increase in scan rate, from 9.52 to 31.8 V/sec, apparently results in a shift of 30 mV for wave I while wave II shifts by 40 mV. Increasing the scan rate from 31.8 to 89.8 V/sec results in an additional 60-mV cathodic shift for both waves. (Experimental error in each voltammetric peak measurement is estimated as ±3–4 mV from scan to scan on the same sample, so shift measurements could involve a maximum of ±8-mV error.)

A portion of the potential shift for both reduction waves I and II is due to uncompensated solution resistance. Separation of uncompensated iR effects from heterogeneous electron transfer effects is often difficult or impossible.[26] However if neglegible charge transfer effects are assumed, then shifts observed for waves III and IV can be used to estimate the uncompensated resistance since these waves have no chemical complications. An average value of 18 ohms is found to account for observed variations from theory.

As scan rate is increased from 9.52 to 31.8 V/sec, reduction wave I shifts 30 mV, wave II shifts 40 mV, wave III shifts 15 mV, and wave IV shifts 18 mV. On going from 31.8 to 89.8 V/sec reduction waves I and II shift 60 mV while waves III and IV shift 40 mV. In systems involving several successive electron transfers the effect of uncom-

pensated resistance should increase progressively from the most anodic to the most cathodic peak. This establishes a practical upper bound to the amount of shift attributable to iR effects. The maximum amount would thus appear to be 10–15 mV of the shifts observed between 9.52 and 31.8 V/sec and 30–40 mV of the shifts seen between 31.8 and 89.8 V/sec. Consequently while iR effects cannot account for the "resolution" of waves I and II, a significant contribution is apparent at scan rates high enough to resolve them.

An additional factor which might contribute to peak shifts such as those seen for reduction waves I and II is a difference in heterogeneous rate constant for electron transfer to the two different species involved. Such an effect is not observable in the present case however since, within experimental error, the potential difference between $(E_{pc})_I$ and $(E_{pc})_{II}$ remains constant as scan rate is increased from 9.52 to 89.8 V/sec.

b. n Values. Using dc polarography it was found that the diffusion current for the most positive reduction wave, $(i_d)_{I+II}$, of the Rh(III) tris and bis dip complexes was twice the magnitude of $(i_d)_{III}$ or of $(i_d)_{IV}$. $((i_d)_{I+II}/(i_d)_{III} = (i_d)_{I+II}/(i_d)_{IV} = 2.00 \pm 0.05.)$

At a scan rate of 0.10 V/sec, using cyclic voltammetry at a platinum electrode, the ratio $(i_{pc})_{I+II}/(i_{pc})_{III} = 2.00 \pm 0.08$ for $[Rh(dip)_2Cl_2]^+$ solutions while for $[Rh(dip)_3]^{3+}$ solutions of approximately the same concentration ($\sim 5 \times 10^{-4}$ M) $(i_{pc})_{I+II}/(i_{pc})_{III} = 1.80 \pm 0.05$. The difference in $(i_{pc})_{I+II}/(i_{pc})_{III}$ between $[Rh(dip)_2Cl_2]^+$ and $[Rh(dip)_3]^{3+}$ suggests that the increase in sweep rate from 0.0033 to 0.10 V/sec results in a more negative $\Delta E^{\circ\prime}$, ($\equiv [E_I^{\circ\prime} - E_I^{\circ\prime}]$) for $[Rh(dip)_3]^{3+}$ so that reduction waves I and II overlap less exactly and lead to a diminished value of $(i_{pc})_{I+II}$. Values of $[E_{pa} - E_{pc}]$ and $[i_{pa}/i_{pc}]$ derived from the same cyclic voltammograms indicated that redox couples III and IV were unequivocally one electron and reversible.

As an independent check of overall n value for the composite waves at 0.10 V/sec, a comparison was made between $(i_{pc})_{I+II}$ for known solutions of $[Rh(dip)_3]^{3-}$ and $[Rh(dip)_2Cl_2]^+$ and (i_{pc}) for a chemically similar but well-characterized standard. The standard chosen was $[Ru(dip)_3]Cl_2 \cdot 5H_2O$ for which it was known that the least negative reduction was a reversible, one-electron transfer.[16] For $[Rh(dip)_3]^{3+}$ solutions, $(i_{pc})_{I+II}/(i_{pc})_{I(Ru)} = 1.83 \pm 0.04$ while for $[Rh(dip)_2Cl_2]^+$ the ratio equalled 2.03 ± 0.05.

The entire reaction sequence for $[Rh(dip)_2Cl_2]^+$ through the second electron transfer process must closely parallel that for $[Rh(dip)_3]^{3+}$. Only if at least an ECE mechanism is also present for $[Rh(dip)_2Cl_2]^+$ with ΔE° somewhat less than zero, can we account for the apparent additivity of current at both dc polarographic and moderate solid-electrode voltammetric scan rates. Again, if ΔE° were >0, it would be expected that $(i_{pc})_{I+II}/(i_{pc})_{I(Ru)} = (2)^{3/2} = 2.82$ since the governing equation for stationary electrode voltammetry shows $i_p \propto n^{3/2}$.

c. Products. At 0.10 V/sec, $(E_{pc})_{I+II} = -0.83$ V for both $[Rh(dip)_2Cl_2]^+$ and $[Rh(dip)_3]^{3+}$, as noted in Tables I and II. Since an ECEC process must be operative, the fact that no additional wave may be resolved for $[Rh(dip)_2Cl_2]^+$ by increasing potential scan rate or by a combination of increased scan rate and potential scan reversal shortly after $(E_{pc})_{I+II}$ may indicate that $(k_f)_I$ for $[Rh(dip)_2Cl_2]^+$ is larger than $(k_f)_I$ for $[Rh(dip)_3]^{3+}$. It definitely suggests that $(k_f)_I$ and $(k_f)_{II}$ for $[Rh(dip)_2Cl_2]^+$ are closer in magnitude than are the same two values for $[Rh(dip)_3]^{3+}$.

At scan rates above 0.10 V/sec, $(E_{pc})_{I+II}$ for $[Rh(dip)_2Cl_2]^+$ shifts cathodically with an increase in scan rate at the same rate observed for $(E_{pc})_{II}$ for $[Rh(dip)_3]^{3+}$. This does not exclude the possibility that the $(k_f)_{II}$'s are similar, nor the possibility that the two species involved in the second electron transfer processes may be similar (Figure 7).

Dc polarographic data offer a clue to the differences in rate of the chemical reaction following reduction wave I for $[Rh(dip)_3]^{3+}$ and $[Rh(dip)_2Cl_2]^+$. Reduction wave V, associated with reduction of free 2,2′-dipyridyl, $(E_{1/2})_V = -2.17$ V *vs.* sce, showed a diffusion current equivalent to $n = 2.18$ for $[Rh(dip)_3]^{3+}$ solutions while in $[Rh(dip)_2Cl_2]^+$ solutions $(i_d)_V$ implied $n = 0.18$.

To further confirm the liberation of 2,2′-dipyridyl at potentials in the vicinity of the composite wave, controlled potential electrolysis was performed on a solution initially containing only $[Rh(dip)_3]Cl_3$. After electrolysis at 0.15 V more negative than $(E_{pc})_{I+II}$, a luminescence spectrum of the resulting solution indicated the presence of $[Rh(dip)_3]^{3+}$, $[Rh(dip)_2Cl_2]^+$, and of free 2,2′-dipyridyl.

Summarizing, polarographic results indicate that a chemical reaction liberating 2,2′-dipyridyl is involved in or after the electron transfer indicated by wave (I + II) for $[Rh(dip)_3]^{3+}$ but not for $[Rh(dip)_2Cl_2]^+$. Luminescence spectra confirm the presence of free 2,2′-dipyridyl in electrolyzed $[Rh(dip)_3]^{3+}$ solutions.

It is reasonable to conclude that the moderately fast irreversible chemical reaction following reduction wave I in $[Rh(dip)_3]^{3+}$ is ligand exchange eliminating 2,2′-dipyridyl. This is consistent with "chemical intuition" since exchange of a bidentate dip for a solvent molecule would proceed at a slower rate than monodentate ligand loss. Consequently, exchange involving dip should be easier to "outrun" by an increase in potential scan rate.

Starting with a solution of $[Rh(dip)_2Cl_2]^+$, if the first very fast following reaction is chloride elimination, the $[Rh(dip)_2Cl]^+$ which results is quite similar in geometry and expected reactivity to the product obtained from

$$[Rh(dip)_3]^{3+} + AN + 1e^- \longrightarrow [Rh(dip)_2(AN)]^{2+} + dip$$

The species $[Rh(dip)_2]^+$ accounts for redox couples found at potentials more negative than the composite wave. Therefore the second electron transfer and the very fast irreversible following reaction for $[Rh(dip)_3]^{3+}$ and $[Rh(dip)_2Cl_2]^+$ starting materials are, respectively

$$[Rh(dip)_2(AN)]^{2+} + 1e^- \rightleftharpoons [Rh(dip)_2(AN)]^+ \longrightarrow [Rh(dip)_2]^+ + AN$$

and

$$[Rh(dip)_2Cl]^+ + 1e^- \rightleftharpoons [Rh(dip)_2Cl]^0 \longrightarrow [Rh(dip)_2]^+ + Cl^-$$

Waves III and IV. Examination of voltammograms of $[Rh(dip)_2]^+$ at 0.10 V/sec reveals that $[E_{pa} - E_{pc}]_{III} = 60$ mV and $[E_{pa} - E_{pc}]_{IV} = 70$ mV. Both charge transfers appear reversible, one electron, and without chemical complication. Comparison of Figure 5 with Figures 1 and 2 indicates a one-to-one correspondence to both in the region from −1.3 to −1.8 V. This then establishes the waves as due to the reactions

$$[Rh(dip)_2]^+ + 1e^- \rightleftharpoons [Rh(dip)_2]^0 \quad \text{(redox couple III)}$$

$$[Rh(dip)_2]^0 + 1e^- \rightleftharpoons [Rh(dip)_2]^- \quad \text{(redox couple IV)}$$

As in dc polarography, waves at more negative potential are associated with reduction of free 2,2′-dipyridyl.

The voltammograms obtained when isolated $[Rh(dip)_2Cl]_2(ClO_4)_2 \cdot 2H_2O$ was dissolved in AN were exactly what would be expected for an equimolar mixture of $[Rh(dip)_2Cl_2]^+$ and $[Rh(dip)_2]^+$. Instead of the general 2:1:1 ratio between peak current for the composite, third and fourth waves observed for Rh(III) starting materials, a 1:1:1 ratio was found. Martin, *et al.*, who originally isolated this complex, indicated that it appeared to disproportionate when redissolved[20] (original preparation involved sodium amalgam reduction of an aqueous suspension). The data above thus appear to support their hypothesis.

While the reduction sequence adduced for the bis and tris dip Rh complexes explains all observed electrochemistry, efforts continue to further characterize intermediate products by electron spin resonance and optical spectroscopy.

Electron Transfer Sequence for (dipH)[Rh(dip)Cl$_3$(OH)]·H$_2$O. Figure 3 indicates that the reduction sequence of $(dipH)[Rh(dip)Cl_3(OH)] \cdot H_2O$ is quite different from those for the bis and tris complexes. The following reactions are proposed for the mono complex

$$[Rh(dip)Cl_3(OH)]^- + 1e^- \longrightarrow \begin{Bmatrix} [Rh(dip)Cl_2(OH)]^- + Cl^- \\ \text{or} \\ [Rh(dip)Cl_3(OH)]^{2-} \end{Bmatrix}$$

$$\begin{Bmatrix} [Rh(dip)Cl_2(OH)]^- + AN \\ \text{or} \\ [Rh(dip)Cl_3(OH)]^{2-} \end{Bmatrix} +$$

$$1e^- = \begin{Bmatrix} [RhCl_2(OH)(AN)]^{2-} \\ \text{or} \\ [RhCl_3(OH)]^{3-} \end{Bmatrix} + dip$$

At all scan rates reported (Table I) $(E_{pc})_I = -0.83$ V and $(E_{pc})_{II} = -1.28$ V. The third wave was not examined at 0.02 V/sec but at 0.20 V/sec $(E_{pc})_{III} = -2.21$ V. The invariance of $[E_{pc} - E_{(p/2)c}]_I$ with an order of magnitude change in scan rate is curious since the electron transfer appears irreversible even at the lower rate, but may lend additional significance to $(E_{pc})_I = -0.83$ V which is also invariant. From the invariance of $(E_{pc})_{II}$ and $[E_{pc} - E_{(p/2)c}]_{II}$ this process can be specified as a reversible, one-electron transfer followed by a fast irreversible chemical reaction. It may be inferred from $(i_{pc})_I/(i_{pc})_{II} = 0.90$ at $\nu = 0.20$ V/sec that the first electron transfer process involves approximately one electron overall. Also, $(i_{pc})_{III}/(i_{pc})_{II} = 5.23$, if $(i_{pc})_{II}$ implies one electron. Recalling that the cation was $(dipH)^+$, a plausible reaction accounting for $n = 5$ is

$$dip + (dipH)^+ + 5e^- \rightarrow 2dip^{2-} + \tfrac{1}{2}H_2$$

The most likely impurity in $(dipH)[Rh(dip)Cl_3(OH)] \cdot H_2O$ is $[Rh(dip)_2Cl_2]Cl \cdot 2H_2O$ which forms readily if heating is attempted during recrystallization from H_2O–acetone. However, any voltammetric peaks attributable to $[Rh(dip)_2Cl_2]^+$ are easily distinguished. In Figure 3b the irreversible wave peaking in the vicinity of −0.83 V *vs.* sce could be due to bis impurity but absence of the third and fourth reduction waves, and the corresponding oxidation waves, is good evidence that the amount of bis present is small and that the irreversible wave (electrochemically and chemically) with $(E_{pc}) = -0.83$ V is characteristic of $[Rh(dip)Cl_3(OH)]^-$.

Redox Orbitals. Rh(III) Complexes. On a platinum surface at scan rates below 0.10 V/sec, no significant difference is observed between the composite wave $E_{1/2}$ values of $[Rh(dip)_3]^{3+}$ and $[Rh(dip)_2Cl_2]^+$. For $[Rh(dip)Cl_3(OH)]^-$ the electron transfer is irreversible making accurate estimate of $E_{1/2}$ impossible so the only meaningful comparison available between all three complexes is between $(E_{pc})_I$ for $[Rh(dip)Cl_3(OH)]^-$ and $(E_{pc})_{I+II}$ for the bis and tris complex ions.

Extensive interaction is expected between bidentate π ligands of a tris complex when substantial π-type bonding to the central metal ion is possible. Since the same degree of interaction, hence same π^* orbital energy, cannot be expected for another complex containing fewer π ligands, a difference in (E_{pc}) is expected for the mono, bis, and tris complexes of this study.

For the tris complex the first electron is expected to add to a π^*-antibonding orbital in which contribution of the dip ring systems predominate. The first electron transferred to a bis moiety could enter either a predominantly π^*-antibonding orbital or possibly a molecular orbital localized on the Rh(III) ion in which d orbital contributions predominate. For the mono complex generally similar alternatives exist except that the orbital in which π character from the dip ring dominates is expected to contain a higher percentage of d orbital character. This difference in orbital character is supported by luminescence spectral data for the tris and bis complexes which indicate that the lowest excited state for $[Rh(dip)_3]^{3+}$ is a ligand π-type state while that for the bis complex indicates a localized d orbital as the lowest excited state.[18]

However, all three Rh(III) dip complexes undergo a first or first composite reduction process showing the same (E_{pc})! One possible explanation is that the redox orbital in each case contains contributions from only *one* dip ring system, *i.e.*, the degree of interaction between dip ring systems in the tris complex is substantially *smaller* than expected.

This is supported by luminescence data for mixed bidentate ligand complexes which suggest that the dip rings of the tris complexes act independently.[27] An electron excited from the ground state in, for instance, the $[Rh(dip)(phen)_2]^{3+}$ ion to a π^* level on the ligand system shows two distinct lifetimes before luminescent decay. One of these is very close to the single lifetime observed for $[Rh(dip)_3]^{3+}$ (2.3×10^{-3} sec *vs.* 2.29×10^{-3} sec for the latter[18]) and the lifetime of a second emission approaches that of the $[Rh(phen)_3]^{3+}$ species.

b. Rh(III) vs. Ru(II) Complexes. The electrochemistry of $[Rh(dip)_3]^{3+}$ and $[Ru(dip)_3]^{2+}$ is largely, but not entirely, consistent with their chemistry. $[Rh(dip)_3]^{3+}$ is obtained in good yield only by special, forcing conditions.[18] $[Rh(dip)Cl_3(OH)]^-$ readily undergoes further ligand exchange yielding $[Rh(dip)_2Cl_2]^+$, clearly the favored species of the three. In contrast, some care is required to obtain anything other than $[Ru(dip)_3]^{2+}$, *i.e.*, $[Ru(dip)_2Cl_2]^0$, and $(dipH)[Ru(dip)Cl_4]$.[28]

This suggests a stability of the Ru tris complex relative to its isoelectronic Rh counterpart apparently borne out by the electrochemical behavior. The value of $(E_{pc})_I = -1.36$ V for $[Ru(dip)_3]^{2+}$ *vs.* approximately −0.83 V for the Rh analog would seem to represent a combination of kinetic and thermodynamic factors. But while a localization of charge in a single dip ring on electrochemical reduction favors the bidentate ligand elimination observed for $[Rh(dip)_3]^{3+}$ after the first electron transfer, the more

extensive delocalization of the redox orbital suggested by *absence* of such a reaction in the Ru analog[16] is normally consistent with reduction at a *less negative* potential, exactly opposite from the effect observed.

Difficulties arise in trying to correlate differences in electrochemical parameters with the spectral differences of $[Ru(dip)_3]^{3+}$ and $[Ru(dip)_3]^{2+}$. Attempts to correlate change in $E°$, a change in free energy, with $h\nu$, a change in internal energy, are problematic in general as has been summarized by Vlcek.[5] For a limited series of isoelectronic metals with the same ligand a linear relationship between $E°$ and $h\nu$ may be noted but even this depends on the spectral transitions being of the same type. The luminescence spectrum of $[Ru(dip)_3]^{2+}$ shows a transition from a lowest unfilled orbital that has substantial d character, *i.e.*, a $(d-\pi)^*$ state, whereas the corresponding orbital for $[Rh(dip)_3]^{3+}$ has little d character and may be characterized as a ligand localized π^* orbital. Therefore, meaningful correlation of optical and electrochemical data is not expected.

References and Notes

(1) Supported by the Army Research Office—Durham (AROD).
(2) R. N. Adams, *J. Electroanal. Chem.*, **8**, 151 (1964).
(3) (a) A. H. Maki and D. H. Geske, *J. Chem. Phys.*, **30**, 1356 (1959); (b) *J. Amer. Chem. Soc.*, **83**, 1852 (1961).
(4) (a) A. Streitweiser, "Molecular Orbital Theory for Organic Chemists," Wiley, New York, N. Y., 1962, pp 173–188; (b) C. K. Mann and K. K. Barnes, "Electrochemical Reactions in Nonaqueous Systems," Marcel Dekker, New York, N. Y., 1970, pp 37–93; (c) R. J. Magee and W. H. Douglas, *J. Inorg. Nucl. Chem.*, **10**, 1707 (1964).
(5) A. A. Vlcek, *Electrochim. Acta*, **13**, 1063 (1968).
(6) (a) A. Davison, N. Edelstein, R. H. Holm, and A. H. Maki, *Inorg. Chem.*, **4**, 55 (1965); (b) *J. Amer. Chem. Soc.*, **85**, 2029 (1963); (c) H. B. Gray, *Transition Metal Chem.*, **1**, 239 (1965).
(7) E. Konig and S. Herzog, *J. Inorg. Nucl. Chem.*, **32**, 585 (1970).
(8) E. Konig, *Z. Naturforsch. A*, **19**, 1139 (1964).
(9) (a) R. E. Dessy, F. E. Stary, R. B. King, and W. Waldrop, *J. Amer. Chem. Soc.*, **88**, 471 (1966); (b) R. E. Dessy, R. B. King, and M. Waldrop, *ibid.*, **88**, 5112 (1966).
(10) (a) D. M. Soignet and L. G. Hargis, *Inorg. Chem.*, **11**, 2349 (1972); (b) A. A. Vlcek, *Nature (London)*, **189**, 393 (1961); (c) N. Tanaka and Y. Sato, *Electrochim. Acta*, **13**, 335 (1968).
(11) (a) T. Ito and N. Tanaka, *Bull. Chem. Soc. Jap.*, **42**, 1021 (1969); (b) Y. Sato and N. Tanaka, *ibid.*, **41**, 2064 (1968); (c) N. Tanaka and Y. Sato, *Inorg. Nucl. Chem. Lett.*, **2**, 359 (1966).
(12) N. Tanaka and Y. Sato, *Bull. Chem. Soc. Jap.*, **41**, 2059 (1968).
(13) (a) W. R. McWhinnie and J. D. Miller, *Advan. Inorg. Chem. Radiochem.*, **12**, 135 (1969); (b) L. F. Lindoy and S. E. Livingstone, *Coord. Chem. Rev.*, **2**, 173 (1967); (c) E. Konig, *ibid.*, **3**, 471 (1968); (d) E. K. Barefield, D. H. Busch, and S. M. Nelson, *Quart. Rev., Chem. Soc.*, **22**, 457 (1968).
(14) R. D. Gillard, J. A. Osborn, and G. Wilkinson, *J. Chem. Soc.*, 4107 (1965).
(15) A. M. Bond, G. A. Heath, and R. L. Martin, *J. Electrochem. Soc.*, **117**, 1362 (1970).
(16) N. Tokel Takvoryan, R. E. Hemingway, and A. J. Bard, *J. Amer. Chem. Soc.*, **95**, 6582 (1973).
(17) C. K. Mann in "Electroanalytical Chemistry," Vol. 3, A. J. Bard, Ed., Marcel Dekker, New York, N. Y., 1969, p 57.
(18) M. K. DeArmond and J. E. Hillis, *J. Chem. Phys.*, **54**, 2247 (1971).
(19) G. C. Kulasingam, W. R McWhinnie, and J. D. Miller, *J. Chem. Soc. A*, 521 (1969).
(20) B. Martin, W. R. McWhinnie, and G. M. Waind, *J. Inorg. Nucl. Chem.*, **23**, 207 (1961).
(21) R. H. Bull and G. C. Bull, *Anal. Chem.*, **43**, 1342 (1971).
(22) Fisher Scientific Co. Product Information Bulletin No. 199 (1972) on Ridox (Stock No. R-30).
(23) M. Mastragostino, L. Nadjo, and J. M. Saveant, *Electrochim. Acta*, **13**, 721 (1968).
(24) R. S. Nicholson and I. Shain, *Anal. Chem.*, **37**, 178 (1965).
(25) R. S. Nicholson and I. Shain, *Anal. Chem.*, **36**, 706 (1964).
(26) R. S. Nicholson, *Anal. Chem.*, **36**, 1351 (1965).
(27) W. Halper and M. K. DeArmond, *J. Luminescence*, **5**, 225 (1972).
(28) (a) F. P. Dwyer, H. A. Goodwin, and E. C. Gyarfas, *Aust. J. Chem.*, **16**, 42, (1963); (b) *ibid.*, **16**, 544 (1963).
(29) Rh containing species below the dotted line under both the "BIS" and "TRIS" headings are identical with the possible exception of one monodentate ligand. Recrystallization of $[Rh(dip)_2Cl_2]ClO_4$ from dry, purified AN yields $[Rh(dip)_2Cl_2]ClO_4 \cdot AN$ according to elemental analysis. This is empirically equivalent to $[Rh(dip)_2Cl(AN)]Cl(ClO_4)$. The reduction of $[Rh(dip)_3]Cl_3 \cdot 5H_2O$ except that absent) exactly parallels that for $[Rh(dip)_3]Cl_3 \cdot 5H_2O$ except that slightly higher concentrations are necessary before values of $[E_{pc} - E_{(p/2)c}]$ and $[E_{pa} - E_{pc}]$ for the various waves exactly correspond to the theoretical values. Since Rh(I) generally forms four-coordinate species it is not surprising that loss of Cl^- from $[Rh(dip)_2Cl]^0$ proceeds at a rate comparable to AN loss from $[Rh(dip)_2AN]^+$. That is, both are expected to be very fast processes. Given additional evidence to support the existence of $[Rh(dip)_2Cl(AN)]^{2+}$ as the bis dip starting material, Figure 7 could be altered to show AN as the only monodentate ligand on Rh appearing below the dotted line.

Mobility of Organic Cations in Cross-Linked Polyelectrolyte Gels. Measurements of the Self-Diffusion of Tetramethylammonium Ion

G. E. Boyd

Oak Ridge National Laboratory, Oak Ridge, Tennessee 37830 *(Received November 30, 1973)*

Publication costs assisted by Oak Ridge National Laboratory

Self-diffusion coefficients were determined for the sodium and for the tetramethylammonium ion in a moderately cross-linked polystyrenesulfonate gel at 5, 25, and 40° by measuring their respective self-exchange reaction rates with 2.3y $^{22}Na^+$ and C-14 labeled Me_4N^+ as tracers. A solution to the diffusion equation for a composite sphere in a limited bath was employed in a computer-assisted, non-linear least-squares fit of the experimental rate data to obtain particle self-diffusion coefficients, D_p, and values of the kinetic mechanism parameter, ξ. The value of D_p for Me_4N^+ at 25° was less than one-fourth that for Na^+ ion and the activation energies for the two ions were 7.0 and 5.2 kcal mol^{-1}, respectively. The strong reduction in the mobility of tetramethylammonium relative to sodium ion in the polyelectrolyte gel was attributed to the difference in the viscous drag effect they experience.

Introduction

A large amount of empirical data on the ion-exchange behavior of organic ions in aqueous solutions has come into existence in recent years, and many astonishing chromatographic separations of closely related species have been reported. At present, however, very little is known about the causes and mechanisms for these unusual results. A discussion of the interactions of organic ions in cross-linked polyelectrolyte gels has been given by Feitelson[1] who has considered the limited information available on the equilibrium behavior of the tetraalkylammonium ions,[2-4] the amino acid cations, and the carboxylic acid anions. Virtually no quantitative measurements on the mobilities of organic ions in ion exchangers have been reported, although it has been observed[5] that the rates of exchange of the tetra-*n*-alkylammonium ions decrease with increasing ion size. Early work[6] with cylindrical packed beds of granular, sulfonic acid-type cation exchangers in the alkali-metal and ammonium form has shown that the ratio of their equivalent conductivities to the equivalent conductances (λ_0^+) of the respective cations in aqueous solutions at infinite dilution is very nearly a constant. If this empirical relation holds for tetramethylammonium ion, its mobility in an ion exchanger would be expected to be approximately the same as for sodium ion because λ_0 for Me_4N^+ (44.9) is only slightly smaller than for Na^- (50.1).

Measurements of the self-diffusion of tetramethylammonium and of sodium ion in a moderately cross-linked polystyrenesulfonate gel have been performed in this research. Diffusion-controlled rates of self-exchange of C-14 labeled and nonlabeled Me_4N^+ ions and of $^{22}Na^+$ and $^{23}Na^+$ ions, respectively, were determined at several temperatures. A superior, new theoretical method was applied to the treatment of the rate data to give accurate ionic self-diffusion coefficients. A criterion for the kinetic mechanism which controls the self-exchange rate also is given by the theory.

Experimental Section

Materials and Procedure. The experimental procedure (limited bath technique) was essentially the same as that applied earlier in this Laboratory.[7] The exchanger was a nominal 8% divinylbenzene (DVB) cross-linked polystyrenesulfonate taken from the same lot as that used in previous thermodynamic studies.[2] The sodium form was wet seived to collect particles with diameters between 0.21 and 0.42 mm, and defective beads were removed by backwashing until a microscopic examination showed the preparation to be nearly 100% spheres. The exchanger was cleaned by cycling it repeatedly from the sodium to the hydrogen form. Finally, it was converted either to the sodium (NaR) or tetramethylammonium (Me_4NR) form by treatment in a column with a large excess of molar chloride solution followed by 0.1 *M* solution and by rinsing with deionized water until a negative test for chloride was obtained.

A predetermined amount (*i.e.*, mequiv) of NaR or Me_4NR was suspended in 270 g of pure water held in a three-neck, round-bottom flask submerged in a water bath held to ±0.05° of the desired temperature. The exchanger was charged with either $^{22}Na^+$ or C-14 labeled Me_4N^+ ion by placing the activity in the water and waiting approximately 24 hr for isotopic equilibration. Conditions were such that virtually all the radioactivity entered the polyelectrolyte gel; the small amount remaining in solution was determined.

The self-exchange reaction which caused radioactivity to reappear in the external solution was initiated by rapidly adding a weighed quantity of electrolyte of known concentration which contained the same cation as in the exchanger.

The external solution was *ca.* 0.10 *N* so that swelling changes or Donnan invasion of the exchanger by electrolyte could be neglected. The rate of attainment of isotopic redistribution equilibrium was measured by withdrawing weighed samples (*i.e.*, *ca.* 0.1 g) of solution from the well-stirred reaction mixture and measuring their radioactivity. The C-14 labeled Me_4N^+ activity in solution was determined by liquid scintillation counting as described previously.[2] Corrections of 1–4% maximum were made for variable quenching caused by the slightly differing amounts of water in the samples. Long-lived, γ-ray emitting (2.6y) Na-22 activity was measured with a 4π geome-

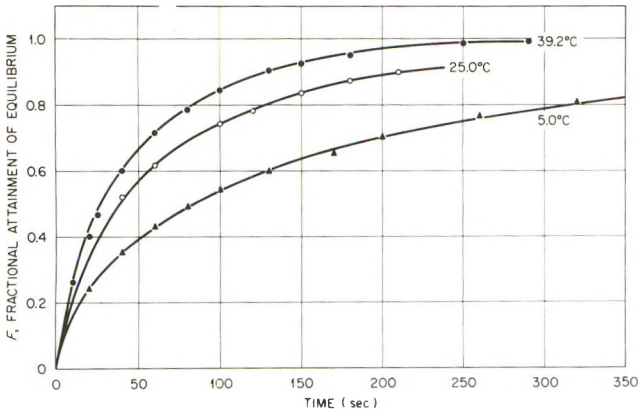

Figure 1. Rate of self-exchange of tetramethylammonium ion in Dowex-50W, X-8, Me_4N form at various temperatures (C-14 labeled Me_4N^+ ions).

try, thalliated NaI crystal scintillation counter. The radiochemical purity of the ^{22}Na preparation was checked by γ spectrum measurements with a multichannel analyzer.

The exchanger was recovered from the reaction flask on completion of the experiment and the average particle size was estimated from microscopic measurements on over 100 spheres submerged in their equilibrium electrolyte solution. The average diameter for the Na^+ form was 0.0301 cm and 0.0326 cm for the Me_4N^+ form. The fractional attainment of isotopic redistribution equilibrium, F, was computed by dividing the corrected activity (counts per min per g of solution) by the activity observed after 24 hr. A typical plot showing the increase of F with time is given in Figure 1.

Treatment of Experimental Results. Two models were applied in the treatment of the $F(t)$ data to derive rate constants for the self-exchange reactions of C-14 labeled Me_4N^+ and $^{22}Na^+$ ions, respectively. Qualitatively the shape of the rate curves (Figure 1) was characteristic of a process controlled by diffusion in and through the polyelectrolyte sphere (*i.e.*, particle or "p-type" diffusion). Therefore, a solution[7] to Fick's equations for a sphere with the appropriate boundary conditions was employed which gives a formula from which the particle diffusion coefficient, D_p, can be derived by fitting the experimental data to the function, $F(t)$. Three quantities, τ, λ_n, and w appear in $F(t)$. The dimensionless variable, τ, which is related to t, D_p, and the particle radius, a, by

$$\tau = D_p t / a^2 \tag{1}$$

the parameters, λ_n, which are the roots of the transcendental equation

$$\lambda_n \cot \lambda_n = 1 + \lambda_n^2/3w \tag{2}$$

and w which is the ratio of the total milliequivalent of ion in the exchanger to that in the ambient solution, and is defined by

$$W = \bar{C}\bar{V}/CV \tag{3}$$

where $\bar{C}$ and C are the concentrations of the diffusing species in the exchanger of volume $\bar{V}$ and in the solution of volume V, respectively. The values of D_p derived by fitting the experimental data to $F(t)$, however, showed a progressive increase with time suggesting that the ion exchanger was nonuniform, or, that a thin film of solution was present at the particle–solution boundary so that a "coupled" film diffusion-particle diffusion process was occurring. Examinations of the spheres with a polarizing microscope did not reveal heterogeneity in the exchanger, hence diffusion in and through a composite sphere was considered.

Several solutions of the mathematics of diffusion in composite spheres for appropriate boundary conditions have been reported,[8,9] however, the recent treatments of Huang[10] for a finite bath and of Span[11,12] for an infinite bath are noteworthy. An important difference in the treatments by these latter authors lies in their assumptions about the concentration profile in the liquid film which encloses the ion-exchange sphere. If a *linear* concentration gradient is assumed, the mathematical solution for a finite bath is

$$F(t) = 1 - \sum_{n=1}^{\infty} \frac{6\xi^2(1+\alpha)\exp(-g_n^2\tau)}{(9/\alpha) + \alpha g_n^2 + 9)\xi^2 - (6+\alpha)g_n^2\xi + \alpha g_n^4} \tag{4}$$

where the g_n are the nonzero roots of

$$\tan g_n/g_n = (3\xi - \alpha g_n^2)/[(\xi - 1)\alpha g_n^2 + 3\xi] \tag{5}$$

with $\alpha = CV/\bar{C}\bar{V} = w^{-1}$ and $\xi = (a/\delta)(D_f/D_p)(C/\bar{C})$, where δ is the film thickness and D_f is the film diffusion coefficient.

Constant values of D_p and estimates of δ, assuming values for D_f published for binary aqueous solutions, were obtained from computer-assisted, non-linear least-square fits of eq 4 and 5 to the data. In making this fit reasonable guesses of the values of ξ and D_p for each system must be made to initiate the computer calculations. The validity of the assumption of a linear concentration profile for our experiments will be discussed in the light of Span's results.

Discussion

A summary of the results is given in Table I where the uncertainties shown for D_p and ξ are the standard deviations of the values listed. The self-diffusion coefficient for Me_4N^+ is seen to be significantly smaller than for Na^+, and the activation energy for the process is distinctly larger. Analogous reductions in the relative mobility of tetramethylammonium ion have been reported[13] in investigations of the electric conductivites of a homogeneous polystyrenesulfonate membrane with a somewhat larger water content (*i.e.*, $\bar{C}(Me_4NR) = 1.59$ mequiv ml^{-1}). Thus, the ratio of the equivalent conductance of the tetramethylammonium to the sodium form of the membrane was 0.44 compared with the ratio of D_p values (Table I) at 25° of 0.23. The reduction in the mobilities of ions in a polyelectrolyte gel from their values in aqueous solutions may be attributed to three effects: (a) a reduction of the cross section for diffusion because of obstruction by the molecular network of the gel; (b) a further reduction because only a fraction of the "free" volume will permit ionic motion in a direction perpendicular to the cross section for diffusion (*i.e.*, tortuosity factor); and (c) a reduction caused by the resistance experienced by a sphere when its diameter approaches the width of the interstices (pores) in the gel network. It may be inferred from the equivalent conductance[6,13] and from ionic self-diffusion coefficient[7] data on the alkali-metal cations that the movement of sodium ion is restricted by a and b, but not by c, because of a decrease in the size of the hydrated ion. Thus, the expected increase in drag with the

TABLE I: Particle Self-Diffusion Coefficient, D_p, and Kinetic Mechanism Parameter, ξ, for the Self-Exchange Reactions of Tetramethylammonium and Sodium Ions in Nominal 8% DVB Cross-Linked Polystyrenesulfonate[a]

Temp, °C	D_p, cm² sec⁻¹ × 10⁷	E_{act}, kcal mol⁻¹	ξ	δ, cm × 10²
		$(CH_3)_4N^+$ Ion		
5.0	0.93 ± 0.01		42.8 ± 3.5	1.6
		7.0 ± 0.3		
25.0	2.17 ± 0.06		39.7 ± 8.6	0.9
39.2	4.46 ± 0.08		9.6 ± 0.4	(1.6)
		Na^+ Ion		
5.0	5.13 ± 0.12		4.6 ± 0.2	2.0
		5.2 ± 0.5		
24.9	9.61 ± 0.38		4.8 ± 0.3	1.2

[a] $\bar{C}$(NaR) = 3.0; $\bar{C}$(Me_4NR) = 2.5 mequiv ml⁻¹.

size of a hydrated alkali-metal cation is compensated by an equivalent reduction in its hydration. The mobility of the large, poorly hydrated Me_4N^+ ion will be reduced by c, and conductance measurements[13] have shown that the mobilities of the larger, symmetrical *n*-alkylammonium ions relative to their mobilities at infinite dilution in water are strongly decreased proportionately to their respective sizes. The role of factor a above in lowering ionic self-diffusion has been shown by recent measurements with $^{22}Na^+$ in aqueous solutions of the model compound, sodium *p*-ethylbenzenesulfonate (see Figure 3, ref 14).

The composite sphere model employed in this research is of interest because of the utility of ξ as a criterion for the mechanism of the rate-controlling step. Helfferich[15], in a consideration of the problem of predicting whether film ("f-type") or particle ("p-type") diffusion will be rate determining, has derived a simple, *approximate* modulus, $(\bar{C}/C)(\bar{D}/D)(\delta/a)(5 + 2\alpha_B^A)$, which predicts particle diffusion control when it is much less than and film diffusion when it is much greater than unity. (α_B^A is unity for isotopic exchange.) It is readily seen that this dimensionless modulus is practically identical with ξ^{-1} which comes directly without approximation from the mathematics of diffusion in a film covered sphere. There is, of course, no sharp boundary between film and particle diffusion control; both mechanisms contribute when their individual rates are comparable.

The values of ξ (Table I) appear to be independent of the temperature, excepting possibly at 39.2° with the Me_4N^+ ion self-exchange reaction. However, the stirring conditions in this experiment may have been different from the others as strict control of this variable in limited bath type measurements is difficult. The parameter ξ is expected to be nearly temperature independent because of the contravariant changes in the ratio (D_f/D_p) and in the film thickness, δ, with temperature. The film diffusion process possesses a lower activation energy than does that for particle diffusion, so that (D_f/D_p) will decrease with temperature. On the other hand, a/δ will increase, largely because of the reduction in viscosity with temperature. Previous measurements[7] have demonstrated that a is independent of the temperature.

The apparent film thickness computed with $D_f(Na^+) = 1.30 \times 10^{-5}$ cm² sec⁻¹ in 0.1 *N* NaCl,[16] and assuming $D_f(Me_4N^+) = 1.1 \times 10^{-5}$ cm² sec⁻¹ in 0.1 *N* Me_4NCl are seen (Table I) to be of reasonable magnitude. These δ values appear to be sufficiently small to support the basic assumption that an immobile film with a *linear concentration profile* existed at the surface of the spherical particle. Calculations by Span[12] have demonstrated that concentration profiles in the films are practically linear when the ratio, (δ/a), is less than 0.1. In our experiments this ratio was 0.055 and 0.080 for tetramethylammonium and sodium ions, respectively.

Acknowledgments The assistance of the late Avraham Schwarz in the rate of self-exchange measurements and of L. D. Hullet in the particle size determinations is gratefully acknowledged.

References and Notes

(1) J. Feitelson in "Ion Exchange," Vol. 2, J. A. Marinsky, Ed., Marcel Dekker, New York, N. Y., 1969, p 135.
(2) A. Schwarz and G. E. Boyd, *J. Phys. Chem.*, **69**, 4268 (1965).
(3) G. E. Boyd and Q. V. Larson, *J. Amer. Chem. Soc.*, **89**, 6038 (1967).
(4) G. E. Boyd, Q. V. Larson, and S. Lindenbaum, *J. Phys. Chem.*, **72**, 2651 (1968).
(5) T. R. E. Kressman and J. A. Kitchener, *J. Chem. Soc.*, 1208 (1949).
(6) E. Heymann and I. J. O'Donnell, *J. Colloid Sci.*, **4**, 405 (1949).
(7) G. E. Boyd and B. A. Soldano, *J. Amer. Chem. Soc.*, **75**, 6091 (1953).
(8) J. Crank, "Mathematics of Diffusion," Oxford University Press, London, 1956, pp 92, 93.
(9) H. S. Carslaw and J. C. Jaeger, "Conduction of Heat in Solids," 2nd ed, Oxford University Press, London, 1959, p 351.
(10) T. C. Huang and K. Y. Li, *Ind. Eng. Chem., Fundam.*, **12**, 50 (1973).
(11) J. Span and M. Ribaric, *J. Chem. Phys.*, **41**, 2347 (1964).
(12) J. Span, *J. Chem. Phys.*, **52**, 3097 (1970).
(13) H. Kawabe, H. Jacobson, I. F. Miller, and H. P. Gregor, *J. Colloid Interface Sci.*, **21**, 79 (1966).
(14) M. J. Pikal and G. E. Boyd, *J. Phys. Chem.*, **77**, 2918 (1973).
(15) F. Helfferich, "Ion Exchange," McGraw-Hill, New York, N. Y., 1962, p 277.
(16) R. Mills, *J. Amer. Chem. Soc.*, **77**, 6116 (1955).

Temperature Dependence of Limiting Heat Capacities of Dissolution of Tetrabutylphosphonium Bromide, Tetraphenylphosphonium Bromide, and Tetraphenylarsonium Chloride in Water and Hydrophobic Hydration

S. Sunder, B. Chawla, and J. C. Ahluwalia*

Department of Chemistry, Indian Institute of Technology, Kanpur-208016, India *(Received May 24, 1973; Revised Manuscript Received November 19, 1973)*

The integral heats of solution ΔH_s, of Bu_4PBr (from 5 to 75°), Ph_4PBr and Ph_4AsCl (from 15 to 75°), and of Ph_4PCl at 25 and 35° in water have been determined at very low concentrations. The heat capacities of dissolution at infinite dilution, $\Delta C_p°$, of these salts in water as a function of temperature have been derived by the integral heat method. The temperature dependence behaviors of $\Delta C_p°$ of Ph_4PBr and Ph_4AsCl are very similar to each other but different from that of Bu_4PBr. The results are compared with those of Bu_4NBr, $NaBPh_4$, and *n*-Am_4NBr reported earlier. The interpretation of certain predominant similar characteristic features such as occurrence of maxima and minima around 40 and 50°, respectively, has been discussed in terms of the various possible structures existing in aqueous solutions of these solutes.

Introduction

The understanding about the exact nature of the interaction of solutes containing large nonpolar groups with water is far from satisfactory. Although a number of studies on the various physicochemical properties of aqueous solutions of such solutes carried out during the past few years have resulted in a great deal of progress, a number of questions have been raised, answers to which are either not available or unsatisfactory.[1] The model compounds chosen in various studies are usually salts containing large alkyl or aryl ions such as R_4N^+, R_4P^+, R_4B^- etc. Because of their ease of dissolution in water, such salts form a convenient tool to study hydrophobic hydration.

The heat capacity changes of the solutes in water is recognized to be one of the most sensitive measures of the gross structural changes brought about by the solutes.[2] The studies on the temperature dependence of heat capacity changes of solutes containing large nonpolar groups not only give an idea about the gross structure of their aqueous solutions at different temperatures but can also shed light on the nature of hydrophobic hydration in a more detailed manner.[3-6] The earlier studies on the temperature dependence of limiting heat capacities of dissolution of $NaBPh_4$,[3] Bu_4NBr,[4,7] and *n*-Am_4NBr[4] had revealed complex behavior (occurrence of maxima and minima in the $\Delta C_p°$-T curve) for $NaBPh_4$ and *n*-Am_4NBr as compared to simple behavior (only a slight decrease if any in $\Delta C_p°$ with increasing temperature) for Bu_4NBr. In these studies[3-5] based on the limited data a certain tentative and speculative explanation was given with regard to the effect of the nature (alkyl or aryl, cation or anion) and size of the large nonpolar group on its interaction with water. In order to obtain a definitive and clear difference in the effect of alkyl and aryl as well as of cationic and anionic nonpolar group and also of the increasing size of the nonpolar group on hydrophobic hydration, we report in this paper the limiting heat capacities of dissolution, $\Delta C_p°$, of Bu_4PBr from 10 to 70° and of Ph_4PBr and Ph_4AsCl from 20 to 70° in water. The limiting heat capacities of dissolution were derived from heats of solution measurements at very low concentrations by the integral heat method.[8,9]

Experimental Section

The precision calorimeter and the procedure for the measurements of integral heats of solution have been described earlier.[3-5] The submarine calorimeter (550-ml glass dewar flask) was immersed in a thermostat whose temperature was kept constant to ±0.002° by a Sargent Welch Thermonitor, Model ST. A 10-kilohm thermistor formed one arm of the Wheatstone bridge which was constructed from precision decade resistors. The signal was fed into an amplifier which in turn drove a Sargent recorder. The minimum temperature change that could be detected was of the order of 2×10^{-5} deg. At 25° the calorimeter was calibrated by measuring heats of solution of KCl in water and that of THAM (tris(hydroxymethyl)-aminomethane) in 0.1 *N* HCl. The values obtained were within 0.2% of those reported by Gunn.[10]

At higher temperatures (up to 75°), the calorimeter was calibrated by measuring heats of solution of NaCl in water. The values obtained were in good agreement with those obtained by Criss and Cobble.[8]

Since the vacuum-sealed empty bulbs gave negligible heat of bulb breaking at all temperatures the sample bulbs were sealed *in vacuo*, thus eliminating the application of somewhat uncertain correction for the heat of empty bulb breaking.

Salts Bu_4PBr and Ph_4PBr were procured from Alfa Inorganics and recrystallized[11] from absolute ethanol by adding absolute ether to the solution; they were dried *in vacuo* at 60° for about 7–8 hr. Ph_4AsCl was obtained from K & K Laboratories and recrystallized[12] from absolute ethanol and ether and then from water free methylene chloride and dried *in vacuo* at 60° for 7–8 hr. The sample bulbs filled with samples were further dried at about 80° for about 12 hr, cooled, weighed to constant mass, and sealed *in vacuo*. The weights of the samples of the salts were chosen so as to result in a calorimeter solution of about 10^{-4} to 10^{-3} *m*. The water used in the calorimeter

was conductivity water obtained by passing distilled water through a Barnsted mixed bed ion-exchange resin column.

Results

The values of the integral heats of solution, ΔH_s, of Bu_4PBr (from 5 to 75°), Ph_4PBr and Ph_4AsCl (from 15 to 75°), and of Ph_4PCl at 25 and 35° at concentrations ranging from 0.3×10^{-4} to 2×10^{-3} m are given in Tables I, II, III, and IV as supplementary material (see paragraph at end of paper regarding supplementary material). The values of the heats of solution at infinite dilution, ΔH_s, were obtained by averaging the values of ΔH_s since the determined values were measured in very dilute solutions wherein any effect of molality is masked by the experimental error. The values of $\Delta H_s°$ of Bu_4PBr, Ph_4PBr, and Ph_4AsCl computed with 95% confidence limits at all temperatures are given in Tables V, VI, and VII, respectively. The values of the limiting heat capacities of dissolution $\Delta C_p°$, of Bu_4PBr from 10 to 70° as derived from the $\Delta H_s°$ values by the integral heat method[8,9] are given in Table V and plotted as a function of temperature in Figure 1. The values of $\Delta C_p°$ of Ph_4PBr and Ph_4AsCl from 20 to 70° are given in Tables VI and VII, respectively, and plotted as function of temperature in Figure 2. Since at 30° the $\Delta C_p°$ value of Ph_4PCl (190 ± 8 cal deg^{-1} mol^{-1}) reported earlier from this laboratory[13] seemed to be inconsistent with the $\Delta C_p°$ value of Ph_4PBr (146 ± 2 cal deg^{-1} mol^{-1}) insofar as the influence of halide ions on the $\Delta C_p°$ values of R_4N^+ and R_4P^+ salts is concerned, it was found desirable to repeat the ΔH_s measurements of Ph_4PCl at 25 and 35°. Ph_4PCl sample was prepared by treating a solution of pure recrystallized Ph_4PBr with freshly precipitated silver hydroxide and HCl. The salt was recrystallized from ethanol and ether and then from dry methylene chloride. The recrystallized salt was dried *in vacuo* at 60° for about 7–8 hr. Measurements of ΔH_s of Ph_4PCl at 25 and 35° which are listed in Table IV of supplementry material were indeed found to be different from the earlier reported values.[13] The present values of $\Delta H_s°$ (−2194 ± 22 cal mol^{-1} at 25° and −691 ± 9 cal mol^{-1} at 35°) are believed to be correct since the value at 25° is in excellent agreement with that reported by Friedman.[14] The error in the earlier reported $\Delta H_s°$ values of Ph_4AsCl is believed to have arisen possibly due to methylene chloride used for recrystallisation not being moisture free.

The revised $\Delta C_p°$ value of Ph_4PCl at 30° (157 ± 3 cal deg^{-1} mol^{-1}) seems to be consistent with that of Ph_4PBr (146 ± 2 cal deg^{-1} mol^{-1}) in that the influence of bromide ion on the $\Delta C_p°$ value of Ph_4P^+ is not much different from that of the chloride ion and the slightly less positive value of $\Delta C_p°$ of Ph_4PBr as compared to that of Ph_4PCl is in line with the view that bromide ion is a better structure breaker than the chloride ion.

Discussion

The partial molal heat capacity at infinite dilution, $\bar{C}_{p_2}°$, can be represented as[15]

$$\bar{C}_{p_2}^0 = C_{p2}(\text{int}) + C_{p2}^0(\text{solv})$$

where $C_{p2}(\text{int})$ represents the intrinsic heat capacity of the ions in the absence of the ion–solvent interaction and $C_{p2}°(\text{solv})$ represents the influence which the ions exert on the solvent structure. Since $\Delta C_p°$, the heat capacity of dissolution at infinite dilution, is given by $\Delta C_p° = \bar{C}_{p2}° - C_{p2}$ where C_{p2} represents the heat capacity of the pure solute, $C_{p2}°(\text{solv})$ can then be represented as

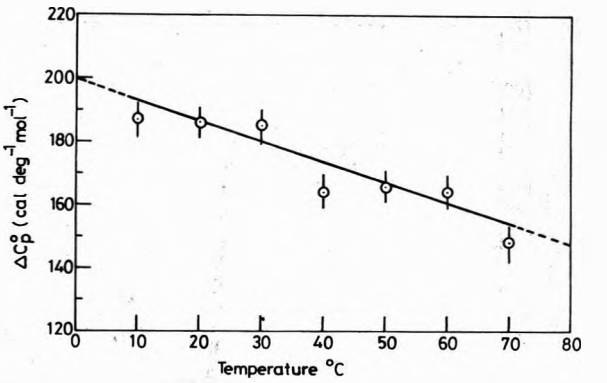

Figure 1. Excess partial molal heat capacities of tetrabutylphosphonium bromide in water as a function of temperature.

TABLE V: Limiting Excess Partial Molal Heat Capacities, $\Delta C_p°$, of Bu_4PBr in Water from 10 to 70°

Temp, °C	$\Delta H_s°$,[a] cal mol^{-1}	Temp, °C	$\Delta C_p°$,[b] cal $°K^{-1}$ mol^{-1}
5	−6883 ± 84		
		10	187 ± 9
15	−5015 ± 39		
		20	186 ± 5
25	−3160 ± 25		
		30	186 ± 3
35	−1305 ± 11		
		40	164 ± 2
45	330 ± 5		
		50	166 ± 2
55	1990 ± 13		
		60	164 ± 2
65	3626 ± 16		
		70	148 ± 4
75	5106 ± 37		

[a] $\Delta H_s°$ values are computed average values with 95% confidence limits. [b] The uncertainty in the $\Delta C_p°$ value at temperature $T(e\Delta C_p°_T)$ is $e\Delta C_p°_T = [1/(T_2 - T_1)][(e\Delta H_s°_{T_1})^2 + (e\Delta H_s°_{T_2})^2]^{1/2}$ where $T = (T_1 + T_2)/2$.

TABLE VI: Limiting Excess Partial Molal Heat Capacities, $\Delta C_p°$, of Ph_4PBr in Water from 20 to 70°

Temp, °C	$\Delta H_s°$,[a] cal mol^{-1}	Temp, °C	$\Delta C_p°$,[b] cal $°K^{-1}$ mol^{-1}
15	622 ± 8		
		20	186 ± 2
25	2486 ± 16		
		30	146 ± 2
35	3946 ± 15		
		40	204 ± 3
45	5986 ± 23		
		50	105 ± 3
55	7037 ± 12		
		60	107 ± 2
65	8105 ± 15		
		70	155 ± 4
75	9656 ± 37		

[a] $\Delta H_s°$ values are computed average values with 95% confidence limits. [b] The uncertainty in the $\Delta C_p°$ value at temperature $T(e\Delta C_p°_T)$ is calculated as follows: $e\Delta C_p{}_T° = [1/(T_2 - T_1)][(\Delta H_s°_{T_1})^2 + (e\Delta H_s°_{T_2})^2]^{1/2}$ where $T = (T_1 + T_2)/2$.

$$C_{p2}^0(\text{solv}) = \Delta C_p^0 + [C_{p2} - C_{p2}(\text{int})]$$

Since the contribution of the term $[C_{p2} - C_{p2}(\text{int})]$ as estimated from the values of C_{p2} and $C_{p2}(\text{int})$ given by Visser and Somsen[15,16] for Bu_4NBr, is rather small compared to the large $\Delta C_p°$ value of highly structure making salts such as reported in this paper, the $\Delta C_p°$ values (in place

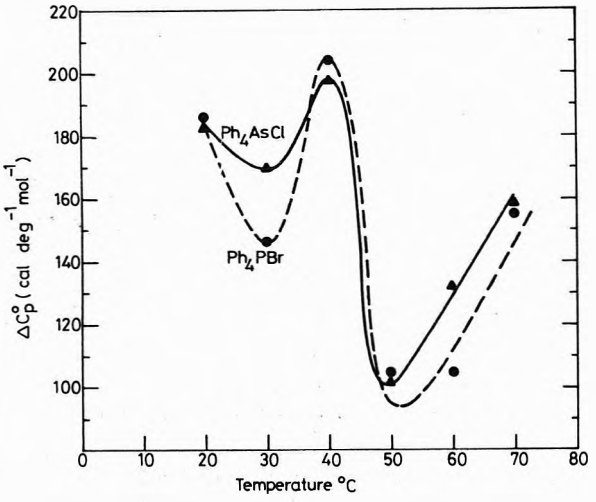

Figure 2. Excess partial molal heat capacities of tetraphenylphosphonium bromide and tetraphenylarsonium chloride in water as a function of temperature: ●, ΔC_p° of Ph_4PBr; ▲, ΔC_p° of Ph_4AsCl.

Table VII: Limiting Excess Partial Molal Heat Capacities, ΔC_p°, of Ph_4AsCl in Water from 20 to 70°

Temp, °C	ΔH_s°,[a] cal mol^{-1}	Temp, °C	ΔC_p°,[b] cal °K^{-1} mol^{-1}
15	−4483 ± 36		
		20	183 ± 4
25	−2654 ± 22		
		30	170 ± 4
35	−956 ± 29		
		40	198 ± 4
45	1023 ± 21		
		50	103 ± 3
55	2055 ± 22		
		60	132 ± 3
65	3375 ± 16		
		70	158 ± 4
75	4952 ± 33		

[a] ΔH_s° values are computed average values with 95% confidence limits. [b] The uncertainty in the ΔC_p° value at temperature T($e\Delta C_p^\circ{}_T$) is calculated as follows: $e\Delta C_p{}_T^\circ = [1/(T_2 - T_1)][(e\Delta H_s^\circ{}_{T_1})^2 + (e\Delta H_s^\circ{}_{T_2})^2]^{1/2}$ where $T = (T_1 + T_2)/2$.

of C_{p2}°(solv) values) could be safely used to discuss the structural changes brought about by the addition of solutes or by the change in temperature.

It may be seen from Tables V, VI, and VII and that the ΔC_p° values of Bu_4PBr, Ph_4PBr, and Ph_4AsCl at 30° are 186 ± 3, 146 ± 2, and 170 ± 4 cal deg^{-1} mol^{-1}, respectively, indicating that all these solutes are good structure makers and that the gross structure-making propensities of these salts are of about the same order of magnitude. However, on examining the ΔC_p°–T plots (see Figures 1 and 2), it is found that the temperature dependence of ΔC_p° of salts (Ph_4PBr and Ph_4AsCl) containing aromatic nonpolar cation resemble each other but are different from that of the salt (Bu_4PBr) containing the aliphatic nonpolar group. Both Ph_4PBr and Ph_4AsCl salts show a complex temperature dependence (see Figure 2) in that a shallow minimum is observed at 30°, followed by a maximum at 40° and another minimum at 50° while the ΔC_p°–T plot for Bu_4PBr (see Figure 1) shows a slight gradual decrease in the ΔC_p° value with increasing temperature. The temperature dependence of C_{p2}°(solv) is not likely to be significantly different from that of ΔC_p° even if the estimated temperature dependence of the term [C_{p2} − C_{p2}(int)][15,16] (which for Bu_4NBr ranges from about −34 cal deg^{-1} mol^{-1} at 5° to about −20 cal deg^{-1} mol^{-1} at 55°) is taken into account. The difference in the behavior of Bu_4PBr from that of Ph_4PBr and Ph_4AsCl may be attributed to the difference in the interaction of butyl and phenyl groups in water.

Although it may be difficult at this stage to explain completely the ΔC_p°–T plots of the solutes containing large aromatic and aliphatic nonpolar groups there are certain predominant similarities as well as differences in the ΔC_p°–T plots of Bu_4NBr,[4,7] Bu_4PBr, Ph_4PBr, Ph_4AsCl, $NaBPh_4$,[3] and n-Am_4NBr[5] which must be accounted for in any theory of interactions of nonpolar moieties with water. For instance, the more or less slight decrease in the ΔC_p° values with increasing temperature from 10 to 70° for Bu_4NBr[4,7] and Bu_4PBr (Figure 1) point out the fact that the overall effect of increasing temperature is not too significant. Less than 20% of the total structure existing at 10° seems to be broken down at 70°. Since the number of clusters of hydrogen-bonded water molecules gets reduced with increasing temperature the decreasing positive contribution to ΔC_p^c with increasing temperature by Bu_4NBr and Bu_4PBr may be correlated with the effect of breakdown of clusters of water molecules stabilized by these salts. These results, however, do not support the theory of Nemethy and Scheraga[17] according to which ΔC_p° of nonpolar solutes in water should increase with increasing temperature. For solutes containing phenyl groups it is interesting to note that there are certain similar predominant features in the ΔC_p°–T plots, *i.e.*, a maximum around 40° and a minimum around 50°. For n-Am_4NBr also corresponding maximum and minimum are found to occur around 50 and 60°, respectively. It seems that the two-state mixture model of hydrogen-bonded and monomers species is inadequate to explain these results. There must be an additional effect or an additional kind of structure which results in increasing positive contribution to ΔC_p° with increasing temperature. It seems logical then to think of the existence of molecular aggregates (nontetrahedral hydrogen-bonded species) in addition to clusters of tetrahedral hydrogen-bonded species; the increasing breakdown of clusters results in an increasing number of molecular aggregates with increasing temperature in the aqueous solutions of the above solutes. The net effect on temperature dependence of ΔC_p° would be the combination of the effect, *i.e.*, (i) melting of clusters which decrease in number with increasing temperature (ΔC_p° decreasing with increasing temperature), and (ii) melting of aggregates[18] which increase in number with increasing temperature (ΔC_p° increasing with increasing temperature) which may thus account for the observed maxima and minima.

An alternative explanation could be that hydrophobic bonding plays an important role in determining the temperature dependence of ΔC_p° of Ph_4PBr, Ph_4AsCl, $NaBPh_4$, and n-Am_4NBr in water. The temperature of maximum hydrophobic bond strength being 42 and 58° for the interactions of aromatic and aliphatic side chains, respectively,[19] may be responsible for the occurrence of minima around 50° for Ph_4PBr, Ph_4AsCl, and $NaBPh_4$ and around 60° for n-Am_4NBr.

The possibility of cage-like structures existing in aqueous solutions of Ph_4PBr, Ph_4AsCl, $NaBPh_4$, and n-Am_4NBr is not ruled out since the rather sharp and drastic reduction in ΔC_p° around 40 to 50° could very well signify the collapse of such a structure.

From the above discussion it seems that although the temperature dependence studies on the limiting heat capacities of dissolution of solutes containing large nonpolar groups have provided some useful information which must be taken into account for any theory of nonpolar group–water interactions, however, these studies alone cannot give complete insight into the nonpolar group–water interactions. It would be worthwhile and desirable that detailed temperature dependence studies on other properties of aqueous solutions of solutes containing nonpolar moieties be also carried out for hopefully complete understanding of hydrophobic hydration.

Acknowledgment. We are thankful to the Council of Scientific and Industrial Research, India, for the award of Junior Research Fellowships to S. Sunder and B. Chawla.

Supplementary Material Available. The detailed listing of ΔH_s values (Tables I, II, III, and IV) will appear following these pages in the microfilm edition of this volume of the journal. Photocopies of the supplementary material from this paper only or microfiche (105 × 148 mm, 24× reduction, negatives) containing all of the supplementary material for the papers in this issue may be obtained from the Journals Department, American Chemical Society, 1155 16th St., N.W., Washington, D. C. 20036. Remit check or money order for $3.00 for photocopy or $2.00 for microfiche, referring to code number JPC-74-738.

References and Notes

(1) T. S. Sarma and J. C. Ahluwalia, *Chem. Soc. Rev.*, **2**, 203 (1973); see also references cited therein.
(2) H. S. Frank and W. Y. Wen, *Discussions Faraday Soc.*, **24**, 133 (1957).
(3) S. Subramanian and J. C. Ahluwalia, *J. Phys. Chem.*, **72**, 2525 (1968).
(4) T. S. Sarma and J. C. Ahluwalia, *Trans. Faraday Soc.*, **67**, 2528 (1971).
(5) R. K. Mohanty, S. Sunder, and J. C. Ahluwalia, *J. Phys. Chem.*, **76**, 2577 (1972).
(6) E. Wicke, *Angew. Chem. Int. Ed. Engl.*, **5**, 106 (1966).
(7) M. J. Mastroianni and C. M. Criss, *J. Chem. Thermodyn.*, **4**, 321 (1971).
(8) C. M. Criss and J. W. Cobble, *J. Amer. Chem. Soc.*, **83**, 3223 (1961).
(9) J. C. Ahluwalia and J. W. Cobble, *J. Amer. Chem. Soc.*, **86**, 5317 (1964).
(10) S. Gunn, *J. Phys. Chem.*, **69**, 2902 (1965).
(11) G. Kalfoglu and L. H. Bowen, *J. Phys. Chem.*, **73**, 2728 (1969).
(12) A. I. Popov and R. E. Humphrey, *J. Amer. Chem. Soc.*, **81**, 2043 (1959).
(13) R. K. Mohanty and J. C. Ahluwalia, *J. Chem. Thermodyn.*, **4**, 53 (1972).
(14) C. V. Krishnan and H. L. Friedman, *J. Phys. Chem.*, **73**, 3934 (1969).
(15) C. De Visser and G. Somsen, *J. Chem. Thermodyn.*, **5**, 147 (1973).
(16) C. De Visser and G. Somsen, *J. Chem. Soc., Faraday Trans. 1*, **69**, 1440 (1973).
(17) G. Nemethy and H. Scheraga, *J. Chem. Phys.*, **36**, 3401 (1962).
(18) H. Ruterjans, F. Schreiner, U. Sage, and Th. Ackermann, *J. Phys. Chem.*, **73**, 986 (1969).
(19) G. Nemethy and H. Scheraga, *J. Phys. Chem.*, **66**, 1773 (1962).

Electronic Absorption Spectra of Ion Radicals and Their Molecular Orbital Interpretation. IV. Anion Radicals of Aromatic and Unsaturated Aliphatic Carbonyl Compounds

Tadamasa Shida,* Suehiro Iwata, and Masashi Imamura

The Institute of Physical and Chemical Research, Wako-shi, Saitama, Japan *(Received September 10, 1973)*

Publication costs assisted by the Institute of Physical and Chemical Research

Electronic absorption spectra of anion radicals of 40 carbonyl compounds have been recorded. For the compounds previously studied, such as fluorenone and benzophenone, the measurement has been extended to shorter wavelengths to find additional absorption bands. The experimental spectra agree systematically with theoretical calculations for the π electronic state of the anions using the method of Longuet-Higgins and Pople plus CI treatment. Some anions are subject to bond scission (benzoyl bromide and ω-bromoacetophenone), enolation (dibenzoylmethane and benzoylacetone), and cis-trans isomerization (dimethylmaleate).

Introduction

The anion radical of aromatic carbonyl compounds has been the subject of a number of esr studies.[1-4] Fraenkel and his coworkers prepared aromatic anion radicals containing aldehyde, acetyl, or amide, as well as other substituents and compared the observed esr spectra with the calculated spin densities.[1] Anion radicals of benzophenone and its analogs have been studied by many authors because of remarkable solvent effect and ion-pair formation.[2-4]

Compared with the esr study, optical studies of the anions are relatively few, and thus far only the visible absorption bands of anions of benzophenone and fluorenone have been investigated in some detail.[4-6] Although the aforementioned tendency of the anions to form ion pairs is by itself an interesting subject in both esr and optical

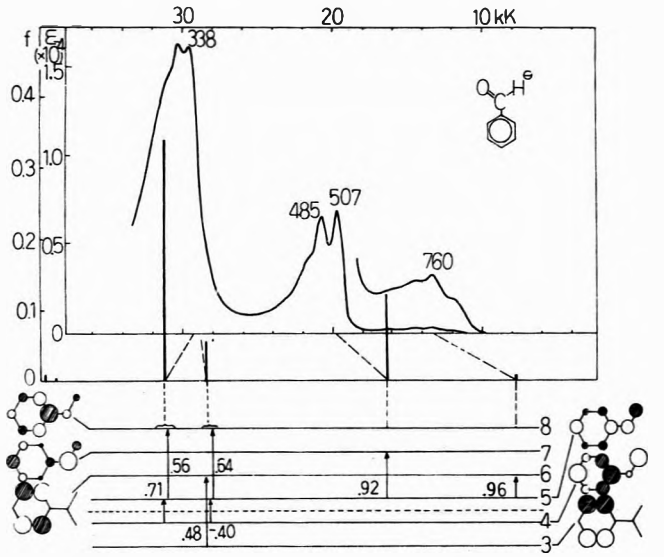

Figure 1. Adsorption spectrum of the benzaldehyde anion. Unless otherwise stated, all spectra were measured for rigic solutions in methyltetrahydrofuran (MTHF) at 77°K. The numbers at the peaks denote the absorption maximum in units of nm. The sticks and MO diagrams represent the result of calculation. The horizontal broken line demarcates the singly occupied orbital from the doubly occupied ones lying below the line. The vertical arrows indicate major configurations whose coefficient in the total wave function exceeds 0.3.

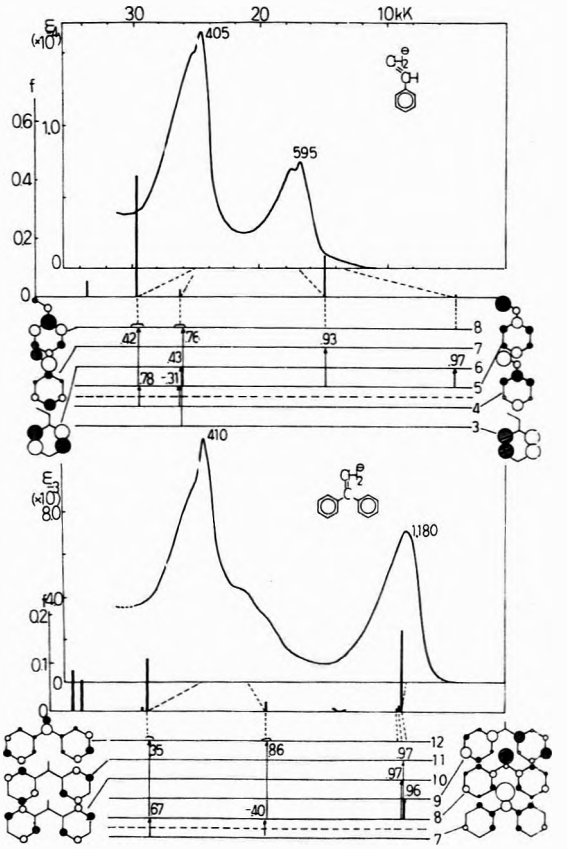

Figure 2. Absorption spectra of the styrene and 1,1-diphenylethylene anions. See cation to Figure 1.

studies, optical spectra perturbed by the countercation or solvent molecules are not suited for the comparison with theoretical spectra calculated for the electronic state of free anions.

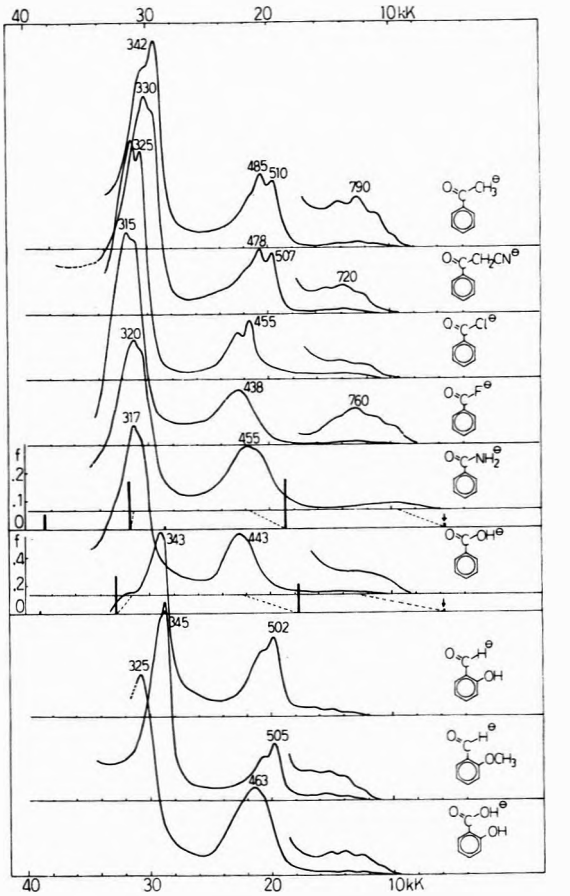

Figure 3. Absorption spectra of the benzaldehyde derivatives anions. See caption to Figure 1. The observed extinction coefficient (ϵ) is not shown to avoid complication in the figure. They are more or less similar to those for the benzaldehyde anion.

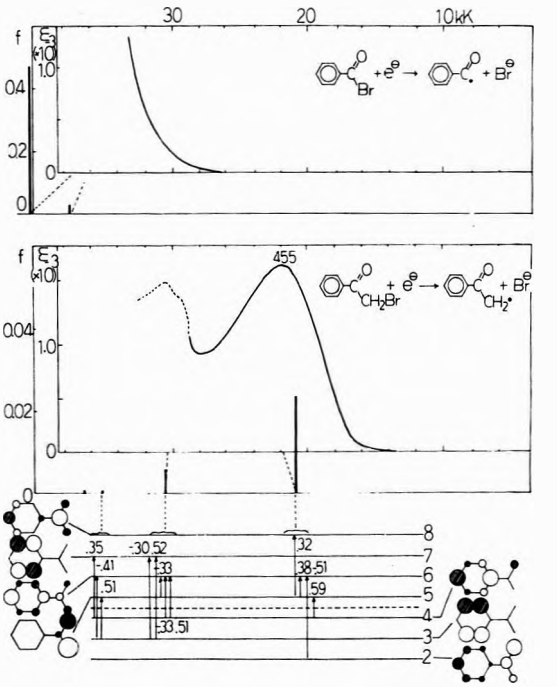

Figure 4. Absorption spectra of benzoyl and benzoylmethyl radicals. See caption to Figure 1. The sticks in the upper spectrum represent the result of a P–P–P type calculation for closed-shell benzaldehyde molecules. Note that the observed ϵ for benzoylmethyl radical is relatively small in agreement with the calculated oscillator strength.

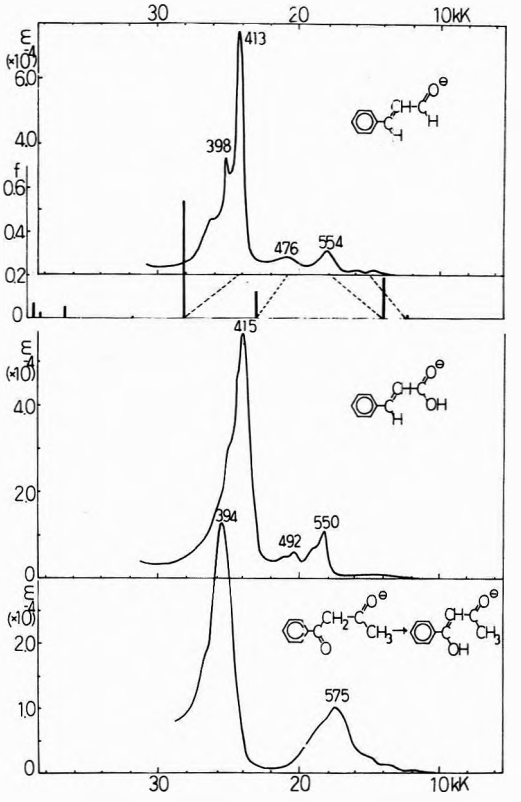

Figure 5. Absorption spectra of the cinnamaldehyde, cinnamic acid, and benzoylacetone anions. See caption to Figure 1. Since the character of the first four transitions of these anions are similar to those of the benzaldehyde anion, the MO diagram as well as the stick spectrum for cinnamic acid are omitted in the figure.

In previous papers we have shown that γ irradiation of frozen ethereal solutions is capable of producing anion radicals for a wide range of substances and providing detailed spectral information about the anions.[7,8] Therefore, the method should improve the long-standing situation of insufficient spectral data on unstable ion radicals. In this paper we have measured the spectra of a number of carbonyl compounds and analyzed the spectra in terms of a conventional π electron MO theory to confirm the experimental results.

Besides spectrochemical interest, a compilation of authentic spectra should be implemental to pulse radiolytic as well as flash photolytic studies dealing with reaction intermediates produced under high excitations. Furthermore, confirmation of the versatility of the present method by studying simpler systems would be desirable before the method is applied to the study of more complicated biological systems involving one-electron reduction and oxidation.[9]

Experimental Section

Since the experimental details are described thoroughly in previous papers,[7,8] only minimum essentials will be given below. All the anion radicals are formed by the reaction of electrons produced by the ionization of an ethereal (2-methyltetrahydrofuran) solution frozen at 77°K, and the spectrum is recorded at the same temperature. The observed spectrum at wavelengths longer than >300 nm can be attributed solely to the anion radical of solute because the radiation "debris" concomitantly produced upon irradiation absorbs only in uv regions. Except for the case where the solute is sparingly soluble the extinction

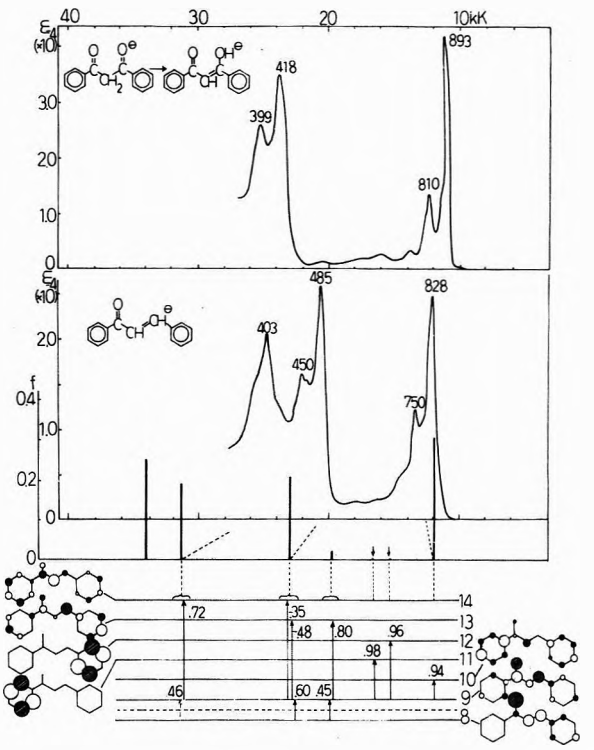

Figure 6. Absorption spectra of the dibenzoylmethane and benzalacetophenone anions. See caption to Figure 1.

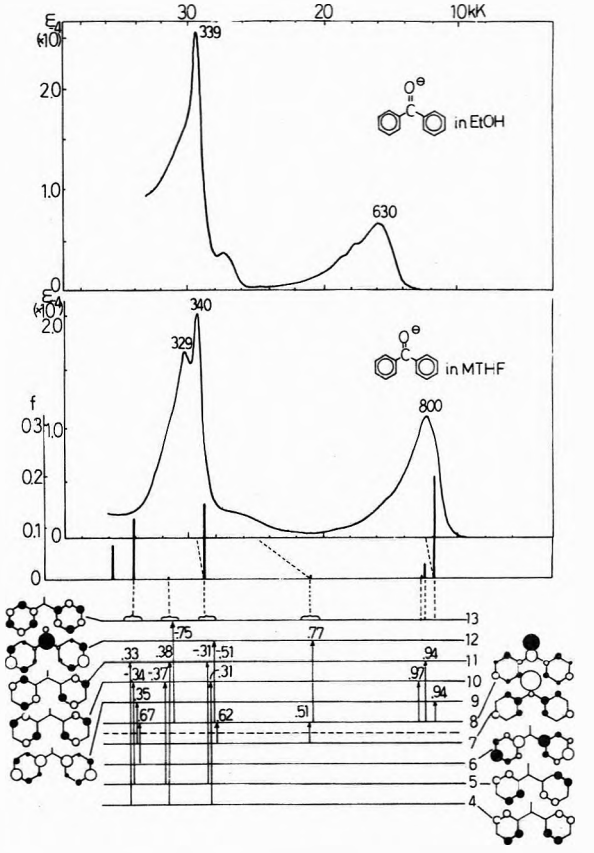

Figure 7. Absorption spectra of the benzophenone anion in ethanol and in MTHF. See caption to Figure 1. The extinction coefficient for the ethanol solution was obtained on the assumption that the yield of the total scavengeable electrons in the alcohol was $G = 2.35$.[18b]

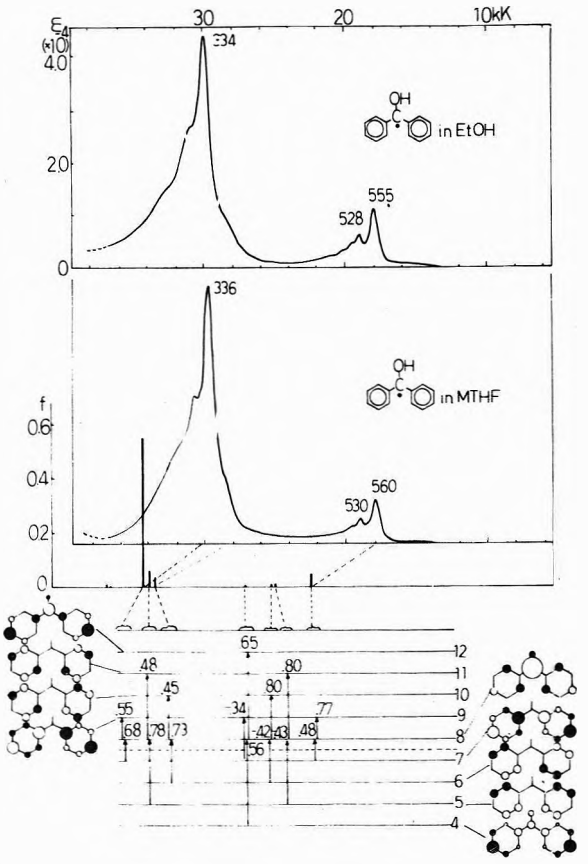

Figure 8. Absorption spectra of the benzophenone ketyl radical in ethanol and in MTHF. See caption to Figure 1.

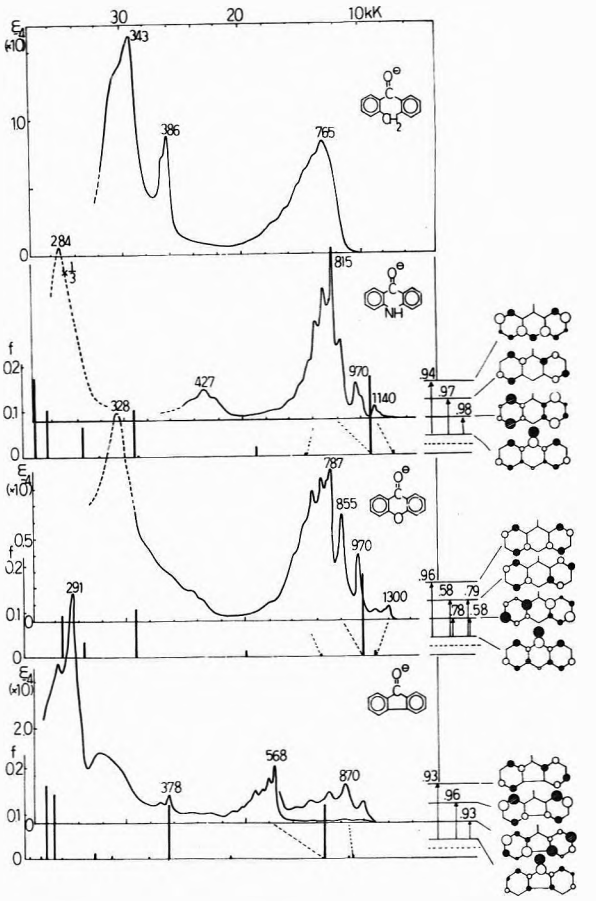

Figure 9. Absorption spectra of the benzophenone analog anions. See caption to Figure 1. The extinction coefficient for acridone could not be determined accurately owing to poor solubility. The MO diagrams are shown only for the first three transitions to demonstrate how the substituents, NH, O, C–C, affect the three MO's involving the e_{2u} orbitals of benzene.

coefficient of the solute anion can be determined fairly accurately.[7,8] Note, however, that care must be exercised when spectra at room temperatures are compared with the spectra in this paper because the absorption band is generally sharpened due to the low measurement temperature.

The MO calculation for π electronic states of anions was made using a standard semiempirical method developed by Longuet-Higgins and Pople as in the previous work.[7,8] The CI procedure with 40 configurations including some with two-electron excitations was applied.

Results and Discussion

(1) Benzaldehyde and Its Simple Derivatives. The anion of benzaldehyde exhibits the absorption spectrum shown in Figure 1. The weak absorption in the near ir (λ >700 nm) can be amplified by a prolonged irradiation as described in previous papers.[7,8] Comparison of the observed spectrum with the theoretical stick spectrum leads to the assignment indicated by the broken lines. The four transitions are characterized mainly by the configurations schematically shown at the bottom of Figure 1. (Since we regard the result of the semiempirical calculation as a confirmatory guide of the experimental result, we are not too much concerned with the numerical discrepancy between the theory and experiment. Thus, only the schematic representation is given in the figures.)

Inspection of the MO diagram shows that the first transition is attributable almost purely to charge transfer from the antibonding carbonyl to the asymmetric e_{2u} orbital of benzene. The second may be visualized as the transition between the states split from the configurations accommodating the odd electron largely in the carbonyl antibonding orbital and in the symmetric e_{2u} orbital of benzene. The two transitions are purely anionic in the sense that the excitation is caused from the half-occupied MO (5) to vacant orbitals. The third and fourth are associated with the near degenerate configurations (5 → 8) and (4 → 5) which have been split by the configuration interaction. It is seen that "molecular" configurations such as (4 → 5) and (3 → 6), that is, excitation of an electron in the orbitals below the horizontal broken line in the figure, begin to appear from the third and fourth transitions.

As will be shown later, the pattern of these four transitions is commonly observed for several other monosubstituted carbonyl compounds such as benzoic acid and cinnamaldehyde, and is also common to the prototype π electron system of styrene anion (upper spectrum of Figure 2). In the spectrum of the latter anion the first absorption band predicted in the near-ir region seems to be overshadowed by the second band having λ_{max} 595 nm. The lowest n–π^* transition expected for the benzaldehyde anion would appear in the near uv as in the case of neutral molecule, and its detection would be more difficult for the anion than for the molecule because of overlapping π–π^* transitions.

Figure 3 demonstrates the spectra of anions of benzaldehyde derivatives. Methyl and cyanomethyl substitution causes little effect on all the three observed bands of the benzaldehyde anion while the hydroxyl and amino groups

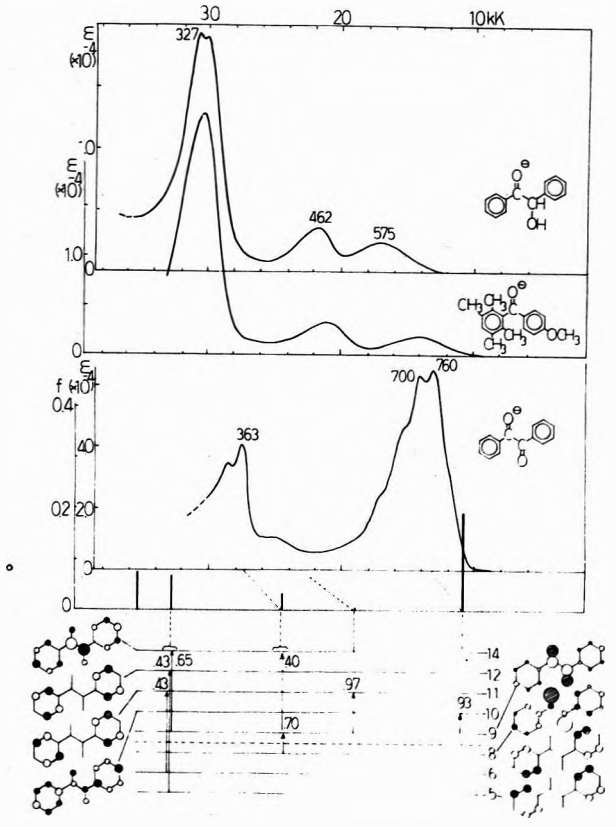

Figure 10. Absorption spectra of the benzoin, *p*-methoxyphenylduro ketone, and benzil anions. See caption to Figure 1.

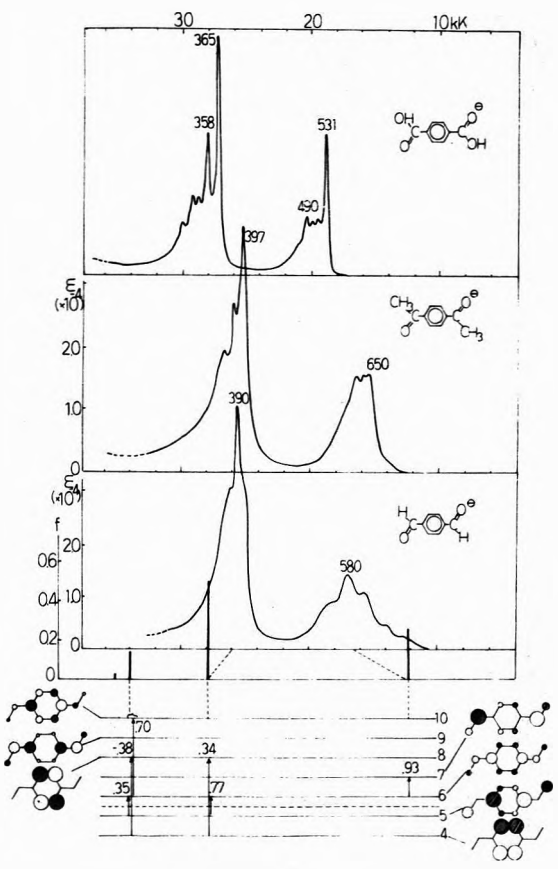

Figure 11. Absorption spectra of the terephthalic compounds anions. See caption to Figure 1. The sparing solubility of terephthalic acid prevents the determination of ϵ. Although omitted in the figure, the result of calculation for the acid indicates that the first transition should be blue shifted relative to terephthalaldehyde (transition energy = 14.37 kK, oscillator strength = 0.287) in qualitative agreement with the experimental result.

blurr the vibrational structure and shift the first band in the near ir toward the red and the second and fourth in the visible-near uv to the blue. The intensity of the second band against the fourth is slightly enhanced. These spectral features are in qualitative agreement with the calculation taking into account the two π electrons on the hydroxyl and amino groups. However, the noticeable red shift of the near-uv band upon the ortho substitution with OH and OCH_3 was not reproduced by the calculation made for both planar and twisted conformations. Whatever the reason for the discrepancy, the similarity of the spectra for the two ortho-substituted ions suggests that the intramolecular hydrogen bond in o-hydroxybenzaldehyde is not crucial in the electronic excitation of the anion.

Contrary to the chloro and fluoro derivatives giving spectra similar to that of benzaldehyde anion, benzoyl bromide yielded a quite different spectrum as shown in Figure 4. Likewise, ω-bromoacetophenone exhibits a spectrum different from the derivatives in Figure 3. The observed spectrum of the latter compound is well reproduced by the calculation of the π electron system of benzoylmethyl radical assumed to be produced by the dissociative electron attachment to ω-bromoacetophenone. By analogy, one may consider that the anion of benzoyl bromide is not stable and decomposes to the benzoyl radical and the bromide anion. If the odd electron in the benzoyl radical remains localized on the carbon atom as a σ electron, the absorption due to the π-π^* transition should be similar to that of the benzaldehyde molecule and occur in the near-uv region. The different behavior of the bromo compounds may be associated with the relatively small bond energy of C-Br compared with C-F and C-Cl. In a previous study of benzoyl chloride an absorption spectrum identifiable with that in Figure 3 has been assigned to benzoyl radical.[10] The result of the present work, however, indicates that the previous assignment is probably in error. Similar correction of assignment seems necessary for the system of cinnamic acylchloride in the previous work in view of the present result of cinnamaldehyde and cinnamic acid in Figure 5.

The character of the calculated first four transitions of the two anions in Figure 5 (cinnamaldehyde and cinnamic acid) is analogous to that of benzaldehyde anion. The predicted red shift of the major three bands as well as the blue shift of the first minor band are realized in the observed spectra, although qualitatively. Since the spectrum of the benzoylacetone anion at the bottom of Figure 5 is similar to the cinnamic compounds rather than the simple benzaldehyde derivatives, the anion appears to be in the enolic form. A brief mention of the enolation of the anion has been made by Bauld.[11] Similar enolation is apparent in the anion of dibenzoylmethane because of the striking resemblance to the spectrum of the benzalacetophenone anion in Figure 6. The anion of dibenzoylmethane has been studied by Bauld[11,12] and by Willigen and Weissman[13] who prepared the anion by alkali metal reduction. The anion has been concluded to take the form of the enolic dianion, $C_6H_5COCH{=}C(C_6H_5)O^{2-} + 2Na^+$, whose optical spectrum is affected sensitively by the metal cation and the solvent. Thus, for example, Li-, Na-, and K-treated MTHF solutions give the absorption maximum at

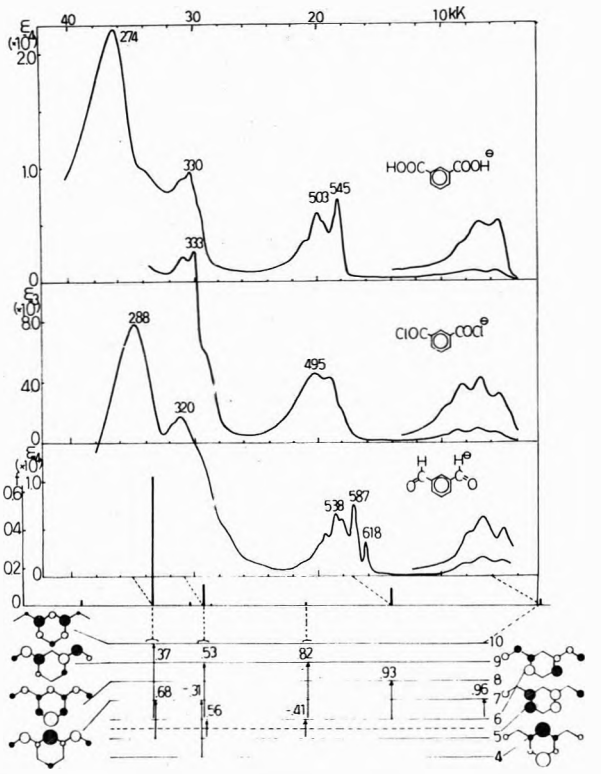

Figure 12. Absorption spectra of the isophthalic compounds anions. See caption to Figure 1.

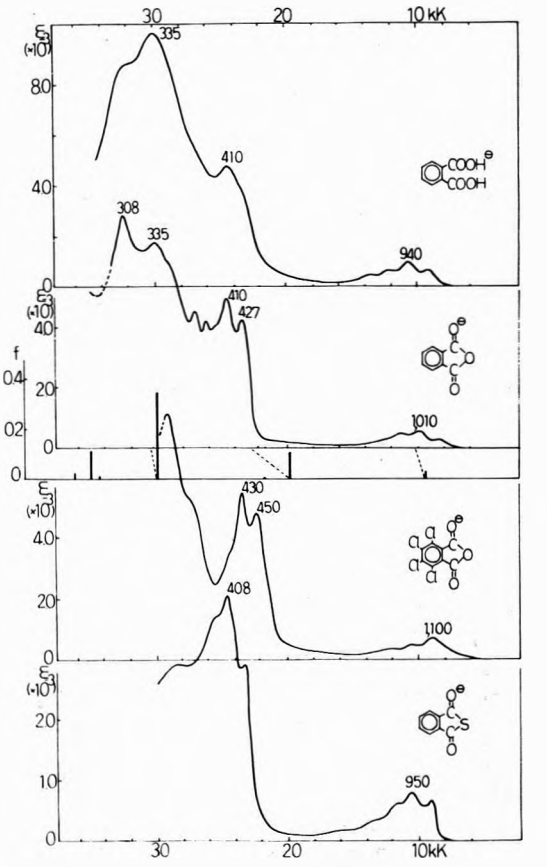

Figure 13. Absorption spectra of phthalic acid, phthalic anhydride, and related anions. See caption to Figure 1.

779, 845, and 900 nm, respectively.[13] Except for the shift and the broadening of the absorption band, the spectrum reported by Willigen and Weissman is in agreement with that in Figure 6. Therefore, the anion of dibenzoylmethane is considered to be enolic whether it is ion paired as in the previous work or free as in the present.

As is seen from comparison of MO diagrams in Figures 6 and 7, the first five transitions of benzalacetophenone bear features common to those of the benzophenone anion which will be discussed below.

The absorption spectrum of benzophenone anion has been studied by many authors,[3-6,14] who paid attention only to the visible band appearing at 600–700 nm arising from the countercation of metals used for the chemical reduction.[3] The remarkable shift upon ion pairing is discussed semiquantitatively by McClelland in terms of the stabilization of the anion in the ground state by pair formation.[5,6] For absorption other than in the visible band Broadhurst, *et al.*, reported a doublet of peaks at 339 (ϵ 1.38×10^4) and 329 nm (1.27×10^4) without showing the whole spectrum.[15]

The lower spectrum in Figure 7 shows that the visible band shifts to the near-ir region while the near-uv bands agree well with those reported by Broadhurst, *et al.*, except for the sharpening of the absorption. In addition to these bands a slight bump is seen at 25–28 kK which becomes distinct upon changing the matrix from MTHF to ethanol (upper spectrum of Figure 7) and upon binding the two phenyl rings by a methylene group (see anthrone in Figure 9). All these absorptions are assigned as in Figure 7. The first three transitions responsible for the near-ir band are associated with the intramolecular charge resonance induced by the charge migration from the carbonyl to the two benzene rings. The bump at 25–28 kK and the strong near-uv band are assigned to a couple of two split transitions. As in the case of benzaldehyde *vs.* styrene, close parallelism is seen for benzophenone and 1,1-diphenylethylene anions (see lower spectrum of Figure 2). As shown in the upper spectrum of Figure 7, the first three transitions are subject to a remarkable blue shift upon change of matrix while the higher transitions are relatively independent of the matrix. Such a difference of the effect of the hydrogen bond is understandable because the local π electron charge on the carbonyl group changes drastically only for the first three transitions.

The slight structure seen at about 560 nm in the upper spectrum of Figure 7 is due to the concomitant formation of a ketyl radical.[14] Almost complete conversion of the anion to the radical could be effected when the sample which showed the upper spectrum was slightly warmed until the blue color due to the anion turned to pink. The pink solution recooled to 77°K gave the spectrum of the ketyl radical in ethanol and MTHF as shown in Figure 8. Although the visible band has been observed repeatedly since the original flash photolytic experiment by Porter,[16] Figure 8 presents a wider scope of the spectrum. Contrary to the benzophenone anion, the solvent shift of the ketyl radical between ethanol and MTHF is relatively small. This is reasonable because the charge density on the oxygen atom, with which the hydrogen bond is formed, is little perturbed by the π electron excitations responsible for the observed absorptions. The unambiguous intensity distribution in the calculated spectrum indicates that the observed strong band at 300–340 nm corresponds to one of the two transitions split from configurations (7 → 8) and (8 → 9), the counterpart being associated with the visible band. Therefore, although the near-uv bands of the benzophenone anion and the ketyl radical are similar in general appearance, the character of the transition is not.

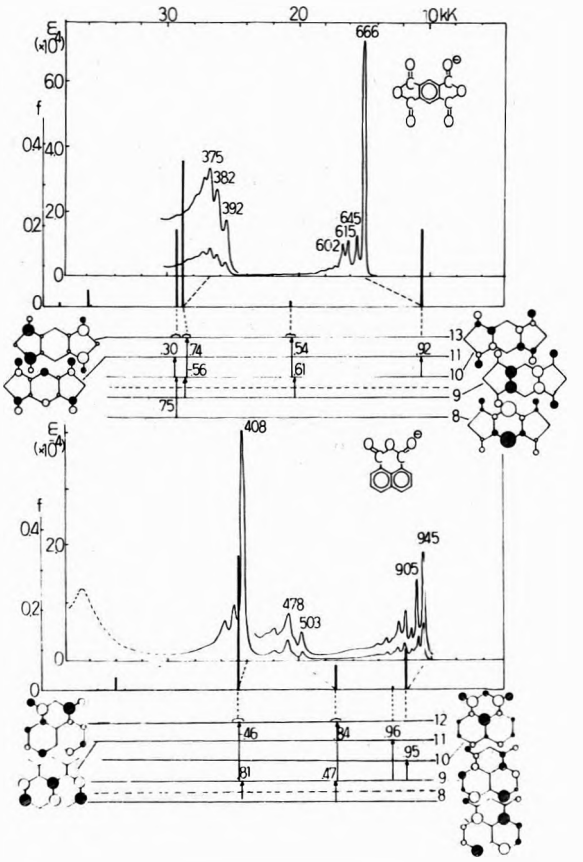

Figure 14. Absorption spectra of the pyromellitic dianhydride and 1,8-naphthalic anhydride anions. See caption to Figure 1.

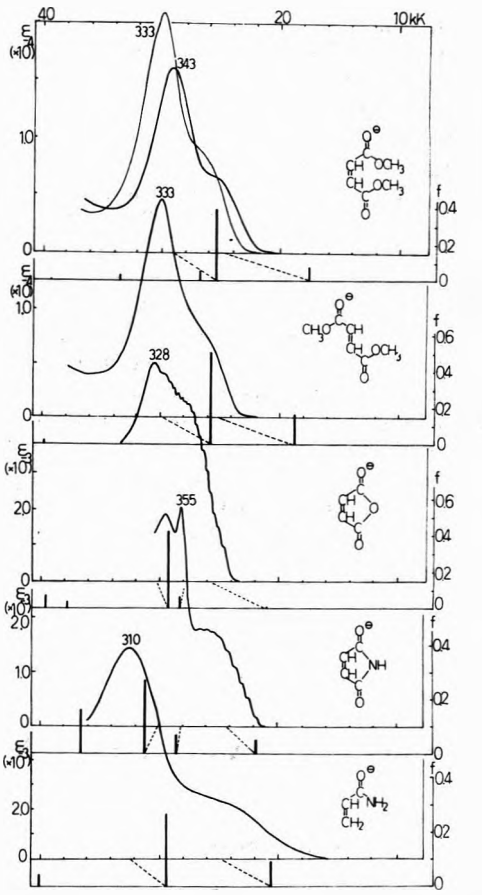

Figure 15. Absorption spectra of the anions of some aliphatic unsaturated ketones. See caption to Figure 1.

Anthrone, with the same π electron system as benzophenone, exhibits a prominent peak at 386 nm which apparently corresponds to the bump observed for benzophenone anion (top of Figure 9). The fixation of the two benzene rings also causes partial revelation of vibrational structure on the first band at 500–1000 nm. For general interest on an analogous series, the anions of acridone, xanthone, and fluorenone were studied (Figure 9). For all three anions theory predicts one strong and two weak transitions involving the charge migration from the carbonyl to two e_{2u} orbitals of benzene to appear at <15 kK as in the case of the benzophenone and 1,1-diphenylethylene anions. The phase of the sym- and asym-e_{2u} orbitals, however, differs among the four anions (benzophenone and the three in Figure 9). The appearance of one or two weak absorptions before the strong one for acridone, xanthone, and fluorenone seems to be in accord with the experiment. Of the first two weak transitions predicted for the fluorenone anion, only the one short-axis polarized seems to have been observed because the finger-like peaks at 600–1100 nm can be analyzed in terms of a fundamental of $\nu \cong 1490\ cm^{-1}$ indicative of a carbonyl stretching.

The middle spectrum of Figure 10 indicates that durosubstitution destroys the coplanarity of benzophenone to make the spectrum of the anion similar to that of simple derivatives of benzaldehyde in Figure 1 and that of benzoin at the top of Figure 10. Since benzil is known to be skewed almost orthogonally in crystal, one might expect, by analogy with the above example, a spectrum similar to that of the benzaldehyde anion. However, the observed spectrum in Figure 10 is compatible with the spectrum calculated on the assumption of a planar trans form. The MO diagram shows that the first two transitions are quite analogous to those of the benzophenone anion while the third transition identifiable with the observed absorption at 320–370 nm is proper to the diketone, that is, the transition is caused mainly between a bonding and an antibonding local orbital on the two carbonyl groups. Calculations were also made for cis planar forms but the general feature of spectrum was not comparable with the experimental. A chemical analysis of reactions of the benzil anion indicates that the anion in solution is probably in a cis form.[17] We regard the discrepancy between the two conclusions as due to the presence of metal cations in the experiment by Bauld[17] which would coordinate with the two adjacent carbonyl oxygens in the cis form.

Figures 11–13 demonstrate systematic differences among the three disubstituted benzene derivatives. The main spectral features of the three isomers can be accounted for by a simple one-electron model as in the case for the corresponding dinitrobenzenes.[7] The fact that the spectrum of the anion of phthalic acid resembles that of the anhydride anion (upper two spectra of Figure 13) seems to indicate that the intramolecular hydrogen bond and the accompanying nonplanarity of phthalic acid is not as influential in the excitation of the π electron system. As is apparent from Figures 13 and 14 (see also Figure 15 below), cyclization in the anhydrides makes the vibrational structure distinct.

Compared with the preceding aromatic compounds, anions of the simple aliphatic compounds in Figure 15 exhibit absorptions in narrower spectral regions. The overlap

of bands for maleic anhydride and maleimide renders the assignment shown by the broken lines less certain. However, the extensive vibrational structures which can be analyzed in terms of a single fundamental of $\nu \cong 305$ cm^{-1} for maleic anhydride and $\nu \cong 620$ cm^{-1} for the imide suggests that the predicted first transition with a small intensity superposes on the second and the third transitions of moderate intensities. The bold curve at the top of Figure 15 represents the absorption of the dimethylmaleate anion. This spectrum changed to that in fine curve upon illumination of light with $\lambda > 350$ nm. The latter spectrum is identical with the spectrum of the dimethylfumarate anion shown in the second part of Figure 15. The result indicates clearly the cis-trans isomerization of dimethylmaleate upon the excitation to its first electronic excited state. Similar isomerization has been observed for stilbene and alkyl disulfides.[18a] It is seen from Figure 15 that the slight blue shift on isomerization is in agreement with the results of calculations.

References and Notes

(1) P. H. Rieger and G. K. Fraenkel, *J. Chem. Phys.*, **37**, 2811 (1962).
(2) P. B. Ayscough and R. Wilson, *J. Chem. Soc.*, 5412 (1963).
(3) N. Hirota in "Radical Ions," E. T. Kaiser and L. Kevan, Ed., Interscience, New York, N. Y., 1968, p 35.
(4) K. Nakamura and N. Hirota, *Chem. Phys. Lett.*, **3**, 134, 137 (1969).
(5) B. J. McClelland, *Trans. Faraday Soc.*, **57**, 1458 (1961).
(6) H. V. Carter, B. J. McClelland, and E. Warhurst, *Trans. Faraday Soc.*, **56**, 455 (1960).
(7) T. Shida and S. Iwata, *J. Phys. Chem.*, **75**, 2591 (1971).
(8) T. Shida and S. Iwata, *J. Amer. Chem. Soc.*, **95**, 473 (1973).
(9) H. Seki, S. Arai, T. Shida, and M. Imamura, *J. Amer. Chem. Soc.*, **95**, 3404 (1973).
(10) S. Noda, K. Fueki, and Z. Kuri, *J. Chem. Phys.*, **49**, 3287 (1968).
(11) N. L. Bauld and M. S. Brown, *J. Amer. Chem. Soc.*, **89**, 5413 (1967).
(12) N. L. Bauld, *J. Amer. Chem. Soc.*, **86**, 2305 (1964).
(13) H. Willigen and S. I. Weissman, *Mol. Phys.*, **11**, 175 (1966).
(14) T. Shida and W. H. Hamill, *J. Amer. Chem. Soc.*, **88**, 3683 (1966).
(15) J. G. Broadhurst, J. C. Chippendale, and E. Warhurst, *Trans. Faraday Soc.*, **64**, 2586 (1968).
(16) G. Porter and F. Wilkinson, *Trans. Faraday Soc.*, 57, 1686 (1961).
(17) N. L. Bauld, *J. Amer. Chem. Soc.*, **87**, 4788 (1965).
(18) (a) T. Shida, *J. Phys. Chem.*, **72**, 2597 (1968); (b) **74**, 3055 (1970).

Sticking Coefficient Curves Expected for Multilayer Adsorption

Isao Kusunoki

Research Institute for Scientific Measurements, Tohoku University, Sendai, Japan

(Received August 17, 1973)

Publication costs assisted by Tohoku University

Assuming multilayer adsorption similar to that seen in the BET model, a series of rate equations, in which beam flux I, the number of adsorption sites N, and two kinds of mean residence times of adatoms labeled τ_1 and τ_2 are only contained as parameters, has been derived to interpret the phenomenon observed in our atomic beam experiments in a previous paper. It has been revealed that some known types of rate equations on adsorption can be deduced from the basic equations. The sticking coefficient has been also expressed as a function of the parameters I/N, τ_1, and τ_2. The sticking coefficient curves are classified into six groups according to the exposure time or the surface coverage. The conditions for the attainment of the adsorption equilibrium or for the vapor condensation have been established by the present model.

Introduction

Although various rate equations for adsorption, among which the Langmuir equation is most famous, have been proposed by many investigators,[1] rate equations applicable to multilayer adsorption are few. Some recent theories on the growth of thin films[2] have treated condensation processes by using various sets of rate equations, and have received a great deal of attention. These equations are, however, very complicated, because many parameters, such as the decay time of the aggregates, lifetime of adatoms on surface, collision probability of aggregates on surface, etc., are involved.

In adsorption experiments using atomic beams, we observed an interesting phenomenon that the sticking coefficient of the potassium atoms on a mica surface changed with the increasing exposure time. That is, in the initial period of exposure the sticking coefficient decreases gradually from unity, but if accumulation of the beam atoms on the surface exceeds a certain value, it increases and gradually approaches a saturated value. To interpret this phenomenon we proposed a series of rate equations in the previous paper.[3] In the present paper the applications of the basic equations will be discussed.

Theory

(*a*) *Model and Basic Equations.* Figure 1 shows the schematic processes of dynamic adsorption in the present model. Beam flux is given by I (molecules cm^{-2} sec^{-1}) and the number of elementary sites on the surface by N (sites cm^{-2}). It is also assumed that the atom impinging on the surface is always trapped at the site, but the atom impinging on the site occupied by the Lth layer is reflected. Atoms trapped on bare sites are assumed to evaporate after a mean residence time τ_1, unless they are confined to the sites by the adsorption of other atoms on the top of them. Atoms adsorbed in the multilayer can only evapo-

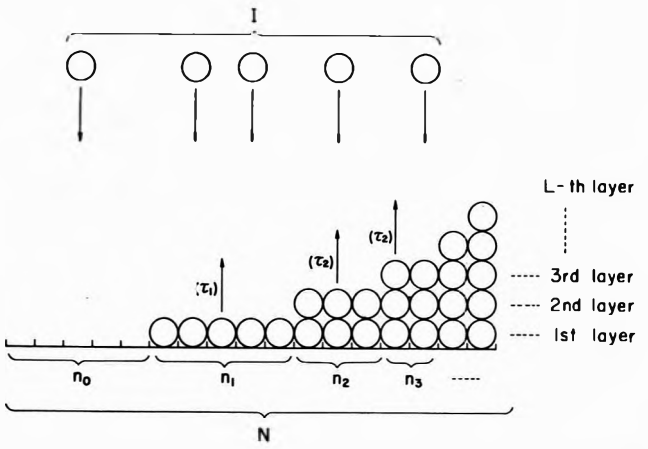

Figure 1. A schematic drawing of the adsorption and desorption processes of atoms in the present model.

rate from the uppermost layer individually, and the mean residence time of the adatoms in every uppermost layer is assumed to have an identical value expressed by τ_2. At time t, the number of bare sites is n_0, that of the sites occupied by the monolayer n_1, those occupied by the double layers n_2, and so on. According to this model, rate equations for multilayer adsorption are given by

$$\frac{dn_0}{dt} = -\frac{In_0}{N} + \frac{n_1}{\tau_1}$$

$$\frac{dn_1}{dt} = \frac{I}{N}(n_0 - n_1) - \frac{n_1}{\tau_1} + \frac{n_2}{\tau_2}$$

$$\frac{dn_2}{dt} = \frac{I}{N}(n_1 - n_2) - \frac{1}{\tau_2}(n_2 - n_3)$$

$$\cdots\cdots$$

$$\frac{dn_L}{dt} = \frac{I}{N}n_{L-1} - \frac{n_L}{\tau_2} \tag{1}$$

where

$$N = \sum_{i=1}^{L} n_i \tag{2}$$

If a sticking coefficient S is defined as

$$S = \sum_{i=1}^{L} i\frac{dn_i}{dt}/I \tag{3}$$

then eq 1 yields

$$S = 1 - \frac{n_1}{\tau_1 I} - \frac{1}{\tau_2 I}\sum_{i=2}^{L} n_i - \frac{n_L}{N} \tag{4}$$

(*b*) $L = 1$ *Case.* In this case, eq 1 are transformed into

$$\frac{dn_1}{dt} = \frac{I}{N}(N - n_1) - \frac{n_1}{\tau_1} \tag{5}$$

which corresponds to the Langmuir equation

$$dv/dt = k_1(v_m - v) - k_2 v$$

where v is the volume of the adsorbed gas and v_m that of the adsorbed gas when all sites of adsorption are covered with a monolayer only. The solution of eq 5 is

$$n_1 = (I/A)[1 - \exp(-At)] \tag{6}$$

where

$$A = (I/N) + (1/\tau_1)$$

Equation 6 indicates that the surface coverage θ_e at the adsorption equilibrium is

$$\theta_e = \frac{I}{AN} = \frac{1}{1 + (N/\tau_1 I)} \tag{7}$$

According to the definition given by eq 3, the sticking coefficient S as a function of the exposure time is obtained by differentiating eq 6, namely

$$S(t) = \frac{1}{I}\frac{dn_1}{dt} = e^{-At} \tag{8}$$

The sticking coefficient S as a function of the surface coverage, $\theta = n_1/N$, can also be obtained from eq 5.

$$S(\theta) = 1 - [1 + (N/\tau_1 I)]\theta \tag{9}$$

(*c*) $L = 2$ *Case.* In this case, the solutions of eq 1 are given by

$$n_1 = \frac{I}{\alpha\beta\tau_2}\left\{1 - \frac{\beta(\alpha\tau_2 - 1)}{\sqrt{H}}e^{-\alpha t} - \frac{\alpha(\beta\tau_2 - 1)}{\sqrt{H}}e^{-\beta t}\right\} \tag{10}$$

and

$$n_2 = \frac{I^2}{\alpha\beta N}\left\{1 + \frac{\beta}{\sqrt{H}}e^{-\alpha t} - \frac{\alpha}{\sqrt{H}}e^{-\beta t}\right\} \tag{11}$$

Here

$$H = (1/\tau_1 - 1/\tau_2)^2 + (4I/N\tau_1)$$

$$\alpha = (B + \sqrt{H})/2$$

$$\beta = (B - \sqrt{H})/2$$

and

$$\alpha\beta = (I/N)^2 + (I/N\tau_2) + (1/\tau_1\tau_2)$$

where

$$B = (2I/N) + (1/\tau_1) + (1/\tau_2)$$

Since $H > 0$, $B > 0$, and $\alpha\beta > 0$, it is clear that $\alpha > 0$ and $\beta > 0$. The total number of adatoms is represented by

$$\sigma(t) = n_1 + 2n_2 = \frac{1}{\alpha\beta}\left(\frac{1}{\tau_2} + \frac{2I}{N}\right)[1 - c_1\exp(-\alpha t) - c_2\exp(-\beta t)] \tag{12}$$

where

$$c_1 = \left(\alpha - \frac{1}{\tau_2} - \frac{2I}{N}\right)\frac{\beta}{\sqrt{H}}\Big/\left(\frac{1}{\tau_2} + \frac{2I}{N}\right)$$

and

$$c_2 = \left(-\beta + \frac{1}{\tau_2} + \frac{2I}{N}\right)\frac{\alpha}{\sqrt{H}}\Big/\left(\frac{1}{\tau_2} + \frac{2I}{N}\right)$$

Then

$$c_1 + c_2 = 1$$

If we have a rate equation expressed by

$$v = v_e[1 - c_1\exp(-\alpha t) - c_2\exp(-\beta t)] \tag{13}$$

the values of τ_1, τ_2, and I/N will be estimated from α, β, and c_1.

Differentiating eq 12, the sticking coefficient as a function of the exposure time can be obtained as

$$S(t) = \frac{1}{\sqrt{H}}\left\{\left(\alpha - \frac{1}{\tau_2} - \frac{2I}{N}\right)e^{-\alpha t} - \left(\beta - \frac{1}{\tau_2} - \frac{2I}{N}\right)e^{-\beta t}\right\} \tag{14}$$

From eq 10 and 11, it is evident that at adsorption equi-

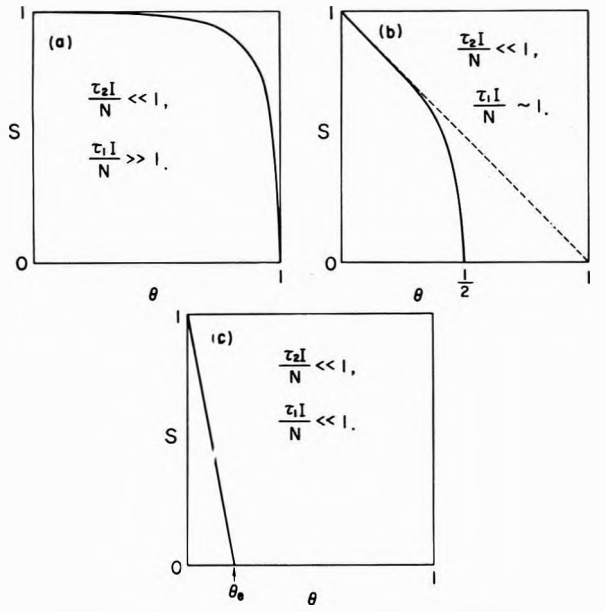

Figure 2. Sticking coefficient curves predicted by various conditions of eq 15.

librium ($t \rightarrow \infty$) n_1 and n_2 are given by $I/\alpha\beta\tau_2$ and $I^2/\alpha\beta N$, respectively, and the ratio of n_2/n_1 is equal to $\tau_2 I/N$. If $\tau_2 I/N \ll 1$, n_2/n_1 is always very small and θ is given by n_1/N. Then, eq 4 results in

$$S(\theta) \simeq 1 - [(N/\tau_1 I) + (N/\tau_2 I)(n_2/n_1)]\theta \quad (15)$$

In this case sticking coefficient curves as shown in Figure 2 are expected.

(*d*) $L = \infty$ *Case.* In the general case of eq 1 the sticking coefficient is defined as

$$S = \lim_{L\to\infty} \sum_{i=1}^{L} i \frac{dn_i}{dt} / I \quad (16)$$

with a plausible assumption

$$\lim_{L\to\infty}(n_L/N) = 0 \quad (17)$$

Now, it is convenient to introduce new parameters as follows: $\theta_i = n_i/N$, $\theta = \Sigma_{i=1}^{\infty} \theta_i$, and $T = It/N$. Using these parameters, eq 1 are rewritten by

$$\begin{aligned} d\theta_1/dT &= 1 - (1 + a)\theta_1 + b\theta_2 - \theta \\ d\theta_2/dT &= \theta_1 - (1 + b)\theta_2 + b\theta_3 \\ &\cdots\cdots \end{aligned} \quad (18)$$

where $a = N/\tau_1 I$ and $b = N/\tau_2 I$. From the above equations, the relations

$$S = 1 - (a - b)\theta_1 - b\theta \quad (19)$$

and

$$d\theta/dT = 1 - a\theta_1 - \theta \quad (20)$$

are obtained.

In the beginning of the exposure θ will be nearly equal to θ_1 as expected from the relations of $d\theta_1/dT = 1$ and $d\theta_i/dT = 0$ ($i \geq 2$) at $T = 0$, and then

$$\theta \cong \frac{1}{1 + a}[1 - e^{-(1+a)T}] = T - \frac{1 + a}{2}T^2 \ldots \quad (21)$$

Since $\lim_{T\to 0}(d\theta/dT) = 1$, the following relations hold

$$\lim_{T\to 0} \frac{dS}{dT} = -a \quad (22)$$

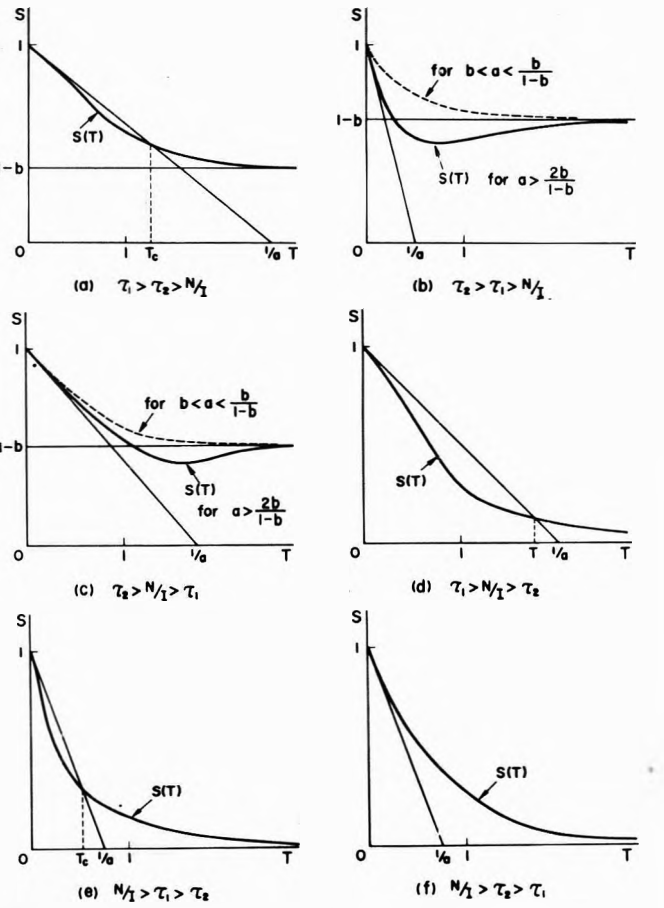

Figure 3. Sticking coefficient curves predicted as a function of T.

and

$$S \simeq 1 - a\theta \simeq 1 - aT \quad \left(\text{for } T \ll \frac{2}{1 + a}\right) \quad (23)$$

(which corresponds to $S = 1 - (t/\tau_1)$ in the S–t coordinate).

The sign of $\Delta S \equiv S - (1 - aT)$ is as follows. If $a > b$, $\Delta S \geq 0$; and if $b > a$, $\Delta S \leq 0$ for $T < T_c$, and $\Delta S \gtrless 0$ for $T > T_c$, where $T_c = [(b/a) - 1](\theta(T_c) - \theta_1(T_c)) + \theta(T_c)$.

If $b < 1$, it is clear that $S > 0$. In this case, the beam atoms will be trapped by the surface and θ will approach unity with exposure time. Then, the extreme conditions can be given by

$$\lim_{T\to\infty} \frac{dS}{dT} = 0 \quad (24)$$

and

$$\lim_{T\to\infty} S = 1 - b \quad (25)$$

If $b > 1$, the adsorption equilibrium can be attained after long exposure time, and the final surface coverage θ_e is obtained from the conditions of $S = 0$ and $d\theta/dT = 0$ as

$$\theta_e = \frac{1}{1 + a - (a/b)} \quad (26)$$

Near the equilibrium, the relation

$$\lim_{T\to\infty} \frac{dS}{dT} = 0 \quad (27)$$

also clearly holds.

TABLE I: Approximate Formulas for Sticking Coefficient

Condition	Sticking coefficient
$a \gg 1$	$S \simeq e^{-aT}$ for $b > 1$ $S: 0 \rightarrow 1 - b$ for $b < 1$ and $T \not\simeq 0$
$a \ll 1 \ll b$	$S \simeq e^{-T}$ for $T \not\simeq 0$
$a \gg 1 \gg b$	$S \simeq 1$
$b \gg 1$	$S = e^{-(1+a)T}$ for $T \not\simeq 0$
$b \ll 1$	$S = 1 + \frac{1}{\sqrt{1 + 4/a}} [e^{-\gamma T} - e^{-\delta T}]$ where $\gamma = 1 + (a/2) + \sqrt{(a/2)^2 + a}$ and $\delta = 1 + (a/2) - \sqrt{(a/2)^2 + a}$

The sign of dS/dT is as follows. If $a < b$, $dS/dT < 0$; if $a > b > 1$, $dS/dT < 0$; if $a > b$ and $b < 1$, the sign changes from negative to positive when $a > 2b/(1 - b)$ but it does not change when $a < b/(1 - b)$.

Considering these relations, six types of S–T curves are expected as shown in Figure 3. Similarly, S–θ curves can be classified into six types as shown in Figure 4.[4] However, b and d in Figure 3 or 4 can not be distinguished from c and e, respectively, unless I/N is known. In the S–T curves it will be difficult to measure the difference of e and f, because the magnitude of ΔS may be very small in these cases. Under some extreme cases, one can find the approximate formulas of the sticking coefficient as shown in Table I.

Discussion

There are two interesting points to be discussed in this model. One of them is the relation of the rate equations in the case of $L = \infty$ to the "BET" isotherm.[5] Under adsorption equilibrium, dn_i/dt in each step in eq 1 can be set equal to zero. Then, one can obtain the relations

$$\tau_1 I/N = n_1/n_0$$

and

$$\tau_2 I/N = n_2/n_1 = n_3/n_2 = \ldots (\equiv 1/b) \qquad (28)$$

Under the condition of $b > 1$, an equation similar to the BET isotherm is obtained by a treatment similar to that described in some textbooks[6]

$$\frac{v}{v_m} = \sum_{i=0}^{\infty} i n_i \Big/ \sum_{i=0}^{\infty} n_i = \frac{c/b}{(1 - 1/b)\{1 + (c - 1)/b\}} \qquad (29)$$

where $c = \tau_1/\tau_2$.

The other point is concerned with nucleation of evaporated film. If the condition of $b < 1 < a$ is satisfied, the growth rate of clusters of adatoms, I/N, is greater than the decay rate of the clusters, $1/\tau_2$, but the condition of $I/N < 1/\tau_1$ makes the bare sites remain as they are. In this case it may also be considered that the surface migration of adatoms will contribute to the formation of clusters of adatoms.

The important problem in future work is how to take mutual interactions of atoms adsorbed in different sites into account. A simple model considered may be that the atoms in the first monolayer have two different residence times, depending on whether the nearest neighbor sites are occupied by adsorbed atoms or not. However, the estimation of the number of the atoms having different residence times seems very difficult. Even if a way to estimate it is found, the rate equations become nonlinear and it will be difficult to solve them.

With regard to the formula of the sticking coefficient, however, a plausible one

$$S = 1 - \frac{N}{I} \sum_i \theta_i/\tau_i \qquad (30)$$

is obtained by generalizing eq 19. This formula holds well even when migration, recombination, and dissociation of adatoms occur on the surface. A discussion of this will appear elsewhere.

Acknowledgment. The author wishes to thank Professor Hokotomo Inouye, Professor Kumasaburo Kodera, and Mr. Shinji Tomoda for their advice and contributions to this work.

Supplementary Material Available. Figure 4 (the procedures used in drawing S–θ curves) will appear following these pages in the microfilm edition of this volume of the journal. Photocopies of the supplementary material from this paper only or microfiche (105 × 148 mm, 24× reduction, negatives) containing all of the supplementary material for the papers in this issue may be obtained from the Journals Department, American Chemical Society, 1155 16th St., N.W., Washington, D. C. 20036. Remit check or money order for $3.00 for photocopy or $2.00 for microfiche, referring to code number JPC-74-748.

References and Notes

(1) G. W. McBain, *Z. Phys. Chem.*, **68**, 471 (1909); I. Langmuir, *J. Amer. Chem. Soc.*, **40**, 1361 (1918); D. H. Bangham and W. Sever, *Phil. Mag.*, **49**, 935 (1925); J. Samejima, *Bull. Chem Soc. Jap.*, **7**, 177 (1932); S. Rosinsky and Ya Zeldovich, *Acta Physicochim.*, **1**, 554, 595 (1934); S. Yu. Elovich and G. M. Zhabrova, *Zh. Fiz. Khim.*, **13**, 1761, 1775 (1939).
(2) G. Zinsmeister, *Vacuum*, **16**, 529 (1966); *Thin Solid Films*, **2**, 497 (1968); **4**, 393 (1969); **7**, 51 (1971); R. M. Logan, *Thin Solid Films*, **3**, 59 (1969).
(3) S. Tomoda, I. Kusunoki, and K. Kodera, *Chem. Lett.*, 669 (1973).
(4) See paragraph at end of paper regarding supplementary material.
(5) S. Brunauer, P. H. Emmett, and E. Teller, *J. Amer. Chem. Soc.*, **60**, 309 (1938).
(6) J. H. deBoer, "The Dynamical Character of Adsorption," Oxford, London, 1953; D. M. Young and A. D. Crowell, "Physical Adsorption of Gases," Butterworths, London, 1962.

Yields of Radiation Products in Sodium Metaphosphate Glasses

Yoshimitsu Kobayashi,[1] Aaron Barkatt,*[1b] and Joseph Rabani

Department of Physical Chemistry, The Hebrew University, Jerusalem 91000, Israel *(Received July 23, 1973; Revised Manuscript Received January 2, 1974)*

Metaphosphate glasses have been irradiated and dissolved in aqueous solutions, where the trapped positive and negative species, MP^+ and MP^-, respectively, reacted with scavengers. I^-, O_2, $Fe(CN)_6^{4-}$, Fe^{3+}, and TMPD have been used to scavenge MP^+ and MP^-. From product analysis, $G(MP^+) = G(MP^-) = 2.2 \pm 0.1$ was calculated. Combining this with absorbance measurements in glasses yields $\epsilon^{500}(MP^+)$ (the extinction coefficient of MP^+ at 500 nm) = $(1.92 \pm 0.17) \times 10^3\ M^{-1}\ cm^{-1}$. MP^- reacts with aqueous O_2 to produce peroxy radicals (O_2^- or MPO_2^-). Whatever peroxy radicals are formed, they decay in water to produce H_2O_2. MP^- does not react with N_2O and does not produce H_2 upon reaction with alcohols in acid solutions. It is concluded that MP^- does not form e_{aq}^- or H upon its interaction with water. Pulse radiolysis experiments show that aqueous solutions of metaphosphate are relatively inert toward e_{aq}^- and OH. $k(e_{aq}^- + MP) < 1 \times 10^6$ and $k(OH + MP) < 5 \times 10^6\ M^{-1}\ sec^{-1}$.

Introduction

Upon irradiation of sodium metaphosphate (MP) glass by ionizing radiations, several absorption bands in the optical and esr spectra appear. These were assigned to electron-deficiency (hole) and electron-excess centers, respectively.[2a]

The processes leading to the formation of these products over an interval of up to 10^{-2} sec after irradiation were previously investigated.[2b]

It is the purpose of the present work to determine the G values of the stable products. The techniques employed here are based on analyzing the effects produced by the dissolution of the irradiated glasses in aqueous solutions. Similar effects have been investigated previously for solids, especially alkali halides, and they include detection of light emission,[3] pH measurements,[4] H_2 analysis,[5] and investigations of redox reactions with solutes. These reactions include the oxidation of I^- to I_3^-,[5] of Fe^{2+} to Fe^{3+},[6] and of tetramethyl-*p*-phenylenediamine (TMPD) to Wurster's blue.[7] Reduction processes investigated included the conversion of tetranitromethane (TNM) to nitroform[7] and the formation of N_2 from N_2O.[8]

Another system utilized in the present work was the reduction of Fe^{3+} to Fe^{2+} in the presence of methanol, previously employed in the radiation chemistry of aqueous solutions.[9]

The use of suitable systems makes it possible to determine the yields of the stable radiation products and their reactivity in aqueous solutions. Comparison with the initial yields of their precursors enables us to test whether the change in optical absorption observed during the stabilization process involve annealing.

Experimental Section

Irradiations were carried out with a Radiation Machinery Corporation ^{137}Cs γ source. The dose rate was measured by means of the Fricke dosimeter taking $G(Fe^{3+}) = 15.6$ molecule/100 eV. (The results agreed within 5% with results obtained by means of Co^{2+}-doped 2-mm thick glass plates calibrated by the Soreq Nuclear Research Center, Israel.)[10] The dose was 6.68×10^{18} eV hr^{-1} g^{-1} unless otherwise stated.

The method of preparation of sodium metaphosphate (MP) glass disks was described earlier.[11]

The chemical composition of these samples was $(NaPO_3)_n$, where $n \cong 50$, and with -OH terminal groups.

The disks were 1.60–1.80-mm thick and weighed 1.0–1.5 g. All the reagents employed were of AR quality. High-purity Ar, O_2, and N_2O (Matheson Co.) were used. Ar and N_2O were purified by bubbling through a trap of V^{2+} (prepared by shaking together NH_4VO_3 and zinc amalgam in concentrated HCl)[12] and subsequently through traps of NaOH and of triply distilled water.

Solutions for the dissolution of the irradiated glasses were prepared using triply distilled water. The optical densities of the dissolved irradiated glass samples were measured with the aid of a Beckman DB-G spectrophotometer against reference solutions containing the same reagents and the same amounts of unirradiated glass. All measurements were carried out at a temperature of 25 ± 2°.

Results

Determination of Yields. The yields of the oxidized and reduced products of the irradiation of MP glass were determined by dissolving the glass samples in the following solutions: air-saturated KI, air-saturated $K_4Fe(CN)_6$, air-saturated TMPD, and Ar-saturated methanol-containing $Fe(ClO_4)_3$.

In all cases, the following precautions had to be taken in order to obtain reproducible results. (1) The glass was crushed into fragments weighing less than 50 mg each before irradiation. During dissolution the water was vigorously stirred. This prevented recombination near the surface, so that the radicals reacted exclusively with the solutes. We have found that a further increase in the rate of stirring did not affect the results under our conditions. (2) The dissolution took place immediately after irradiation to minimize the effect of thermal decay.

In all cases, 500-mg MP samples were dissolved in 25-ml scavenger solutions. Dissolution was usually complete within 20 min. Optical densities obtained with samples irradiated for long periods (in the KI system) were read after appropriate dilution.

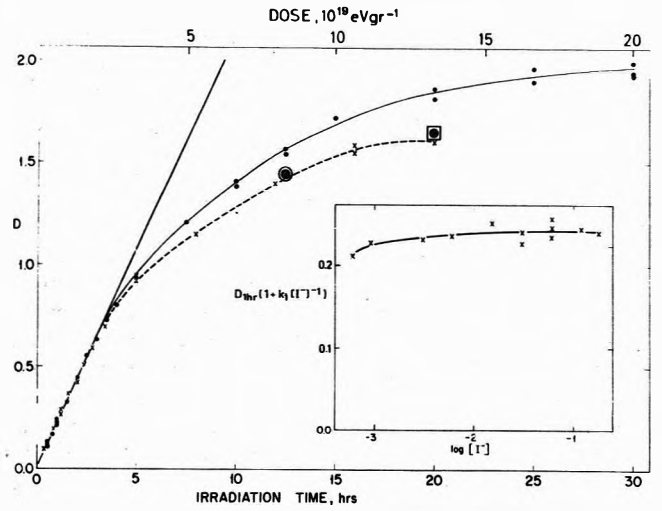

Figure 1. Dissolution of irradiated MP in air-saturated 0.06 *M* KI (λ 353 nm, *l* = 1 cm): (●) dose rate 6.68 × 10^{18} eV g^{-1} hr^{-1}; (⊙) 20-hr delay before dissolution; (⊡) 30-hr delay before dissolution; (×) dose rate 2.67 × 10^{18} eV g^{-1} hr^{-1}, time scale divided by 2.5.

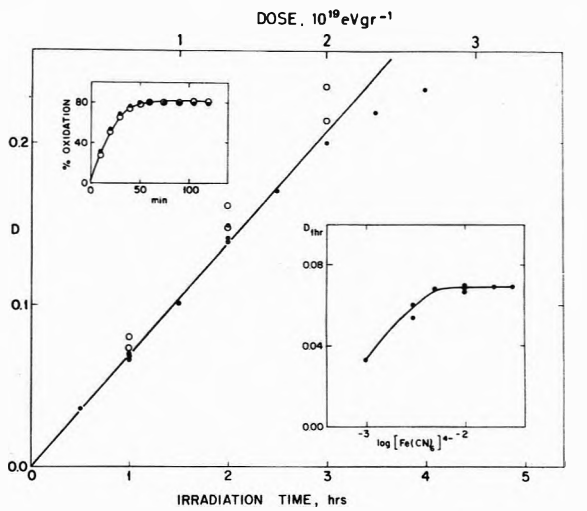

Figure 2. Dissolution of irradiated MP in air-saturated 0.01 *M* $K_4Fe(CN)_6$ (λ 420 nm, *l* = 4 cm): (●) pH 2.1, 75–90 min after dissolution; (○) pH 4.5, 20 min after dissolution; (upper inset) oxidation of 0.01 *M* $K_4Fe(CN)_6$ by 1 × 10^{-5} *M* H_2O_2: (○) 0.2 *M* MP, 0.05 *M* H_2SO_4 (pH 2.1); (●) 0.01 *M* H_2SO_4 (pH 2.1).

(*a*) *Aerated KI.* The extent of the oxidation of KI to iodine was determined by reading the optical density *D* due to I_3^- at 353 nm, where $\epsilon = (25{,}700 \pm 300)$ M^{-1} cm^{-1}.[13] Corrections were carried out for the equilibrium

$$I_2 + I^- \underset{}{\overset{K_1}{\rightleftharpoons}} I_3^- \quad (K_1 = 774\ M^{-1})^{14} \qquad (1)$$

The results obtained for the optical density at 353 nm as a function of irradiation time are given in Figure 1. Note that $D_{1hr}(1 + (K_1[I^-])^{-1})$ represents the optical density which would have been obtained had all the iodine been in the form of I_3^- irrespective of $[I^-]$. Air-saturated aqueous solutions acidified with H_2SO_4 were employed, and the optical densities were read 10–15 min after the end of the dissolution. The results were independent of $[H^+]$ over the range of pH 2–5. They were also not changed by saturation with O_2 instead of air. No concentration effect on the total iodine ($I_3^- + I_2$) can be observed within experimental error at $>10^{-3}$ *M* KI. From Figure 1 it can also be seen that the total iodine production is linearly dependent on the irradiation time of the sample up to 3 hr (2 × 10^{19} eV g^{-1}), yielding (9.6 ± 0.4) × 10^{-6} *M* total iodine/hr. The same initial slope is obtained at a dose rate lower by a factor of 2.5.

The difference between the high and the low dose rate curves (Figure 1) is due to some thermal annihilation which is more important at low dose rates (longer irradiation time). This effect has been confirmed by direct observation of the visible absorption in undissolved glasses (see Figure 5). It can be seen from both figures that irradiation at a high dose rate and subsequent delay gave practically the same results as irradiation with the same dose at a slower rate over the same overall period of time.

(*b*) *I^- Saturated with O_2, N_2O, or Ar at pH 2 and 4.* The results obtained upon dissolving the irradiated glasses in O_2-saturated solutions were identical with those obtained in aerated solutions. When Ar or N_2O were used instead of O_2, only about 10% of the I_3^- was obtained. When I_2 (~5 × 10^{-5} *M*) was initially present in the Ar- or N_2O-saturated 6 × 10^{-2} *M* I^- solution, no effect on $[I_3^-]$ could be observed upon dissolving the irradiated glass.

(*c*) *Aerated $K_4Fe(CN)_6$.* The solutions were prepared in 0.05 *M* H_2SO_4, and the pH after introduction of 20 g $l.^{-1}$ of MP was 2.1. The production of $Fe(CN)_6^{3-}$ was measured 75–90 min after the end of the dissolution by reading the optical density at 420 nm. The absorption of $Fe(CN)_6^{3-}$ at this wavelength was found to be independent of the presence of MP, with a molar extinction coefficient of (1000 ± 50) M^{-1} cm^{-1} in agreement with previous data.[15] The dependence of $Fe(CN)_6^{3-}$ absorption on irradiation time was linear in 0.01 *M* ferrocyanide up to 3 hr at least (see Figure 2), and the resulting yield of $[Fe(CN)_6^{3-}]$ was (17 ± 1) × 10^{-6} *M*/hr. We found that using a constant dose (1-hr irradiation) *D* increased with $Fe(CN)_6^{4-}$. Above 5 × 10^{-3} *M* ferrocyanide, *D* became independent of [ferrocyanide] (Figure 2).

(*d*) *Aerated TMPD.* In the case of air-saturated TMPD the production of Wurster's blue was measured at 600 nm. The introduction of MP did not change the absorption at this wavelength and the value used for ε was accordingly 10,100 M^{-1} cm^{-1}.[16] The oxidation of TMPD by air over the dissolution time (<20 min) was very slight and was corrected for by measuring the absorbance against a reference solution which contained unirradiated MP dissolved under the same conditions in the same concentration of TMPD. The [product] dependence on irradiation time at 1 m*M* TMPD was linear up to at least 4 hr (see Figure 3) yielding (10.3 ± 0.4) × 10^{-6} *M* product/hr. At constant dose (1-hr irradiation) *D* increased with [TMPD]. *D* became independent of [TMPD] at concentrations >5 × 10^{-4} *M* (see Figure 3). As in the case of I^-, there was no effect of $[O_2]$ which was varied from 2.6 × 10^{-4} to 1.3 × 10^{-3} *M*. Replacing the O_2 by Ar or N_2O resulted in the elimination of the product (Wurster's blue).

(*e*) *Ar-Saturated Methanol-Containing $Fe(ClO_4)_3$.* Aqueous 1,10-phenanthroline (5 ml of 0.25% solution) was added at the end of the dissolution in a Fe^{3+}–methanol aqueous solution. The optical density of the Fe^{2+}–1,10-phenanthroline complex was read at 515 nm. Although MP apparently forms a complex with Fe^{3+}, suppressing its yellow color, it has no effect on the absorption of Fe^{2+}–1,10-phenanthroline at pH 3, where it was found to have a molar extinction coefficient of (11,000 ± 300) M^{-1} cm^{-1} in accordance with previous data.[17] The data (for a total volume of 30 ml) is presented in Figure 4, where a linear

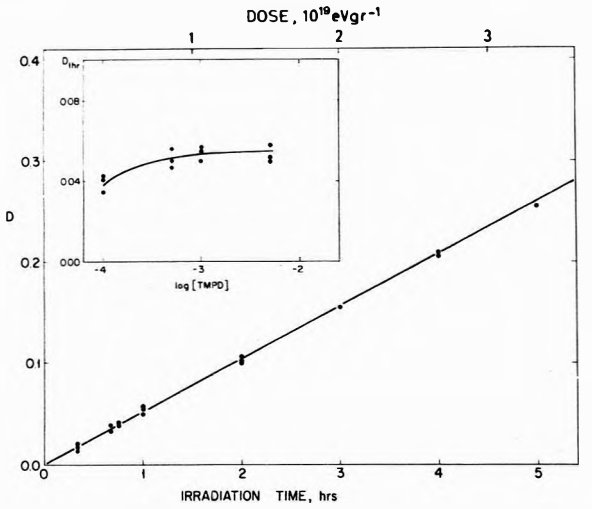

Figure 3. Dissolution of irradiated MP in air-saturated 10^{-3} *M* TMPD (λ 600 nm, *l* = 1 cm).

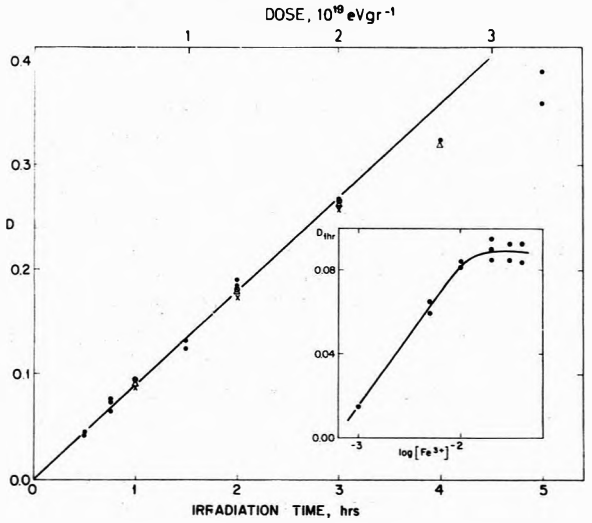

Figure 4. Dissolution of irradiated MP in Ar-saturated 0.02 *M* $Fe(ClO_4)_3$ + CH_3OH + o-phenanthroline (λ 515 nm, *l* = 1 cm): (○) 0.1 *M* CH_3OH; (●) 0.2 *M* CH_3OH; (×) 0.5 *M* CH_3OH; (△) glasses doped with 0.1 *m* Cd^{2+}, 0.2 *M* CH_3OH.

dependence on irradiation time is observed at 0.02 *M* Fe^{3+} and 0.2 *M* CH_3OH up to 3 hr. After normalization to 25 ml we obtain $(9.8 \pm 0.5) \times 10^{-6}$ *M* Fe^{2+}/hr. *D* became independent of $[Fe^{3+}]$ at concentrations $>1 \times 10^{-2}$ *M*. Varying the $[CH_3OH]$ over the range 0.1–0.5 *M* does not have any significant effect on the results (see Figure 4).

Mechanism. The results presented in the previous sections are in agreement with the following general mechanism.

$$\text{metaphosphate glass} \rightarrow \text{intermediates} \rightarrow MP^+ + MP^- \quad (2)$$

where MP^- and MP^+ represent the "trapped electron" and "trapped positive hole," respectively. Note that MP^+ and MP^- are free radicals, the nature of which has been discussed.[2] Upon dissolving the glass in O_2-containing water, reaction 3 or 3′ takes place.

$$MP^- + O_2 \longrightarrow MP + O_2^- \quad (3)$$

$$MP^- + O_2 \longrightarrow MPO_2^- \quad (3')$$

As we measure final products we are unable to discriminate between reaction 3 and 3′. If O_2^- is produced, it is in equilibrium with HO_2, $pK(HO_2) = 4.8$.[18,19] The peroxy radicals are expected to oxidize the solute X (X ≡ I^-, $Fe(CN)_6^{4-}$, TMPD), according to reaction 4 or 4′.[20,21]

$$2H^+ + O_2^- + X \longrightarrow X^+ + H_2O_2 \quad (4)$$

$$2H^+ + MPO_2^- + X \longrightarrow X^+ + H_2O_2 + MP \quad (4')$$

(X^+ is $\frac{1}{2}(I_2 + I_3^-)$, $Fe(CN)_6^{3-}$, or Wurster's blue.)

Indeed, we have identified H_2O_2 as a product in such solutions. When solid KI was added (up to 0.1 *M*) to the solution that contained the dissolved irradiated metaphosphate glass, I_3^- was produced, although at a relatively low concentration (35% of the concentration obtained when I^- was initially present). If the solution was treated for 20 min by 10^{-8} *M* catalase at pH 4.5, prior to the addition of KI, no oxidation of I^- could be observed. This indicates that either reaction 3′ is not important, or reaction 4′ proceeds as written, so that no peroxide other than H_2O_2 is formed (catalase acts as a specific catalyst for the decomposition of H_2O_2).[22] The low yield (35%) can be rationalized since back reactions between MPO_2^- or O_2^- and MP^+ may take place when I^- is absent. However, formation of some H_2O_2 may be expected from O_2^- produced in reaction 3 or 3′.

MP^+ is assumed to react with X according to reaction 5. We have previously shown that MP^+ is a strong oxidizing agent.[2b] The yield of X^+ depends on the fate of H_2O_2. When X ≡ I^-, H_2O_2 oxidizes two equivalents of X, according to the general reaction

$$MP^+ + X \rightarrow MP + X^+ \quad (5)$$

$$H_2O_2 + 2X \longrightarrow 2OH^- + 2X^+ \quad (6)$$

The results at pH 2.1 (X ≡ ferrocyanide) are in agreement with the proposed mechanism. We have confirmed that the oxidation of ferrocyanide by H_2O_2 at pH 2.1 is not stoichiometric, but proceeds to 81 ± 2%, in agreement with previous data.[23] This oxidation is independent of the metaphosphate concentration (see Figure 2). Measurements were also carried out at pH 4.5, where after 20 min two ferricyanide ions are produced per each H_2O_2 molecule. (The reaction is not stoichiometric, and the concentration of ferricyanide depends on the time.[23] The results at pH 2.1, where the optical density of ferricyanide does not change after 1 hr, are more reliable.) Indeed, higher ferricyanide yields were obtained at pH 4.5. The kinetics and the material balance observed in the oxidation of ferrocyanide ions at both pH 2 and 4.5 are in agreement with the assumption that H_2O_2 is produced upon the dissolution of the irradiated glasses.

The oxidation of TMPD by H_2O_2 was found to be relatively slow, and reaction 6 could be neglected under our conditions. Thus, in iodide–O_2 solutions, $G(I_3^-) = \frac{1}{2}[G(MP^+) + 3G(MP^-)] = 4.3 \pm 0.2$, in ferrocyanide–$O_2$ at pH 2.1, G(ferricyanide) = $G(MP^+) + 2.62G(MP^-) = 7.8 \pm 0.3$, in ferrocyanide–$O_2$ at pH 4.5, G(ferricyanide) = $G(MP^+) + 3G(MP^-) = 8.6 \pm 0.6$, and in TMPD–$O_2$, G(Wurster's blue) = $G(MP^+) + G(MP^-) = 4.6 \pm 0.2$.

In the Fe^{3+}, CH_3OH deaerated solutions, MP^- reduces Fe^{3+} to Fe^{2+}. MP^+ presumably reacts with methanol to produce radicals which reduce additional Fe^{3+}.

$$MP^- + Fe^{3+} \longrightarrow MP + Fe^{2+} \quad (7)$$

$$MP^+ + CH_3OH \longrightarrow MP + CH_2OH + H^+ \quad (8)$$

$$MP^+ + CH_3OH \longrightarrow (MPCH_2OH)^+ \quad (8')$$

$$CH_2OH + Fe^{3+} \longrightarrow CH_2O + Fe^{2+} + H^+ \quad (9)$$

$$(MPCH_2OH)^+ + Fe^{3+} \longrightarrow CH_2O + Fe^{2+} + 2H^+ + MP \quad (9')$$

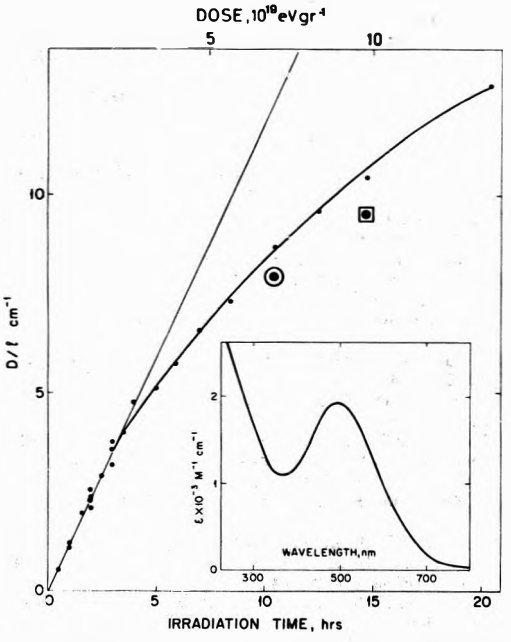

Figure 5. Spectrum and intensity (at 500 nm) of absorption in irradiated pure MP disks: (●) no delay; (⊙) 15-hr delay; (⊡) 25-hr delay.

$G(Fe^{2+}) = G(MP^+) + G(MP^-) = 4.4 \pm 0.2$.

From the results obtained in all four systems one can calculate $G(MP^+) = G(MP^-) = (2.2 \pm 0.1)$. The equivalence of $G(MP^+)$ and $G(MP^-)$ follows from the requirement for electrical balance. It is in agreement with the results presented above, and with the lack of change in $[I_3^-]$, when both I^- and iodine were present before the dissolution of the glasses.

N_2O did not increase the yield of $(I_3^- + I_2)$ in comparison to Ar, as might have been expected if N_2O could convert MP^- into OH, as it does to e_{aq}^-. The low yield of $(I_3^- + I_2)$ observed in Ar and N_2O is probably due to the incomplete removal of adsorbed O_2. This conclusion is in agreement with gas chromatographic measurements which showed that the yield of N_2 was less than 0.02 molecule/100 eV.

Molar Extinction Coefficients of MP^+ and MP^-. Feldmann, Treinin, and Volterra reported the absorption spectrum of irradiated metaphosphate glass disks.[11]

We have carried out similar work and confirmed their results (see Figure 5). The absorbance at 500 nm was linear with dose up to at least 3 hr of irradiation. Moreover, combined pulse radiolysis and spectrophtometric techniques showed absorbance changes of less than 3% at 500 nm in the time range 30 msec–4 hr. Combining absorbance measurements with dosimetry yields $G(MP^+) \times \epsilon^{500}(MP^+) = 4.2 \times 10^3\ M^{-1}\ cm^{-1}\ (100\ eV)^{-1}$ molecules, hence $\epsilon^{500}(MP^+) = (1.92 \pm 0.17) \times 10^3\ M^{-1}\ cm^{-1}$. The spectrum in Figure 5 represents both MP^+ and MP^-. Above 500 nm only MP^+ absorbs, and $\epsilon = \epsilon(MP^+)$.

Properties of MP^-. (*a*) *Gas Chromatography.* No H_2 was detected upon dissolving the irradiated glasses in 1 *M* 2-propanol or 1 *M* methanol at pH 1. This shows that MP^- produces neither e_{aq}^- nor H atoms upon its interaction with water. This conclusion is in agreement with the N_2O experiments which show that MP^- does not react with N_2O, and hence it does not react similarly to e_{aq}^-.

(*b*) *Light Emission.* An RCA 1P28 photomultiplier, sensitive in the wavelength range 200–650 nm, showed no light emission upon the dissolution of an irradiated glass sample (250 hr) at pH 4–6. Experiments with irradiated NaCl, under identical conditions, showed strong emission, in agreement with previous results.[3b] The dissolution of MP takes 20 min, as compared with 1 min for NaCl. However, surrounding the dissolution vessel by a Kodak ASA 400 film showed no darkening in the case of MP, and intense darkening in NaCl. These experiments demonstrate the different nature of products in NaCl and in MP. Had MP^- produced e_{aq}^- and MP^+ produced OH upon reaction with water, the emission results would have been similar in both MP and NaCl. It has been proposed that the production of e_{aq}^- is responsible for the emission in irradiated NaCl.[24]

(*c*) *Pulse Radiolysis of MP Solutions.* The possibility of producing oxidized and reduced products of MP through reactions with the active irradiation products of water, *viz.*, e_{aq}^-, H, and OH, was investigated using pulse radiolytic techniques. The accelerator, the optical analyzing system and the handling of solutions were described previously.[25] For all MP solutions used (in concentrations up to 1 *M*) no formation of absorbing products other than those of the medium could be observed upon pulsing with 1.5 μsec, 3×10^{20} eV $l.^{-1}$, 5-MeV electron pulses. Such negative results were obtained at pH 5–5.5, 1–2 ($HClO_4$), and 11–12 (NH_4OH, NaOH) in solutions saturated with Ar, N_2O, air, and O_2, in the presence and in the absence of alcohols.

These observations were in agreement with another series of measurements, where 1 *M* MP was found to have no noticeable effect on the yield or lifetime of e_{aq}^- as measured by direct observation, on the reduction of 5×10^{-5} *M* $KMnO_4$,[26] both in Ar-saturated solutions at pH 5–5.5 and in N_2O-saturated solutions at pH 1–2 ($HClO_4$), and on the oxidation of aerated 10^{-3} *M* KSCN[27] solutions at pH 5–5.5.

These results lead to the conclusion that the rate constants for the reactions of MP with e_{aq}^- and H are $<1 \times 10^6\ M^{-1}\ sec^{-1}$ and that for the reaction with OH is $<5 \times 10^6\ M^{-1}\ sec^{-1}$. MP is therefore much less reactive toward the radiation products of water than the monomeric phosphate anions.[28]

Concluding Remark

It can be concluded that although MP is unreactive toward e_{aq}^- and H (on the basis of the pulse radiolysis results), the reverse reaction of the negative radiation product MP^-, to form e_{aq}^- or H in solution, does not proceed either. In this manner, MP differs from NaCl, which produces e_{aq}^- upon irradiation and dissolution.[8]

MP is unreactive toward OH, but in this case the reverse reaction of the positive radiation product of MP to form OH in solution cannot be ruled out, as no significant differences were found between the reactivity of MP^+ in the present experiments and the known data concerning OH radicals.

Doped Glasses. In the experiments described up to now, we measured the yield of the permanent radiation products of MP glass. In a previous work[2b] we observed that the absorption of the radiation products at 25° undergoes several consecutive changes in the 10^{-7} to 10^{-2} sec range. After 30 msec, no more changes in the spectrum were observed and no appreciable decrease in intensity occurred for several hours. We sought to determine whether the absorption changes prior to stabilization involve short-range annihilation, or, as indicated by kinetic evidence,[2b,29] are

due only to changes in the spectrum due to interaction with the medium, whereas the annihilation at 25° commences only at the 10^4 sec time scale.

In order to clarify this point, we dissolved MP glasses doped with 0.1 *m* Cd^{2+} (as $CdSO_4$) in Ar-saturated 0.02 *M* $Fe(ClO_4)_3$ solution containing 0.2 *M* CH_3OH. From earlier pulse radiolysis work[2b] we know that 0.1 *m* Cd^{2+} traps 95% of the precursors of MP^-, and that the trapping takes place in $<5 \times 10^{-8}$ sec. Careful examinations showed that the absorption of Cd^- remains unchanged up to several hours after the irradiation, and that Cd^{2+} does not affect the positive holes. The present results obtained in the dissolution of the Cd^{2+}-doped glasses were identical with those obtained with the pure glass (see Figure 4), leading to the conclusion that the yield of initially produced electrons trapped as Cd^+ is the same as that of stabilized MP^- in the pure glass.

Acknowledgment. We wish to thank Mr. J. Ogdan for maintenance of the equipment, and Professor M. Ottolenghi and Mr. Dan Meisel for valuable discussions.

This research was supported by The Ministry of Education of Israel and The Authority for Research and Development, The Hebrew University, Jerusalem 91000, Israel.

References and Notes

(1) (a) Visiting research student from the Department of Pure and Applied Sciences, University of Tokyo, Komaba, Tokyo, Japan. (b) In partial fulfillment of the requirements for a Ph.D. Degree.
(2) (a) A. Treinin in "Radical Ions," E. T. Kaiser and L. Kevan, Ed., Interscience, New York, N. Y., 1968, p 525; (b) A. Barkatt, M. Ottolenghi, and J. Rabani, *J. Phys. Chem.*, **76**, 203 (1972).
(3) (a) G. Ahnstrom and G. von Ehrenstein, *Acta Chem. Scand.*, **13**, 855 (1959); (b) T. Westermark and B. Grapengiesser, *Nature (London)*, **188**, 395 (1960).
(4) M. Hacskaylo and D. Otterson, *J. Chem. Phys.*, **21**, 552 (1953); **21**, 1434 (1953).
(5) W. G. Burns and T. F. Williams, *Nature (London)*, **175**, 1043 (1955).
(6) T. Westermark, B. Grapengiesser, and N. Biesert, *Ark. Kemi.*, **17**, 151 (1961).
(7) J. P. Mittal and J. Shankar, *Radiochem. Radioanal. Lett.*, **6**, 115 (1971).
(8) C. Gopinathan, P. S. Damle, and E. J. Hart, *J. Phys. Chem.*, **76**, 3694 (1972).
(9) J. H. Baxendale and G. Hughes, *Z. Phys. Chem (Frankfurt am Main)*, **14**, 306 (1958).
(10) H. Fricke and E. J. Hart, "Radiation Dosimetry," Vol. 2, F. H. Attix and W. C. Roesch, Ed., Academic Press, New York, N. Y., 1966, Chapter 12.
(11) T. Feldmann, A. Treinin, and V. Volterra, *J. Chem. Phys.*, **42**, 3366 (1965).
(12) J. P. Candlin, J. Halpern, and D. L. Trimm, *J. Amer. Chem. Soc.*, **86**, 1019 (1964).
(13) G. V. Buxton and F. S. Dainton, *Proc. Roy. Soc., Ser. A*, **287**, 427 (1965).
(14) M. Davies and E. Gwynne, *J. Amer. Chem. Soc.*, **74**, 2748 (1952).
(15) D. Zehavi and J. Rabani, *J. Phys. Chem.*, **76**, 3703 (1972).
(16) J. K. Thomas, *Trans. Faraday Soc.*, **66**, 621 (1970).
(17) J. P. Mehlig and H. R. Hulett, *Ind. Eng. Chem., Anal. Ed.*, **14**, 869 (1942).
(18) J. Rabani and S. O. Nielson, *J. Phys. Chem.*, **73**, 3736 (1969).
(19) D. Behar, G. Czapski, J. Rabani, L. M. Dorfman, and H. A. Schwarz, *J. Phys. Chem.*, **74**, 3209 (1970).
(20) G. E. Adams, J. W. Boag, and B. D. Michael, *Trans. Faraday Soc.*, **61**, 492 (1965).
(21) P. B. Ayscough, C. E. Burchill, K. J. Ivin, and S. R. Logan, *J. Chem. Educ.*, **44**, 349 (1967).
(22) A. S. Brill, *Compr. Biochem.*, **14**, 447 (1962).
(23) J. Sobkowski, *Rocz. Chem.*, **43**, 1729 (1969).
(24) (a) G. Ahnstrom, *Acta Chem. Scand.*, **19**, 300 (1965); (b) J. P. Mittal, *Radiat. Res., Proc. Int. Congr., 4th, 1970*, 147 (1971).
(25) D. Zehavi and J. Rabani, *J. Phys. Chem.*, **75**, 1738 (1971).
(26) J. H. Baxendale, J. P. Keene, and D. A. Stott in "Pulse Radiolysis," M. Ebert, J. P. Keene, A. J. Swallow, and J. H. Baxendale, Ed., Academic Press, London, 1965, p 107.
(27) G. E. Adams, J. W. Boag, J. Currant, and B. D. Michael, ref 26, p 117.
(28) E. D. Black and E. Hayon, *J. Phys. Chem.*, **74**, 3199 (1970).
(29) A. Barkatt, M. Ottolenghi, and J. Rabani, *J. Phys. Chem.*, **77**, 2857 (1973).

COMMUNICATIONS TO THE EDITOR

On the Mechanism of the Hydrolysis of Triethylethoxysilane at the Silica–Carbon Tetrachloride Interface

Sir: We would like to present the following remarks concerning the mechanism of this reaction as proposed by Bascom and Timmons.[1] (1) It is difficult to imagine that water molecules covering only 15% of a silica surface[1] can form a continuous hydrogen-bonded network sufficiently strong to assure protons transfer. (2) In Bascom and Timmon's mechanism, it is not obvious why it is necessary to cover all the existing surface hydroxyl groups, independently of their concentration (their experiments on surfaces treated at 750 and 550°) before an abrupt increase in hydrolysis rate can be observed.

We are therefore proposing an alternative mechanism based on the supposition that in a silica surface the effect of π bonding between the free electron pairs of oxygen and the empty 3d orbitals of a silicon atom prevails on the positive inductive effect, which the oxygen is exercizing on a silicon. As a result, one would observe a change in polarity of the Si-O bond from $Si^{+\delta}-O^{-\delta}$ to $Si^{-\delta}-O^{+\delta}$. This could be responsible for an increase of the ionic character of hydroxyl groups of a silica surface. These hydroxyl groups would then become active sites for adsorption of water and TEES molecules.

When the number of adsorbed water molecules is not sufficient to cover all hydroxyl groups, there exist on a silica surface three competitive sites for adsorption of TEES: free hydroxyl groups, free hydroxyl groups with adsorbed water molecules, and vicinal hydroxyl groups with adsorbed water molecules.[2] We have also to consider the effect of a $(p \rightarrow d)\pi$ bonding between a silicon atom of the silica surface and an oxygen of the surface hydroxyl group. This effect would manifest itself most strongly in the hydrogen bond formed between the proton of the surface hydroxyl group and the alkoxyoxygen of the TEES molecule. The Bascom and Timmons' experiments seem also to suggest that the noncovered isolated hydroxyl groups would form the strongest hydrogen bonds with TEES molecules and would then be the preferable sites for their adsorption. The change of the stretching frequency of these groups on triethylethoxysilane adsorption quoted by Bascom and Timmons was from 3700 to about 3500–3000 cm^{-1}. These sites however are inactive for the hydrolysis reaction. Due to the low relative concentration of adsorbed TEES molecules (with respect to the number of surface hydroxyl groups), one must cover practically all the existing hydroxyl groups with water molecules before the adsorption of TEES on hydrated sites, followed by the hydrolysis reaction, can take place. As soon as all hydroxyl groups are covered by adsorbed water molecules, there is competition between the two active sites formed on (a) vicinal hydroxyl groups and (b) isolated hydroxyl groups. It seems logical that due to the cumulative effect of the two surface silicon atoms, the hydrogen bond formed between the hydrogen of the adsorbed water and the oxygen of $(C_2H_5)_3SiOC_2H_5$ molecule would be stronger in the case of adsorption on vicinal than on isolated hydroxyl groups.

Due to the effect of $(p \rightarrow d)\pi$ bonding mentioned above, the silicon atom of a silica surface can supply some polarizing field. A decrease of the activation energy for the dissociation of adsorbed water molecules would result in a reduction of the energy of the transition state. The polarizing field generated by silicon atom would then create favorable conditions for the hydrolysis reaction of the adsorbed TEES. If the hydrogen atom involved in hydrogen bonding with an alkoxyoxygen of TEES is sufficiently acidic and the oxygen atom sufficiently basic, the hydrogen can be transfered as a proton to form a covalent bond with this oxygen. If, at the same time, the position of the adsorbed TEES molecule is such that the silicon of TEES finds itself in the vicinity of the oxygen of the adsorbed water molecule, the hydrolysis reaction of TEES can take place.

It seems to us that our mechanism of the hydrolysis reaction of TEES by water molecules adsorbed on a silica surface suggests not only an explanation for the "go," "no-go" behavior of the kinetic data obtained by Bascom and Timmons but also foresees the existence of optimal conditions for this reaction. An increase of concentration of vicinal hydroxyl groups covered by adsorbed water would increase the hydrolysis rate due to an increase in concentration of active sites. On the other hand, the increase in concentration of surface hydroxyl groups would result in a decrease of the polarizing ability of the silica surface. (Due to a kind of a saturation effect, the influence of π bond is smaller, the higher the concentration of surface hydroxyl groups.) It is this last effect which would limit the rate of the reaction of hydrolysis of TEES on a silica surface. We therefore consider that experiments should be conducted in a way to control the concentration of vicinal hydroxyl groups.[3]

Acknowledgment. I thank Professors J. J. Fripiat, G. Thomaes, and J. Nasielski for the helpful discussions.

References and Notes

(1) W. D. Bascom and R. B. Timmons, *J. Phys. Chem.*, **76**, 3192 (1972).
(2) W. Hertl and M. L. Hair, *Nature (London)*, **223**, 1150 (1969).
(3) In the experiments of Bascom and Timmons, the vicinal hydroxyl groups were formed in the rehydroxylation process. The only indication about their concentration could be inferred from the degree of reversibility of the dehydroxylation process for two temperatures for which their heat treatments were made. Taking into account that silica–water is a dynamic system, the duration of all the experiments should be well defined and always comparable. The hydration of the silica surface should be sufficient to cover all the hydroxyl groups present. According to K. Klier, J. H. Shen, and A. C. Zettlemoyer (*J. Phys. Chem.*, **77**, 1458 (1973)), this would be achieved for a coverage equal to about 1.5 of the apparent monolayer. The concentration of the TEES molecules should be such as to cover all the sites active for hydrolysis.

Service de Chimie Physique E.P.
Faculté des Sciences Appliquées
Université Libre de Bruxelles
Brussels, Belgium

Maryna Prigogine

Received April 2, 1973

On the Mechanism of the Hydrolysis of Triethylethoxysilane at the Silica–Carbon Tetrachloride Interface. A Reply

Publication costs assisted by the Office of Naval Research

Sir: We wish to respond to Prigogine's criticisms of our proposed mechanism of the surface hydrolysis of triethylethoxysilane[1] and also to comment on the model which she proposes as an alternative.[2] Her first objection is that the water coverage was only 15% of the surface area and finds it difficult to imagine that this low a coverage can form a continuous H-bonded network. This objection ignores the more pertinent point that this amount of water represents complete coverage of the surface hydroxyls which themselves covered only 15% of the surface. If we make the reasonable assumption that the hydroxyls are randomly distributed over the surface, a scale drawing will show that even at as low a coverage of 15% the hydroxyls are close enough to be bridged by water molecules in the fashion we proposed. A much higher water coverage was needed in the work of Fripiat than in our study because their silica had been less intensely dried and therefore had a higher surface hydroxyl content.[3]

The most surprising result of the hydrolysis study was the, go-no go, aspect of the kinetics. Prigogine does not accept our hypothesis that this is the result of the sudden formation of a H-bonded water–hydroxyl network. Instead, she suggests that the triethylethoxysilane (TEES) is so strongly H bonded to nonhydrated surface hydroxyls that until the latter are all hydrated, there is no adsorption of TEES on the hydrated hydroxyls and, thus, no reaction.

We find it difficult to understand why the bonding of the TEES should be so different to the two types of sites when H bonding is undoubtedly involved in both cases. We would agree that there might be a distribution that *favors* TEES···HO-Si≡ adsorption but that in equilibrium with the TEES adsorbed to nonhydrated hydroxyls there would be some adsorption on the hydrated sites. Therefore, there should have been some hydrolysis, albeit small, prior to complete water coverage of the hydroxyls. None was observed.

One of the difficulties we encountered in justifying our proposed network formation was that it required a particular orientation of the adsorbed water molecule, *i.e.*, a SiOH donon, H_2O acceptor configuration (structure I).[4]

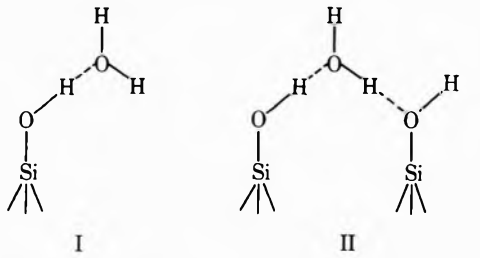

I II

Recently, a study of the infrared bands of adsorbed water in the 4500-9000-cm^{-1} region indicated that the configuration that we assumed is in fact the only orientation consistent with the observed spectra.[5] Furthermore, if the preferred H-bonding role of the ≡Si-OH is that of a donor, then the bridging of water molecules between hydroxyls, which involves the ≡Si-OH as an acceptor (structure II), will not occur until nearly all of the hydroxyls are covered by a water molecule. In other words, extensive bridging and the formation of a network is not expected until the hydroxyl–water molecule ratio is nearly unity, which is consistent with the model proposed in the hydrolysis study.

References and Notes

(1) W. D. Bascom and R. B. Timmons, *J. Phys Chem.*, **76**, 3192 (1972).
(2) M. Prigogine, *J. Phys. Chem.*, **78**, 757 (1974).
(3) J. J. Fripiat, A. Jelli, G. Poncelet, and J. Andri *J. Phys. Chem.*, **69**, 2185 (1965).
(4) W. D. Bascom, *J. Phys. Chem.*, **76**, 3188 (1972).
(5) K. Klier, J. H. Shen, and A. C. Zettlemoyer, *J. Phys. Chem.*, **77**, 1458 (1973).

Code 6170 **Willard D. Bascom***
Naval Research Laboratory
Washington, D. C. 20375

Chemistry Department **Richard B. Timmons**
Catholic University of America
Washington, D. C. 20017

Received September 14, 1973

Interaction of Molecular Hydrogen with Magnesium Oxide Defect Surface

Sir: We have studied the interaction of molecular H_2 with high defect concentration MgO surfaces, freshly prepared by vacuum decomposition of high-purity $Mg(OH)_2$ powders. It was found that molecular H_2 at 1–6 bars is capable of reacting with such MgO surfaces giving rise to a pronounced conductivity maximum at about 130°.

The methods employed were dc conductivity and dielectric loss factor measurements in the frequency range from 100 Hz to 10 kHz, using a cell with circular Al electrodes, 40 mm diameter with a 0.1-mm gap. The results obtained with dc and ac were essentially the same, which indicates that no polarization effects occur. The higher pressure range, up to 200 bars, is presently under investigation.

A typical experiment was carried out as follows, and the results are shown in Figure 1.

The cell loaded with about 0.1 g of $Mg(OH)_2$ and contained in the pressure recipient was first evacuated to 10^{-2} Torr and heated at 3°/min to near 400°. Prior to the dehydration of $Mg(OH)_2$ which starts around 250° a conductivity maximum is observed, shown by curve 1. This maximum, already reported elsewhere,[1] occurs under vacuum as well as under H_2 or inert gas pressure. It is not due to a gas–solid reaction, but rather due to a proton tunnelling mechanism operative in $Mg(OH)_2$ prior to decomposition.[2]

After partial dehydration the sample was slowly cooled under vacuum to room temperature. High-purity H_2 gas was then introduced to 6 bars pressure, and the sample was heated again at 3°/min to not more than 250°. Curve 2 shows an increased conductivity but no maximum.

The sample was then again allowed to cool slowly, first under H_2 pressure to about 150°, then under vacuum to room temperature. After thorough evacuation at room temperature 6 bars H_2 pressure were again applied and

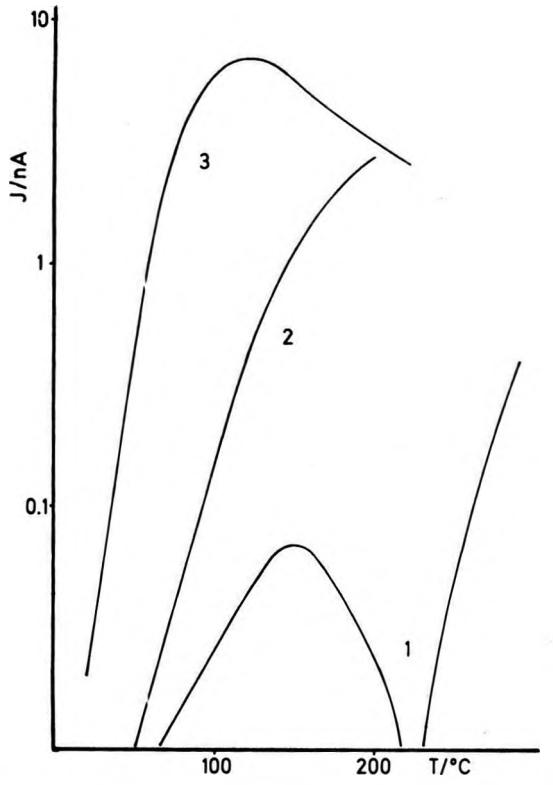

Figure 1. Results of conductivity *vs.* temperature measurements.

the sample was once more heated to about 250°. Curve 3 shows that the conductivity has again markedly increased and now goes through a pronounced maximum at about 130°.

Repeating the same cycling does not further increase the conductivity nor does it increase the intensity of the maximum. On the contrary, the maximum decreases and eventually vanishes after eight–ten cycles.

The following features of the conductivity maximum were established. First, no maximum was observed, if in between the heating was performed under either N_2 or O_2, but the maximum reappeared nearly as strong as before during the next run under H_2 pressure. Second, after the maximum had disappeared, due to repeated cycling, the activity could largely be restored by heating the sample again above 300°, causing new dehydration to occur.

We think that the conductivity effects reported here can be connected with the presence of O^- centers on the MgO defect surface. Mass spectroscopic studies have shown that, when high-purity $Mg(OH)_2$ is heated under vacuum, molecular hydrogen is evolved between 300 and 550°, followed by an oxygen evolution around 700°.[3] As discussed briefly elsewhere in connection with preliminary work done on partially deuterioxylated MgO samples,[4] the hydrogen evolution can be explained by a thermal dissociation of pairs of OH^- groups neighboring an oxygen vacancy, schematically

$$OH^- \ldots\ldots OH^- \rightarrow O^- \ldots\ldots O^- + H_2$$

Concomitantly O^- ions are formed on the MgO defect surface, which become unstable at high temperatures, giving off oxygen.

The present conductivity measurements seem to indicate that above reaction can be reversed by applying H_2 at higher pressure

$$O^- \ldots H{-}H \ldots O^- \rightarrow OH^- \ldots\ldots OH^-$$

A quite similar description has been proposed by Boudart, *et al.*,[5] to explain the H_2/D_2 isotope exchange reaction taking place at temperatures as low as 77 K on V_I centers on MgO surfaces. Between 77 K and room temperature, the range studied by Boudart and coworkers, H_2 and D_2 seem to form adsorption complexes permitting the isotope exchange but not annihilating the V_I center. The present conductivity study indicates that above room temperature a true reaction seems to take place between H_2 and some O^- centers which slowly destroys the active sites.

The V_I center is thought to consist of a cluster of O^- ions, probably three in a triangular array, and closely connected with an oxygen vacancy and an OH^- group.[5] Derouane, *et al.*,[6] have found that the V_I center is active for the H_2/D_2 exchange only, if traces of H_2O are present. We also found that the conductivity maximum appears strongly only, if traces of H_2O are present during the heating cycle. Too much H_2O, however, veils the effect by the formation of a tightly bound H_2O film on the MgO defect surface.[7]

A full discussion and detailed description of the experimental results, including electron spin resonance data, will be published shortly.

References and Notes

(1) W. Gieseke, H. Nägerl, and F. Freund, *Naturwissenschaften*, **57**, 493 (1970).
(2) To be submitted for publication.
(3) F. Freund, N. Scheik Ol Eslami, and H. Gentsch, to be submitted for publication.
(4) See discussion following the paper cited in ref 6.
(5) M. Boudart, A. Delbouille, E. G. Derouane, V. Indovina, and A. B. Walters, *J. Amer. Chem. Soc.*, **94**, 6622 (1972).
(6) E. G. Derouane, V. Indovina, A. B. Walters, and M. Boudart in "Reactivity of Solids," J. S. Anderson, M. W. Roberts and F. S. Stone, Ed., Butterworths, London, 1972, p 703.
(7) R. Martens, H. Nägerl, and F. Freund, *Ind. Chim. Belg.*, **38**, 519 (1973).

IV. Physikalisches Institut der Universität Göttingen D-3400 Göttingen, Germany — **W. Gieseke, H. Nägerl**

Mineralogisch-Petrographisches Institut der Universität Köln D-5000 Köln-41, Germany — **F. Freund***

Received July 6, 1973

Effect of Pressure on the Thermodynamically Reversible Gelation of 12-Hydroxystearic Acid in Carbon Tetrachloride[1]

Publication costs assisted by the Research Institute of Science and Engineering, Ritsumeikan University

Sir: In a thermodynamically reversible gel, the cross links are known to be caused by secondary forces, such as hydrogen bonds (H bonds), hydrophobic, and electrostatic interactions, rather than by covalent bonds. The gel of 12-hydroxystearic acid ($CH_3(CH_2)_5CH(OH)(CH_2)_{10}COOH$) in carbon tetrachloride (CCl_4) has been investigated by

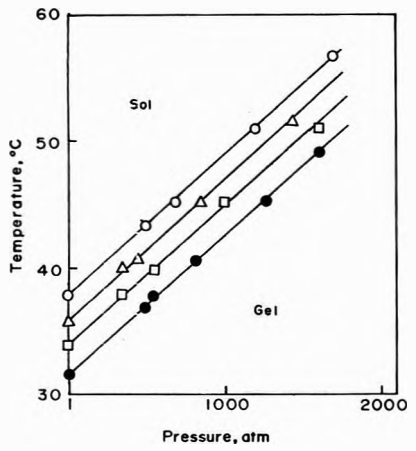

Figure 1. Sol-gel phase diagram of 12-hydroxystearic acid–CCl_4 system at various concentrations: (●) 3.3×10^{-2}; (□) 4.95×10^{-2}, (△) 6.6×10^{-2}; (○) 9.9×10^{-2} *M*.

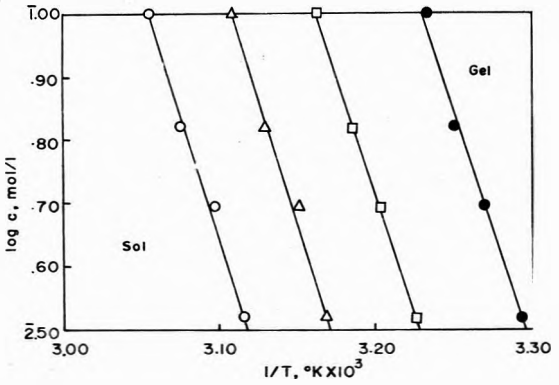

Figure 2. Relationship between the logarithm of the acid concentrations and the reciprocal of the absolute temperature of the sol to gel transformation at each pressure: (●) 1; (□) 500; (△) 1000; (○) 1500 atm.

means of thermal analysis and ir spectrophotometric measurements by Tachibana and coworkers.[2] These authors showed that cross links are formed by the intermolecular H bonding between hydroxyl groups (OH) and oxygen atoms of carbonyl groups (C=O).

In a previous study of the pressure effect on thermodynamically reversible gelation in aqueous solutions, we have found that for gelatin, poly(vinyl alcohol), and methyl cellulose the formation of intermolecular H bonded cross links results in negative values of both ΔH (enthalpy change) and ΔV (volume change). In this paper we report on the effect of pressure on gel formation of 12-hydroxystearic acid in CCl_4. In this solvent one may expect that H bonds between individual acid molecules will be more pronounced than in aqueous solution.

The method for the determination of the sol to gel transformation was the same as the previous paper.[3] The error in the pressure accompanying the measurement of the transformation was about ±50 to 100 atm. The sample of 12-hydroxystearic acid was furnished from Tokyo Kasei Kogyo Chemicals Co. and recrystallized five times from acetone, mp 79.0–80.0°, lit. mp 79.3–79.8°[4] and 80.5–81°.[5]

Figure 1 shows the sol-gel diagram of 12-hydroxystearic acid at concentrations from 3.3×10^{-2} to 9.9×10^{-2} *M* CCl_4. The phase above each curve is a sol, while the phase below each curve is a gel. It can be seen from Figure 1 that gelation is promoted by compression. If plots of the logarithm of the concentrations of acid *vs.* the reciprocal of the absolute temperature of the sol to gel transformation are made, straight lines are obtained at each pressure (Figure 2). According to an analysis presented by Eldridge and Ferry,[6] the ΔH values for the formation of 1 mol of cross links out of 2 mol of cross linking sites are then obtained from

$$\log c = (\Delta H/2.303R)1/T + \text{constant} \quad (1)$$

The ΔH value per mole of H bond, which has been reported on many compound in CCl_4 for OH---O bond, is well established to fall within the range of 4–4.5 kcal/mol.[7] If we assume that the average strength for 1 mol of H bond of 12-hydroxystearic acid in CCl_4 system is 4.25 kcal/mol, the number of H bond per cross link can be estimated. Table I with ΔH values per cross link shows the number of H bonds per cross link to be about 8 to 9. Since one H bond per molecule is in principle sufficient for gelation, the much higher value of 8 to 9 found per cross link probably mean that a lot of dimerization occurs which leads to "wasted H bonds" as far as infinite network formation is concerned.

Assuming that the sol to gel transformation can be treated as a phase transition, the ΔV accompanying the formation of a cross link, which is derived from the Clausius–Clapeyron and Eldridge–Ferry equations at constant temperature, is obtained from the following equation

$$\log c = ((\Delta V - RTk_s)/2.303RT)P + \text{constant} \quad (2)$$

where k_s is the compressibility of CCl_4 and was calculated by the Tait equation.[8] Table II show ΔV values calculated from the linear relation between the logarithm of the acid concentration and the transformation pressure at various temperatures in Figure 3. The ΔV values accompanying the formation of 1 mol of H bond also can be calculated

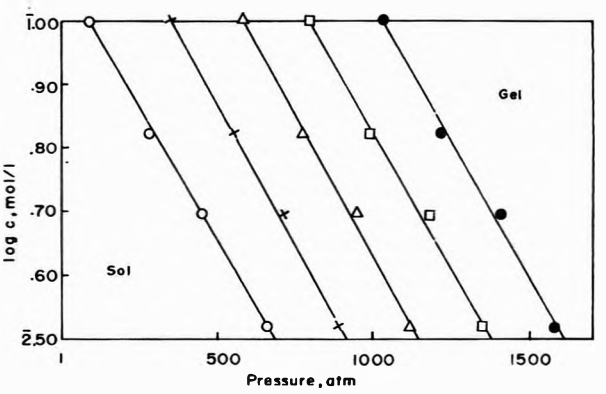

Figure 3. Relationship between the logarithm of the acid concentrations and the pressure of the sol to gel transformation at each temperature: (○) 40.0; (×) 42.5; (△) 45.0; (□) 47.5; (●) 50.0°.

TABLE I: ΔH Values and the Number of H Bonds per Mole of Cross Link Formed at the Gel Point under Various Pressures

Pressure, atm	1	500	1000	1500
$-\Delta H$, kcal/mol	35.2	34.7	36.9	37.5
No. of H bonds	8.3	8.2	8.7	8.8

TABLE II: ΔV Values per Mole of Cross Link Formed at the Gel Point at Various Temperatures

Temp, °C	40.0	42.5	45.0	47.5	50.0
$-\Delta V$, ml/mol	47.8	50.8	50.8	49.3	49.6

from the ΔV values per cross link in gel formation and the average number of H bonds in each cross link (Table I). The average value of ΔV for the formation of an H bond is then found to be about −5.5 ml/mol, which seems to be reasonable in comparison with the value for OH---O bond formation, −6.0 ml/mol obtained in the dimerization of formic acid,[9] −4.64 ml/mol for the association of *n*-butyl alcohol in CS_2.[10]

Acknowledgment. Financial support given by the Ministry of Education in Japan is gratefully acknowledged.

References and Notes

(1) Part of this article was presented at the 22nd International Congress of Pure and Applied Chemistry, Sydney, Australia, Aug 1969, p 104.
(2) K. Imanega, H. Kambara, and T. Tachibana, presented at the 20th Annual Meeting of Chemical Society of Japan, Osaka, 1968, No. 22216.
(3) K. Suzuki, Y. Taniguchi, and T. Enomoto, *Bull. Chem. Soc. Jap.*, **45**, 336 (1972).
(4) T. Tachibana and H. Kambara, *Bull. Chem. Soc. Jap.*, **42**, 3422 (1969).
(5) K. Serck-Hanssen, *Chem. Ind. (London)*, 1554 (1958).
(6) J. E. Eldridge and J. D. Ferry, *J. Phys. Chem.*, **58**, 992 (1954).
(7) G. C. Pimental and A. L. McClellan, "The Hydrogen Bond," W. H. Freeman, San Francisco, Calif., 1960 p 218.
(8) R. E. Gibson and O. H. Loeffler, *J. Amer. Chem. Soc.*, **63**, 898 (1941).
(9) K. Suzuki, Y. Taniguchi, and T. Watanabe, *J. Phys. Chem.*, **77**, 1918 (1973).
(10) E. Fishman and G. H. Drickamer, *J. Chem. Phys.*, **24**, 548 (1956).

Department of Chemistry **Yoshihiro Taniguchi***
Faculty of Science and Engineering **Keizo Suzuki**
Ritsumeikan University
Kita-ku, Kyoto, 603, Japan

Received July 30, 1973

Noise Spectra of Ion Transport Across an Anion Membrane

Publication costs assisted by City College of New York

Sir: We have, over the past several years, studied transport across cation membranes by measuring noise power spectra.[1] From this work, we were able to draw certain conclusions, at least for H^+ ion, as to the transport mechanism.[1d] In our initial paper,[1a,b] we reported some limited results on anion membranes. These results indicated that, unlike the cation membrane spectra, anion membrane spectra showed $1/f$ noise, and sometimes $1/f^{3/2}$ noise. Since these results on anion membranes have not been followed by a systematic evaluation, the initial data have been left unconfirmed. Recent work by Hooge and coworkers[2] has renewed interest in $1/f$ noise, and there is a significant difference in the transport mechanism indicated by $1/f$ noise and $1/f^{3/2}$. For these reasons, a brief reinvestigation of the noise spectra generated by ion transport across an anion membrane seemed appropriate at this time.

The technique is unchanged from that previously described,[1d] except that only room temperature measurements were made. The LA260V Applied Cybernetics amplifier was replaced by a Model LA460V (or by an AD-YU Model 1027C for some higher noise measurements). Solutions of H_3PO_4 were prepared as follows: solution 1, 0.034 *M*; solution 2, 0.018 *M*, solution 3, 0.0081 *M*, solution 4, 0.0019 *M*. Also, solutions of HCl were prepared: solution 1, 0.1024 *M*, solution 2, 0.017 *M*, solution 3, 0.0080 *M*, solution 4, 0.003 *M*.

TABLE I: Slopes of Noise Spectra for Various Concentrations and Currents[a]

Concn, *M*	Current density, A/m²	*a*	*b*[b]	*c*	f_B,[c] Hz
		HCl Spectra			
0.024	96			1.8	
	178	0.9	2.2		5,000
0.017	70			1.7	
	74			1.8	
	82			1.9	
	95			1.6	
	119			1.7	
	125	1.3	3.0		13,000
0.0080	43			1.7	
	50			1.6	
	62			1.5	
	71	1.3	2.1		4,500
	80			1.4	
	95	0.9	3		20,000
0.0038	42			1.8	
	49			2.0	
	59			1.7	
	89			1.7	
	96			1.8	
		H_3PO_4 Spectra			
0.034	96			1.4	
	101			1.4	
	125			1.5	
	178			1.5	
0.018	42			1.6	
	53			1.7	
	74			1.6	
	95			1.4	
	101			1.6	
	131	1.1	1.8		9,000
0.0081	42			1.4	
	61			1.7	
	71	1.1	1.9		4,500
	78			1.7	
	119	1.0	1.8		8,000
0.0019	42	1.2	2.6		15,000
	50	1.6	2.0		15,000
	55	1.1	3.0		20,000
	59	1.5	2.6		15,000
	71	1.1	3.0		20,000
	77	1.3	2.3		15,000

[a] Slopes as $-\mathrm{d}\log \text{power}/\mathrm{d}\log f$. [b] For values of $f_B \geq 10^4$ Hz, the *b* slopes are based on a small number of points, and have a relatively large error. [c] Frequency at which curves of two slopes meet, ±20%.

The anion membrane was Ionac Type MA 3236, with an exposed surface of 8.4×10^{-6} m².

The spectra were taken, as before, with a Tektronix 3L5 spectrum analyzer in the frequency range 300–80 kHz; in this work, the center frequency settings were checked with an IEC Model F34 function generator. No other changes in procedure were made from the previous work.[1d]

The results are summarized in Table I. As can be seen, two types of spectra exist: those in which an approximate $f^{-3/2}$ slope was found, and those in which an f^{-1} slope was found at lower frequencies, with an approximate f^{-2} at higher frequencies. It is relatively simple to deal with the −1.5 slope cases, as these are normally characteristic of diffusion.[3] Furthermore, with cation membranes at low current densities, diffusion appears to dominate the

noise.[1d] It is probably safe to conclude that for the more concentrated H_3PO_4 solutions, this is equally true.

However, the other form of spectrum is not comparable to any found with the cation membranes. Here, $1/f$ noise does appear over an appreciable frequency range. The fact that a steeper slope appears at higher frequencies gives a strong hint as to the source of the noise, however. It has long been known that a distribution of relaxtion times could produce $1/f$ noise between the lower and upper frequency limits of the distribution, and that, above the upper frequency limit, f^{-2} noise should result.[4] This is fairly close to the behavior observed here. The fact that, even in the more dilute solutions, single slope spectra which are usually between 1.5 and 2.0 occur suggests that the relaxation processes do not exclude the simultaneous presence of diffusion. If the two contributions are of similar magnitude (as is indicated by the fact that either one may be found with only a relatively small change in conditions) it is possible for them to combine so as to produce a spectrum which takes this form, within experimental error.

Current-voltage curves for anion membranes do not produce clearly defined plateaus at a critical current density, as cation membranes do;[1a] this behavior was found again in this system. Of the systems studied here, only the most concentrated H_3PO_4 solution remains ohmic in its behavior throughout the range of current densities in which noise spectra were taken. This solution gave only diffusion spectra. No spectra showing two slopes appeared at current densities less than that at which non-ohmic behavior began (within experimental error, ± 8 A/m^2), although single slope spectra, as in the case of the least concentrated HCl solution, appeared well above this point.

Above the critical current density, cation membranes show a spectrum fairly close to two straight lines of slope -3, -5, and this could be interpreted as due to turbulence.[1d,5] Although the anion membrane spectra sometimes showed a steeper spectrum following a less steep one, and a -1 slope can appear between -3 and -5, the steeper slope for the anion case did not approach -5, and no evidence of a -3 slope was found at low frequency. Therefore, it appears that turbulence does not occur with anion membranes as it does with cation membranes.

The following conclusions can be drawn. (1) At current densities lower than that for the start of non-ohmic behavior, the noise spectra are dominated by diffusion noise. (2) At higher current densities, the spectra often are of a type which would be characteristic of a distribution of relaxation times. (3) In contrast to cation membranes, these spectra show no evidence of turbulent flow.

References and Notes

(1) (a) M. E. Green and M. Yafuso, *J. Phys. Chem.*, **72**, 4072 (1968); (b) *ibid.*, **73**, 1626 (1969); (c) M. Yafuso and M. E. Green, *ibid.*, **75**, 654 (1971); (d) S. H. Stern and M. E. Green, *ibid.*, **77**, 1567 (1973).
(2) (a) F. N. Hooge and J. L. M. Gaal, *Philips Res. Rep.*, **26**, 77 (1971); (b) F. N. Hooge, *Phys. Lett.*, **33A**, 169 (1970); (c) F. N. Hooge, *Physica*, **45**, 386 (1969).
(3) M. Lax, *Rev. Mod. Phys.*, **32**, 25 (1960).
(4) R. H. Kingston and A. L. McWhorter, *Phys. Rev.*, **103**, 534 (1956).
(5) C. M. Tchen, *Phys. Rev. A*, **8**, 500 (1973).

Department of Chemistry
The City College of the
City University of New York
New York, New York 10031

Michael E. Green

Received December 10, 1973

The leading American journal devoted to general organic chemistry:

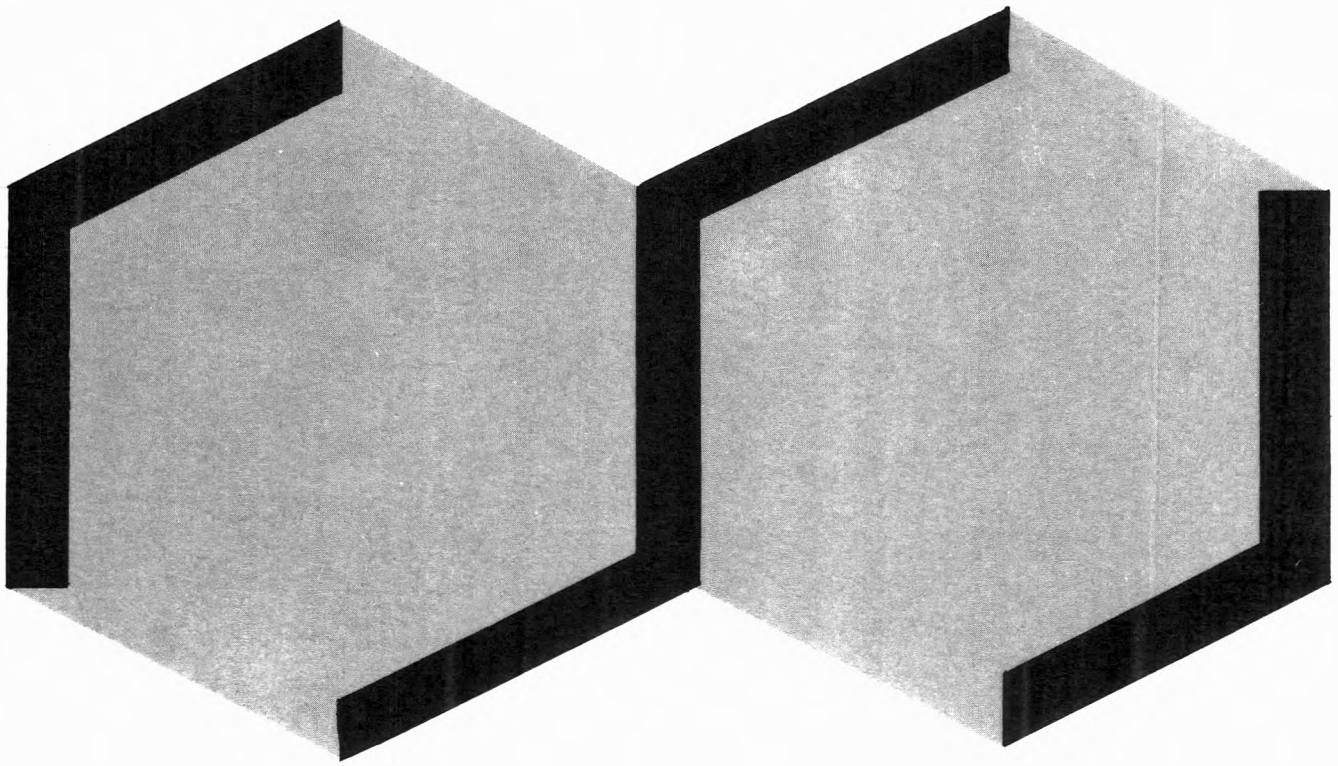

The Journal of Organic Chemistry

The career wise way to keep up with current thinking in the field. You get the *total picture* presented through forty some papers per biweekly issue. Areas of emphasis include:

- Organic reactions
- Natural products
- Studies of mechanism
- Theoretical organic chemistry
- Various aspects of spectroscopy related to organic chemistry

You get all of this, in the 1100 articles and NOTES (brief, concise accounts of studies of smaller scope) and over 4000 pages a year from your big informative issues of THE JOURNAL.

You owe it to your career to find out for yourself why The Journal of Organic Chemistry is the leader in its field.

Send your order today.

. . . *another ACS service*

The Journal of Organic Chemistry
American Chemical Society
1155 Sixteenth Street, N.W.
Washington, D.C. 20036

1974

Yes, I would like to receive THE JOURNAL OF ORGANIC CHEMISTRY at the one-year rate checked below:

	U.S.	*Canada***	*Latin America***	*Other Nations***
ACS Member One-Year Rate*	☐ $20.00	☐ $25.00	☐ $25.00	☐ $26.00
Nonmember	☐ $60.00	☐ $65.00	☐ $65.00	☐ $66.00

Bill me ☐ Bill company ☐ Payment enclosed ☐

Air freight rates available on request.

Name _____

Street _____ Home ☐ Business ☐

City _____ State _____ Zip _____

*NOTE: Subscriptions at ACS member rates are for personal use only. **Payment must be made in U.S. currency, by international money order, UNESCO coupons, U.S. bank draft, or order through your book dealer.

50 good reasons why you should have been reading Environmental Science & Technology

Features

1 Environmental protection: new navy duty by Alexander Ogrinz

2 Law and science team up to preserve environmental quality by William Butler, EDF

3 TVA's chief chemical engineer A. V. Slack evaluates stack gas cleaning for SO_2

4 EPA's Carl Shy and John Finklea explain the CHESS program for air pollution effects

5 Metal finishing is not an ecological scourge say James Zievers and Charles Novotny

6 Metcalf & Eddy's James Fife discusses incineration and pyrolysis of solid waste

7 Office of Saline Water's Fred Witmer looks at desalination technology

8 ISIS's Herschel Cutler outlines transportation hangups in recycling

9 EPA's Ellison Burton discusses computer management of air quality

10 Rendering plant odors are controllable—EPA's Carey, Murthy and Prof. Bethea

11 Storing hot water from utilities in wells is explored by GE's Meyer and Prof. Todd

12 The renovated water-health connection—Shuval and Gruener, Hebrew University

13 Additives help utility emissions, says Apollo Chemical's Ira Kukin

14 Dow's Stacy Daniels and Daniel Parker discuss phosphorus removal technology

15 AWARE's Carl E. Adams tells how to take nitrogen out of waste water

16 Digital Equipment's Epler tells how minicomputers help with data gathering

17 Tracing water pollutants to the source by Lysyj of Rockwell International

18 Sludge disposal is explained by Gruninger and Westerhoff of Malcolm Pirnie, Inc.

19 Wheelabrator-Frye's Culhane on air pollution control with fabric filters

20 U.S. Coast Guard's Lt. Ard and Thomas Scarano on marine waste water systems

21 Orion Research's Martin Frant tells how to detect pollutants with electrodes

22 Picatinny Arsenal's Irving Forsten talks about munitions waste cleanup

23 IKOR's E. Karl Bastress assesses air pollution from aircraft

24 ESI's Ford and Eller and Kellogg's Patterson on petrochemical wastes

25 Jerome Klaff emphasizes the necessity of a national materials policy

26 Honeywell's Blakeley and Thomas explain instruments for waste water

27 Lawrence Berkeley Lab's Hollowell and McLaughlin on air pollution instruments

28 Chem-Seps' Higgins on the use of continuous ion exchange techniques

29 Cal Tech's Friedlander calls attention to small particles in air

Interviews

30 Art Stromberg tells of URS Systems' role as a consulting engineering firm

31 Beckman Instruments' Ballhaus monitors environmental progress

32 Joseph Lawler tells of Camp Dresser & McKee's role in consulting engineering

33 Harold Gershowitz's Waste Management is number two and trying harder

34 John McConnaughy tells of Peabody Galion's role in environmental cleanup

35 Advisory Committee's Martha Sager speaks out on effluent standards

36 American Air Filter's Jesse Shaver talks about air pollution cleanup

Special report

37 A comprehensive national energy policy seems to be a long way off

38 Water pollution control is a real headache for state officials

39 Air pollution control companies find their business is growing and growing

40 Rosemount municipal sewage plant is on the cutting edge of technology

41 Sonic gas cooling systems cut air pollution control costs three ways

42 Department of Commerce takes instrument and equipment companies abroad

43 United Nations Environment Program has come a long way since Stockholm

44 Du Pont faces a divergence of cleanup regulations in its European activity

Outlooks

45 Oregon banned the bottle but all parties are not happy with results

46 Deep well injection is still a popular practice for waste water disposal

47 Stratified charge engine looms larger in emission control strategy

48 Public service organization, Keep America Beautiful, marks its 20th year

49 Clean air law again under the gun as the energy needs surface

50 A myriad of methods separate refuse for recovery, but none are yet commercial